Crystal Engineering of Functional Coordination Polymers

Shin-ichiro Noro

2003

Crystal Engineering of Functional Coordination Polymers

Shin-ichiro Noro

2003

Acknowledgement

This work has been carried out from 1997 to 1999 at Department of Chemistry, Graduate School of Science, Tokyo Metropolitan University, from 2000 to 2002 at Department of Synthetic Chemistry and Biological Chemistry, Graduate School of Engineering, Kyoto University, and from 2001 to 2002 at the RIKEN (The Institute of Physical and Chemical Research), under the direction of Prof. Susumu Kitagawa (Kyoto University), Prof. Masahiro Yamashita (Tokyo Metropolitan University), and Dr. Tatsuo Wada (RIKEN). The author is greatly indebted to Prof. Susumu Kitagawa, Prof. Masahiro Yamashita, and Dr. Tatsuo Wada for their continuing guidance and very hearty encouragement.

The author wishes to gratefully acknowledge Prof. Hiroyuki Matsuzaka (Osaka Prefecture University), Associate Prof. Tadashi Mizutani (Kyoto University), Associate Prof. Mitsuru Kondo (Sizuoka University), Associate Prof. Tomohiko Ishii (Kagawa University), Dr. Ho-Chol Chang (Kyoto University), Dr. Hitoshi Miyasaka (Tokyo Metropolitan University), Dr. Takashi Okubo (Japan Advanced Institute of Science & Technology), Dr. Masaaki Iwata, Dr. Masahisa Osawa, Dr. Tetsuya Aoyama, Dr. Takafumi Sassa, and Dr. Shigeru Ikeda (RIKEN), Dr. Shinya Matsumoto (Yokohama National University), for hearty advice, informative discussion, and continuous encouragement.

The author would like to express gratitude to Dr. Kazuhiro Fukata (Tokyo Metropolitan University) and Dr. Yasuhiro Iimura (RIKEN) for the technical advises in the XRPD measurements. The author is sincerely grateful to Dr. Hisae Shirakawa and Dr. Kazuo Wakasugi (Tokyo Metropolitan University) for the measurements of the elemental analysis. The author wishes to express his gratitude to Dr. Kenji Seki (Osaka Gas Company) and Mr. Ryo Kitaura (Kyoto University) for the measurements of gas adsorption. The author thanks the Instrument Center, the Institute for Molecular Science, for assistance in obtaining the X-ray crystal structures by RAXIS-IV imaging plate diffractometer. The author is indebted to the Rigaku Corporation for the measurements of temperature dependence of XRPD patterns. The author would like to express his grateful acknowledgement to Miss Kimiko Kobayashi for the direction and measurement of X-

ray diffraction analysis by RAXIS-CS imaging plate diffractometer.

The author is grateful to the secretaries Mrs. Hiroko Hirohata and Miss Mieko Yamakado for doing office works.

The author wishes to express his gratitude to all members of Kitagawa, Yamashita, and Wada laboratories for their continuous encouragement.

The author expresses gratitude to RIKEN for supporting him as a Junior Research Associate (JRA).

Finally, the author wishes to offer special thanks to his parents Syoji Noro and Mihoko Noro, his brother Takashi Noro, his step-parents Akio Hirata and Naomi Hirata, his step-sister Yoshiko Hirata, his step-grandmother Fusako Hirata, his wife Tomoko Noro, his son Kazuya Noro, and his daughter Wakaba Noro, for their all patience, warm-hearted encouragement, and both material and spiritual supports.

Shin-ichiro Noro

Department of Synthetic Chemistry and Biological Chemistry

Graduate School of Engineering

Kyoto University

December 2002

Contents

General Introduction

Self-Assembled Coordination Polymers

Coordination polymers have infinite frameworks constructed from metal ions and bridging ligands (Scheme 0.1). Coordination bond plays an important role in construction of extended structures as well as other weak attractive interactions such as hydrogen bond, π-π, CH-π, and van der Waals interaction, and so on. This synthetic chemistry is just like a play with building blocks, therefore one can control the coordination frameworks by modifying geometries of the components. Generally, the formation process proceeds automatically and, therefore, is called "a sort of self-assembly" one. In particular, crystalline coordination polymers are of great use because their structures can be exclusively determined by X-ray crystallographic method, and have demonstrated that they have unique network motifs, structural diversities, and available for physical and chemical properties ranging from magnetism, conductivity, optical properties to porous functions such as adsorption, exchange, separation, catalysis and so on. The size and geometry of those components control topology and spatial dimensionality of networks, and functionality of ligands determines the strength of coordination bonds, resulting in stability of frameworks. Weakly coordinating anions influence not only local structure of metal ions but also an overall framework, therefore so-called a framework-regulator. It is worth noting that protic solvent molecules are involved in hydrogen-bonding links in frameworks, forming a complementary linking net. As compared with assemblies of discrete metal complexes, infinite coordination polymers have advantages for (1) a construction of a stable framework, which leads to microporous functions such as zeolites and activated carbons, (2) a desired arrangement of metal ions with spins, which is related to a magnetostructural study, and (3) a diverse framework topology (chain, ladder, helix, fish-bone, square, rectangular, herringbone, bilayer, honeycomb, pillared-layer, diamond, octahedral net, etc) and a control of overall crystal symmetry. These natures are tunable by a reaction condition (temperature, pressure, PH, and solvent), a selection of proper metal ions and counter anions, a fine modification of organic ligands,

a choice of solvents, and their combinations. Many reviews concerning coordination polymers have been hitherto reported.[1-11]

Scheme 0.1

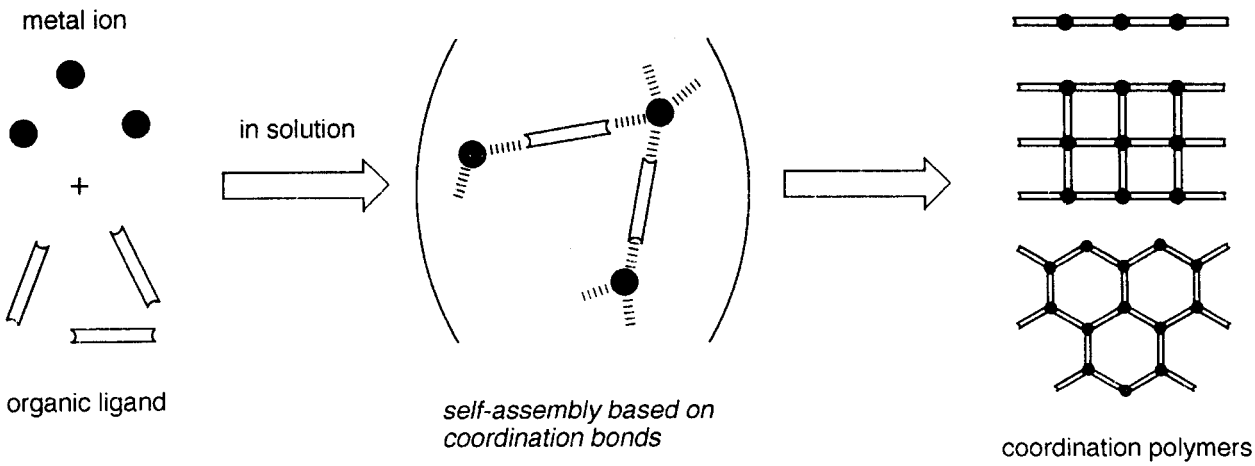

Building Blocks: Connectors and Linkers

There are mainly two kinds of building blocks, that is, connector and linker in construction of the coordination polymers.

The important part of connector is a metal ion. A transition metal ion is often utilized as versatile connectors in the construction of coordination polymers. Depending on metal element and valence for its ion, there are various coordination geometries, which are linear, trigonal-planar, T-shaped, tetrahedral, square-planar, square-pyramidal, trigonal-bipyramidal, octahedral, trigonal-prismatic, pentagonal-bipyramidal, and their distorted forms as shown in Scheme 0.2.

A large number of lanthanide-based frameworks have been synthesized, by utilizing polydentate ligands such as sulfoxides, carboxylates, nitrile, pyridones and lactams.[12-45] Contrary to difficulty in controlling coordination number, its high number from 7 to 10 of lanthanide makes f-block metal ions attractive for the discovery of new and unusual network topologies. In addition, the open vacant sites on a metal ion tend to be generated after removal of coordinated solvent molecules. The vacant sites could be utilized in chemical adsorption and heterogeneous catalysis. Furthermore, lanthanide ions have their potential utility as luminescent and sensory materials.

Scheme 0.2

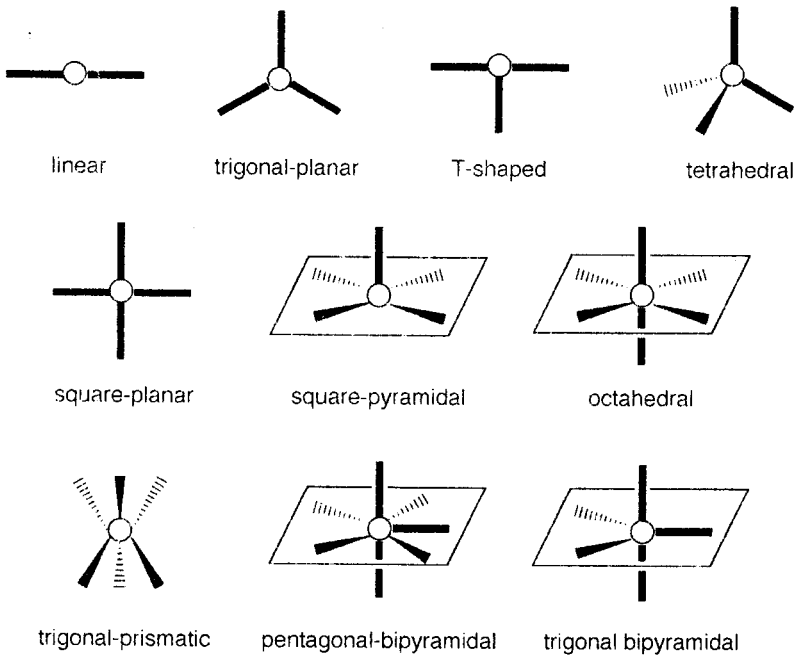

Multidentate linkers such as carboxylates provide rigid frameworks due to their ability to aggregate metal ions into M-O-C polynuclear units, which are recently referred as secondary building units (SBUs).[4,35,46-63] The SBUs are sufficiently rigid because the metal ions are locked into their positions by the carboxylates; thus, instead of employing one transition metal ion at a network vertex (as is the case in M-bipyridine compounds), now the SBUs are available to produce extended frameworks of high structural stability. In several clusters with terminal ligands, their coordination sites may be opened to allow the study of metal site reactivity, which is also shown in the case of the lanthanide ions. Dinuclear complexes of Mo, W, Re, Rh and Ru are useful connectors for the design of infinite networks with the aim of other bridging ligands.[64-89] One can envisage a variety of interesting phenomena that may be exhibited by materials composed of M-M connectors; these include unusual optical, electronic and magnetic properties.

Metal complex connectors have an advantage to control a joint angle; coordination sites for no use can be blocked by chelating or macrocyclic ligands directly bound to a connector metal ion, and therefore, special sites remain for linker. This "ligand-regulation" of a connector is quite useful.[90-109]

The linkers are classified in three categories: inorganic, organic, and organic-inorganic hybrid types. Halides (F, Cl, Br, and I) are smallest and simplest inorganic linkers of all bridging ligands.[110-116] CN^- and SCN^- have the similar bridging ability to halides with the aim of other organic ligands.[117-120]

Cyanometallate anions show various geometries, e.g. linear, as in $[M(CN)_2]^-$ (M = Au[121,122] and Ag[123-125]), trigonal, as in $[Cu(CN)_3]^{2-}$,[126] tetrahedral, as in $[Cd(CN)_4]^{2-}$,[127-130] square planar, as in $[M(CN)_4]^{2-}$ (M = Ni,[131,132] Pd,[25,28,133] and Pt[16,25]), octahedral, as in $[M(CN)_6]^{3-}$ (M = Fe,[44,94,100,101,134] Co,[134-136] Cr,[18,96,137] and Mn[138,139]), pentagonal bipyramidal, as in $[Mo(CN)_7]^{4-}$.[140-143] Especially, octacyanometallates, $[M(CN)_8]^{n-}$ (M = Mo and W), as one of these potential connectors, may show various geometrical structures, e.g. square-antiprism, dodecahedron, or bicapped trigonal-prism.[143-145] This diversity in structure makes cyanometallates as modules useful and practical.

Typical organic ligands are shown in Scheme 0.3. Most famous neutral organic ligands are pyz and 4,4'-bpy.[6-8,10] Recent efforts have been devoted to a utilization of long bridging ligands with appropriate spaces.[146-151]

Di-,[4,152-154] tri-,[4,61,155] tetra-,[156,157] and hexa-[13,158] carboxylate molecules are representative anionic linkers. Coordination polymers having non-symmetric anionic ligands generally described as Pyridine–X–COO^- (X = spacer) have been widely studied.[5] 1,4-Dihydroxy-2,5-benzoquinone and its derivatives provide a variety of frameworks, which play a straight linker in coordination polymers.[159]

The examples of coordination polymers with cationic organic ligands are almost nothing, due to a very low coordination power for cationic metal ions. Developed were novel cationic ligands based on N-aryl pyridiniums and viologen derivatives.[160,161]

In order to functionalize micro-pores and/or -channels and construct dimetallic compounds for molecular-based magnets, newly invented is a donor-type building block, composed of molecularly inorganic-organic hybrid bridging ligand, so-called metalloligand.[162-179]

Scheme 0.3

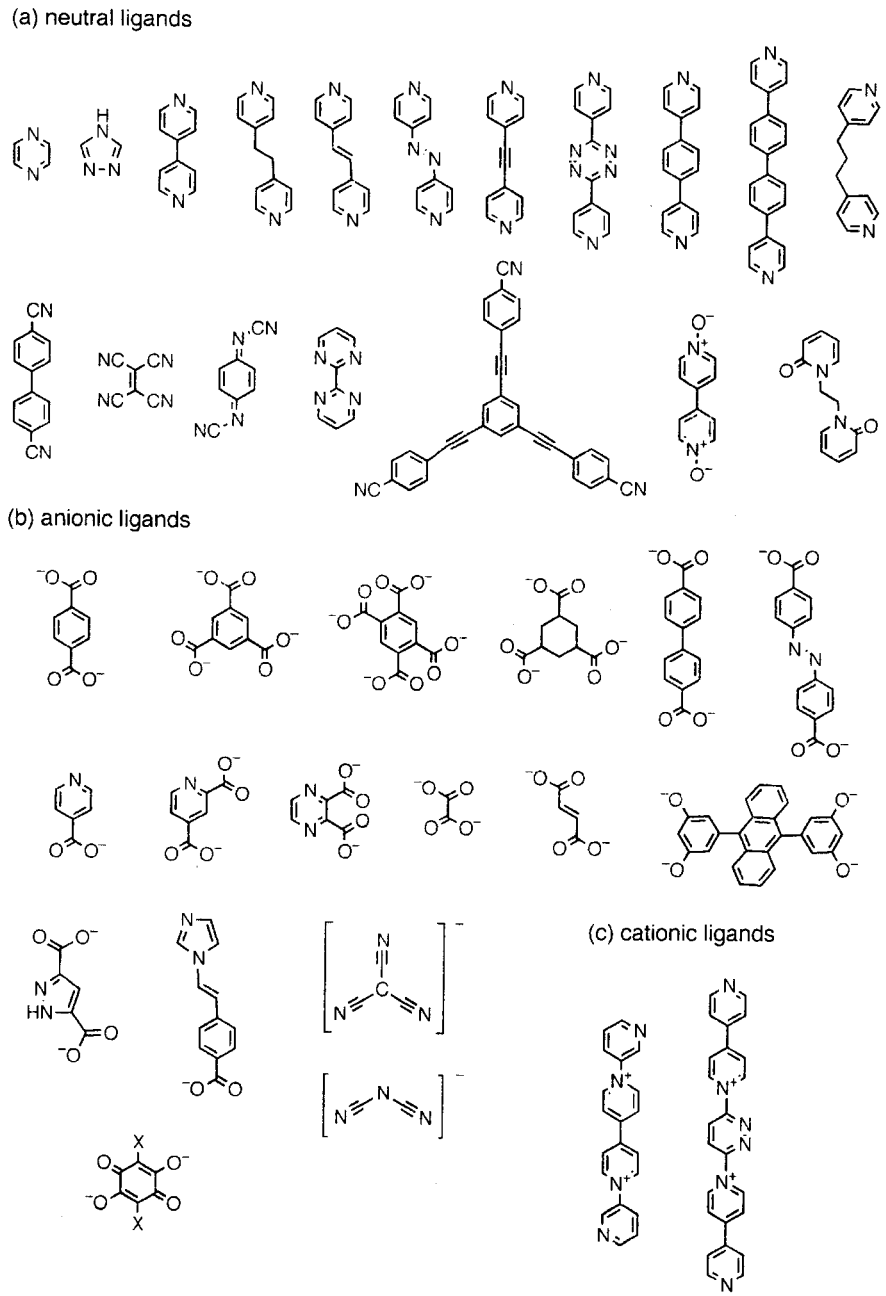

Other Building Blocks Supporting Coordination Frameworks

When neutral bridging ligands such as bipyridine derivatives are used as linkers, counter anions coexist in the framework due to requirement of neutrality in overall charge. Furthermore, other several roles of the anions can be expected, i.e. coordination and hydrogen bonding linker, guest for vacant space, eventually resulting in framework-regulator.

Various solvents are used not only for reaction media, but also for regulation of framework topology.[180-182] Solvent molecules often occur in microspace formed by coordination polymer motifs. In other words, crystal structures of coordination polymers happen to be controlled by template effect of solvent molecules. There has been a vast body of compounds having this aspect.

Motifs for Infinite Structures

Dimensionless combination of building blocks mentioned above creates a variety of characteristic structural motifs. Representative examples of 1-D, 2-D, and 3-D coordination polymer motifs are illustrated in Scheme 0.4.

An interpenetration frequently occurs in the 2-D and 3-D coordination polymers with large grid or space. In some cases the frameworks do generate spacious voids, cavities, and channels, which may account for more than half the volume of the crystal. These large spaces are usually occupied by highly disordered, essentially liquid solvent. In other cases remarkable interpenetrating structures are formed in which the voids associated with one framework are occupied by one or more independent frameworks; an inherent feature of such entangled structures is that they can be disentangled only by breaking internal connections.

Crystal Engineering of Coordination Polymers

Rationally synthesizing coordination polymers with desired bonds, environments, and overall shapes, is a final goal for synthetic chemists. This is called as "crystal engineering". Up to date, reported are a large number of coordination polymers, many of which frequently afford unexpected frameworks because of the presence of a lot of structure-determining factors such as several building blocks, reaction conditions and techniques, which is in sharp contrast to the case of organic compounds. Therefore, the regulation of "crystal engineering" is one of the current interests.

Scheme 0.4

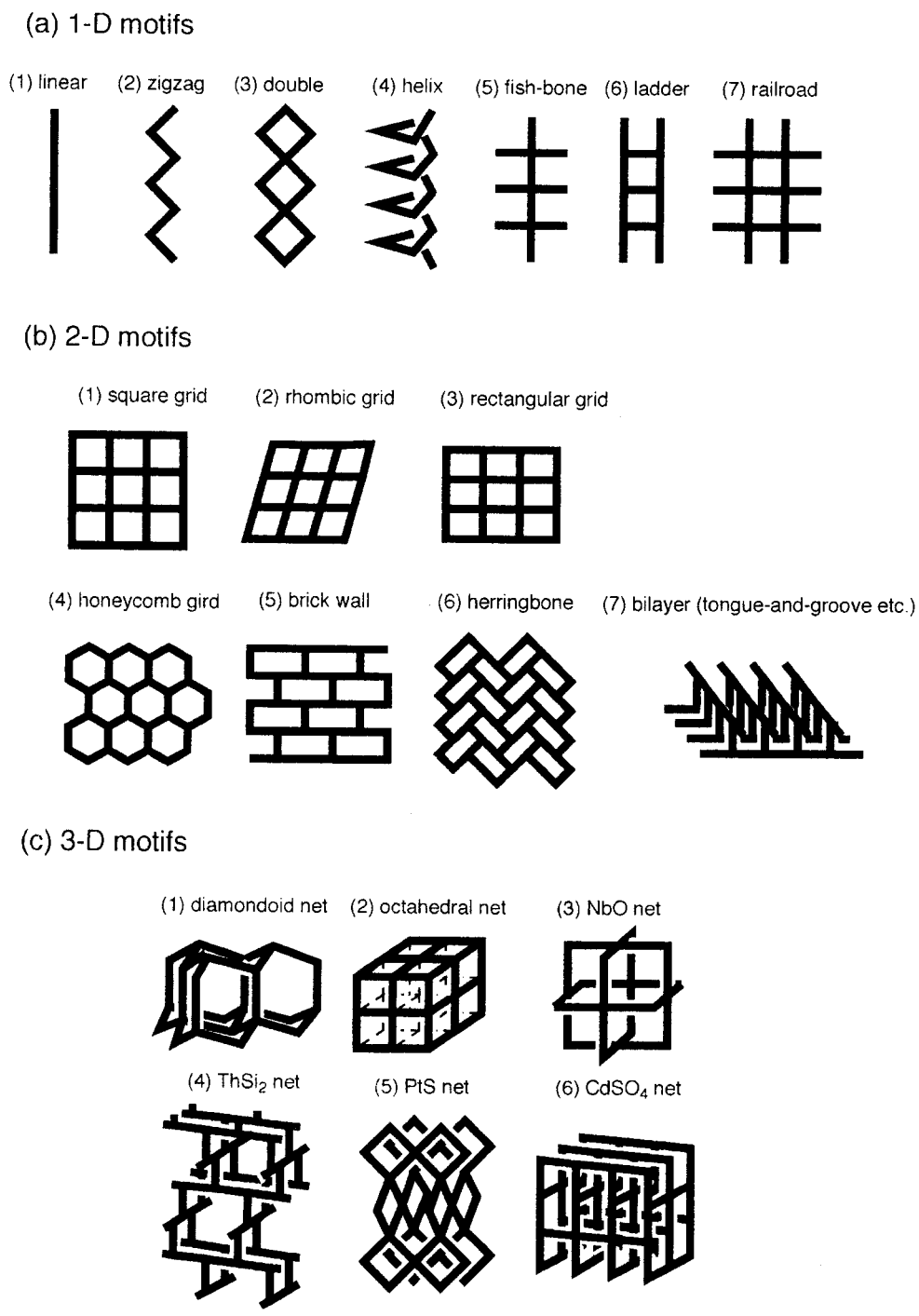

From Structural Studies to Functionalities

Since the crystallization for the coordination polymer has been difficult by the middle of the 20th century due to the insolubility of the polymeric compounds, the well-characterized commands

have still been limited. However recent efforts of many researchers in the past decade enable us to obtain a good quality of single crystals of the coordination polymers by means of some synthetic techniques, for examples, diffusion method, hydro(solvo)thermal method, and microwave method. Therefore, the interest of the chemists is rapidly changing from the structures to the functionalities such as magnetism,[108,175,183-189] conductivity,[190-194] spin-crossover,[123,195-205] host-guest chemistry,[4,7,170,206,207] and nonlinear optical (NLO) properties.[5,41,57,208-217] Of course, the information of crystal structures is indispensable to discuss their functionalities in detail and realize more sophisticated materials. For examples, the length between spin species and their 3-D arrangement determine the magnitude and the type of magnetic interaction. For synthesis of the materials with second-order NLO properties noncentrosymmetric arrangements of molecular chromophores are prerequisite. In this thesis, the main interest of the author focused on microporosity of coordination polymers, research of which has been started at the threshold of the 1990s.

Porous Compounds

Inorganic porous compounds such as a large number of zeolites and activated carbons with high stability of their frameworks are great available in our ordinary life due to their unique functionalities such as adsorption, separation, catalysis, exchange, nonlinear optics, electro devices, ship in bottle synthesis, and so on. Therefore, many researchers have hitherto devoted themselves to study such materials in detail. The zeolites have regular channels or cavities, that is, a high crystallinity, but a low porosity because of a thick pore wall. On the other hand, the activated carbons with a high porosity possess several sizes of channels or cavities, which causes the presence of an ineffective space. In addition, hard synthetic condition for both compounds makes it difficult to control the frameworks. Recently, organic porous compounds linked by hydrogen bonds have been reported by Aoyama et al. However, many of them are liable to destruct or change their original frameworks after the removal of guest molecules into the micropores. The coordination polymer is mainly constructed from coordination bonds and resulting network is robust. The bridging organic ligands as building block can be modified easily and enable us to make desired structures, and the transition metal ions for catalytic sites can be easily introduced in the pore, not by inorganic

compounds. Moreover, the pore walls are constructed from organic molecules, producing a 'light material'. Thus, the field of porous coordination polymer chemistry has shown quite spectacular advances in the last decade.

Classification of Porous Coordination Polymers

Porous coordination polymers are classified in three categories (Scheme 0.5). The first generation compounds provide frameworks with microcavities and/or channels supported by guest molecules, which are collapsed by the removal of all guest molecules. The second ones have robust porous frameworks even after removal of guest molecules. The third ones bear dynamic frameworks, which change themselves responding to external physical stimuli, such as electric or magnetic field and light, and chemical stimuli by guest molecules. Zeolites and activated carbons constructed from covalent bonds are representative of porous solid and classified in the second generation compounds. On the other hand, porous coordination polymers could afford not only stable "second generation compounds" but also dynamic "third generation ones". In the followings described are typical examples of the second and third generation coordination polymers and their porous properties. Representative examples of coordination polymers with several porous functions are listed in Table 0.1.[59,218-224]

Scheme 0.5

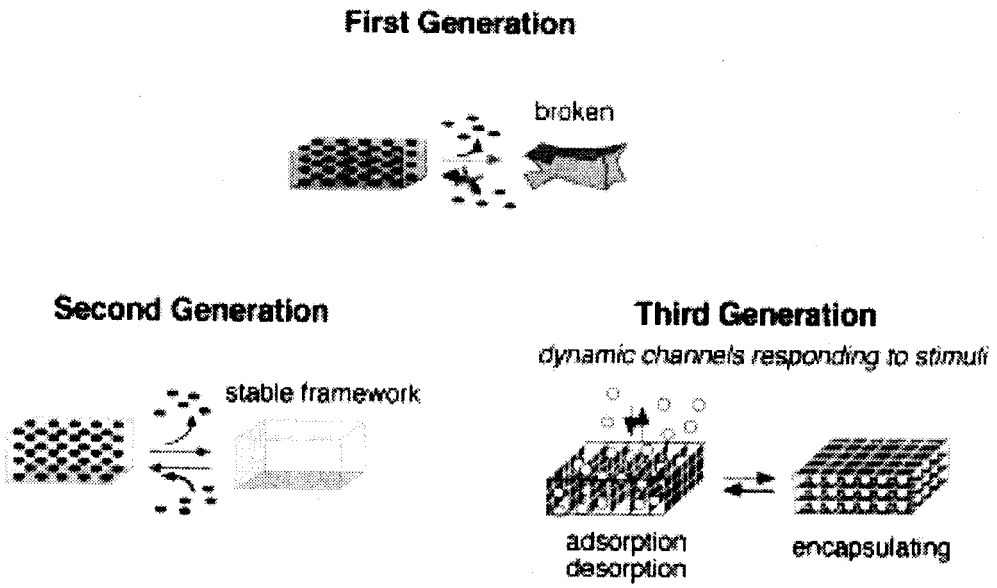

Table 0.1. Representative Examples of Porous Function.

	Function	Compound	Guests or Substrates	Appeared in
2nd Gen.[a]	adsorption (gas)	$[Co_2(NO_3)_4(4,4'\text{-bpy})_3]_n$	CH_4, O_2, N_2	1997[218]
	adsorption (vapor)	$[Zn_4O(1,4\text{-BDC})_3]_n$[c]	CH_2Cl_2, CCl_4, C_6H_{12}, etc	1999[219]
	anion-exchange	$[Cu(L1)]_n$[d]	BF_4^-, PF_6^-	1990[220]
3rd Gen.[b]	adsorption (gas)	$\{[Cu(BF_4)_2(4,4'\text{-bpy})(H_2O)_2]\cdot 4,4'\text{-bpy}\}_n$	Ar, N_2, CO_2	2001[221]
	adsorption (vapor)	$[Ag(CF_3SO_3)(3\text{-TEB})]_n$[e]	C_6H_6	1995[222]
	anion-exchange	$[Ag(EDTPN)]_n$[f]	NO_3^-, $CF_3SO_3^-$, ClO_4^-	2000[223]
	catalysis	$[Cd(NO_3)_2(4,4'\text{-bpy})_2]_n$	aldehydes and $SiMe_3CN$	1994[224]
		$\{[Zn_3O(L2)_6]\cdot 2H_3O\cdot 12H_2O\}_n$[g]	ester and alcohols	2000[59]

[a] second generation compound, [b] third generation compound, [c] 1,4-BDC = 1,4-benzenedicarboxylate, [d] L1 = 4,4',4'',4'''-tetracyanotetraphenylmethane, [e] 3-TEB = 1,3,5-tris(3-ethynylbenzonitrile)benzene, [f] EDTPN = ethylenediaminetetrapropionitrile, [g] L2 is shown below.

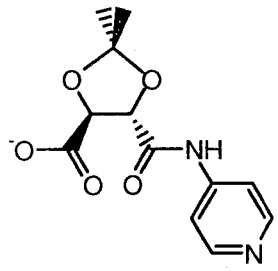

Gas Adsorption Property

An adsorption property of several gases is of great interest due to their fascinating applications such as the storage and transport of natural gas. For the creation of such adsorbents, the researchers have been devoted to synthesize a stable framework after the removal of guest molecules, namely second generation compounds. First report on the gas adsorption properties of coordination polymers at ambient temperature appeared in 1997, whose framework is best described as tongue-and-groove (bilayer) structure. $\{[M_2(NO_3)_4(4,4'\text{-bpy})_3]\cdot xH_2O\}_n$ (M = Co, x = 4; Ni, x = 4; Zn, x = 2) is formed from $M(NO_3)_2$ and 4,4'-bpy.[218] The effective microchannel cross section for dried sample is obtained as about 3 Å x 6 Å (after consideration of van der Waals radii). This apohost reversibly adsorbs CH_4, N_2, and O_2 in the pressure range of 1-36 atm without collapsing of the crystal framework. Similar coordination polymers capable of the gas adsorption have been synthesized.[40,47,52,219,221,225-243] In this century other types of complexes with high capacity have been successively synthesized. $[Zn_4O(L)_3]_n$ (L = several dicarboxylate ligands) with a CH_4 adsorption property affords a 3-D cubic porous network, in which an oxide-centered Zn_4O tetrahedron is edge-bridged by six carboxylates to give the octahedron-shaped SBU.[47,219] It should be noted that its 3-D porous system can be functionalized with the organic groups –Br, $-NH_2$, $-OC_3H_7$, $-OC_5H_{11}$, $-C_2H_4$, $-C_4H_4$ and that its pore size can be expanded with the long molecular struts biphenyl, tetrahydropyrene, pyrene, and terphenyl, with retention of an original framework topology. To data, the highest value of surface area (3265 $m^2\cdot g^{-1}$) is obtained in 3-D coordination polymer $[Cu_2(4,4'\text{-biphenyldicarboxylate})_2(TED)]_n$ (TED = triethylenediamine).[233]

Dynamic Third Generation Porous Compounds

Several third generation compounds with flexible channels have been recently prepared. Compound of $\{[Cu(BF_4)_2(4,4'\text{-bpy})(H_2O)_2]\cdot 4,4'\text{-bpy}\}_n$ has 1-D linear chains linked by metal-free 4,4'-bpy molecules via hydrogen bonds with coordinated H_2O molecules, forming 2-D non-interpenetrated sheets.[244] The adsorption of N_2, Ar, and CO_2 suddenly begins at a certain relative pressure ('gate pressure') regardless of almost nil adsorption below the gate pressure.[221] Such a

unique adsorption phenomenon is associated with the hydrogen bond links. Our labolatory previously refined the third-generation compound as three categories as shown in Scheme 0.6.[245]

1) The "recoverable collapsing" framework (type I): the framework in this species collapses due to the close-packing force on removal of the guest molecules; however, it regenerates under the initial conditions.[93,243,245,246]

2) The " guest-induced transformation" framework (type II): this framework has the property that structural shifts in the network are induced by the simultaneous exchanging of guest molecules.[223,247]

3) The "guest-induced reformation" framework (type III): this framework has the property that removal or addition of guest molecules makes a structural change in the network; however, it reverts to the original structure under the initial conditions.[22,221,245,248,249]

Interestingly, compounds of type II and III show "crystal-to crystal transformation". In a sense, this property results from the molecular inorganic-organic hybrid system.

Scheme 0.6

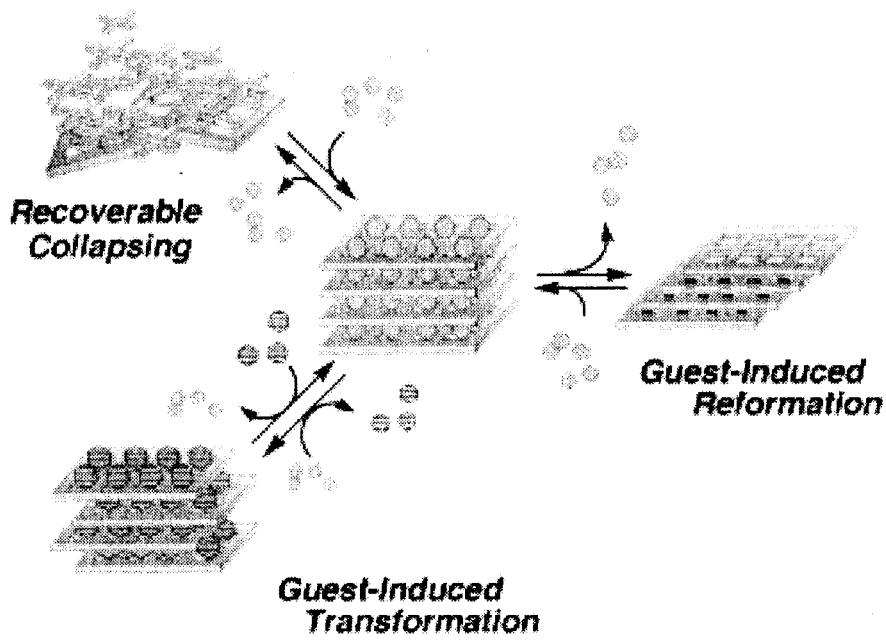

Adsorption or Exchange of Vapors

Adsorption or exchange of several vapors and small molecules is most energetically investigated in porous functionalities.[17,22,39,46,47,53,56,58,59,91-93,95,219,222,227,228,241,245,246,248-260] Properties such as guest removal and exchange within a host crystal are investigated for $[Ag(CF_3SO_3)(4\text{-TEB})]_n$ (4-TEB = 1,3,5-tris(4-ethynylbenzonitrile)benzene).[250] The nitrile moieties of the trigonal phenylacetylene ligand coordinate end-on to the trigonal pyramidal silver cation to form a 3-D (3,3)-connected net topologically analogous to the inorganic structure type $ThSi_2$. There are six interpenetrated $ThSi_2$-type networks with large channels with cross sections of 15 Å x 22 Å in the final structure. Guest exchange of nonfunctionalized aliphatic and aromatic molecules makes no changes in the original framework. However, crystals containing alcoholic aromatic molecules can be indexed to the 2-D rectangular. A hysteretic adsorption and desorption profile accompanied by a transformation of the crystal structure is observed for $\{[Cu_2(pzdc)_2(dpyg)]\cdot 8H_2O\}_n$ (pzdc = pyrazine-2,3-dicarboxylate; dpyg = 1,2-di(4-pyridyl)glycol), which possesses a pillared-layer structure, on exposure to H_2O or MeOH vapor under pressure.[249] Selectivities for adsorbed organic molecules, which determines by size, shape, kinds of substituent groups, are important properties due to the possibility of separating a mixture.[53,93,224,245,246,256] Structural diversity and easy modification of the pore in coordination polymers could give higher selectivities that zeolites and activated carbons. $\{[Co(HBTC)(pyridine)_2]\cdot 2/3pyridine\}_n$ (BTC = 1,3,5-benzenetricarboxylate) selectively adsorbs aromatic molecules by the π-π interaction.[256] The selective uptake for guests with hydrogen bonding sites, in some case, involving size and shape recognition, is also observed in several coordination polymers containing coordinatively unsaturated metal centers,[53,246] amide sites,[245] and both carboxylate and pyridine sites[93] for the guest binding.

Anion-Exchange Property

It is well known that porous zeolites show cation-exchange properties due to their anionic frameworks, while porous coordination polymers constructed from cationic metal ions and neutral bridging ligands could exchange the counteranions included in the frameworks.[220,223,247,261-264] An anion-exchange property, which happens in a solid-liquid interface, was first reported in 1990.[220]

$\{[Cu(4,4',4'',4'''\text{-tetracyanotetraphenylmethane})]\cdot BF_4\cdot xC_6H_5NO_2\}_n$ contains a diamond-related cationic framework, which generates very large admanantane-like cavities occupied by disordered $C_6H_5NO_2$ together with BF_4^- anions. This crystal undergoes ready anion-exchange with PF_6^- anions. Recently, the structural transformations in the crystalline state are observed concomitant with the anion-exchange.[223,247]

Adsorption of Salts and Metal Complexes

Porous coordination polymers that adsorb the molecules such as salts and metal complexes have been also found.[59,93,95,243] The X-ray crystal structure of $\{[Cu(pymo)_2]\cdot NH_4ClO_4\}_n$ (Hpymo = 2-hydroxypyrimidine) reveals that the combination of square-planar Cu(II) ion with 120 ° bond angles provided by Hpymo generates a 3-D porous framework with ammonium and ClO_4^- and H_2O molecules included in the pores.[243] This complex reversibly and selectively sorbs $AClO_4$ salts (A = NH_4, Li, Na, K, Rb) when exposed to $AClO_4$ aqueous solutions giving highly crystalline $\{[Cu(pymo)_2]\cdot AClO_4\}_n$ clathrates. $\{[Ni_3(C_{20}H_{32}N_8)_3(CTC)_2]\cdot 16H_2O\}_n$ ($C_{20}H_{32}N_8$ = 1,8-(4-pyridylmethyl)-1,3,6,8,10,13-hexaazacyclotetradecane macrocyclic ligand, CTC = *cis*,*cis*-1,3,5-cyclohexanetricarboxylate) indicates that each Ni(II) macrocyclic unit binds two CTC^{3-} ions in *trans* position and each CTC^{3-} ion coordinates three Ni(II) macrocyclic complexes to form a 2-D layer, in which pendant pyridine rings are involved in the hydrogen bonding and the herringbone π-π interaction.[93,95] The XRPD patterns indicate that the framework is deformed upon removal of H_2O guests but restored upon rebinding of H_2O. The host solid binds $\{[Cu(NH_3)_4]\cdot 2ClO_4\}$ in MeCN.

Heterogeneous Catalysis

Metal ions play key roles in organic transformations. Many investigators work with soluble species in a homogeneous solution. An advantage of heterogeneous catalysts is their ready recoverability, and they are important in industry. However, solid catalysts have so far been almost exclusively inorganic materials. Especially useful are microporous inorganic zeolites. Despite much recent interest in metal-organic solids with zeolitic guest-binding properties, their catalytic activities are largely unexplored.[17,59,224,257,265,266] $[Cd(NO_3)_2(4,4'\text{-bpy})_2]_n$, which consists of 2-D networks,

shows a catalytic activity for the cyanosilylation of aldehydes with shape specificity.[224] A homochiral open-framework solid, whose formula is given as $\{[Zn_3O(L)_6]\cdot 2H_3O\cdot 12H_2O\}_n$ (L is shown in the bottom of Table 0.1), reveals the enantioselective catalytic activity for the transesterification.[59] Zr, Ti, and lanthanide complexes also show characteristic activities.[17,257,266] Utilization of a metalloligand as a building unit could provide a novel porous coordination polymer with highly catalytic activity because coordinatively unsaturated metal center acting as activation sites in the homogeneous catalyst can be located in channel wall, metal ion of which undergoes a less steric hindrance for an attack of organic molecules than that in the nodal position.

Survey of This Thesis

The main purpose of this thesis is to establish rational syntheses ("crystal engineering") by finding a general principle for controlling frameworks and to elucidate the correlation between crystal structures and the microporous properties or dynamic phenomena of frameworks of coordination polymers. Bridging or chelating ligands used in this study are given in Scheme 0.7 along with their abbreviations.

Scheme 0.7

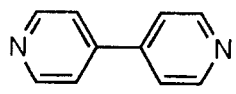

4,4'-bipyridine
(4,4'-bpy)

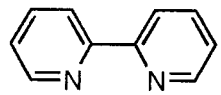

2,2'-bipyridine
(2,2'-bpy)

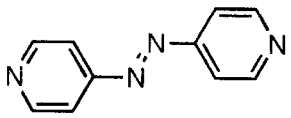

4,4'-azopyridine
(azpy)

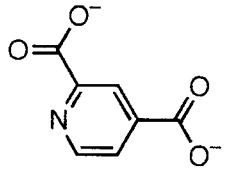

pyridine-2,4-dicarboxylate
(2,4-pydca)

In Part 1 of this thesis, which consists of Chapters I, II, and III, the exploration of rational synthetic methods for the construction of desired coordination polymers, namely, "crystal engineering", is studied.

Chapter I deals with the preparation and structural transformation of Fe(II) coordination polymers, $\{[Fe(NCS)_2(azpy)(MeOH)_2]\cdot azpy\}_n$ (**I-1**·2MeOH), $\{[Fe(NCS)_2(4,4'\text{-bpy})(H_2O)_2]\cdot azpy\}_n$ (**I-2**·$2H_2O$), $\{[Fe(NCS)_2(azpy)_2]\cdot 3H_2O\}_n$ (**I-3**), and $\{(H_2 4,4'\text{-bpy})[Fe_3(SO_4)_4(4,4'\text{-bpy})_3(H_2O)_6]\cdot 10H_2O\}_n$ (**I-4**), synthesized by the reaction of Fe(II) salts with linear azpy or 4,4'-bpy ligands. **I-1**·2MeOH and **I-2**·$2H_2O$ easily release the coordinated solvent molecules of MeOH and H_2O, respectively, by heating to form new crystal phases of **I-1** and **I-2**, which show 2-D sheets with square or rhombic grids. Especially, the magnetic property of **I-1** reveals the occurrence of a spin-crossover of the Fe(II) ions, which is in contrast to that of a precursory of **I-1**·2MeOH.

Chapter II demonstrates the development of new synthetic method of porous coordination polymer, $\{[ZnCu(2,4\text{-pydca})_2(H_2O)_3(DMF)]\cdot DMF\}_n$ (**II-1**), by utilization of a metalloligand, $\{[Cu(2,4\text{-pydca})_2(H_2O)]\cdot 2Et_3NH\}$ (**III-1**·$2Et_3NH$), as a building unit, in which the Zn(II) ion at the node of the network acts as a connector and the Cu(II) ion in channel wall is available for guest-coordination.

Chapter III describes rational design and bond engineering of coordination polymers by a Cu(II) metalloligand, $\{[Cu(2,4\text{-pydca})_2(H_2O)]\cdot 2Et_3NH\}$ (**III-1**·$2Et_3NH$), which was prepared by a deprotonation of a precursory metalloligand $[Cu(2,4\text{-pydca})_2(H_2O)_2]$ (**III-1**·2H). 1-D coordination polymers with homo- and hetero-metallic ions, $\{[MCu(2,4\text{-pydca})_2(H_2O)_4]\cdot 2H_2O\}_n$ (M = Co (**III-2**), Cu (**III-3**), Zn (**III-4**)), show a similar type of chain bridged by 4-carboxylate donors of metalloligand **III-1**. In addition, several 2-D coordination polymers constructed from the metalloligand **III-1** have also been isolated and characterized. $[MCu(2,4\text{-pydca})_2(H_2O)_4]_n$ (M = Mn (**III-5**), Fe (**III-6**)) forms a 2-D thick sheet-like structure, in which 1-D mixed-metallic zigzag chains of $[MCu(2,4\text{-pydca})_2]_n$ are linked by the weak coordination between the oxygen atoms of 4-carboxylate group and the Cu(II) atoms. $\{[Cu(2,2'\text{-bpy})Cu(2,4\text{-pydca})_2]\cdot 3H_2O\}_n$ (**III-7**) consists of metalloligand **III-1** and metal complex connector of $[Cu(2,2'\text{-bpy})]^{2+}$, producing 1-D zigzag

chains bridged by 4-carboxylate groups of **III-1**. These chains are bound by the weak coordination between the oxygen atom of 2-carboxylate unit and the Cu(II) atom to create a 2-D undulated sheet structure. $[ZnCu(2,4\text{-pydca})_2(H_2O)_2(MeOH)_2]_n$ (**III-8**) consists of 1-D linear chains, which are linked by weak coordination and hydrogen bonds to form a 2-D network. It is worth nothing that the regular coordination bonds of these polymers and $\{[ZnCu(2,4\text{-pydca})_2(H_2O)_3(DMF)]\cdot DMF\}_n$ (**II-1**) can be predictably controlled, following to an Irving-Williams order. Also attempted was the reaction of Ag(I) ion with metalloligand **III-1**, which generate a 3-D network of $[Ag_2Cu(2,4\text{-pydca})_2]_n$ (**III-9**). **III-9** is composed of Ag_2 dimer unit and bridging metalloligand **III-1**. Both 2- and 4-carboxylates of metalloligands link to the Ag-Ag dimers to form a 3-D network. These structural results clearly demonstrate that the metalloligand **III-1** has a variety of coordination modes, depending on second metal ion units employed.

Part 2 of this thesis, which consists of Chapters IV, V, and VI, is a summary of microporous functionalities of coordination polymers, which include framework stability, gas adsorption, anion-exchange, and dynamic properties.

Chapter IV demonstrates the syntheses, crystal structures, and CH_4 adsorption properties of highly porous coordination polymers, $[Cu(AF_6)(4,4'\text{-bpy})_2]_n$ (A = Si (**IV-1**), Ge (**IV-2**), and Ti (**IV-3**)), each of which affords a stable, 3-D, microporous network. The channel size of each compound is *ca.* 8 Å × 8 Å along the *c*-axis and 6 Å × 2 Å along the *a*- or *b*-axes. It should be noted that **IV-1** has the high specific surface area of 1337 $m^2\cdot g^{-1}$ and the high CH_4 adsorption ability at ambient temperature and low pressure, which is superior to that of any zeolites, and thus opens up a new possibility for CH_4 storage materials.

Chapter V describes a framework engineering by anions and dynamic anion-exchange properties of Cu(II)/4,4'-bpy coordination polymers. When compounds **IV-1-3** were immersed in water, a conversion of 3-D networks (**IV-1-3**) to interpenetrated ones $\{[Cu(4,4'\text{-bpy})_2(H_2O)_2]\cdot AF_6\}_n$ (A = Si (**V-1**), Ge (**V-2**), and Ti (**V-3**)) (*2-D Interpenetration*) took place. The 2-D interpenetrating network **V-1** shows unique dynamic anion-exchange properties, which accompany drastic structural conversions. A series of novel Cu(II) coordination polymers, $\{[Cu_2(4,4'\text{-bpy})_5(H_2O)_4]\cdot anions\cdot 2H_2O\cdot 4EtOH\}_n$ (anions = $4PF_6^-$ (**V-4**·$2H_2O$·4EtOH), $2PF_6^-$ +

$2ClO_4^-$ (**V-5**·$2H_2O$·4EtOH)) (*2-D Double-Layer*), $\{[Cu_2(PF_6)(NO_3)(4,4'\text{-bpy})_4]\cdot 2PF_6\cdot 2H_2O\}_n$ (**V-6**·$2PF_6$·$2H_2O$) (*3-D Undulated Grid*), $\{[Cu(PF_6)(4,4'\text{-bpy})_2(MeCN)]\cdot PF_6\cdot 2MeCN\}_n$ (**V-7**·2MeCN) (*2-D Grid*), and $\{[Cu(4,4'\text{-bpy})_2(H_2O)_2]\cdot PF_6\cdot BF_4\}_n$ (**V-8**) (*2-D Grid*), were synthesized from the combination of framework-builder (Cu(II) ion and 4,4'-bpy ligand) and framework-regulator (PF_6^- and coexistent anions). The three modes of PF_6^- anions are observed. **V-6**·$2PF_6$·$2H_2O$ has rare PF_6^- bridges. The PF_6^- and NO_3^- monoanions alternately link to the Cu(II) centers in the undulated 2-D sheets of $[Cu(4,4'\text{-bpy})_2]_n$ to form a 3-D porous network. The free PF_6^- anions are included in the channels. **V-7**·2MeCN affords both free and terminal-bridged PF_6^- anions. **V-4**·$2H_2O$·4EtOH, **V-5**·$2H_2O$·4EtOH, and **V-8** bear free PF_6^- anions. All of the anion in **V-4**·$2H_2O$·4EtOH and **V-5**·$2H_2O$·4EtOH are freely located in the channels constructed from a host network. Interestingly, these Cu(II) frameworks are rationally controlled by counter anions and selectively converted to other ones.

Chapter VI describes the reaction of several metal(II) ions with rich π-conjugated azpy ligand as linker. Ten coordination polymers, $\{[Mn(NO_3)_2(azpy)(H_2O)_2]\cdot 2EtOH\}_n$ (**VI-1**·2EtOH) (*1-D linear chain*), $\{[Cd(azpy)_3(H_2O)_2]\cdot 2PF_6\cdot azpy\}_n$ (**VI-2**) (*1-D fishbone-type chain*), $\{[M_2(azpy)_6(H_2O)_5]\cdot 4PF_6\cdot azpy\cdot H_2O\}_n$ (M = Ni (**VI-3**), Zn (**VI-4**)) (*1-D defective zigzag chain*), $\{[Ag(azpy)]\cdot PF_6\}_n$ (**VI-5**) (*1-D linear chain*), $\{[Mn(NCS)_2(azpy)(MeOH)_2]\cdot azpy\}_n$ (**VI-6**) (*1-D linear chain*), $\{[Mn(NCS)_2(azpy)_2]\cdot azpy\}_n$ (**VI-7**) (*2-D square sheet*), $\{[Ni(NCS)_2(azpy)_2]\cdot 3toluene\}_n$ (**VI-8**·3toluene) (*2-D rhombic sheet*), and $\{[Ni_2(NCS)_4(azpy)_4]\cdot alcohol\}_n$ (alcohol = MeOH (**VI-9**·MeOH), EtOH (**VI-9**·EtOH)) (*2-D interpenetrating sheet*), have been synthesized and crystallographically characterized. It should be noted that the interpenetration and π-π interaction play an important role in the framework stability of azpy-containing coordination polymers. **VI-9**·MeOH and **VI-9**·EtOH afford perpendicularly interpenetrating structures of rhombic 2-D sheets, resulting in small microporous channels with dimensions of *ca.* 2 Å x 2 Å along the *c*-axis. These channels are filled with guest alcohol molecules (MeOH and EtOH). The TGA data and XRPD patterns reveal that **VI-9**·H_2O retains the channel network after the removal of guest molecules, while non-interpenetrating network of **VI-7** destroys with a release of guest azpy molecules. Compound **VI-9** shows N_2 and CH_4 adsorption activities

for the microporous channels, despite of larger sizes of the N_2 and CH_4 (*ca.* 3 Å and 4 Å, respectively) than that of the channel window (2 Å), which clearly indicates that this interpenetrating network has soft dynamic channels, namely, new type of third-generation microporous compounds.

References

(1) Kitagawa, S.; Munakata, M. *Trends Inorg. Chem.* **1993**, *3*, 437-462.

(2) Munakata, M. *Adv. Inorg. Chem.* **1998**, *46*, 173-303.

(3) Blake, A. J.; Champness, N. R.; Hubberstey, P.; Li, W.-S.; Withersby, M. A.; Schröder, M. *Coord. Chem. Rev.* **1999**, *183*, 117-138.

(4) Eddaoudi, M.; Moler, D. B.; Li, H.; Chen, B.; Reineke, T. M.; O'Keeffe, M.; Yaghi, O. M. *Acc. Chem. Res.* **2001**, *34*, 319-330.

(5) Evans, O. R.; Lin, W. *Acc. Chem. Res.* **2002**, *35*, 511-522.

(6) Hagrman, P. J.; Hagrman, D.; Zubieta, J. *Angew. Chem., Int. Ed. Engl.* **1999**, *38*, 2638-2684.

(7) Kitagawa, S.; Kondo, M. *Bull. Chem. Soc. Jpn.* **1998**, *71*, 1739-1753.

(8) Moulton, B.; Zaworotko, M. J. *Chem. Rev.* **2001**, *101*, 1629-1658.

(9) Zaworotko, M. J. *Chem. Soc. Rev.* **1994**, 283-288.

(10) Zaworotko, M. J. *Chem. Commun.* **2001**, 1-9.

(11) Batten, S. R.; Robson, R. *Angew. Chem., Int. Ed. Engl.* **1998**, *37*, 1460-1494.

(12) Carrad, L. H.; Goodgame, D. M. L.; Hill, S. P. W.; Williams, D. J. *J. Chem. Soc., Dalton Trans.* **1993**, 1003-1008.

(13) Chui, S. S.-Y.; Siu, A.; Feng, X.; Zhang, Z. Y.; Mak, T. C. W.; Williams, I. D. *Inorg. Chem. Commun.* **2001**, *4*, 467-470.

(14) Cui, Y.; Ngo, H. L.; White, P. S.; Lin, W. *Chem. Commun.* **2002**, 1666-1667.

(15) Doyle, G. A.; Goodgame, D. M. L.; Hill, S. P. W.; Williams, D. J. *Chem. Commun.* **1993**, 207-209.

(16) Du, B.; Meyers, E. A.; Shore, S. G. *Inorg. Chem.* **2001**, *40*, 4353-4360.

(17) Evans, O. R.; Ngo, H. L.; Lin, W. *J. Am. Chem. Soc.* **2001**, *123*, 10395-10396.

(18) Figuerola, A.; Diaz, C.; Fallah, M. S. E.; Ribas, J.; Maestro, M.; Mahía, J. *Chem. Commun.* **2001**, 1204-1205.

(19) Goodgame, D. M. L.; Menzer, S.; Ross, A. T.; Williams, D. J. *Inorg. Chim. Acta* **1996**, *251*, 141-149.

(20) Goodgame, D. M. L.; Menzer, S.; Smith, A. M.; Williams, D. J. *Chem. Commun.* **1997**, 339-340.

(21) Goodgame, D. M. L.; Hill, S. P. W.; Williams, D. J. *Inorg. Chim. Acta* **1998**, *272*, 131-140.

(22) Kiritsis, V.; Michaelides, A.; Skoulika, S.; Golhen, S.; Ouahab, L. *Inorg. Chem.* **1998**, *37*, 3407-3410.

(23) Knoeppel, D. W.; Shore, S. G. *Inorg. Chem.* **1996**, *35*, 1747-1748.

(24) Knoeppel, D. W.; Shore, S. G. *Inorg. Chem.* **1996**, *35*, 5328-5334.

(25) Knoeppel, D. W.; Liu, J.; Meyers, E. A.; Shore, S. G. *Inorg. Chem.* **1998**, *37*, 4828-4837.

(26) Lee, E.; Heo, J.; Kim, K. *Angew. Chem., Int. Ed. Engl.* **2000**, *39*, 2699-2701.

(27) Liang, Y.; Hong, M.; Su, W.; Cao, R.; Zhang, W. *Inorg. Chem.* **2001**, *40*, 4574-4582.

(28) Liu, J.; Meyers, E. A.; Shore, S. G. *Inorg. Chem.* **1998**, *37*, 5410-5411.

(29) Liu, Q.-D.; Li, J.-R.; Gao, S.; Ma, B.-Q.; Liao, F.-H.; Zhou, Q.-Z.; Yu, K.-B. *Inorg. Chem. Commun.* **2001**, *4*, 301-304.

(30) Long, D.-L.; Blake, A. J.; Champness, N. R.; Schröder, M. *Chem. Commun.* **2000**, 1369-1370.

(31) Long, D.-L.; Blake, A. J.; Champness, N. R.; Wilson, C.; Schröder, M. *J. Am. Chem. Soc.* **2001**, *123*, 3401-3402.

(32) Long, D.-L.; Blake, A. J.; Champness, N. R.; Wilson, C.; Schrëder, M. *Angew. Chem., Int. Ed. Engl.* **2001**, *40*, 2444-2447.

(33) Long, D.-L.; Blake, A. J.; Champness, N. R.; Wilson, C.; Schröder, M. *Chem. Eur. J.* **2002**, *8*, 2026-2033.

(34) Ma, L.; Evans, O. R.; Foxman, B. M.; Lin, W. *Inorg. Chem.* **1999**, *38*, 5837-5840.

(35) Ma, B.-Q.; Zhang, D.-S.; Gao, S.; Jin, T.-Z.; Yan, C.-H.; Xu, G.-X. *Angew. Chem., Int. Ed. Engl.* **2000**, *39*, 3644-3646.

(36) Mao, J.-G.; Zhang, H.-J.; Ni, J.-Z.; Wang, S.-B.; Mak, T. C. W. *Polyhedron* **1999**, *18*, 1519-1525.

(37) Pan, L.; Woodlock, E. B.; Wang, X.; Zheng, C. *Inorg. Chem.* **2000**, *39*, 4174-4178.

(38) Pan, L.; Huang, X.; Li, J.; Wu, Y.; Zheng, N. *Angew. Chem., Int. Ed. Engl.* **2000**, *39*, 527-530.

(39) Reineke, T. M.; Eddaoudi, M.; Fehr, M.; Kelley, D.; Yaghi, O. M. *J. Am. Chem. Soc.* **1999**, *121*, 1651-1657.

(40) Reineke, T. M.; Eddaoudi, M.; O'Keeffe, M.; Yaghi, O. M. *Angew. Chem., Int. Ed. Engl.* **1999**, *38*, 2590-2594.

(41) Shi, J.-M.; Xu, W.; Liu, Q.-Y.; Liu, F.-L.; Huang, Z.-L.; Lei, H.; Yu, W.-T.; Fang, Q. *Chem. Commun.* **2002**, 756-757.

(42) Wu, C.-D.; Lu, C.-Z.; Yang, W.-B.; Lu, S.-F.; Zhuang, H.-H.; Huang, J.-S. *Eur. J. Inorg. Chem.* **2002**, 797-800.

(43) Wu, C.-D.; Lu, C.-Z.; Zhuang, H.-H.; Huang, J.-S. *Acta Cryst.* **2002**, *C58*, m283-285.

(44) Yan, B.; Wang, H.-D.; Chen, Z.-D. *Polyhedron* **2001**, *20*, 591-597.

(45) Zhang, R.-H.; Ma, B.-Q.; Bu, X.-H.; Wang, H.-G.; Yao, X.-K. *Polyhedron* **1997**, *16*, 1123-1127.

(46) Eddaoudi, M.; Kim, J.; O'Keeffe, M.; Yaghi, O. M. *J. Am. Chem. Soc.* **2002**, *124*, 376-377.

(47) Eddaoudi, M.; Kim, J.; Rosi, N.; Vodak, D.; Wachter, J.; O'Keeffe, M.; Yaghi, O. M. *Science* **2002**, *295*, 469-472.

(48) Vodak, D. T.; Braun, M. E.; Kim, J.; Eddaoudi, M.; Yaghi, O. M. *Chem. Commun.* **2001**, 2534-2535.

(49) Kim, J.; Chen, B.; Reineke, T. M.; Li, H.; Eddaoudi, M.; Moler, D. B.; O'Keeffe, M.; Yaghi, O. M. *J. Am. Chem. Soc.* **2001**, *123*, 8239-8247.

(50) Eddaoudi, M.; Kim, J.; Wachter, J. B.; Chae, H. K.; O'Keeffe, M.; Yaghi, O. M. *J. Am. Chem. Soc.* **2001**, *123*, 4368-4369.

(51) Braun, M. E.; Steffek, C. D.; Kim, J.; Rasmussen, P. G.; Yaghi, O. M. *Chem. Commun.* **2001**, 2532-2533.

(52) Chae, H. K.; Eddaoudi, M.; Kim, J.; Hauck, S. I.; Hartwig, J. F.; O'Keeffe, M.; Yaghi, O. M. *J. Am. Chem. Soc.* **2001**, *123*, 11482-11483.

(53) Yaghi, O. M.; Davis, C. E.; Li, G.; Li, H. *J. Am. Chem. Soc.* **1997**, *119*, 2861-2868.

(54) Yaghi, O. M.; Jernigan, R.; Li, H.; Davis, C. E.; Groy, T. L. *J. Chem. Soc., Dalton Trans.* **1997**, 2383-2384.

(55) Kumagai, H.; Akita-Tanaka, M.; Inoue, K.; Kurmoo, M. *J. Mater. Chem.* **2001**, *11*, 2146-2151.

(56) Evans, O. R.; Lin, W. *Inorg. Chem.* **2000**, *39*, 2189-2198.

(57) Lin, W.; Wang, Z.; Ma, L. *J. Am. Chem. Soc.* **1999**, *121*, 11249-11250.

(58) Gutschke, S. O. H.; Price, D. J.; Powell, A. K.; Wood, P. T. *Eur. J. Inorg. Chem.* **2001**, 2739-2741.

(59) Seo, J. S.; Whang, D.; Lee, H.; Jun, S. I.; Oh, J.; Jeon, Y. J.; Kim, K. *Nature* **2000**, *404*, 982-986.

(60) Bourne, S. A.; Lu, J.; Mondal, A.; Moulton, B.; Zaworotko, M. J. *Angew. Chem., Int. Ed. Engl.* **2001**, *40*, 2111-2113.

(61) Gutschke, S. O. H.; Price, D. J.; Powell, A. K.; Wood, P. T. *Angew. Chem., Int. Ed. Engl.* **2001**, *40*, 1920-1923.

(62) Tao, J.; Tong, M.-L.; Shi, J.-X.; Chen, X.-M.; Ng, S. W. *Chem. Commun.* **2000**, 2043-2044.

(63) Lin, W.; Evans, O. R.; Yee, G. T. *J. Solid State Chem.* **2000**, *152*, 152-158.

(64) Aquino, M. A. S. *Coord. Chem. Rev.* **1998**, *170*, 141-202.

(65) Barral, M. C.; Jiménez-Aparicio, R.; Pérez-Quintanilla, D.; Priego, J. L.; Royer, E. C.; Torres, M. R.; Urbanos, F. A. *Inorg. Chem.* **2000**, *39*, 65-70.

(66) Beck, E. J.; Drysdale, K. D.; Thompson, L. K.; Li, L.; Murphy, C. A.; Aquino, M. A. S. *Inorg. Chim. Acta* **1998**, *279*, 121-125.

(67) Bonnet, L.; Cukiernik, F. D.; Maldivi, P.; Giroud-Godquin, A.-M.; Marchon, J.-C. *Chem. Mater.* **1994**, *6*, 31-38.

(68) Campana, C.; Dunbar, K. R.; Ouyang, X. *Chem. Commun.* **1996**, 2427-2428.

(69) Cotton, F. A.; Kim, Y. *J. Am. Chem. Soc.* **1993**, *115*, 8511-8512.

(70) Cotton, F. A.; Kim, Y.; Lu, J. *Inorg. Chim. Acta* **1994**, *221*, 1-4.

(71) Cotton, F. A.; Kim, Y.; Ren, T. *Inorg. Chem.* **1992**, *31*, 2723-2726.

(72) Cotton, F. A.; Kim, Y.; Ren, T. *Polyhedron* **1993**, *12*, 607-611.

(73) Cotton, F. A.; Pedersen, E. *Inorg. Chem.* **1975**, *14*, 388-391.

(74) Cukiernik, F. D.; Giroud-Godquin, A.-M.; Maldivi, P.; Marchon, J.-C. *Inorg. Chim. Acta* **1994**, *215*, 203-207.

(75) Cukiernik, F. D.; Luneau, D.; Marchon, J.-C.; Maldivi, P. *Inorg. Chem.* **1998**, *37*, 3698-3704.

(76) Handa, M.; Sayama, Y.; Mikuriya, M.; Nukada, R.; Hiromitsu, I.; Kasuga, K. *Chem. Lett.* **1996**, 201-202.

(77) Handa, M.; Sayama, Y.; Mikuriya, M.; Nukada, R.; Hiromitsu, I.; Kasuga, K. *Bull. Chem. Soc. Jpn.* **1998**, *71*, 119-125.

(78) Handa, M.; Yamada, K.; Nakao, T.; Kasuga, K.; Mikuriya, M.; Kotera, T. *Chem. Lett.* **1993**, 1969-1972.

(79) Handa, M.; Yoshioka, D.; Yasuyoshi, S.; Shiomi, K.; Mikuriya, M.; Hiromitsu, I.; Kasuga, K. *Chem. Lett.* **1999**, 1033-1034.

(80) Lu, J.; Harrison, W. T. A.; Jacobson, A. J. *Chem. Commun.* **1996**, 399-400.

(81) Miyasaka, H.; Campos-Fernández, C. S.; Clérac, R.; Dunbar, K. R. *Angew. Chem., Int. Ed. Engl.* **2000**, *39*, 3831-3835.

(82) Miyasaka, H.; Campos-Fernández, C. S.; Galán-Mascarós, J. R.; Dunbar, K. R. *Inorg. Chem.* **2000**, *39*, 5870-5873.

(83) Miyasaka, H.; Clérac, R.; Campos-Fernández, C. S.; Dunbar, K. R. *J. Chem. Soc., Dalton Trans.* **2001**, 858-861.

(84) Miyasaka, H.; Clérac, R.; Campos-Fernández, C. S.; Dunbar, K. R. *Inorg. Chem.* **2001**, *40*, 1663-1671.

(85) Ouyang, X.; Campana, C.; Dunbar, K. R. *Inorg. Chem.* **1996**, *35*, 7188-7189.

(86) Sayama, Y.; Handa, M.; Mikuriya, M.; Nukada, R.; Hiromitsu, I.; Kasuga, K. *Chem. Lett.* **1998**, 777-778.

(87) Schiavo, S. L.; Bruno, G.; Zanello, P.; Laschi, F.; Piraino, P. *Inorg. Chem.* **1997**, *36*, 1004-1012.

(88) Telser, J.; Drago, R. S. *Inorg. Chem.* **1984**, *23*, 3114-3120.

(89) Wesemann, J. L.; Chisholm, M. H. *Inorg. Chem.* **1997**, *36*, 3258-3267.

(90) Carlucci, L.; Ciani, G.; Gramaccioli, A.; Proserpio, D. M.; Rizzato, S. *CrystEngComm* **2000**, *29*, 1-10.

(91) Choi, H. J.; Suh, M. P. *Inorg. Chem.* **1999**, *38*, 6309-6312.

(92) Ko, J. W.; Min, K. S.; Suh, M. P. *Inorg. Chem.* **2002**, *41*, 2151-2157.

(93) Min, K. S.; Suh, M. P. *Chem. Eur. J.* **2001**, *7*, 303-313.

(94) Colacio, E.; Domínguez-Vera, J. M.; Chazi, M.; Kivekäs, R.; Klinga, M.; Moreno, J. M. *Chem. Commun.* **1998**, 1071-1072.

(95) Choi, H. J.; Lee, T. S.; Suh, M. P. *J. Incl. Phenom.* **2001**, *41*, 155-162.

(96) Marvilliers, A.; Parsons, S.; Rivière, E.; Audière, J.-P.; Kurmoo, M.; Mallah, T. *Eur. J. Inorg. Chem.* **2001**, 1287-1293.

(97) Kou, H.-Z.; Gao, S.; Bai, O.; Wang, Z.-M. *Inorg. Chem.* **2001**, *40*, 6287-6294.

(98) Ohba, M.; Usuki, N.; Fukita, N.; Okawa, H. *Inorg. Chem.* **1998**, *37*, 3349-3354.

(99) Fukita, N.; Ohba, M.; Okawa, H. *Mol. Cryst. Liq. Cryst.* **2000**, *342*, 217-224.

(100) Kou, H.-Z.; Bu, W.-M.; Liao, D.-Z.; Jiang, Z.-H.; Yan, S.-P.; Fan, Y.-G.; Wang, G.-L. *J. Chem. Soc., Dalton Trans.* **1998**, 4161-4164.

(101) Miyasaka, H.; Matsumoto, N.; Okawa, H.; Re, N.; Gallo, E.; Floriani, C. *J. Am. Chem. Soc.* **1996**, *118*, 981-994.

(102) Miyasaka, H.; Okawa, H.; Matsumoto, N. *Mol. Cryst. Liq. Cryst.* **1999**, *335*, 1015-1023.

(103) Re, N.; Crescenzi, R.; Floriani, C.; Miyasaka, H.; Matsumoto, N. *Inorg. Chem.* **1998**, *37*, 2717-2722.

(104) Miyasaka, H.; Okawa, H.; Miyazaki, A.; Enoki, T. *Inorg. Chem.* **1998**, *37*, 4878-4883.

(105) Matsumoto, N.; Sunatsuki, Y.; Miyasaka, H.; Hashimoto, Y.; Luneau, D.; Tuchagues, J. P. *Angew. Chem., Int. Ed. Engl.* **1999**, 171-173.

(106) Miller, J. S.; Epstein, A. J. *Chem. Commun.* **1998**, 1319-1325.

(107) Hibbs, W.; Rittenberg, D. K.; Sugiura, K.; Burkhart, B. M.; Morin, B. G.; Arif, A. M.; Liable-Sands, L.; Rheingold, A. L.; Sundaralingam, M.; Epstein, A. J.; Miller, J. S. *Inorg. Chem.* **2001**, *40*, 1915-1925.

(108) Miller, J. S.; Calabrese, J. C.; McLean, R. S.; Epstein, A. J. *Adv. Mater.* **1992**, *4*, 498-501.

(109) Mikami, S.; Sugiura, K.; Maruta, T.; Maeda, Y.; Ohba, M.; Usuki, N.; Okawa, H.; Akutagawa, T.; Nisihara, S.; Nakamura, T.; Iwasaki, K.; Miyazaki, N.; Hino, S.; Asato, E.; Miller, J. S.; Sakata, Y. *J. Chem. Soc., Dalton Trans.* **2001**, 448-455.

(110) Okamoto, H.; Yamashita, M. *Bull. Chem. Soc. Jpn.* **1998**, *71*, 2023-2039.

(111) Clark, R. J. H. *Chem. Soc. Rev.* **1990**, *19*, 107-131.

(112) Scott, B.; Willett, R.; Porter, L.; Williams, J. *Inorg. Chem.* **1992**, *31*, 2483-2492.

(113) Yaghi, O. M.; Li, G. *Angew. Chem., Int. Ed. Engl.* **1995**, *34*, 207-209.

(114) Kawata, S.; Kitagawa, S.; Kumagai, H.; Iwabuchi, S.; Katada, M. *Inorg. Chim. Acta* **1998**, *267*, 143-145.

(115) Blake, A. J.; Brooks, N. R.; Champness, N. R.; Cooke, P. A.; Deveson, A. M.; Fenske, D.; Hubberstey, P.; Li, W.-S.; Schröder, M. *J. Chem. Soc., Dalton Trans.* **1999**, 2103-2110.

(116) Chesnut, D. J.; Kusnetzow, A.; Birge, R. R.; Zubieta, J. *Inorg. Chem.* **1999**, *38*, 2663-2671.

(117) Ibrahim, A. M. A.; Siebel, E.; Fischer, R. D. *Inorg. Chem.* **1998**, *37*, 3521-3525.

(118) Chesnut, D. J.; Plewak, D.; Zubieta, J. *J. Chem. Soc., Dalton Trans.* **2001**, 2567-2580.

(119) Healy, P. C.; Pakawatchai, C. P.; Papasergio, R. I.; Patrick, V. A.; White, A. H. *Inorg. Chem.* **1984**, *23*, 3769-3776.

(120) Blake, A. J.; Brooks, N. R.; Champness, N. R.; Crew, M.; Hanton, L. R.; Hubberstey, P.; Parsons, S.; Schröder, M. *J. Chem. Soc., Dalton Trans.* **1999**, 2813-2817.

(121) Leznoff, D. B.; Xue, B.-Y.; Batchelor, R. J.; Einstein, F. W. B.; Patrick, B. O. *Inorg. Chem.* **2001**, *40*, 6026-6034.

(122) Yeung, W.-F.; Wong, W.-T.; Zuo, J.-L.; Lau, T.-C. *J. Chem. Soc., Dalton Trans.* **2000**, 629-631.

(123) Niel, V.; Muñoz, M. C.; Gaspar, A. B.; Galet, A.; Levchenko, G.; Real, J. A. *Chem. Eur. J.* **2002**, *8*, 2446-2453.

(124) Iwamoto, T.; Soma, T. *Inorg. Chem.* **1996**, *35*, 1849-1856.

(125) Bowmaker, G. A.; Effendy; Reid, J. C.; Rickard, C. E. F.; Skelton, B. W.; White, A. H. *J. Chem. Soc., Dalton Trans.* **1998**, 2139-2146.

(126) Nishikiori, S. *J. Coord. Chem.* **1996**, *37*, 23-38.

(127) Yun, S.-S.; Kim, Y.-P.; Kim, C.-H. *Acta Cryst.* **1999**, *C55*, 2026-2028.

(128) Kitazawa, T.; Kikuyama, T.; Ugajin, H.; Takahashi, M.; Takeda, M. *J. Coord. Chem.* **1996**, *37*, 17-22.

(129) Yuge, H.; Kim, C.-H.; Iwamoto, T.; Kitazawa, T. *Inorg. Chim. Acta* **1997**, *257*, 217-224.

(130) Nishikiori, S.; Iwamoto, T. *J. Incl. Phenom.* **1985**, *3*, 283-295.

(131) Iwamoto, T. *Inclusion Compounds*; Oxford University Press, 1991; Vol. 5, Chapter 6, pp 172-212.

(132) Iwamoto, T. *Inclusion Compounds*; Academic Press: London, 1984; Vol. 1, Chapter 2, pp 29-57.

(133) Munakata, M.; Zhong, J. C.; Ino, I.; Kuroda-Sowa, T.; Maekawa, M.; Suenaga, Y.; Oiji, N. *Inorg. Chim. Acta* **2001**, *317*, 268-275.

(134) Eriksen, J. O.; Hazell, A.; Jensen, A.; Jepsen, J.; Poulsen, R. D. *Acta Cryst.* **2000**, *C56*, 551-553.

(135) Ferbinteanu, M.; Tanase, S.; Andruh, M.; Journaux, Y.; Cimpoesu, F.; Strenger, I.; Riviere, E. *Polyhedron* **1999**, *18*, 3019-3025.

(136) Mondal, N.; Dey, D. K.; S., M.; Gramlich, V. *Polyhedron* **2001**, *20*, 607-613.

(137) Kou, H.-Z.; Gao, S.; Zhang, J.; Wen, G.-H.; Su, G.; Zheng, R. K.; Zhang, X. X. *J. Am. Chem. Soc.* **2001**, *123*, 11809-11810.

(138) Ziegler, B.; Witzel, M.; Schwarten, M.; Babel, D. *Z. Naturforsch.* **1999**, *54b*, 870-876.

(139) Babel, D.; Kurtz, W. *Studies in Inorganic Chemistry* **1982**, *3*, 593-596.

(140) Larionova, J.; Kahn, O.; Golhen, S.; Ouahab, L.; Clérac, R. *Inorg. Chem.* **1999**, *38*, 3621-3627.

(141) Kahn, O.; Larionova, J.; Ouahab, L. *Chem. Commun.* **1999**, 945-952.

(142) Larionova, J.; Kahn, O.; Gohlen, S.; Ouahab, L.; Clérac, R. *J. Am. Chem. Soc.* **1999**, *121*, 3394-3356.

(143) Sra, A. K.; Rombaut, G.; Lahitête, F.; Golhen, S.; Ouahab, L.; Mathonière, C.; Yakhmi, J. V.; Kahn, O. *New J. Chem.* **2000**, *24*, 871-876.

(144) Zhong, Z. J.; Seino, H.; Mizobe, Y.; Hidai, M.; Verdaguer, M.; Ohkoshi, S.; Hashimoto, K. *Inorg. Chem.* **2000**, *39*, 5095-5101.

(145) Rombaut, G.; Golhen, S.; Ouahab, L.; Mathonière, C.; Kahn, O. *J. Chem. Soc., Dalton Trans.* **2000**, 3609-3614.

(146) Banfi, S.; Carlucci, L.; Caruso, E.; Ciani, G.; Proserpio, D. M. *J. Chem. Soc., Dalton Trans.* **2002**, 2714-2721.

(147) Biradha, K.; Fujita, M. *Chem. Commun.* **2001**, 15-16.

(148) Withersby, M. A.; Blake, A. J.; Champness, N. R.; Cooke, P. A.; Hubberstey, P.; Schröder, M. *J. Am. Chem. Soc.* **2000**, *122*, 4044-4046.

(149) Abrahams, B. F.; Hardie, M. J.; Hoskins, B. F.; Robson, R.; Sutherland, E. E. *Chem. Commun.* **1994**, 1049-1050.

(150) Fujita, M.; Aoyagi, M.; Ibukuro, F.; Ogura, K.; Yamaguchi, K. *J. Am. Chem. Soc.* **1998**, *120*, 611-612.

(151) Pschirer, N. G.; Ciurtin, D. M.; Smith, M. D.; Bunz, U. H.; zur Loye, H.-C. *Angew. Chem., Int. Ed. Engl.* **2002**, *41*, 583-585.

(152) Choi, K.-Y.; Chun, K. M.; Suh, I.-H. *Polyhedron* **2001**, *20*, 57-65.

(153) Zhang, H.-X.; Kang, B.-S.; Xu, A.-W.; Chen, Z.-N.; Zhou, Z.-Y.; Chan, A. S. C.; Yu, K.-B.; Ren, C. *J. Chem. Soc., Dalton Trans.* **2001**, 2559-2566.

(154) Burrows, A. D.; Harrington, R. W.; Mahon, M. F.; Price, C. E. *J. Chem. Soc., Dalton Trans.* **2000**, 3845-3854.

(155) Prior, T. J.; Rosseinsky, M. J. *Chem. Commun.* **2001**, 495-496.

(156) Murugavel, R.; Krishnamurthy, D.; Sathiyendiran, M. *J. Chem. Soc., Dalton Trans.* **2002**, 34-39.

(157) Kumagai, H.; Kepert, C. J.; Kurmoo, M. *Inorg. Chem.* **2002**, *41*, 3410-3422.

(158) Endres, H.; Knieszner, A. *Acta Cryst.* **1984**, *C40*, 770-772.

(159) Kitagawa, S.; Kawata, S. *Coord. Chem. Rev.* **2002**, *224*, 11-34.

(160) Zhang, J.; Matsushita, M. M.; Kong, X. X.; Abe, J.; Iyoda, T. *J. Am. Chem. Soc.* **2001**, *123*, 12105-12106.

(161) Matsushita, M. M.; Morikawa, M.; Kawai, T.; Iyoda, T. *Mol. Cryst. Liq. Cryst.* **2000**, *343*, 87-96.

(162) Pei, Y.; Kahn, O.; Sletten, J.; Renard, J.-P.; Georges, R.; Gianduzzo, J.-C.; Curely, J.; Xu, Q. *Inorg. Chem.* **1988**, *27*, 47-53.

(163) Baron, V.; Gillon, B.; Cousson, A.; Mathonière, C.; Kahn, O.; Grand, A.; Öhrström, L.; Delley, B.; Bonnet, M.; Boucherle, J.-X. *J. Am. Chem. Soc.* **1997**, *119*, 3500-3506.

(164) Stumpf, H. O.; Ouahab, L.; Pei, Y.; Bergerat, P.; Kahn, O. *J. Am. Chem. Soc.* **1994**, *116*, 3866-3874.

(165) Ciurtin, D. M.; Smith, M. D.; zur Loye, H.-C. *Chem. Commun.* **2002**, 74-75.

(166) Dong, Y.-B.; Smith, M. D.; zur Loye, H.-C. *Inorg. Chem.* **2000**, *39*, 1943-1949.

(167) Horikoshi, R.; Mochida, T.; Moriyama, H. *Inorg. Chem.* **2002**, *41*, 3017-3024.

(168) Dong, G.; Hong, M.; Chun-ying, D.; Feng, L.; Qing-jin, M. *J. Chem. Soc., Dalton Trans.* **2002**, 2593-2594.

(169) Carlucci, L.; Ciani, G.; Porta, F.; Proserpio, D. M.; Santagostini, L. *Angew. Chem., Int. Ed. Engl.* **2002**, *41*, 1907-1911.

(170) Goldberg, I. *Chem. Eur. J.* **2000**, *6*, 3863-3870.

(171) Abrahams, B. F.; Hoskins, B. F.; Michail, D. M.; Robson, R. *Nature* **1994**, *369*, 727-729.

(172) Sharma, C. V. K.; Broker, G. A.; Huddleston, J. G.; Baldwin, J. W.; Metzger, R. M.; Rogers, R. D. *J. Am. Chem. Soc.* **1999**, *121*, 1137-1144.

(173) Diskin-Posner, Y.; Patra, G. K.; Goldberg, I. *Eur. J. Inorg. Chem.* **2001**, 2515-2523.

(174) Zhong, Z. J.; Matsumoto, H.; Okawa, H.; Kida, S. *Chem. Lett.* **1990**, 87-90.

(175) Tamaki, J.; Zhong, Z. J.; Matsumoto, N.; Kida, S.; Koikawa, M.; Achiwa, N.; Hashimoto, Y.; Okawa, H. *J. Am. Chem. Soc.* **1992**, *114*, 6974-6979.

(176) Decurtins, S.; Schmalle, H. W.; Oswald, H. R.; Linden, A.; Ensling, J.; Gütlich, P.; Hauser, A. *Inorg. Chim. Acta* **1994**, *216*, 65-73.

(177) Carling, S. G.; Mathonière, C.; Day, P.; Abdul Malik, K. M.; Coles, S. J.; Hursthouse, M. B. *J. Chem. Soc., Dalton Trans.* **1996**, 1839-1843.

(178) Larionova, J.; Mombelli, B.; Sanchiz, J.; Kahn, O. *Inorg. Chem.* **1998**, *37*, 679-684.

(179) Okawa, H.; Mitsumi, M.; Ohba, M.; Kodera, M.; Matsumoto, N. *Bull. Chem. Soc. Jpn.* **1994**, *67*, 2139-2144.

(180) Hennigar, T. L.; MacQuarrie, D. C.; Losier, P.; Rogers, R. D.; Zaworotko, M. J. *Angew. Chem., Int. Ed. Engl.* **1997**, *36*, 972-973.

(181) Blake, A. J.; Brooks, N. R.; Champness, N. R.; Crew, M.; Deveson, A.; Fenske, D.; Gregory, D. H.; Hanton, L. R.; Hubberstey, P.; Schröder, M. *Chem. Commun.* **2001**, 1432-1433.

(182) Withersby, M. A.; Blake, A. J.; Champness, N. R.; Cooke, P. A.; Hubberstey, P.; Li, W.-S.; Schröder, M. *Inorg. Chem.* **1999**, *38*, 2259-2266.

(183) Clérac, R.; Miyasaka, H.; Yamashita, M.; Coulon, C. *J. Am. Chem. Soc.* **2002**, *124*, 12837-12844.

(184) Inoue, K.; Imai, H.; Ghalsasi, P. S.; Kikuchi, K.; Ohba, M.; Okawa, H.; Yakhmi, J. V. *Angew. Chem., Int. Ed. Engl.* **2001**, *40*, 4242-4245.

(185) Caneschi, A.; Gatteschi, D.; Lalioti, N.; Sangregorio, C.; Sessoli, R.; Venturi, G.; Vindigni, A.; Rettori, A.; Pini, M. G.; Novak, M. A. *Angew. Chem., Int. Ed. Engl.* **2001**, *40*, 1760-1763.

(186) Kahn, O.; Larionova, J.; Yakhmi, J. V. *Chem. Eur. J.* **1999**, *5*, 3443-3449.

(187) Ohba, M.; Okawa, H.; Fukita, N.; Hashimoto, Y. *J. Am. Chem. Soc.* **1997**, *119*, 1011-1019.

(188) Pei, Y.; Verdaguer, M.; Kahn, O. *J. Am. Chem. Soc.* **1986**, *108*, 7428-7430.

(189) Kumagai, H.; Inoue, K. *Angew. Chem., Int. Ed. Engl.* **1999**, *38*, 1601-1603.

(190) Sinzger, K.; Hünig, S.; Jopp, M.; Bauer, D.; Beitsch, W.; von Schütz, J. U.; Wolf, H. C.; Kremer, R. K.; Metzenthin, T.; Bau, R.; Khan, S. I.; Lindbaum, A.; Lengauer, C. L.; Tillmanns, E. *J. Am. Chem. Soc.* **1993**, *115*, 7696-7705.

(191) Aumüller, A.; Erk, P.; Klebe, G.; Hünig, S.; von Schütz, J. U.; Werner, H.-P. *Angew. Chem., Int. Ed. Engl.* **1986**, *25*, 740-741.

(192) Coronado, E.; Galan-Mascaros, J. R.; Gomez-Garcia, C. J.; Laukhin, V. *Nature* **2000**, *408*, 447-449.

(193) Hünig, S.; Kemmer, M.; Meixner, H.; Sinzger, K.; Wenner, H.; Bauer, T.; Tillmanns, E.; Lux, F. R.; Hollstein, M.; Groβ, H.-G.; Langohr, U.; Werner, H.-P.; von Schütz, J. U.; Wolf, H.-C. *Eur. J. Inorg. Chem.* **1999**, 899-916.

(194) Kato, R.; Kobayashi, H.; Kobayashi, A. *J. Am. Chem. Soc.* **1989**, *111*, 5224-5232.

(195) Garcia, Y.; van Koningsbruggen, P. J.; Codjovi, E.; Lapouyade, R.; Kahn, O.; Rabardel, L. *J. Mater. Chem.* **1997**, *7*, 857-858.

(196) van Koningsbruggen, P. J.; Garcia, Y.; Codjovi, E.; Lapouyade, R.; Kahn, O.; Fournès, L.; Rabardel, L. *J. Mater. Chem.* **1997**, *7*, 2069-2075.

(197) Moliner, N.; Muñoz, M. C.; Létard, S.; Salmon, L.; Tuchagues, J.-P.; Bousseksou, A.; Real, J. A. *Inorg. Chem.* **2002**, *41*, 6997-7005.

(198) Ozarowski, A.; Shunzhong, Y.; McGarvey, B. R.; Mislankar, A.; Drake, J. E. *Inorg. Chem.* **1991**, *30*, 3167-3174.

(199) Reger, D. L.; Little, C. A.; Rheingold, A. L.; Lam, M.; Concolino, T.; Mohan, A.; Long, G. J. *Inorg. Chem.* **2000**, *39*, 4674-4675.

(200) Garcia, Y.; Kahn, O.; Rabardel, L.; Chansou, B.; Salmon, L.; Tuchagues, J. P. *Inorg. Chem.* **1999**, *38*, 4663-4670.

(201) Gütlich, P.; Hauser, A.; Spiering, H. *Angew. Chem., Int. Ed. Engl.* **1994**, *33*, 2024-2054.

(202) Kahn, O.; Martinez, C. J. *Science* **1998**, *279*, 44-48.

(203) Niel, V.; Martinez-Agudo, J. M.; Muñoz, M. C.; Gaspar, A. B.; Real, J. A. *Inorg. Chem.* **2001**, *40*, 3838-3839.

(204) Real, J. A.; Andrés, E.; Muñoz, M. C.; Julve, M.; Granier, T.; Bousseksou, A.; Varret, F. *Science* **1995**, *268*, 265-267.

(205) Vreugdenhil, W.; van Diemen, J. H.; de Graaff, R. A. G.; Haasnoot, J. G.; Reedijk, J.; van der Kraan, A. M.; Kahn, O.; Zarembowitch, J. *Polyhedron* **1990**, *9*, 2971-2979.

(206) Kitagawa, S.; Kitaura, R. *Comments Inorg. Chem.* **2002**, *23*, 101-126.

(207) Yaghi, O. M.; Li, H.; Davis, C.; Richardson, D.; Groy, T. L. *Acc. Chem. Res.* **1998**, *31*, 474-484.

(208) Ayyappan, P.; Evans, O. R.; Cui, Y.; Wheeler, K. A.; Lin, W. *Inorg. Chem.* **2002**, *41*, 4978-4980.

(209) Hou, H.; Wei, Y.; Fan, Y.; Du, C.; Zhu, Y.; Song, Y.; Niu, Y.; Xin, X. *Inorg. Chim. Acta* **2001**, *319*, 212-218.

(210) Hou, H.; Song, Y.; Fan, Y.; Zhang, L.; Du, C.; Zhu, Y. *Inorg. Chim. Acta* **2001**, *316*, 140-144.

(211) Hou, H.; Meng, X.; Song, Y.; Fan, Y.; Zhu, Y.; Lu, H.; Du, C.; Shao, W. *Inorg. Chem.* **2002**, *41*, 4068-4075.

(212) Hou, H.; Wei, Y.; Song, Y.; Zhu, Y.; Li, L.; Fan, Y. *J. Mater. Chem.* **2002**, *12*, 838-843.

(213) Huang, S. D.; Xiong, R.-G. *Polyhedron* **1997**, *16*, 3929-3939.

(214) Huang, S. D.; Xiong, R.-G.; Han, J.; Weiner, B. R. *Inorg. Chim. Acta* **1999**, *294*, 95-98.

(215) Janiak, C.; Scharmann, T. G.; Albrecht, P.; Marlow, F.; Macdonald, R. *J. Am. Chem. Soc.* **1996**, *118*, 6307-6308.

(216) Xiong, R.-G.; Xue, X.; Zhao, H.; You, X.-Z.; Abrahams, B. F.; Xue, Z. *Angew. Chem., Int. Ed. Engl.* **2002**, *41*, 3800-3803.

(217) Kisida, H.; Matsuzaki, H.; Okamoto, H.; Manabe, T.; Yamashita, M.; Taguchi, Y.; Tokura, Y. *Nature* **2000**, *405*, 929-932.

(218) Kondo, M.; Yoshitomi, T.; Seki, K.; Matsuzaka, H.; Kitagawa, S. *Angew. Chem., Int. Ed. Engl.* **1997**, *36*, 1725-1727.

(219) Li, H.; Eddaoudi, M.; O'Keeffe, M.; Yaghi, O. M. *Nature* **1999**, *402*, 276-279.

(220) Hoskins, B. F.; Robson, R. *J. Am. Chem. Soc.* **1990**, *112*, 1546-1554.

(221) Li, D.; Kaneko, K. *Chem. Phys. Lett.* **2001**, *335*, 50-56.

(222) Venkataraman, D.; Gardner, G. B.; Lee, S.; Moore, J. S. *J. Am. Chem. Soc.* **1995**, *117*, 11600-11601.

(223) Min, K. S.; Suh, M. P. *J. Am. Chem. Soc.* **2000**, *122*, 6834-6840.

(224) Fujita, M.; Kwon, Y. J.; Washizu, S.; Ogura, K. *J. Am. Chem. Soc.* **1994**, *116*, 1151-1152.

(225) Kondo, M.; Okubo, T.; Asami, A.; Noro, S.; Yoshitomi, T.; Kitagawa, S.; Ishii, T.; Matsuzaka, H.; Seki, K. *Angew. Chem., Int. Ed. Engl.* **1999**, *38*, 140-143.

(226) Chen, B.; Eddaoudi, M.; Hyde, S. T.; O'Keeffe, M.; Yaghi, O. M. *Science* **2001**, *291*, 1021-1023.

(227) Eddaoudi, M.; Li, H.; Yaghi, O. M. *J. Am. Chem. Soc.* **2000**, *122*, 1391-1397.

(228) Chen, B.; Eddaoudi, M.; Reineke, T. M.; Kampf, J. W.; O'Keeffe, M.; Yaghi, O. M. *J. Am. Chem. Soc.* **2000**, *122*, 11559-11560.

(229) Li, H.; Eddaoudi, M.; Groy, T. L.; Yaghi, O. M. *J. Am. Chem. Soc.* **1998**, *120*, 8571-8572.

(230) Mori, W.; Hoshino, H.; Nishimoto, Y.; Takamizawa, S. *Chem. Lett.* **1999**, 331-332.

(231) Mori, W.; Inoue, F.; Yoshida, K.; Nakayama, H.; Takamizawa, S.; Kishita, M. *Chem. Lett.* **1997**, 1219-1220.

(232) Seki, K. *Phys. Chem. Chem. Phys.* **2002**, *4*, 1968-1971.

(233) Seki, K.; Mori, W. *J. Phys. Chem. B* **2002**, *106*, 1380-1385.

(234) Seki, K.; Takamizawa, S.; Mori, W. *Chem. Lett.* **2001**, 122-123.

(235) Seki, K.; Takamizawa, S.; Mori, W. *Chem. Lett.* **2001**, 332-333.

(236) Seki, K. *Chem. Commun.* **2001**, 1496-1497.

(237) Barthelet, K.; Marrot, J.; Riou, D.; Férey, G. *Angew. Chem., Int. Ed. Engl.* **2002**, *41*, 281-284.

(238) Li, D.; Kaneko, K. *J. Phys. Chem. B* **2000**, *104*, 8940-8945.

(239) Nukada, R.; Mori, W.; Takamizawa, S.; Mikuriya, M.; Handa, M.; Naono, H. *Chem. Lett.* **1999**, 367-368.

(240) Takamizawa, S.; Mori, W.; Furihata, M.; Takeda, S.; Yamaguchi, K. *Inorg. Chim. Acta* **1998**, *283*, 268-274.

(241) Chui, S. S.-Y.; Lo, S. M.-F.; Charmant, J. P. H.; Orpen, A. G.; Williams, I. D. *Science* **1999**, *283*, 1148-1150.

(242) Soldatov, D. V.; Ripmeester, J. A. *Chem. Mater.* **2000**, *12*, 1827-1839.

(243) Tabares, L. C.; Navarro, J. A. R.; Salas, J. M. *J. Am. Chem. Soc.* **2001**, *123*, 383-387.

(244) Blake, A. J.; Hill, S. J.; Hubberstey, P.; Li, W. S. *J. Chem. Soc., Dalton Trans.* **1997**, 913-914.

(245) Uemura, K.; Kitagawa, S.; Kondo, M.; Fukui, K.; Kitaura, R.; Chang, H.-C.; Mizutani, T. *Chem. Eur. J.* **2002**, *8*, 3587-3600.

(246) Li, H.; Davis, C. E.; Groy, T. L.; Kelley, D. G.; Yaghi, O. M. *J. Am. Chem. Soc.* **1998**, *120*, 2186-2187.

(247) Jung, O.-S.; Kim, Y. J.; Lee, Y.-A.; Park, J. K.; Chae, H. K. *J. Am. Chem. Soc.* **2000**, *122*, 9921-9925.

(248) Beauvais, L. G.; Shores, M. P.; Long, J. R. *J. Am. Chem. Soc.* **2000**, *122*, 2763-2772.

(249) Kitaura, R.; Fujimoto, K.; Noro, S.; Kondo, M.; Kitagawa, S. *Angew. Chem., Int. Ed. Engl.* **2002**, *41*, 133-135.

(250) Gardner, G. B.; Kiang, Y.-H.; Lee, S.; Asgaonkar, A.; Venkataraman, D. *J. Am. Chem. Soc.* **1996**, *118*, 6946-6953.

(251) Manakov, A. Y.; Soldatov, D. V.; Ripmeester, J. A.; Lipkowski, J. *J. Phys. Chem. B* **2000**, *104*, 12111-12118.

(252) Carlucci, L.; Ciani, G.; Moret, M.; Proserpio, D. M.; Rizzato, S. *Angew. Chem., Int. Ed. Engl.* **2000**, *39*, 1506-1510.

(253) Edgar, M.; Mitchell, R.; Slawin, A. M. Z.; Lightfoot, P.; Wright, P. A. *Chem. Eur. J.* **2001**, *7*, 5168-5175.

(254) Forster, P. M.; Cheetham, A. K. *Angew. Chem., Int. Ed. Engl.* **2001**, *41*, 457-459.

(255) Yaghi, O. M.; Li, H.; Groy, T. L. *J. Am. Chem. Soc.* **1996**, *118*, 9096-9101.

(256) Yaghi, O. M.; Li, G.; Li, H. *Nature* **1995**, *378*, 703-706.

(257) Sawaki, T.; Dewa, T.; Aoyama, Y. *J. Am. Chem. Soc.* **1998**, *120*, 8539-8640.

(258) Gardner, G. B.; Venkataraman, D.; Moore, J. S.; Lee, S. *Nature* **1995**, *374*, 792-795.

(259) Lee, E.; Kim, J.; Heo, J.; Whang, D.; Kim, K. *Angew. Chem., Int. Ed. Engl.* **2001**, *40*, 399-402.

(260) Su, X.-C.; Zhu, S.; Lin, H.-K.; Leng, X.-B.; Chen, Y.-T. *J. Chem. Soc., Dalton Trans.* **2001**, 3163-3168.

(261) Yaghi, O. M.; Li, H.; Groy, T. L. *Inorg. Chem.* **1997**, *36*, 4292-4293.

(262) Pan, L.; Woodlock, E. B.; Wang, X.; Lam, K.-C.; Rheingold, A. L. *Chem. Commun.* **2001**, 1762-1763.

(263) Jung, O.-S.; Kim, Y. J.; Lee, Y.-A.; Yoo, K. H. *Chem. Lett.* **2002**, 500-501.

(264) Jung, O.-S.; Kim, Y. J.; Kim, K. M.; Lee, Y.-A. *J. Am. Chem. Soc.* **2002**, *124*, 7906-7907.

(265) Naito, S.; Tanibe, T.; Saito, E.; Miyao, T.; Mori, W. *Chem. Lett.* **2001**, 1178-1179.

(266) Sawaki, T.; Aoyama, Y. *J. Am. Chem. Soc.* **1999**, *121*, 4793-4798.

Part 1

Crystal Engineering of Coordination Polymers

Chapter I

Syntheses and Crystal Structures of Fe(II) Coordination Polymers with azpy and 4,4'-bpy : 2-D Networks Supported by Hydrogen Bond, $\{[Fe(NCS)_2(azpy)(MeOH)_2]\cdot azpy\}_n$ and $\{[Fe(NCS)_2(4,4'\text{-}bpy)(H_2O)_2]\cdot 4,4'\text{-}bpy\}_n$, 2-D Network, $\{[Fe(NCS)_2(azpy)_2]\cdot 3H_2O\}_n$, and 3-D Porous Network, $\{(H_2 4,4'\text{-}bpy)[Fe_3(SO_4)_4(4,4'\text{-}bpy)_3(H_2O)_6]\cdot 10H_2O\}_n$

Abstract: New Fe(II) coordination polymers, $\{[Fe(NCS)_2(azpy)(MeOH)_2]\cdot azpy\}_n$ (**I-1**·2MeOH), $\{[Fe(NCS)_2(4,4'\text{-bpy})(H_2O)_2]\cdot 4,4'\text{-bpy}\}_n$ (**I-2**·$2H_2O$), and $\{[Fe(NCS)_2(azpy)_2]\cdot 3H_2O\}_n$ (**I-3**), have been synthesized and characterized. Both compounds of **I-1**·2MeOH and **I-2**·$2H_2O$ contain two types of bridging ligands; one is coordination-bonding type, directly bridging Fe(II) centers to form a 1-D chain of [Fe(L)] (L = azpy or 4,4'-bpy), while the other links these chains by hydrogen bond between the pyridine nitrogen atom and coordinated MeOH or H_2O molecules, resulting in a 2-D sheet with rectangular grids. No interpenetration occurs in the sheets, which stack with spacer of NCS^- anion in the grid. Crystal structure of **I-3** shows a 2-D layer with rhombic grids, each of which slip to the direction, thus resulting in no channel. Cyclic voltammograms (CV) in the solid state show that **I-1**·2MeOH has single coupled wave at $E_{1/2}$ = -0.66 V, attributable to redox reaction of the hydrogen-bonding azpy. The magnetic susceptibilities were measured from 1.9 to 300 K, indicative of no appreciable magnetic exchange interaction between the adjacent Fe(II) ions.

I-1·2MeOH and **I-2**·$2H_2O$ easily release the coordinated solvent molecules of MeOH and H_2O, respectively, by the heat treatment to form new crystal phases of $[Fe(NCS)_2(azpy)_2]_n$ (**I-1**) and $[Fe(NCS)_2(4,4'\text{-bpy})_2]_n$ (**I-2**), which afford 2-D sheets with square or rhombic grids. Especially, the magnetic property of **I-1** reveals the occurrence of a spin-crossover of the Fe(II) ions, which is in contrast to that of a precursor of **I-1**·2MeOH.

A new sulfate-bridged coordination polymer, $\{(H_2 4,4'\text{-bpy})[Fe_3(SO_4)_4(4,4'\text{-bpy})_3(H_2O)_6]\cdot 10H_2O\}_n$ (**I-4**), was synthesized and crystallographically characterized. This complex shows a novel 3-D *log-cabin* type structure constructed from 1-D $[Fe(4,4'\text{-bpy})(H_2O)_2]_n$ cationic

chain, free protonated 4,4'-bpy, and sulfate dianion. This structure shows microporous channels with dimensions of about 3 Å × 4 Å.

I. 1 Introduction

Square grid type sheets constructed from a metal ion with an octahedral environment and a rod-like bridging ligand are of great interest due to the versatility of the crystal structures, physical properties, and catalytic reactivities.[1-12] Heterogeneous catalysis and spin-crossover behavior were observed in a 2-D porous structure of $[Cd(NO_3)_2(4,4'\text{-bpy})_2]_n$[1] and a perpendicularly interpenetrating network of $[Fe(NCS)_2(bpethe)_2]_n$ (bpethe = 1,2-bis(4-pyridyl)ethene),[10] respectively. As far as sheet structures with bipyridine derivatives are concerned, two types of networks are known (Scheme I.1); type 1 is constructed from only coordination bonds, by which metal ions and ligands are directly linked, while type 2 consists of both coordination bonds for 1-D chains and hydrogen bonds for interchain links. Bridging ligands, pyrazine (pyz),[7,11,12] 4,4'-bpy,[1,3,7-9] and bpethe,[10] afford type 1 structures, whose channel shape is a square or rhombic (if distorted) grid form. On the other hand, type 2, which provides a larger channel size and non-square grid, dissimilar to type 1, has been restricted to the case of a 4,4'-bpy ligand.[2-6] In this chapter, Fe(II) ion as a connector, azpy and 4,4'-bpy ligands as linkers, were chosen for the construction of

Scheme I.1

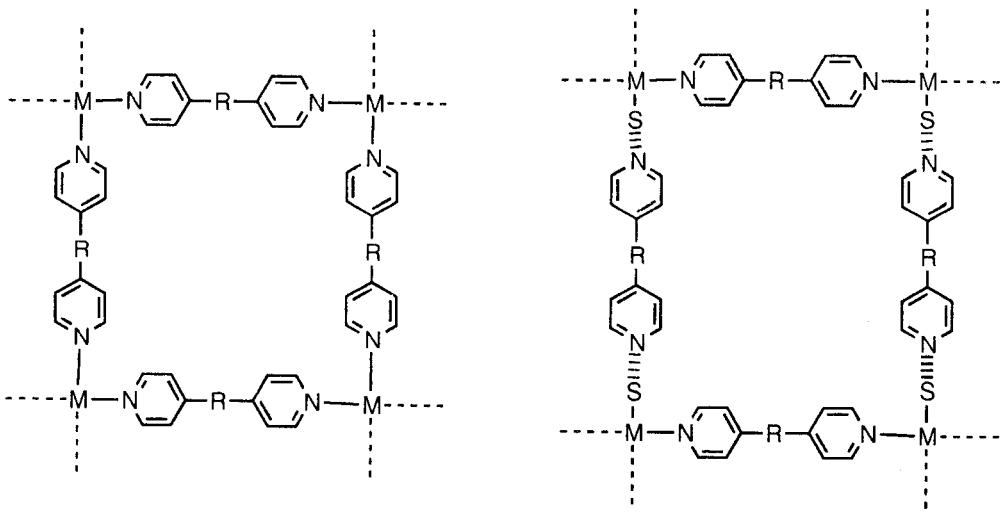

Type 1 Type 2

M = metal ion
R = spacer
S = solvent or anion with hydrogen bonding sites

a new functional coordination network. Especially, azpy ligand gives a longer metal-metal distance than that of 4,4'-bpy, and thus the type 2 coordination polymer affords a larger channel size that those with 4,4'-bpy. Interestingly, azpy has a redox activity,[13] and a redox active coordination network is expected. Described herein is the syntheses, crystal structures, redox properties, and structural conversion of Fe(II) coordination polymers with azpy and 4,4'-bpy as illustrated in Scheme I.2.

Scheme I.2

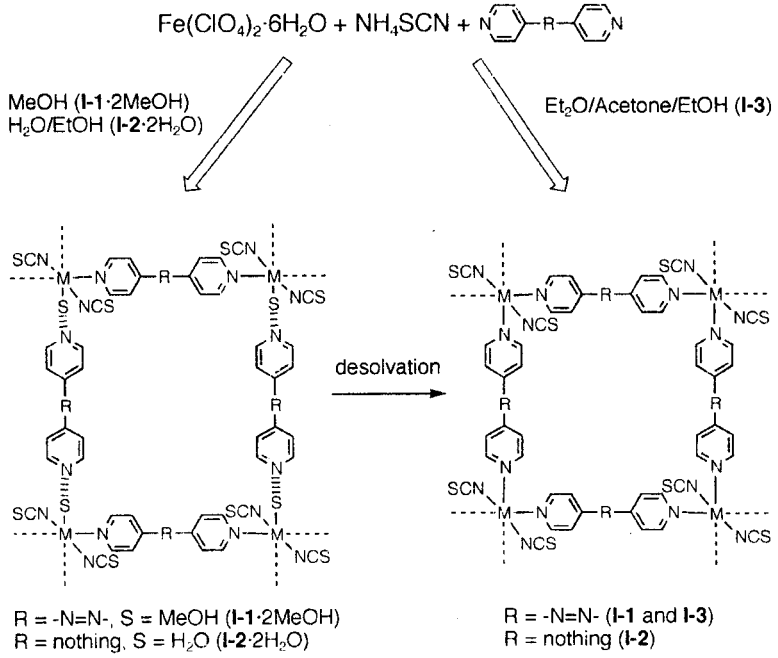

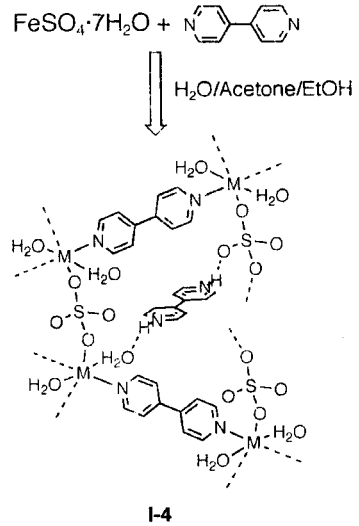

I-4

I. 2 Experimental

I. 2. 1 Physical Measurements

Elemental analyses were taken on Yanaco C,H,N Corder MT-5. IR spectra were recorded on a Hitachi I-5040 FT-IR spectrometer with samples prepared as KBr pellets. X-ray powder diffraction data were collected on a MAC Science MXP21TA-PO by using Cu Kα radiation. Thermal gravimetric analyses (TGA) were carried out with a Seiko Instruments SSC5200 instrument in a nitrogen atmosphere (heating rate: 5 $K \cdot min^{-1}$). .

The cyclic voltammograms (CV) were taken on a BAS CV-50W polarographic analyzer. A SCE electrode was used as a reference. Each bulk sample of compounds **I-1**·2MeOH and **I-3** was added to carbon paste (graphite and mineral oil) and mixed well. By using this mixture a working electrode was prepared; the mixture was set in a cavity on a Teflon rod, connected to a platinum wire. Another platinum wire was used as a counter electrode. Three-electrode systems were carried out in 0.1 $mol \cdot dm^{-3}$ $NaClO_4$ aqueous solution, using a scan rate of 10 $mV \cdot s^{-1}$ in the range from -1.2 to 1.2 V. Magnetic susceptibilities were recorded over the temperature range 1.9-300 K at 0.3 T (**1**·2MeOH and **I-2**·$2H_2O$) and 1 T (**I-1**) with a superconducting quantum interference device (SQUID) susceptometer (Quantum Design, San Diego, CA) interfaced with a HP Vectra computer system. All the values were corrected for diamagnetism that were calculated from Pascal's table.[14]

I. 2. 2 Syntheses

Materials. $Fe(ClO_4)_2 \cdot 6H_2O$ and NH_4SCN were obtained from Aldrich Chemical Co. and Wako Co., respectively. 4,4'-Bpy was purchased from Tokyo Kasei Chemical Co. $FeSO_4 \cdot 7H_2O$ was obtained from Kanto Chemical Co. Azpy was prepared according to the literature method.[15,16]

Synthesis of $\{[Fe(NCS)_2(azpy)(MeOH)_2] \cdot azpy\}_n$ (I-1·2MeOH). A methanol solution (20 mL) of azpy (0.75 g, 4.1 mmol) was added to a methanol solution (40 mL) containing a mixture of $Fe(ClO_4)_2 \cdot 6H_2O$ (0.75 g, 2.1 mmol) and NH_4SCN (0.31 g, 4.0 mmol). The black microcrystals were collected by filtration, washed with methanol, and dried under vacuum for 2 h. Yield: 1.03 g (1.70 mmol, 85 %) Anal. Calcd for $C_{24}H_{24}FeN_{10}O_2S_2$: C, 47.69; H, 4.00; N, 23.17.

Found: C, 48.13; H, 4.09; N, 23.58. IR (KBr pellet): 3063 w, 2996 w, 2937 w, 2876 w, 2830 w, 2732 bm, 2542 m, 2074 s, 1597 s, 1567 m, 1486 w, 1457 w, 1437 w, 1412 s, 1319 w, 1223 m, 1187 w, 1136 w, 1087 w, 1048 m, 1027 m, 1007 m, 954 w, 846 m, 835 m,797 w, 738 w, 569 m, 543 m, 526 m, 476 w cm^{-1}.

After the microcrystals were collected, standing of the filtrate for a few weeks provided single crystals. One of these was used for single X-ray analysis. The homogeneity of the bulk product was confirmed by comparison of the observed and calculated powder diffraction patterns obtained from single crystal data.

Synthesis of $[Fe(NCS)_2(azpy)_2]_n$ (I-1). A desolvated compound **I-1** was obtained by heating **I-1**·2MeOH at 100 °C under vacuum for 5 hours. Anal. Calcd for $C_{22}H_{16}FeN_{10}S_2$: C, 48.90; H, 2.98; N, 25.92. Found: C, 48.19; H, 2.90; N, 25.79. IR (KBr pellet): 3073 w, 2881 w, 2099 w, 2053 s, 1598 m, 1566 m, 1486 w, 1412 m, 1321 w, 1223 m, 1044 w, 1009 w, 841 m, 567 m, 543 w, 528 w cm^{-1}.

Synthesis of $\{[Fe(NCS)_2(4,4'\text{-bpy})(H_2O)_2]\cdot 4,4'\text{-bpy}\}_n$ (I-2·2H$_2$O). An ethanol solution (20 mL) containing 4,4'-bpy (0.64 g, 4.1 mmol) was added to an aqueous solution (20 mL) containing a mixture of $Fe(ClO_4)_2\cdot 6H_2O$ (0.72 g, 2.0 mmol) and NH_4SCN (0.30 g, 3.9 mmol). The red powder was collected by filtration, washed with water and ethanol, and dried under vacuum for 2 h. Yield: 0.78 g (1.50 mmol, 77 %) Anal. Calcd for $C_{22}H_{20}FeN_6O_2S_2$: C, 50.77; H, 3.87; N, 16.15. Found: C, 50.79; H, 3.75; N, 16.05. IR (KBr pellet): 3385 m, 3064 w, 2878 w, 2824 w, 2091 s, 1605 m, 1597 m, 1536 w, 1488 w, 1405 m, 1320 w, 1217 w, 1059 w, 1044 w, 1000 w, 942 w, 854 w, 808 m, 785 w, 729 w, 676 w, 663 w, 629 m, 574 w, 544 w, 471 w cm^{-1}.

Single crystals suitable for X-ray analysis were prepared by the careful diffusion of an ethanol solution of 4,4'-bpy into an aqueous solution containing $Fe(ClO_4)_2\cdot 6H_2O$ and NH_4SCN. The homogeneity of the bulk product was confirmed by comparison of the observed and calculated powder diffraction patterns obtained from single-crystal data.

Synthesis of $[Fe(NCS)_2(4,4'\text{-bpy})_2]_n$ (I-2). A desolvated compound **I-2** was obtained by heating **I-2**·2H$_2$O at 100 °C under vacuum for 5 hours. Anal. Calcd for $C_{22}H_{16}FeN_6S_2$: C, 54.55; H, 3.33; N, 17.35. Found: C, 53.87; H, 3.25; N, 17.26. IR (KBr pellet): 3040 w,

2880 w, 2780 w, 2092 m, 2053 s, 1603 m, 1533 w, 1486 w, 1409 m, 1320 w, 1217 w, 1068 w, 1045 w, 1005 w, 854 w, 807 m, 730 w, 674 w, 663 w, 626 m, 574 w, 485 w cm^{-1}.

Synthesis of $\{[Fe(NCS)_2(azpy)_2]\cdot 3H_2O\}_n$ (I-3). A diethyl ether solution (20 mL) of azpy (0.050 g, 0.27 mmol) was added to a mixture of acetone (10 mL) and ethanol (10 mL) solution containing a mixture of $Fe(ClO_4)_2\cdot 6H_2O$ (0.049 g, 0.14 mmol) and NH_4SCN (0.020 g, 0.27 mmol). The dark purple powder was collected by filtration, washed with diethyl ether, acetone and ethanol, and dried under vacuum for 2 h. Yield: 0.052 g (0.09 mmol, 64 %) Anal. Calcd for $C_{22}H_{22}FeN_{10}O_3S_2$: C, 44.45; H, 3.73; N, 23.56. Found: C, 44.40; H, 3.76; N, 24.30. IR (KBr pellet): 2102 s, 2046 s, 1637 w, 1599 m, 1566 w, 1520 w, 1489 w, 1414 m, 1223 w, 1194 w, 1049 w, 1012 w, 844 m, 569 m, 528 w cm^{-1}.

Synthesis of $\{(H_2$4,4'-bpy$)[Fe_3(SO_4)_4$(4,4'-bpy$)_3(H_2O)_6]\cdot 10H_2O\}_n$ (I-4). An EtOH solution (20 ml) of 4,4'-bpy (312 mg, 2 mmol) was added to a H_2O solution (20 ml) of $FeSO_4\cdot 7H_2O$ (278 mg, 1 mmol). The obtained yellow solution was filtered, and diffusion of acetone in the filtrate gave orange single crystals after a few weeks.

I. 2. 3 X-Ray Structure Determination

Single crystals of **I-1**·2MeOH, **I-2**·$2H_2O$, and **I-4**, were sealed in a glass capillary. A suitable crystal of **I-3** was mounted on a glass fiber and coated with epoxy resin. X-ray data collections were carried out by an oscillation method using a Rigaku RAXIS-IV imaging-plate system on a rotating-anode X-ray generator operated at 50 kV and 100 mA. Laue group and unit-cell parameters were determined by data-processing software (PROCESS) attached to the RAXIS system. Lorentz-polarization corrections were applied. For **I-1**·2MeOH, the structure was solved by a direct method using the SHELXS86 program[17] and expanded using Fourier techniques.[18] For **I-2**·$2H_2O$, **I-3**, and **I-4**, the structure was solved by a direct method using the SIR92 program[19] and expanded using Fourier techniques.[18] In the case of **I-4**, disordered oxygen atoms of one sulfate dianion were refined isotropically and other non-hydrogen atoms were refined anisotropically. The non-hydrogen atoms of other complexes were refined anisotropically. All hydrogen atoms, which were placed in idealized positions, were included but not refined. The refinements were carried out

using full-matrix least squares techniques. Crystal data and details of the structure determinations are summarized in Table I.1. All calculations were performed using the teXsan[20] crystallographic software package of Molecular Structure Corporation.

Table I.1. Crystallographic Data for $\{[Fe(NCS)_2(azpy)(MeOH)_2]\cdot azpy\}_n$ (**I-1**·2MeOH), $\{[Fe(NCS)_2(4,4'\text{-bpy})(H_2O)_2]\cdot 4,4'\text{-bpy}\}_n$ (**I-2**·$2H_2O$), $\{[Fe(NCS)_2(azpy)_2]\cdot 3H_2O\}_n$ (**I-3**), and $\{(4,4'\text{-bpyH}_2)[Fe_3(4,4'\text{-bpy})_3(SO_4)_4(H_2O)_6]\cdot 10H_2O\}_n$ (**I-4**).

compound	**I-1**·2MeOH	**I-2**·$2H_2O$	**I-3**	**I-4**
formula	$C_{24}H_{24}FeN_{10}S_2O_2$	$C_{22}H_{20}FeN_6S_2O_2$	$C_{22}H_{22}FeN_{10}S_2O_3$	$C_{40}H_{66}Fe_3N_8S_4O_{32}$
fw	604.49	520.41	594.45	520.41
crystal color	red	orange	dark red	orange
crystal system	monoclinic	triclinic	monoclinic	triclinic
a, Å	7.232(4)	9.017(1)	17.267(1)	12.000(3)
b, Å	16.960(3)	10.222(1)	13.515(3)	12.611(4)
c, Å	11.950(3)	7.489(1)	14.691(1)	11.526(3)
α, deg		104.318(9)		115.75(2)
β, deg	94.65(3)	96.65(1)	113.684(5)	106.99(2)
γ, deg		107.454(10)		69.34(2)
V, Å^3	1460.9(7)	624.5(2)	3139.5(6)	1449.9(8)
space group	$P2_1/c$ (No.14)	$P\bar{1}$ (No.2)	$C2/c$ (No.15)	$P\bar{1}$ (No.2)
Z	2	1	4	1
ρ(calcd), g·cm^{-3}	1.374	1.384	1.258	1.680
F(000)	624.00	268.00	1224.00	760.00
μ(Mo Kα), cm^{-1}	6.99	8.00	6.51	9.85
diffractometer	RAXIS-IV	RAXIS-IV	RAXIS-IV	RAXIS-IV
radiation (γ, Å)	0.71069	0.71069	0.71069	0.71069
temp., °C	23	23	-20	22
GOF	1.423	2.036	3.914	2.375
no. of obsd data	1168 ($I > 2.50\sigma(I)$)	1580 ($I > 3.00\sigma(I)$)	2323 ($I > 3.00\sigma(I)$)	2706 ($I > 3.00\sigma(I)$)
no. of variables	179	152	184	410
R[a]	0.0634	0.0467	0.0623	0.0775
R_w[b]	0.0638	0.0541	0.0833	0.0970

[a] $R = \Sigma\||Fo| - |Fc|\|/\Sigma|Fo|$. [b] $R_w = [(\Sigma w\,(|Fo| - |Fc|)^2/\Sigma wFo^2)]^{1/2}$.

I. 3 Results and Discussion

I. 3. 1 Crystal Structures

I. 3. 1. 1 Crystal Structures of $\{[Fe(NCS)_2(azpy)(MeOH)_2]\cdot azpy\}_n$ (I-1·2MeOH) and $\{[Fe(NCS)_2(4,4'\text{-bpy})(H_2O)_2]\cdot 4,4'\text{-bpy}\}_n$ (I-2·2H$_2$O)

An ORTEP view around the Fe(II) center of **I-1**·2MeOH is shown in Figure I.1(a) with numbering scheme, where the metal sites are on crystallographic inversion centers. The Fe(II) has a distorted elongated octahedral environment with two thiocyanate nitrogen donors and two methanol molecules in the basal plane, and two pyridine nitrogen donors in the axial sites. The *trans* N-Fe-N (NCS), N-Fe-N (py), and O-Fe-O bond angles are crystallographically 180 °. On the other hand, *cis* N-Fe-O and N-Fe-N bond angles range from 85.9(2) ° to 91.1(3) °, indicative of a distorted octahedral environment. The NCS ligands are coordinated to the Fe(II) atom in a bent fashion with the angle Fe(1)-N(5)-C(11) of 169.8(7) °. The NCS ligand itself is almost linear, N(5)-C(11)-S(1) 177.9(8) °. The Fe(1)-O(1)-C(12) (CH_3OH) bond angle is 129.0(5) °.

All azpy ligands show a *trans* form. There are two types of association for the azpy molecules in the crystal. One is a coordination type, which shows direct bridging between the Fe centers to form Fe-azpy-Fe chains (Figure I.1(b)) with the Fe•••Fe separation of 13.46 Å. The other is a hydrogen bonding type and bridges the coordinated CH_3OH molecules in the nearest neighbor chains to form a Fe-($HOCH_3$)-azpy-(CH_3OH)-Fe link [$O(CH_3OH)$-N(py) = 2.685(9) Å]. The interchain distance of the Fe•••Fe pair is 16.96 Å. The chain of Fe-($HOCH_3$)-azpy-(CH_3OH)-Fe affords a 2-D structure having rectangular grids (Figure I.1(c)).

The structure of compound **I-2**·2H$_2$O is similar to that of analogs of cobalt and manganese with type 2 framework.[2,3] An ORTEP view around the Fe(II) center of **I-2**·2H$_2$O is shown in Figure I.2(a) with a numbering scheme, where the metal sites are on crystallographic inversion centers. The Fe(II) has an elongated octahedral environment with two thiocyanate nitrogen donors and two water ligands in the equatorial positions, and two pyridine nitrogen donors in the axial positions. The Fe-N (py), Fe-N (NCS) and Fe-O bond distances [2.216(3), 2.134(4), and 2.135(4) Å, respectively] are shorter than those of the manganese compound (average 2.278, 2.175 and 2.198 Å,

respectively)[2] and longer than those of the cobalt compound [2.162(2), 2.095(2), and 2.096(2) Å, respectively][3]. These results are expected from the metal ion radii (Mn^{2+}, 0.970; Fe^{2+}, 0.920; and Co^{2+}, 0.885 Å). There are two types of association modes for the 4,4'-bpy ligand in the crystal as in **I-1**·2MeOH. One is a coordination bridge between the Fe(II) centers to form linear Fe-(4,4'-bpy)-Fe chains (Figure I.2(b)). The other is a hydrogen-bonding type and bridges the coordinated H_2O molecules in the nearest neighbor chains. The sheet also shows a stepwise 2-D structure of rectangular grids as shown in Figure I.2(c).

Both compounds **I-1**·2MeOH and **I-2**·$2H_2O$ afford a sheet composed of rectangular-shaped grids with dimensions of *ca.* 13.5 Å x 17.0 Å and *ca.* 11.5 Å x 15.8 Å, respectively. These grids are larger than those of type 1 of coordination polymers solely coordinated by 4,4'-bpy (*ca.* 11.5 Å x 11.5 Å).[1,3,8] Coordination polymers with 4,4'-bpy showing type 2 structure[2-6] have a grid shape (rectangular) and size (*ca.* 11.5 Å x 15.8 Å), similar to that of **I-2**·$2H_2O$. Complex **I-1**·2MeOH also forms a 2-D structure having rectangular-type grid (Figure I.1(c)). The grids defined by four Fe centers in the sheet have a size of *ca.* 13.5 Å x 17.0 Å, which is larger than those of **I-2**·$2H_2O$ and the coordination polymers having similar type 2 structure (*ca.* 11.5 Å x 15.8 Å).[2-6] Complex **I-1**·2MeOH is the first example in which methanol molecules are involved in hydrogen-bonding links instead of water molecules for a type 2 structure. It is to be noted that **I-1**·2MeOH and **I-2**·$2H_2O$ show non-interpenetrating networks regardless of the presence of the large grids, probably because each grid in a layer is occupied by a NCS anion provided by the adjacent layer. A similar structural aspect has been found for the 4,4'-bpy complex $\{[Cu(BF_4)_2(4,4'\text{-bpy})(H_2O)_2]\cdot 4,4'\text{-bpy}\}_n$.[5]

The crystal structure of compound **I-1**·2MeOH is comprised of two types of sheets, which are related to each other by the glide plane symmetry, leading to alternative stacks of these different sheets as demonstrated in Figure I.3(a). The two pyridine rings of the azpy ligands are constrained by the symmetry of the crystal to be coplanar, and alternate π stacks for A and B types of the azpy ligand are obtained, the separation being about 3.29 Å. The Fe(II) in an adjacent layer lies above or below the center of the rectangular-type grid. The shortest Fe•••Fe separation between the nearest-neighbor sheets is 10.37 Å. In **I-2**·$2H_2O$ there is only one type of sheet in the crystal as shown in Figure I.3(b). The two pyridine rings of 4,4'-bpy ligands are constrained by the symmetry of the

crystal to be coplanar, and alternate π stacks for A and B types of the 4,4'-bpy ligand are obtained, the separation being about 3.43 Å. The Fe(II) in an adjacent layer lies above or below the center of this rectangle. The shortest Fe•••Fe separation between the sheets is 9.07 Å. A similar stacking form of the sheet is found in $\{[Cu(BF_4)_2(4,4'\text{-bpy})(H_2O)_2]\cdot 4,4'\text{-bpy}\}_n$.[5] In the network of **I-2**·$2H_2O$, coordinated (A) and hydrogen-bonded (B) 4,4'-bpy ligands in the sheet are arranged in a parallel fashion, while the molecular plane of the corresponding azpy ligands of **I-1**·2MeOH show a dihedral angle of 26°.

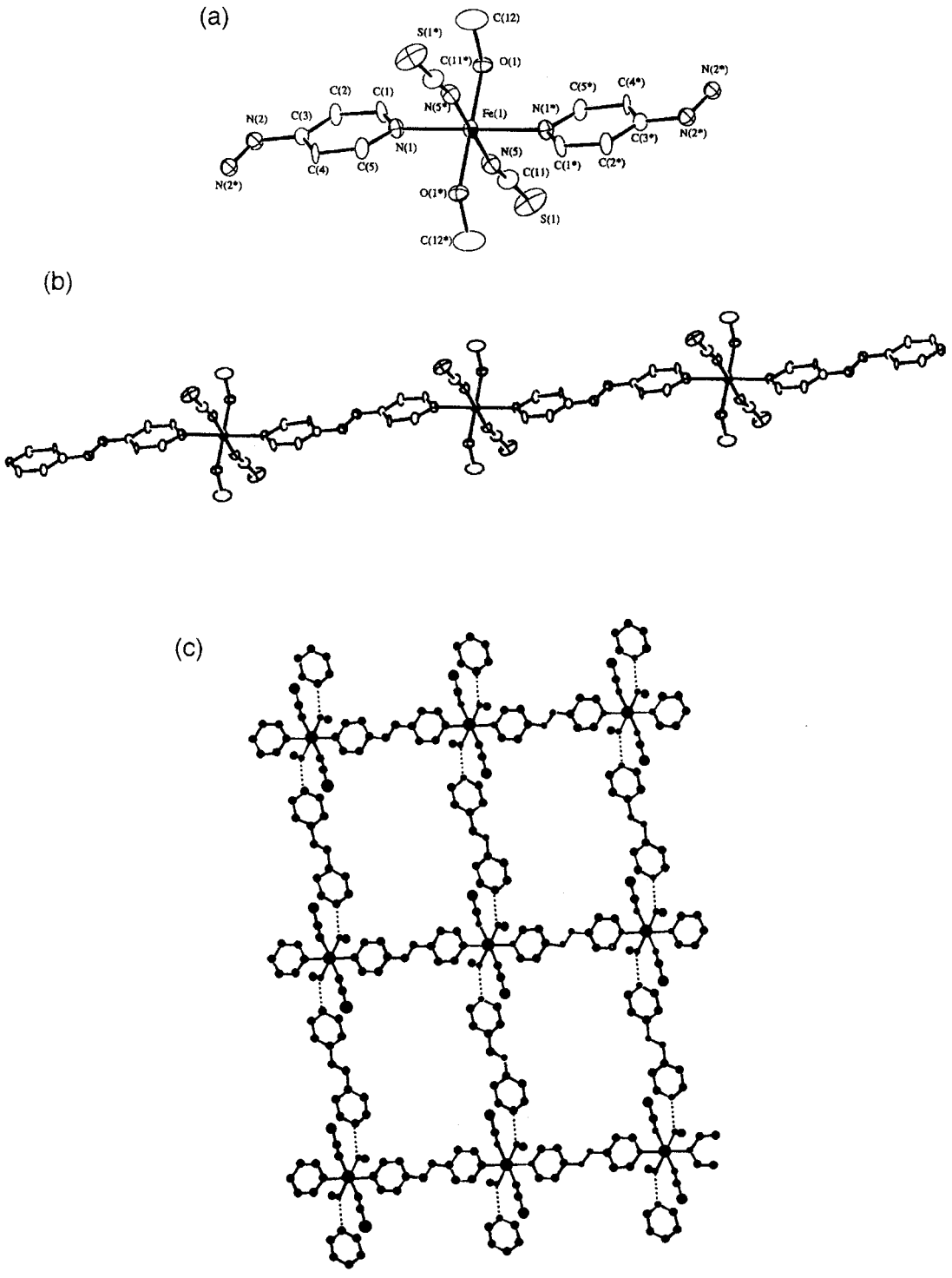

Figure I. 1. (a) ORTEP drawing around a Fe(II) center of **I-1**·2MeOH at the 30 % probability level. In regard to all figures, the hydrogen atoms are omitted for clarity. (b) ORTEP view of a 1-D chain structure of **I-1**·2MeOH at the 30 % probability level. (c) View of a 2-D network with rectangular grids of **I-1**·2MeOH.

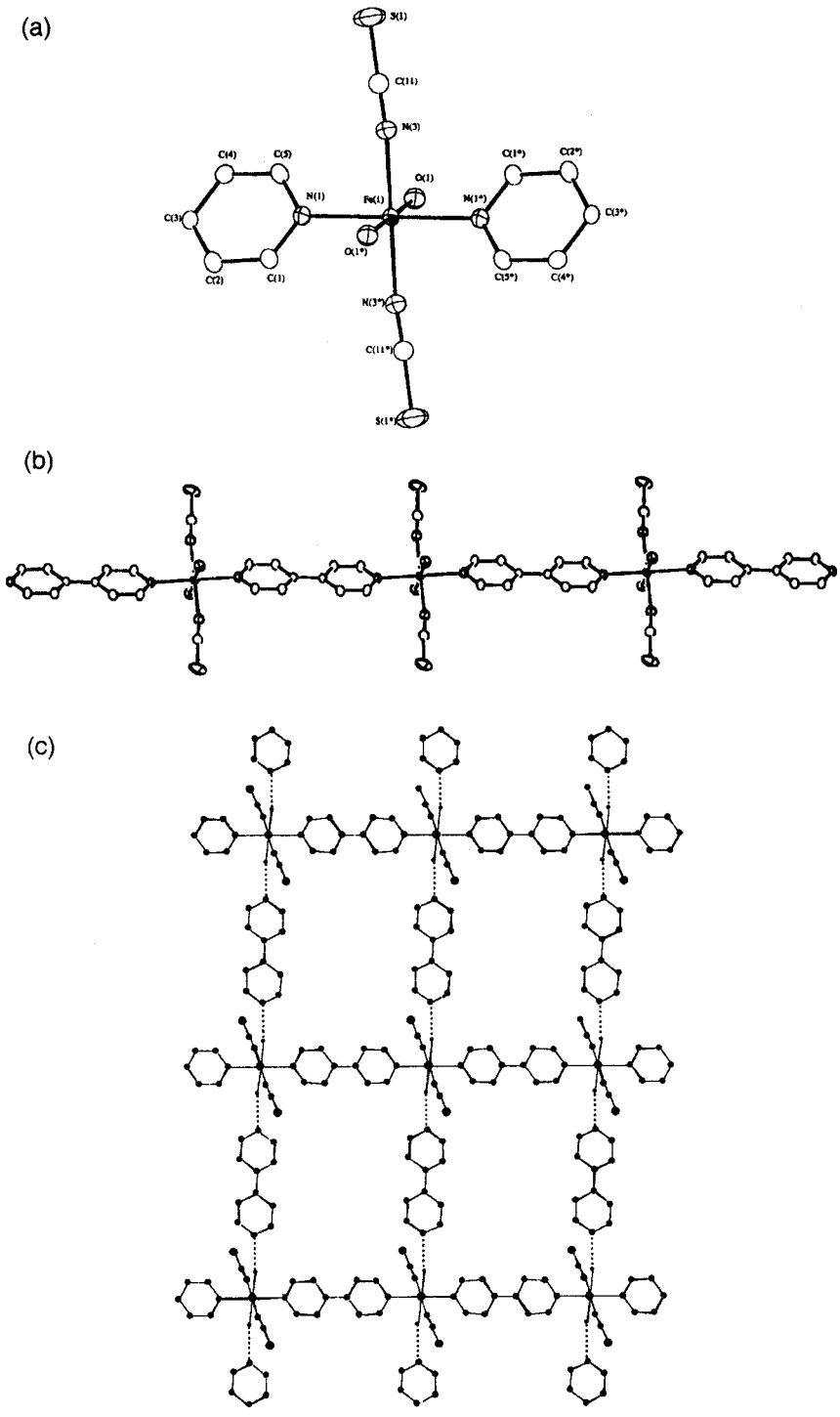

Figure I.2. (a) ORTEP drawing around a Fe(II) center of **I-2**·2H_2O at the 30 % probability level. (b) ORTEP view of a 1-D chain structure of **I-2**·2H_2O at the 30 % probability level. (c) View of a 2-D network with rectangular grids of **I-2**·2H_2O.

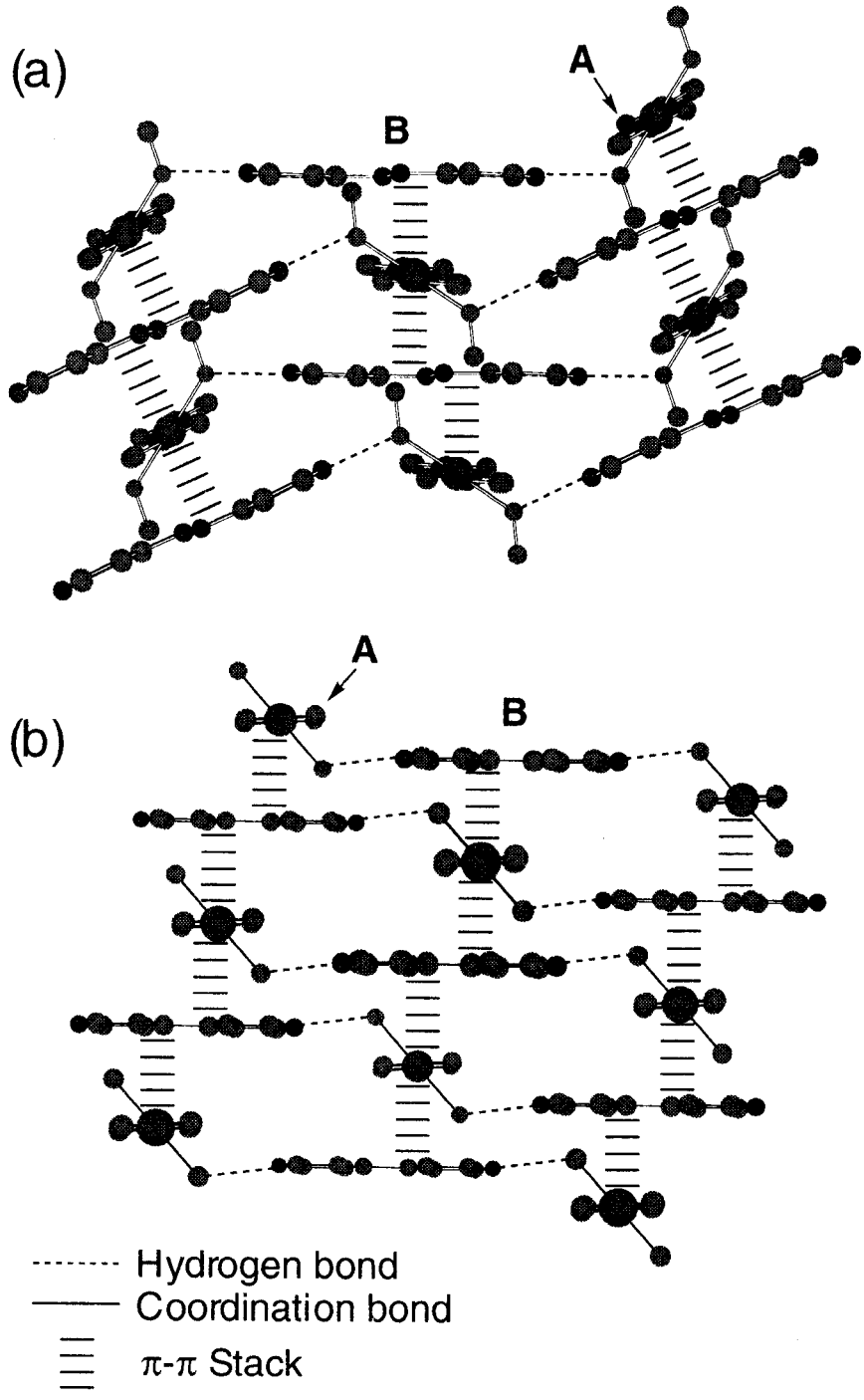

Figure I.3. View of the stacking forms of the sheets in (a) **I-1**·2MeOH and (b) **I-2**·2H_2O; the NCS anions are omitted for clarity.

I. 3. 1. 2 Crystal Structure of $\{[Fe(NCS)_2(azpy)_2]\cdot 3H_2O\}_n$ (I-3)

An ORTEP view around the Fe(II) center of **I-3** is shown in Figure I.4(a) with numbering scheme. The Fe(II) has a distorted elongated octahedral environment with four pyridine nitrogen donors in the basal plane, and two thiocyanate nitrogen donors in the axial sites. The *trans* N-Fe-N bond angles are 173.1(2), 174.3(2), and 180 °, and the *cis* N-Fe-N bond angles range from 86.5(1) ° to 93.5(1) °, indicative of a distorted octahedral environment. The NCS ligands are coordinated to the Fe(II) atom in a more bent fashion with the angle Fe(1)-N(5)-C(11) of 159.3(4) ° than those of **I-1**·2MeOH and **I-2**·$2H_2O$ because of steric repulsion in the Fe(II) center. The NCS ligand itself is almost linear, N(5)-C(11)-S(1) 178.6(5) °.

All azpy ligands show a *trans* form. There are only one type of association for the azpy ligand in the crystal. It is a coordination type, which shows direct bridging between the Fe(II) centers to form 2-D *rhombus*-type sheets with corner angles of about 99 ° and 88 °(Figure I.4(b)). The Fe•••Fe separations in the sheet are *ca.* 13.52 and 13.57 Å. These sheets, which have large grids (*ca.* 10 Å x 10 Å), stack without interpenetration as shown in Figure I.4(c), the distance between adjacent sheets being about 4.8 Å. Because the mutual sheets slip to the direction, thus resulting in no channel. Each grid in a layer is occupied by a NCS anion provided by the adjacent layer. No interaction between these sheets is observed. The Fe(II) in an adjacent layer lies above or below the center of this rhombic grid. The shortest Fe•••Fe separation between the sheets is *ca.* 8.66 Å. In the crystal, two kinds of azpy ligands are observed. One is a disordered azpy ligand A, and the other is a ordered azpy ligand B. Each pyridine ring of azpy A, in which N=N group is disordered, is twisted by a dihedral angle of *ca.* 61 °. On the other hand, each pyridine ring of azpy B is almost coplanar. Previously, a similar coordination polymer has been reported,[10] in which $\{[Fe(NCS)_2(bpethe)_2]\cdot MeOH\}_n$ makes a same 2-D rhombic sheet. In comparison with **I-3**, these 2-D sheets take perpendicularly interpenetrating structure.

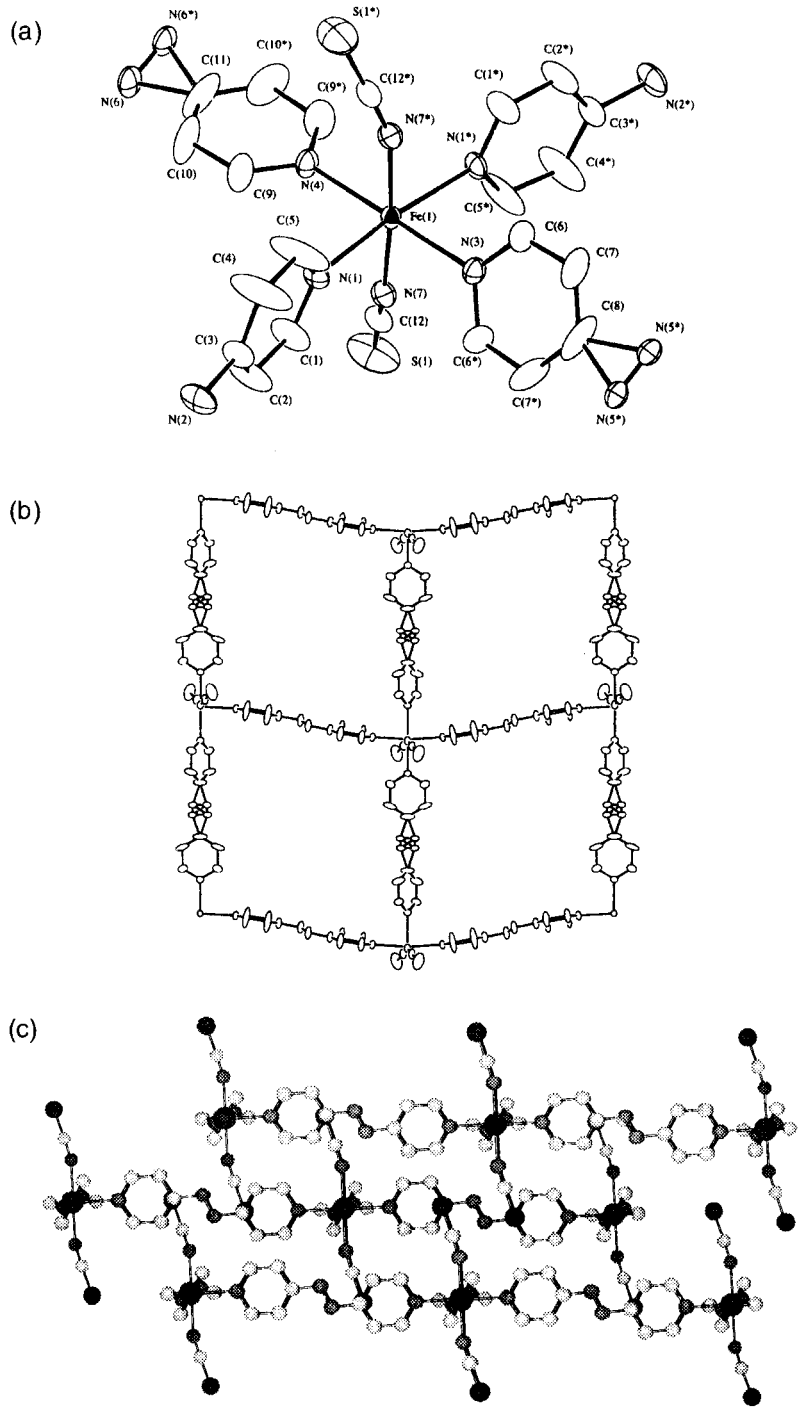

Figure I.4. (a) ORTEP drawing around a Fe(II) center of **I-3** at the 30 % probability level. (b) ORTEP view of a 2-D structure of **I-3** at the 30 % probability level. (c) View of a stacking form of 2-D sheets of **I-3**.

I. 3. 1. 3 Crystal Structure of $\{(H_2$4,4'-bpy$)[Fe_3(SO_4)_4($4,4'-bpy$)_3(H_2O)_6]\cdot 10H_2O\}_n$ (I-4)

The compound **I-4** consists of the 1-D chain of $[Fe(4,4'\text{-bpy})(H_2O)_2]_n$, protonated 4,4'-bpy, and sulfate dianion. The aspect of sulfate-linking is shown in Figures I.5(a) and I.5(b). In the crystal, there are three independent Fe(II) atoms, which sit on the crystallographically inversion center. Each Fe(II) center, which has a similar coordination environment, is based on a distorted octahedron with two pyridine nitrogen donors (Fe-N = av. 2.194 Å), two sulfate oxygen donors (Fe-O = av. 2.136 Å), and two water molecules (Fe-O = av. 2.135 Å). Each ligand occupies a *trans* position, and the *trans* N-Fe-N and O-Fe-O bond angles are crystallographically linear. The *cis* N-Fe-O and O-Fe-O bond angles are slightly deviated from 90 ° (range from 84.4 to 90.4 °). Two pyridine rings of each 4,4'-bpy ligand are co-planar.

The crystal structure affords 3-D neutral framework. In the crystal, the two types of layers (A and B) are formed as shown in Figure I.5(c). Type A layer consists of only linear $[Fe(4,4'\text{-bpy})(H_2O)_2]_n$ cationic chains. On the other hand, type B layer consists of linear $[Fe(4,4'\text{-bpy})(H_2O)_2]_n$ cationic chains, which run parallel along the *c*-axis, and protonated 4,4'-bpy. The directions of these two types of chains are mutually oriented at 53 °. Both A and B layers are perpendicular to the *ab*-plane, and alternately stack as shown in Figure I.5(b).

Sulfate dianion shows an important role for the construction of the 3-D neutral network. The 1-D chains in the A and the adjacent B layers are linked by coordination bond of sulfate bridges (see Figures I.5(a) and I.5(b)). In addition to this, the sulfate dianion of the 1-D chains in the A layer is hydrogen bonded to both the coordinating water molecule in the next A layer and protonated 4,4'-bpy in the adjacent B layer; the O (SO_4) - O (H_2O) and O (SO_4) - N ($H_2$4,4'-bpy) distances are 2.71 and 2.67 Å as shown in Figure I.5(d). As a result, 3-D neutral framework is built up. This unique structure is described as *log-cabin* type network (Figure I.5(d)). In the 3-D network, parallel π-π interaction (*ca.* 3.4 Å) is observed between 4,4'-bpy molecules in the adjacent layers.

The framework of this complex creates the channels along the (a - b) vector with dimensions of about 3 Å × 4 Å. The aspect is illustrated in Figure I.5(e). These channels are occupied with

crystallized water molecules, which are hydrogen bonded to the sulfate oxygen atoms (O-O = *ca.* 2.9 Å) and coordinated water oxygen atoms (O-O = *ca.* 2.8 Å).

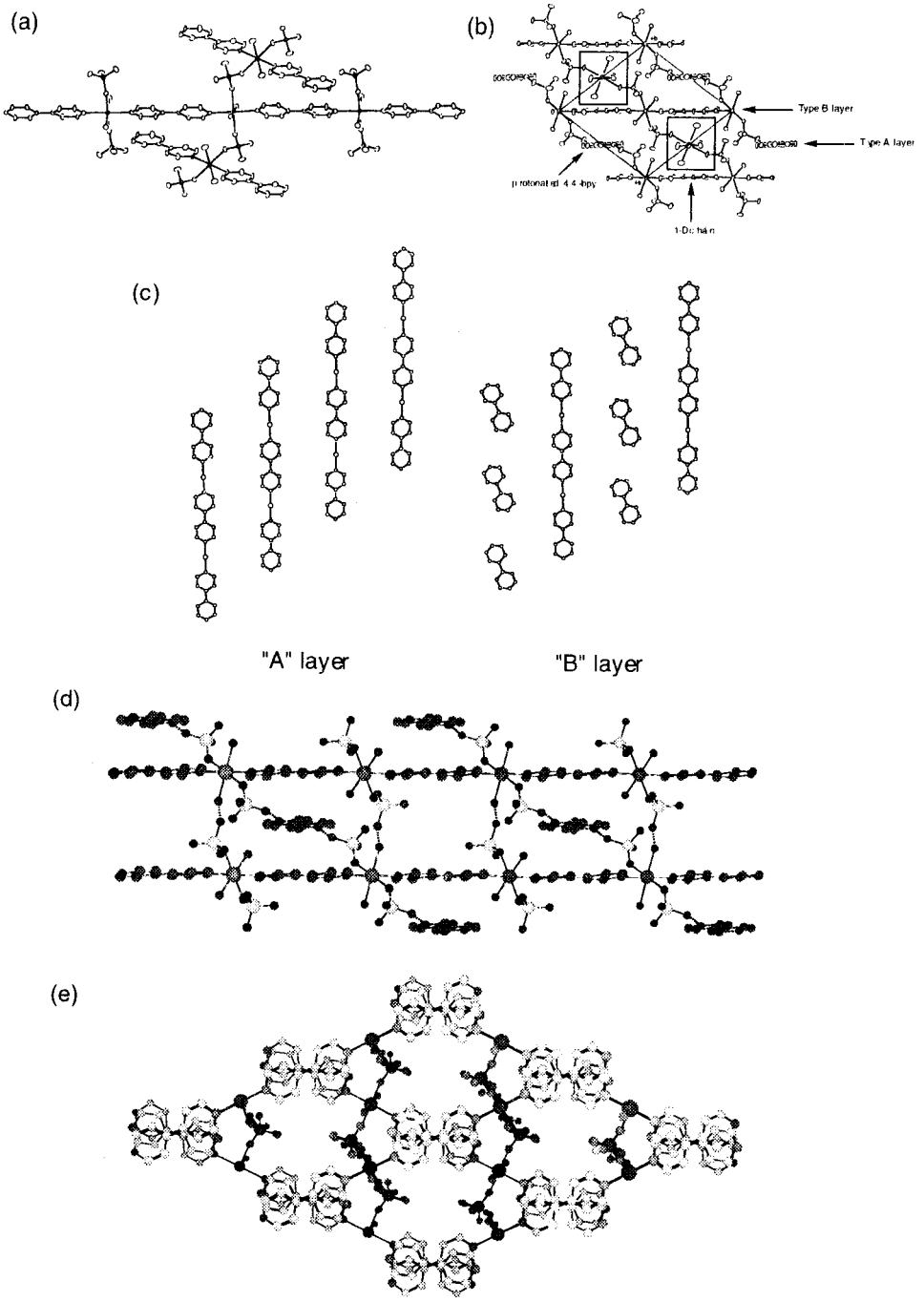

Figure I.5. (a) ORTEP view of the $[Fe(SO_4)]_n$ undulating chain that serves to interconnect $[Fe(4,4'\text{-bpy})]_n$ linear chains of **I-4**. (b) ORTEP view of the crystal cell of **I-4** along the *c*-axis. (c) Structural aspects of two types of layers of **I-4**; the coordinated sulfate dianion and H_2O are omitted for clarity. (d) A view of the *log-cabin* type structure of **I-4**. (e) A space-filling model of *log-cabin* type structure of **I-4**, indicating the small channel structure.

I. 3. 2 Magnetic and Thermal Properties

The magnetic susceptibilities of compounds **I-1**·2MeOH and **I-2**·2H_2O as a function of temperature (1.9-300 K) were measured. As shown in Figure I.6, the temperature dependence of the magnetic susceptibilities obeys Curie-Weiss law: $\chi_M = C/(T-\theta)$ (C = 3.11 emu·K·mol^{-1} and θ = 0 K in **I-1**·2MeOH, C = 2.62 emu·K·mol^{-1} and θ = 0 K in **I-2**·2H_2O). Thus, there is practically no magnetic interaction between the neighboring Fe(II) ions through the azpy or 4,4'-bpy bridges. A weak temperature dependence at low temperature of $\chi_M T$ is observed for both complexes due to the combined effect of spin-orbit coupling and axial distortion of the Fe(II) atom, exhibiting maxima at about 28 and 15 K for **I-1**·2MeOH and **I-2**·2H_2O, respectively, where the $\chi_M T$ value can be estimated to be 3 emu·K·mol^{-1} (S = 2) only in the case of the absence of the spin-orbit interaction.

The thermal decomposition behaviors of compounds **I-1**·2MeOH and **I-2**·2H_2O are very similar to that reported for $\{[Mn(NCS)_2(4,4'\text{-bpy})(H_2O)_2]\cdot 4,4'\text{-bpy}\}_n$[2] and $\{[Co(NCS)_2(4,4'\text{-bpy})(H_2O)_2]\cdot 4,4'\text{-bpy}\}_n$.[3] They were heated to 500 ℃ under N_2. The TGA data for **I-1**·2MeOH show two steps of weight loss as shown in Figure I.7(a). In the first region 80-110 °C, it loses two methanol molecules (observed 11.95, calculated 10.60 %). On further heating, it loses one azpy ligand (observed 29.09, calculated 30.47 %) between 150 and 200 ℃, immediately followed by the other azpy ligand and decomposition of $Fe(NCS)_2$ above 210 ℃. The weight loss continues up to 300 ℃, and the final residue is black and amorphous. The TGA data for **I-2**·2H_2O show two steps of weight loss as shown in Figure I.7(b). In the first region 80-110 °C, it loses two water molecules (observed 7.02, calculated 6.92%). On further heating, it loses one 4,4'-bpy ligand (observed 29.23, calculated 30.01%) between 150 and 200 ℃, immediately followed by the other 4,4'-bpy ligand and decomposition of $Fe(NCS)_2$ above 210 ℃. The weight loss continues up to 300 ℃, and the final residue is black and amorphous. All TGA data reveal that the methanol or water molecules are readily liberated from the Fe(II) ion and the hydrogen bonded networks may be more brittle than coordination bonded networks. Consequently, the coordination networks with hydrogen-bonding linkage afford flexible structures and retain the electrochemical reactivity of the azpy.

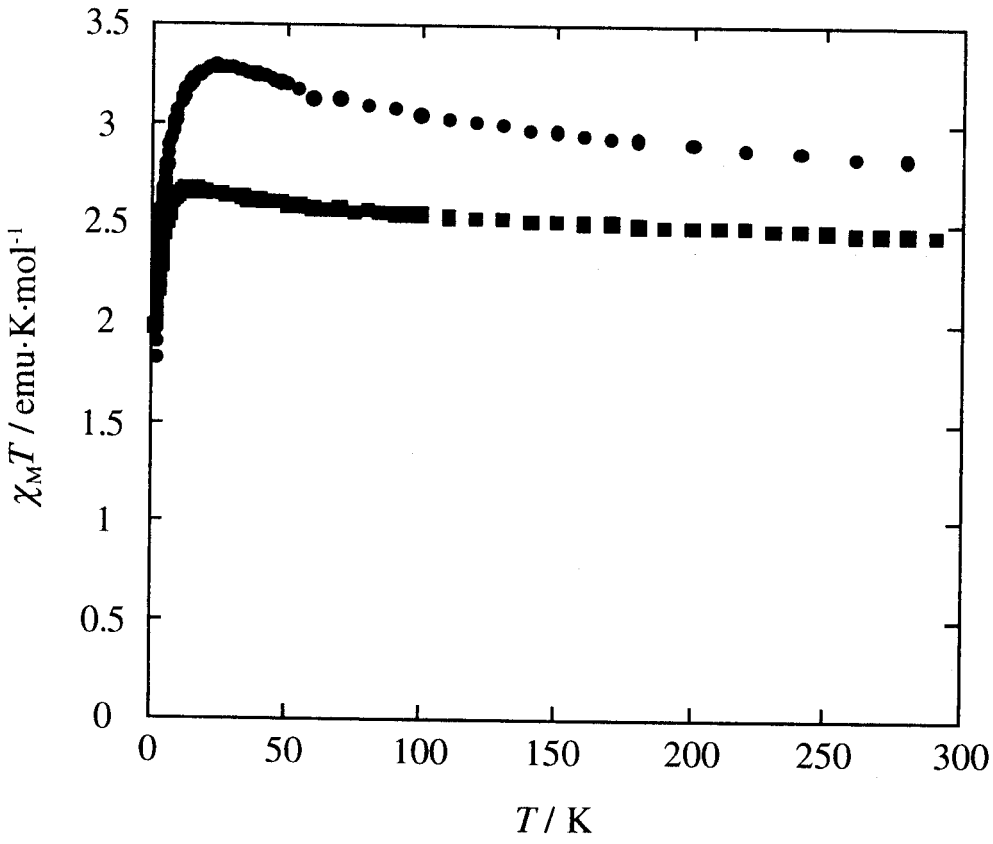

Figure I.6. Plots of the temperature dependence of $\chi_M T$ for **I-1**·2MeOH (closed circle) and **I-2**·2H_2O (closed square).

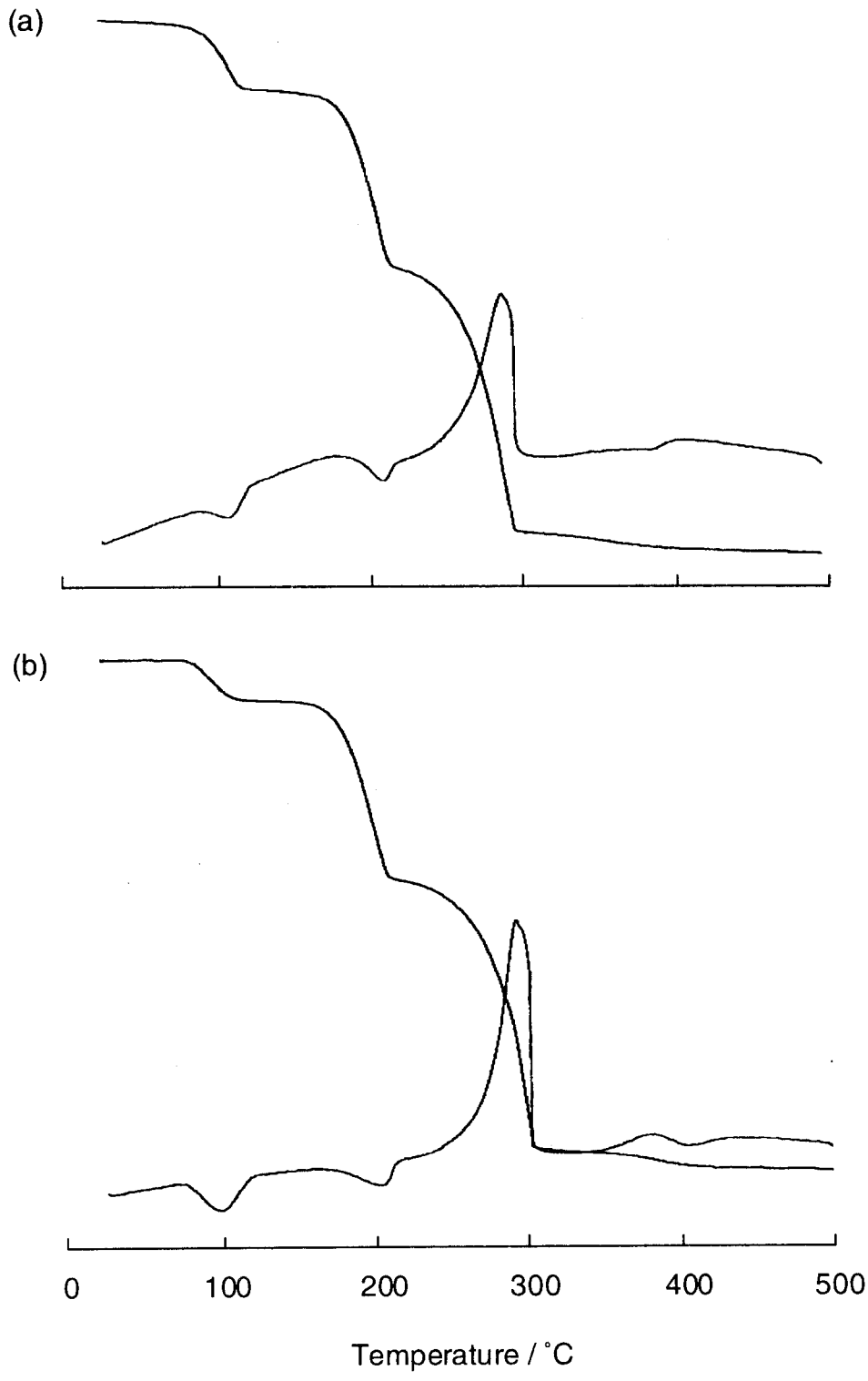

Figure I.7. Thermogravimetric analysis data for (a) **I-1**·2MeOH and (b) **I-2**·2H_2O.

I. 3. 3 Redox Properties

The electrochemical behaviors of compounds **I-1**·2MeOH and **I-3** were characterized by the measurement of the cyclic voltammograms in the solid state. One of the unique characteristics of azo-type compounds is the redox properties.[13] The electrochemical behavior of azpy, which depends on the properties of the solution, has been hitherto studied. It is reduced in two monoelectronic steps in DMF or acetonitrile solutions,[21,22] providing two coupled waves ($E_{1/2}$ = -0.84 and -1.58 V *vs.* SCE in DMF, -1.67 and -2.29 V in acetonitrile). On the other hand, azpy in an aqueous buffer solution (pH 7) undergoes a reversible two-electron reduction,[13] which appears as a single coupled wave ($E_{1/2}$ = -0.13 V *vs.* SCE for a gold electrode, -0.07 V for a Metrohm hanging mercury drop electrode). These results suggest that a single coupled wave is observed when a proton donor coexists.

Measurements of cyclic voltammograms in the solid state were carried out by using the carbon paste method. Free azpy diluted in carbon paste shows a single coupled wave ($E_{p,c}$ = -0.61 V, $E_{p,a}$ = 0.14 V *vs.* SCE, ΔE = 0.75 V), as shown in Figure I.8(a). This one-step reduction process is similar to that of azpy observed in aqueous buffer solution, based on the following mechanism.

$$\text{py-N=N-py} + 2e^- + 2H^+ \rightleftharpoons \text{py-}\underset{H}{N}\text{-}\underset{H}{N}\text{-py}$$

The cyclic voltammogram of compound **I-1**·2MeOH in the solid state shows similar behavior to that of free azpy, as shown in Figure 8(b) ($E_{p,c}$ = -0.66 V and $E_{p,a}$ = 0.13 V *vs.* SCE, ΔE = 0.79 V). Compound **I-1**·2MeOH contains two types of azpy ligands; one directly bonded to the Fe(II) center, the other contacts the Fe(II) ion through a hydrogen bonding.

In order to understand the redox properties of the azpy ligands in **I-1**·2MeOH, the cyclic voltammogram of **I-3** was measured under the same conditions (Figure I.8(c)). As described earlier, **I-3** has only coordinated azpy molecules and is free from the hydrogen bond supported by non-coordinated azpy units. In sharp contrast to the case of **I-1**·2MeOH, **I-3** shows no redox waves between -1.2 and 1.2 V, indicative of no apparent redox activity of the coordinated azpy

ligands. These results demonstrate that the clear reversible redox wave observed for **I-1**·2MeOH is attributed to the hydrogen-bonding supported azpy.

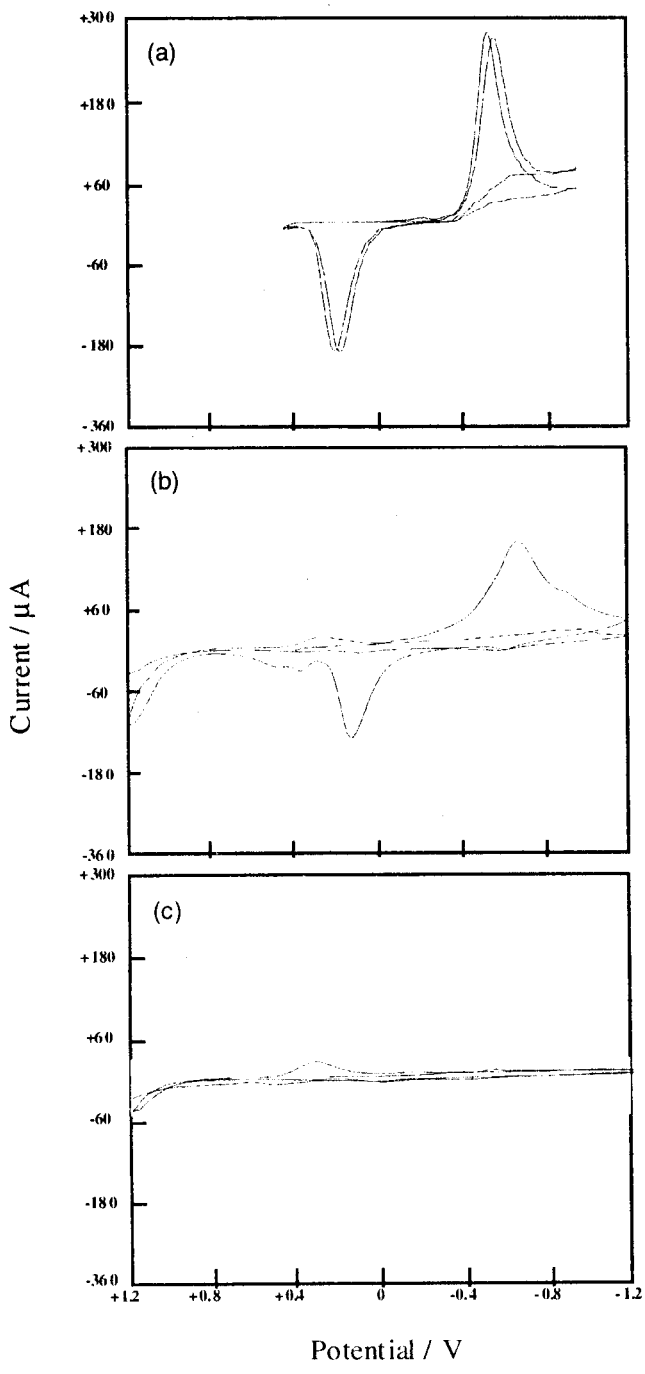

Figure I.8. Cyclic voltammograms of (a) free azpy, (b) **I-1**·2MeOH, and (c) **I-3**, in carbon paste.

I. 3. 4 Structural Conversion by Removal of Capped Solvents and Concomitant Spin-Crossover Phenomenon

An interesting feature of **I-1**·2MeOH and **I-2**·2H_2O is that the 2-D coordination- and hydrogen-bonding networks of **I-1**·2MeOH and **I-2**·2H_2O are transformed into the 2-D coordination-bonding networks of **I-1** and **I-2**, respectively, by the heat treatment in the solid phase. The EA, IR, TGA, and XRPD measurements reveal the conversion to **I-1** and **I-2**. The IR measurements show that stretching bands for MeOH or H_2O molecules disappear. Moreover, as illustrated in Figures I.9 and I.10, the XRPD patterns of **I-1** and **I-2** are in good agreement with the simulated pattern calculated from the crystallographic data of **I-3** and observed pattern of $[Co(NCS)_2(4,4'\text{-bpy})_2]_n$, respectively. $[Co(NCS)_2(4,4'\text{-bpy})_2]_n$, which has been previously synthesized by Jacobson et al.,[3] affords a 2-D coordination-bonding network.

The magnetic properties of **I-1**·2MeOH and desolvated **I-1** expressed in the form of $\chi_M T$ versus T curves are shown in Figure I.11. At 300 K, the $\chi_M T$ product of **I-1** is 3.46 emu·K·mol^{-1}. The value of $\chi_M T$ gradually increases when cooling to around 230 K and then diminishes gradually to reach a value *ca.* 3.27 emu·K·mol^{-1} at 60 K. Finally, $\chi_M T$ diminishes rapidly down to 1.44 emu·K·mol^{-1} at 2 K. The first $\chi_M T$ drop is consistent with around 5 % of HS ions undergoing $S = 2 \leftrightarrow S = 0$ spin conversion. The second $\chi_M T$ drop can be ascribed to zero-field splitting in the orbital singlet $S = 2$ ground state arising from the strongly distorted coordination sphere of the remaining HS Fe(II) ions.

It is well-known that ligands such as bpethe, 1,4-bis(4-pyridyl)butadiyne (bpb), and 4,4'-bis-1,2,4-triazole (btr) represent good examples of rodlike bifunctional ligands well-suited for the synthesis of spin-crossover coordination polymers.[10,23,24] Upon reaction of these ligands with [Fe(II)/2NCX$^-$] solution (X = S, Se), the solvent molecules of the first coordination sphere of the metal ion are usually replaced yielding square-grid motifs as observed in the $\{[Fe(NCX)_2(btr)_2]\cdot H_2O\}_n$ (X = S, Se),[23,25] $\{[Fe(NCS)_2(bpethe)_2]\cdot MeOH\}_n$,[10] and $\{[Fe(NCS)_2(bpb)_2]\cdot 0.5MeOH\}_n$[24] spin-crossover systems. Further, the synthesis of the $\{[Fe(btr)_3]\cdot 2ClO_4\}_n$ 3-D polymeric spin-crossover compound through substitution of pseudo-halide anions with non-coordinating anions such as ClO_4^- has been recently reported.[26] In the case of **I-**

1·2MeOH, the Fe(II) center has a $[N_4O_2]$ coordination environment, which generally shows no spin-crossover phenomenon due to a weak ligand field splitting energy (LFSE). However, the removal of coordinated MeOH molecules induces a structural transformation, namely, coordination of free azpy ligands to Fe(II) centers, which generate a $[N_6]$ coordination environment. Therefore, the spin-crossover successfully happens due to the resulting strengthened LFSE. Such a regulation of the spin-crossover by the desolvation of guests is quite rare and opens up a new possibility for functional materials. At present, the study on the measurement of Mössbauer spectra and reversibility by guest molecules is in progress.

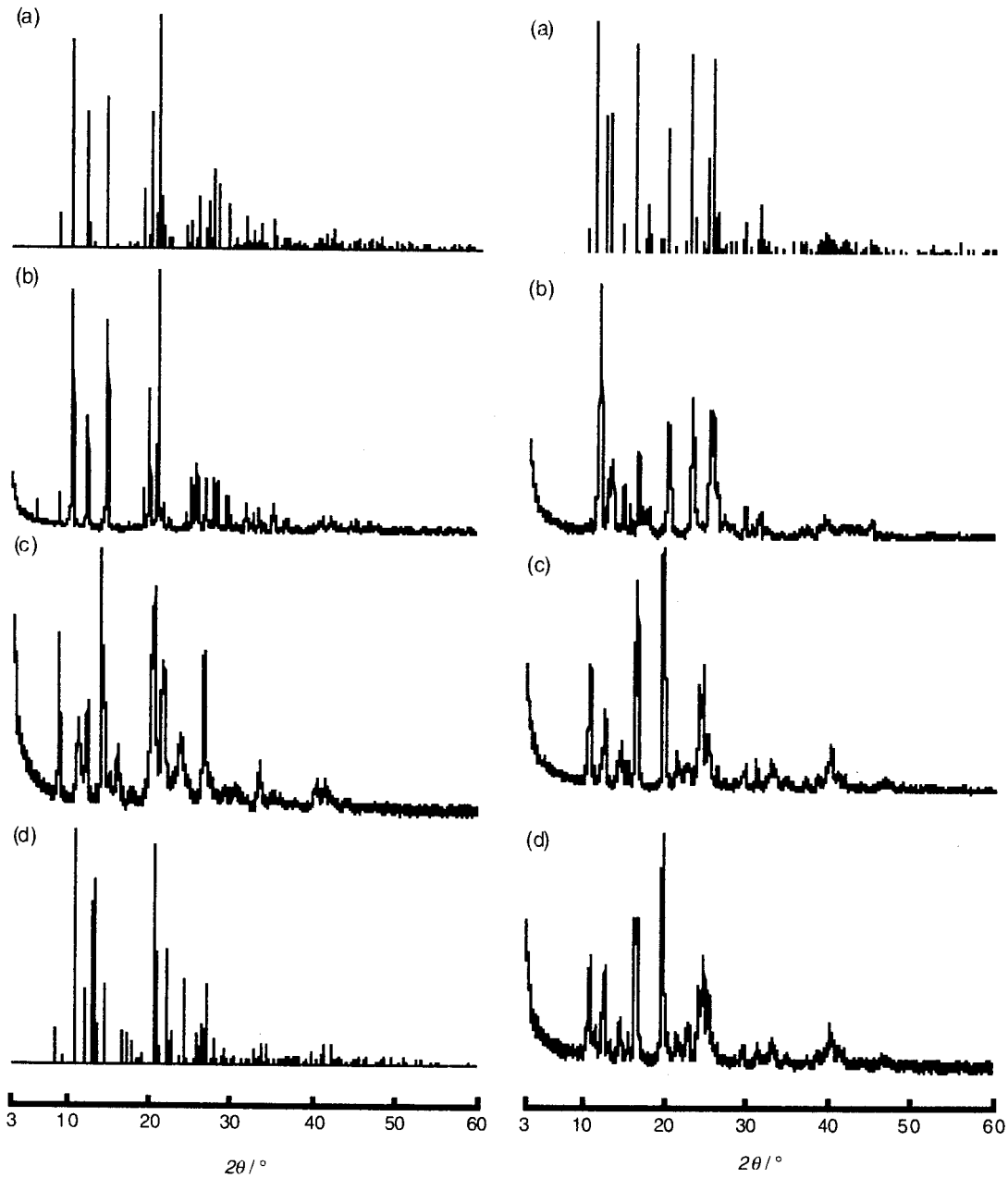

Figure I.9 (left). XRPD patterns of **I-1**·2MeOH ((a) simulation and (b) observed patterns), (c) **I-1**, and (d) a simulation pattern of **I-3**.

Figure I.10 (right). XRPD patterns of **I-2**·$2H_2O$ ((a) simulation and (b) observed patterns), (c) **I-2**, and (d) $[Co(NCS)_2(4,4'\text{-bpy})_2]_n$.[3]

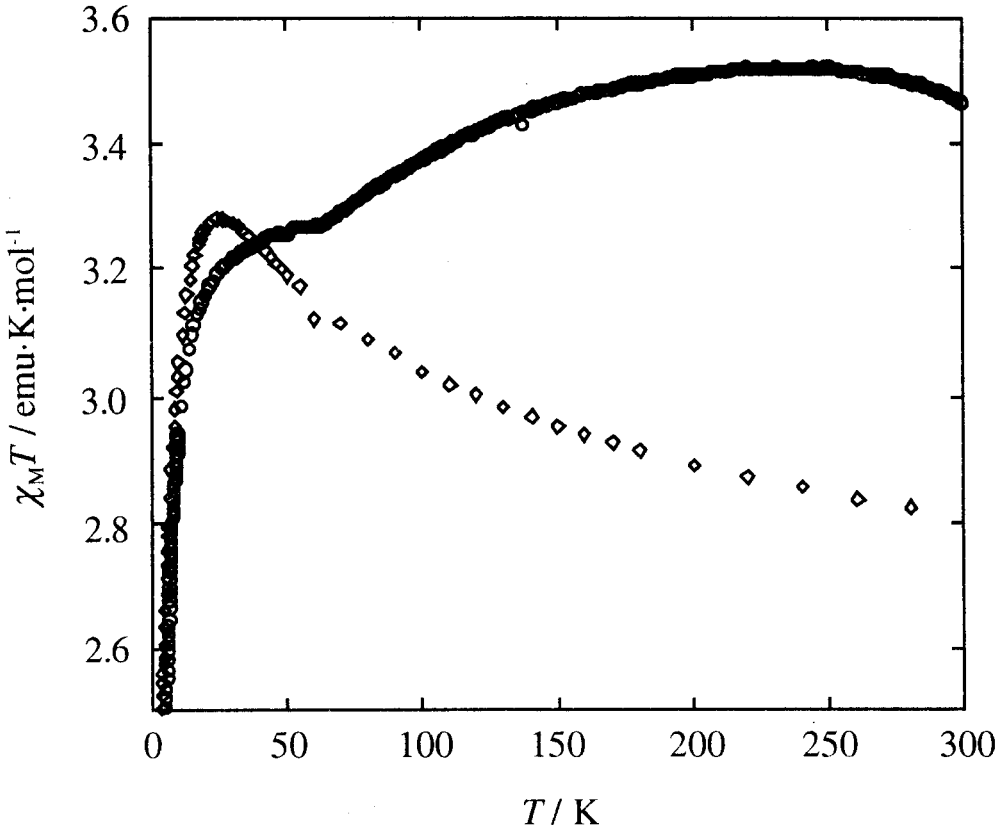

Figure I.11. Plots of the temperature dependence of $\chi_M T$ for **I-1**·2MeOH (open rhombus) and **I-1** (open circle).

I. 4 Conclusion

Syntheses, crystal structures, and properties of Fe(II) coordination polymers, $\{[Fe(NCS)_2(azpy)(MeOH)_2]\cdot azpy\}_n$ (**I-1**·2MeOH), $\{[Fe(NCS)_2(4,4'\text{-bpy})(H_2O)_2]\cdot azpy\}_n$ (**I-2**·$2H_2O$), $\{[Fe(NCS)_2(azpy)_2]\cdot 3H_2O\}_n$ (**I-3**), and $\{(H_2 4,4'\text{-bpy})[Fe_3(SO_4)_4(4,4'\text{-bpy})_3(H_2O)_6]\cdot 10H_2O\}_n$ (**I-4**), were described. Cyclic voltammograms of **I-1**·2MeOH and **I-3** demonstrate that the directly bridging azpy ligands show no apparent redox activity and a reversible redox wave observed for **I-1**·2MeOH is attributed to the hydrogen-bonding supported azpy. **I-1**·2MeOH and **I-2**·$2H_2O$ have 2-D rectangular grids constructed by both coordination and hydrogen bonds. They easily release the coordinated solvent molecules of MeOH and H_2O by heating to form new crystal phases of **I-1** and **I-2**, which show 2-D coordination-bonding sheets with square or rhombic grids. Especially, the magnetic property of **I-1** reveals the occurrence of a spin-crossover of the Fe(II) ions, which is in contrast to that of a precursor of **I-1**·2MeOH. It is noteworthy that the control of the spin-crossover phenomenon was achieved by the structural transformation induced by the release of the coordinated solvent molecules.

I. 5 References

(1) Fujita, M.; Kwon, Y. J.; Washizu, S.; Ogura, K. *J. Am. Chem. Soc.* **1994**, *116*, 1151-1152.

(2) Li, M.-X.; Xie, G.-Y.; Gu, Y.-D.; Chen, J.; Zheng, P.-J. *Polyhedron* **1995**, *14*, 1235-1239.

(3) Lu, J.; Paliwala, T.; Lim, S. C.; Yu, C.; Niu, T.; Jacobson, A. J. *Inorg. Chem.* **1997**, *36*, 923-929.

(4) Carlucci, L.; Ciani, G.; Proserpio, D. M.; Sironi, A. *J. Chem. Soc., Dalton Trans.* **1997**, 1801-1803.

(5) Blake, A. J.; Hill, S. J.; Hubberstey, P.; Li, W. S. *J. Chem. Soc., Dalton Trans.* **1997**, 913-914.

(6) Chen, X. M.; Tong, M. L.; Luo, Y. J.; Chen, Z. N. *Aust. J. Chem.* **1996**, *49*, 835-838.

(7) Tong, M.-L.; Chen, X.-M.; Yu, X. L.; Mak, T. C. W. *J. Chem. Soc., Dalton Trans.* **1998**, 5-6.

(8) Gable, R. W.; Hoskins, B. F.; Robson, R. *Chem. Commun.* **1990**, 1667-1668.

(9) MacGillivray, L. R.; Groeneman, R. H.; Atwood, J. L. *J. Am. Chem. Soc.* **1998**, *120*, 2676-2677.

(10) Real, J. A.; Andrés, E.; Muñoz, M. C.; Julve, M.; Granier, T.; Bousseksou, A.; Varret, F. *Science* **1995**, *268*, 265-267.

(11) Real, J. A.; Munno, G. D.; Muñoz, M. C.; Julve, M. *Inorg. Chem.* **1991**, *30*, 2071-2074.

(12) Kawata, S.; Kitagawa, S.; Kondo, M.; Furuchi, I.; Munakata, M. *Angew. Chem., Int. Ed. Engl.* **1994**, *33*, 1759-1761.

(13) Haladjian, J.; Pilard, R.; Bianco, P.; Asso, L. *Electrochimica Acta* **1985**, *30*, 695-699.

(14) Kahn, O. In *Molecular Magnetism*; VCH: New York, 1993.

(15) Brown, E. V.; Granneman, G. R. *J. Am. Chem. Soc.* **1975**, *97*, 621-627.

(16) Campbell, N.; Henderson, A. W.; Taylor, D. *J. Chem. Soc.* **1953**, 1281-2185.

(17) Sheldrick, G. M. **1985**, In "Crystallographic Computing 3" (Eds G.M. Sheldrick, C. Kruger and R. Goddard) Oxford University Press, pp. 175-189.

(18) Beurskens, P. T.; Admiraal, G.; Beurskens, G.; Bosman, W. P.; de Gelder, R.; Israel, R.; Smits, J. M. M. **1994**, The DIRDIF-94 program system, Technical Report of the Crystallography Laboratory, University of Nijmegen, The Netherlands.

(19) Altomare, A.; Burla, M. C.; Camalli, M.; Cascarano, M.; Giacovazzo, C.; Guagliardi, A.; Polidori, G. *J. Appl. Cryst.* **1994**, *27*, 435.

(20) Crystal Structure Analysis Package, Molecular Structure Corporation (1985 & 1999).

(21) Sadler, J. L.; Bard, A. J. *J. Am. Chem. Soc.* **1968**, *90*, 1979-1989.

(22) Bellamy, A. J.; MacKirdy, I. S.; Niven, C. E. *J. Chem. Soc., Perkin Trans.* **1983**, 183-185.

(23) Vreugdenhil, W.; van Diemen, J. H.; de Graaff, R. A. G.; Haasnoot, J. G.; Reedijk, J.; van der Kraan, A. M.; Kahn, O.; Zarembowitch, J. *Polyhedron* **1990**, *9*, 2971-2979.

(24) Moliner, N.; Muñoz, C.; Létard, S.; Solans, X.; Menéndez, N.; Goujon, A.; Varret, F.; Real, J. A. *Inorg. Chem.* **2000**, *39*, 5390-5393.

(25) Ozarowski, A.; Shunzhong, Y.; McGarvey, B. R.; Mislankar, A.; Drake, J. E. *Inorg. Chem.* **1991**, *30*, 3167-3174.

(26) Garcia, Y.; Kahn, O.; Rabardel, L.; Chansou, B.; Salmon, L.; Tuchagues, J. P. *Inorg. Chem.* **1999**, *38*, 4663-4670.

Chapter II

New Microporous Coordination Polymer Affording Guest-Coordination Sites at Channel Walls

Abstract: Utilization of a metalloligand, $\{[Cu(2,4\text{-pydca})_2(H_2O)]\cdot 2Et_3NH\}$, as a building unit has provided a novel porous coordination polymer, $\{[ZnCu(2,4\text{-pydca})_2(H_2O)_3(DMF)]\cdot DMF\}_n$ (**II-1**), in which the Zn(II) ion at the node of the network acts as a connector and the Cu(II) ion in channel wall is available for guest-coordination.

II. 1 Introduction

If coordinatively unsaturated metal ions can be incorporated not in nodal sites but in channel walls, new porous properties would be created on the basis of coordination of a guest molecule.[1-3] However, the synthesis of such compounds by "one-step self-assembly" method is very difficult because metal ions tend to occur in nodes of frameworks and therefore all the coordination sites are occupied by bridging ligands and/or counter anions. In order to create a porous framework containing coordinatively unsaturated metal centers, the author developed a new synthetic scenario, that is, "two-step self-assembly". Firstly, synthesized is a metalloligand, which acts as not only a framework linker but also a coordinatively unsaturated metal center (M^1). Secondly, the metalloligand is added to another metal ion (M^2), which acts as a nodal unit of a framework. Consequently, two kinds of metal centers coexist in a framework (Scheme II.1), and a larger space around the metal ion at the channel wall could be obtained, relevant for an attack of guest molecules. In this chapter, new porous coordination polymer $\{[ZnCu(2,4\text{-}pydca)_2(H_2O)_3(DMF)]\cdot DMF\}_n$ (**II-1**) with metal ions in the channel walls was successfully synthesized and crystallographically characterized by using a new synthetic method, "two-step self-assembly".

Scheme II.1

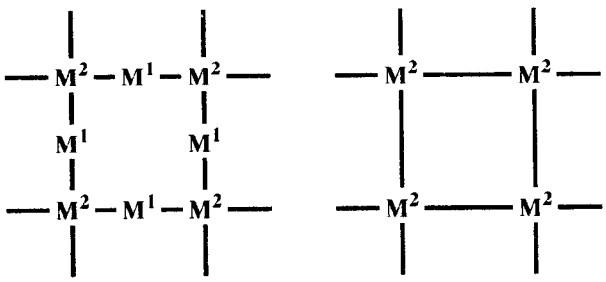

II. 2 Experimental

II. 2. 1 Physical Measurements

The physical measurements were performed as described in Chapter I.

II. 2. 2 Synthesis

Materials. $Zn(NO_3)_2 \cdot 6H_2O$ was obtained from Wako Co. The synthesis and detailed description of metalloligand $\{[Cu(2,4\text{-pydca})_2(H_2O)] \cdot 2Et_3NH\}$ (**III-1**·$2Et_3NH$) is explained in Chapter III.

Synthesis of $[ZnCu(2,4\text{-pydca})_2(H_2O)_3(DMF)] \cdot DMF\}_n$ (II-1). To a hot DMF solution (30 mL) of **III-1**·$2Et_3NH$ (300 mg, 0.487 mmol) was added a DMF solution (5 mL) of $Zn(NO_3)_2 \cdot 6H_2O$ (144 mg, 0.484 mmol). After the obtained powder was filtered, the filtrate was kept for a few weeks to give sky-blue crystals, which were filtered, washed with acetone, and dried under vacuum. Anal. Calcd for $C_{20}H_{26}CuN_4O_{13}Zn$: C, 36.43; H, 3.97; N, 8.50. Found: C, 36.53; H, 4.02; N, 8.57. IR (KBr pellet): 3184 bm, 1663 s, 1646 s, 1614 s, 1552 s, 1473 m, 1439 m, 1387 s, 1327 s, 1257 m, 1087 m, 1035 w, 895 w, 843 w, 779 m, 746 m, 731 m, 694 m, 663 m, 472 w cm^{-1}.

II. 2. 3 X-Ray Structure Determination

Suitable crystal was mounted on a glass fiber and coated with epoxy resin. All measurements were made on a Rigaku RAXIS-RAPID imaging plate diffractometer with graphite monochromated Mo-Kα radiation. A symmetry-related adsorption correction using the program ABSCOR[4] was applied. The data were corrected for Lorentz and polarization effects. The structure was solved by a direct method using the MITHRIL90 program[5] and expanded using Fourier techniques.[6] The non-hydrogen atoms were refined anisotropically. All hydrogen atoms, which were placed in idealized positions, were included but not refined. The refinements were carried out using full-matrix least squares techniques. Crystal data and details of the structure determinations are summarized in Table II.1. All calculations were performed using the teXsan[7] crystallographic software package of Molecular Structure Corporation.

Table II.1. Crystallographic Data for $\{[ZnCu(2,4\text{-pydca})_2(H_2O)_3(DMF)]\cdot DMF\}_n$ (**II-1**).

formula	$C_{20}H_{26}CuN_4O_{13}Zn$
fw	659.37
crystal system	triclinic
a, Å	10.5857(9)
b, Å	20.308(2)
c, Å	6.3289(6)
α, deg	92.801(4)
β, deg	107.034(4)
γ, deg	92.175(5)
V, Å^3	1297.3(2)
space group	$P\bar{1}$ (No.2)
Z	2
ρ(calcd), g·cm^{-3}	1.688
F(000)	674.00
μ(Mo Kα), cm^{-1}	18.17
diffractometer	RAXIS-RAPID
radiation (λ, Å)	0.71069
temp., °C	25
GOF	1.240
no. of observns	5731 (all data)
no. of variables	355
R^a ($I > 2.00\sigma(I)$, all data)	0.0479, 0.0726
$R_w{}^b$ ($I > 2.00\sigma(I)$, all data)	0.1098, 0.1164

[a] $R = \Sigma||Fo| - |Fc||/\Sigma|Fo|$. [b] $R_w = [(\Sigma w (|Fo| - |Fc|)^2/\Sigma wFo^2)]^{1/2}$.

II. 3 Results and Discussion

II. 3. 1 Crystal Structure of Porous Coordination Polymer {[ZnCu(2,4-pydca)$_2$(H_2O)$_3$(DMF)]·DMF}$_n$ (II-1).

An ORTEP view around metal centers of **II-1** is shown in Figure II.1(a). In the crystal, there are three crystallographically independent metal centers, Cu(1), Cu(2), and Zn. Each Cu(II) center is based on an elongated octahedral environment with the two oxygen atoms and the two nitrogen atoms of 2,4-pydca^{2-} ligands in the equatorial plane, and the two oxygen atoms of H_2O and DMF molecules at the axial positions for Cu(1) and Cu(2), respectively. On the other hand, the Zn(II) center shows a distorted octahedron with the three oxygen atoms of H_2O molecules, the two oxygen atoms of the 4-carboxylate in a semi-chelating fashion,[8,9] and the oxygen atom of another 4-carboxylate in a monodentate fashion. The O-Zn-O bond angles for *trans* and *cis* orientation range from 152.2(1) ° to 177.7(1) °, and 59.0(1) ° to 104.0(1) °, respectively. It is worth noting that the coordination environment of **III-1** used as a building block is almost retained even in the extended structure. As a result, the ligand 2,4-pydca^{2-} shows a characteristic coordination feature in the framework; the carboxylate group at 2-position for both Cu(II) ions is involved in a chelating mode together with the nitrogen atom while that at 4-position is alone coordinated to Zn(II) ion, taking semi-chelating and monodentate coordination modes.

The 2,4-pydca^{2-} ligands bridge the Cu and Zn ions alternately to provide an undulated 1-D chain structure of •••Zn-Cu(2)-Zn-Cu(1)-Zn-Cu(2)•••, in which a Cu(1)-Zn-Cu(2) angle is 116 °. The intrachain distances of Cu(1)-Zn and Cu(2)-Zn are 8.90 and 8.75 Å, respectively. As shown in Figure II.1(b), these chains are linked by H_2O molecules, which bridge between the Zn and Cu(1) ions (Zn-O = 2.178(3) Å, Cu(1)-O = 2.713(3) Å).[10] The bridging H_2O molecules are also supported by 4-carboxylates (Hydrogen bond A : O-O = 2.665(4) Å). In addition, their chains are connected via hydrogen bonds between coordinated H_2O molecules at the Zn centers and the oxygen atoms of 2-carboxylates (Hydrogen bond B : 2.818(4) Å). These two linkages create a 2-D network of a large grid. Each sheet is linked to adjacent one by hydrogen bonds

among coordinated H_2O molecules at the Zn centers and the oxygen atoms of 2- and 4-carboxylates (av. 2.740 Å) to form parallelogrammic cavities with a dimension of *ca.* 15 Å x 5 Å as shown in Figure II.1(c). These cavities are filled with two types of DMF molecules. One is weakly coordinating to the Cu(2) center (Cu(2)-O = 2.513(4) Å), and the other is connected to a coordinated H_2O molecule at the Zn(II) center via a hydrogen bond (Hydrogen bond C : O-O = 2.662(5) Å) as illustrated in Figure II.1(b).

There are eight metal units per one cavity as illustrated in Figure II.1(d). The two Cu(1) units act only as a node. On the other hand, the Cu(2) units are located on the both side of cavity, accompanying DMF molecules at the axial sites. The four Zn sites are coordinatively saturated, essentially located in nodal positions but provide one of the coordinated water molecules as a hydrogen bond donor/acceptor toward the channel cavity. Therefore, the residual DMF molecules are trapped by a hydrogen bond. As compared with the Zn sites at the nodal positions, the Cu(2) ions at channel walls have enough space to trap more larger guest molecules at the axial sites.

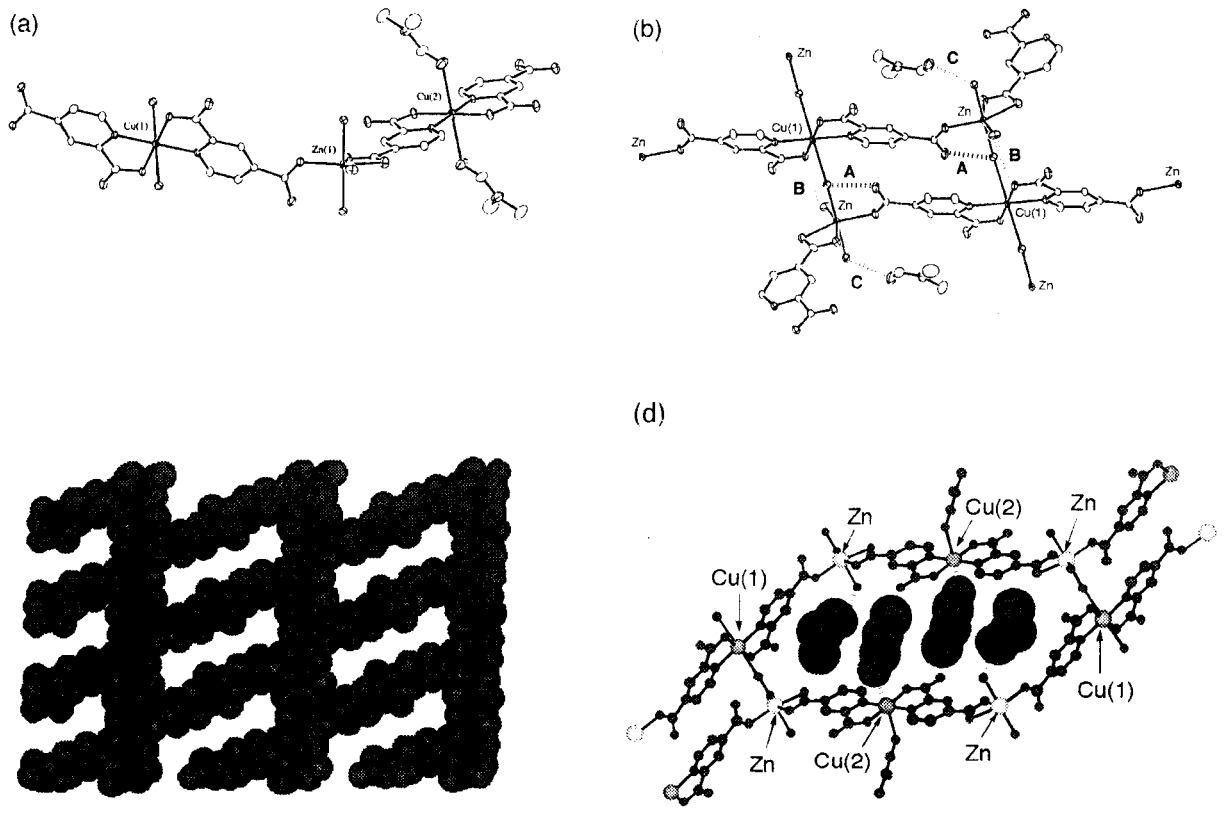

Figure II.1 (a) ORTEP drawing around metal centers of **II-1** at the 30 % probability level. In all figures, the hydrogen atoms are omitted for clarity. (b) ORTEP drawing of a bridging mode between 1-D chains of **II-1**. The dotted line represents a hydrogen bond. (c) View of a microporous network of **II-1** along the *c*-axis. The guest DMF molecules are omitted for clarity. (d) View of one cavity of **II-1**. The guest DMF molecules are represented by a space filling model.

II. 3. 2 Guest-Exchange Property

II-1 was immersed in a H_2O solution for one day, subsequently filtered and dried under vacuum. The resulting compound, $\{[ZnCu(2,4\text{-pydca})_2(H_2O)_4]\cdot xH_2O\}_n$ (**II-2**), shows that all the DMF molecules are replaced with H_2O ones, from the results of EA, IR, and TGA measurements. As illustrated in Figure II.2, **II-2** keeps high crystallinity during a guest exchange process as indicated by sharp peaks observed in the XRPD pattern. The pattern is, however, slightly different from that of **II-1**, indicating that the cavity is so flexible that H_2O molecules may be incorporated instead of DMF molecules without collapsing or decomposition.

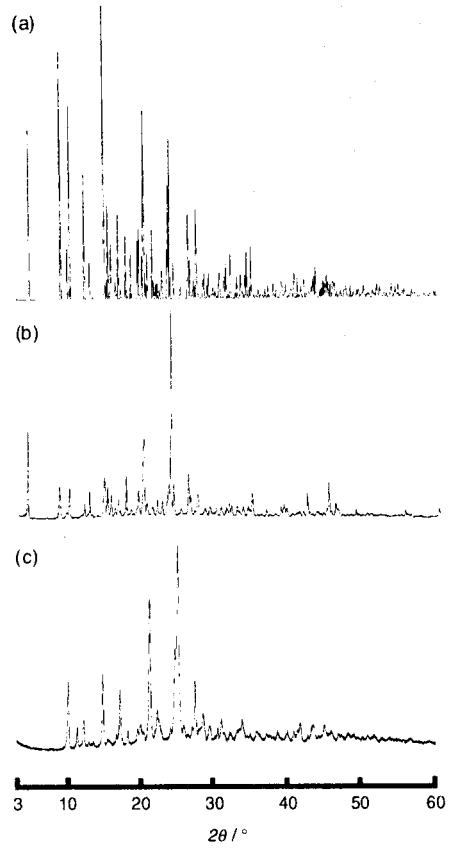

Figure II.2 XRPD data : (a) simulation pattern of **II-1**, (b) observed pattern of **II-1**, and (c) observed pattern of **II-2** replaced by H_2O molecules.

II. 4 Conclusion

The author succeeded in obtaining a novel porous coordination polymer {[ZnCu(2,4-pydca)$_2$(H_2O)$_3$(DMF)]·DMF}$_n$ (**II-1**) by two step synthesis with the aid of the metalloligand, which could be relevant for chemical modification of channel cavities.

II. 5 References

(1) Reineke, T. M.; Eddaoudi, M.; Fehr, M.; Kelley, D.; Yaghi, O. M. *J. Am. Chem. Soc.* **1999**, *121*, 1651-1657.

(2) Li, H.; Davis, C. E.; Groy, T. L.; Kelley, D. G.; Yaghi, O. M. *J. Am. Chem. Soc.* **1998**, *120*, 2186-2187.

(3) Sawaki, T.; Dewa, T.; Aoyama, Y. *J. Am. Chem. Soc.* **1998**, *120*, 8539-8640.

(4) Higashi, T. **1995**, Program for Adsorption Correction, Rigaku Corporation, Tokyo, Japan.

(5) Gilmore, C. J. **1990**, MITHRIL – an integrated direct methods computer program. Univ. of Glasgow, Scotland.

(6) Beurskens, P. T.; Admiraal, G.; Beurskens, G.; Bosman, W. P.; de Gelder, R.; Israel, R.; Smits, J. M. M. **1994**, The DIRDIF-94 program system, Technical Report of the Crystallography Laboratory, University of Nijmegen, The Netherlands.

(7) Crystal Structure Analysis Package, Molecular Structure Corporation (1985 & 1999).

(8) Guilera, G.; Steed, J. W. *Chem. Commun.* **1999**, 1563-1564.

(9) Addison, C. C.; Logan, N.; Wallwork, S. C.; Chang, N.-C. *Quart. Rec. Chem. Soc.* **1971**, *25*, 289.

(10) Brooks, N. R.; Blake, A. J.; Champness, N. R.; Cunningham, J. W.; Hubberstey, P.; Teat, S. J.; Wilson, C.; Schröder, M. *J. Chem. Soc., Dalton Trans.* **2001**, 2530-2538.

Chapter III

Control of Frameworks by a Multi-Functional Metalloligand: New Synthetic Approach toward Crystal Engineering

Abstract: Rational design and bond engineering of coordination polymers by a Cu(II) metalloligand, $\{[Cu(2,4\text{-pydca})_2(H_2O)]\cdot 2Et_3NH\}$ (**III-1**$\cdot 2Et_3NH$), which was prepared by a deprotonation of a precursory metalloligand $[Cu(2,4\text{-pydca})_2(H_2O)_2]$ (**III-1**$\cdot 2H$), have been succeeded for first periodic transition metal ions (Mn(II), Fe(II), Co(II), Cu(II), and Zn(II)), following to an Irving-Williams order. 1-D coordination polymers with homo- or hetero-metallic ions, $\{[MCu(2,4\text{-pydca})_2(H_2O)_4]\cdot 2H_2O\}_n$ (M = Co (**III-2**), Cu (**III-3**), Zn (**III-4**)), show a similar type of 1-D chain bridged by 4-carboxylate donors of metalloligand **III-1**. In addition, several 2-D coordination polymers constructed from the metalloligand **III-1** have also been isolated and characterized. $[MCu(2,4\text{-pydca})_2(H_2O)_4]_n$ (M = Mn (**III-5**), Fe (**III-6**)) forms a 2-D thick sheet-like structure, in which 1-D mixed-metallic zigzag chains of $[MCu(2,4\text{-pydca})_2]_n$ are linked by the weak coordination between the oxygen atoms of 4-carboxylate group and the Cu(II) atoms. $\{[Cu(2,2'\text{-bpy})Cu(2,4\text{-pydca})_2]\cdot 3H_2O\}_n$ (**III-7**) consists of metalloligand **III-1** and metal complex connector of $[Cu(2,2'\text{-bpy})]^{2+}$, producing 1-D zigzag chains bridged by 4-carboxylate groups of **III-1**. These chains are bound by the weak coordination between the oxygen atom of 2-carboxylate unit and the Cu(II) atom to create a 2-D undulated sheet structure. $[ZnCu(2,4\text{-pydca})_2(H_2O)_2(MeOH)_2]_n$ (**III-8**) consists of 1-D linear chains, which are linked by weak coordination and hydrogen bonds to form a 2-D network. It is worth nothing that the regular coordination bonds of these polymers and $\{[ZnCu(2,4\text{-pydca})_2(H_2O)_3(DMF)]\cdot DMF\}_n$ (**II-1**), which is reported in Chapter II, were predictably controlled. Also attempted was the reaction of Ag(I) ion with metalloligand **III-1**, which generated a 3-D network of $[Ag_2Cu(2,4\text{-pydca})_2]_n$ (**III-9**). **III-9** is composed of Ag_2 dimer unit and bridging metalloligand **III-1**. Both 2- and 4-carboxylates of metalloligands link to the Ag-Ag dimers to form a 3-D network. These structural results clearly demonstrate that the metalloligand **III-1** has a variety of coordination modes,

depending on second metal ion units employed. Magnetic properties of 2-D bimetallic compounds **III-5** and **III-6** represent the weak ferrimagnetic behaviors.

III. 1 Introduction

According to current synthetic methodology of coordination polymers, choice of building blocks is of significance at initial stage of preparation, and principal building blocks have so far been found. One is a transition metal ion (M), which could provide various spatial and electronic structures, i.e. coordination number, geometry, oxidation and spin state. The other is a bridging ligand (L), which is usually commercially available or obtained from modification of a simple ligand such as families of bipyridines, dicarboxylates, oxocarbons, and so on. Combination of these two building blocks forms a wide variety of frameworks. In order to develop the chemistry, where fruitful structures and novel properties would be realized, newly invented is the third building block, so-called inorganic-organic hybrid bridging ligand (metalloligand, L-M-L).

The metalloligand has several advantages that are listed as follows.

(1) Simple process to prepare multi-functional ligands. Organic bridging ligands having multi-functionalities require many intricate synthetic steps while metalloligands with multi-functionalities can be obtained from combination of simple building blocks (M and L).

(2) Modification of coordination ability. Metalloligand is relevant for modifying coordination power of functional groups because of Lewis-acidity and electrostatic effect of metal ions.

(3) Amphoteric properties. In addition to Lewis-basic coordination sites, metalloligands also provide Lewis-acid sites supplied from the metal ion.

(4) Introduction of two types of metal ions. Two roles of metal ions can be utilized, one is to link building block to afford a backbone of a framework. The other is to make a branch for the backbone, and in a sense, to create chemical or physical properties. Not only homo-metallic coordination polymers but also hetero-metallic ones can be systematically synthesized.

Reports on coordination polymers with metalloligand are still sparse in comparison with those with organic ligands.[1-21] Most famous examples of metalloligands are Cu(II) complexes reported by Kahn's group,[8-14,22-29] where metalloligands have oxamate, oxamide, benzoate, and propionate groups and bridge second transition metal ions such as Mn(II), Co(II), Ni(II), and Cu(II). For recent instances, several mixed-metallic coordination polymers of Cu(II)-M parts (M =

Ag(I), Cu(I), Hg(II), and Cd(II)) have been synthesized by using the metalloligands [Cu(2-pyrazinecarboxylate)$_2$] and [Cu(2-methylpyrazine-5-carboxylate)$_2$(H_2O)].[15-20] These, however, dissolve only in hot water, the use as a ligand being restricted.

The author developed a new metalloligand, namely [Cu(2,4-Hpydca)$_2$(H_2O)$_2$] (**III-1**·2H), by utilizing a 2,4-H_2pydca ligand, which has three coordination sites with different coordination abilities as shown in Scheme III.1. One is a chelation site with N,O-set from pyridyl and 2-carboxylate groups. Another is a remaining oxygen atom of the 2-carboxylate groups, and the other is oxygen atoms of the 4-carboxylate groups. The chelation site can be strongly coordinated to a metal ion to afford a metalloligand **III-1**·2H. The coordination ability of the remaining sites (another oxygen atom of 2-carboxylate and each oxygen atom of 4-carboxylate) becomes weaker than that of the parent ligand because of an introduction of the Lewis-acid metal ion. Therefore, **III-1**·2H could be readily isolated. By deprotonating the 4-carboxylic acid moiety, the coordination ability of the metal-free sites increases, giving rise to a useful linker of {[Cu(2,4-pydca)$_2$(H_2O)]·2Et_3NH} (**III-1**·2Et_3NH) for the construction of coordination polymers. The four coordination sites (A and B in Scheme III.1) afford various frameworks, where terminal, bridging, chelating, and its combinations occur (Scheme III.2). The coexistence of several hydrogen-bonding sites from each carboxylate

Scheme III.1

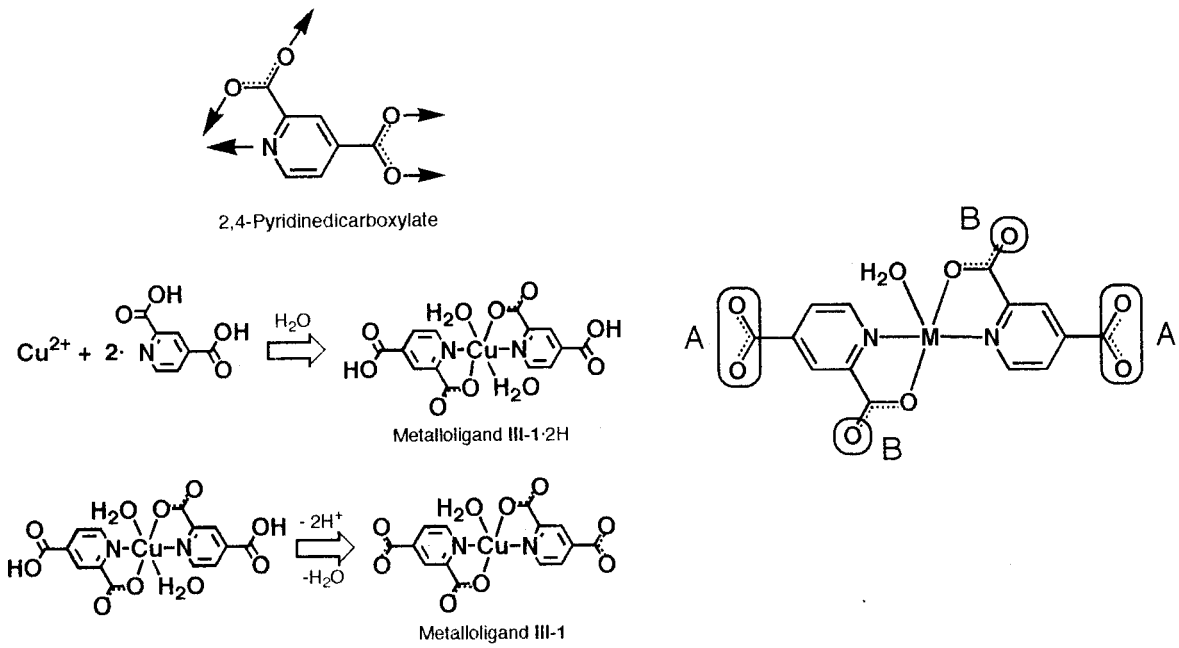

and Lewis-acidic sites at the Cu(II) ion supports the stability of frameworks. Furthermore, since this deprotonated metalloligand **III-1**·2Et_3NH is easily soluble in polar H_2O, MeOH, and DMF solvents without decomposition, the reaction for preparation of coordination polymers can be carried out in a mild condition.

Crystal engineering of coordination polymers by the self-assembly method is at the forefront of modern research, but still limited are examples that researchers succeeded in syntheses of desired frameworks: unprecedented structures are often observed. The author focused on two different coordination sites in the metalloligand **III-1** as illustrated in the right of Scheme III.1. Site A is a regular carboxylate linker, while site B has a character that each oxygen atom of site B carboxylate is less anionic and has a weaker electron-donating power than that of site A carboxylate, due to the coordination to the cationic and Lewis-acidic Cu(II) ion. Therefore, one could easily predict the bonding selectivity of each carboxylate site for the first periodic transition metal units, according to an Irving-Williams order,[30] that is, site B preferably coordinates to Mn(II) and Fe(II) and site A to Cu(II) and Zn(II).

Scheme III.2

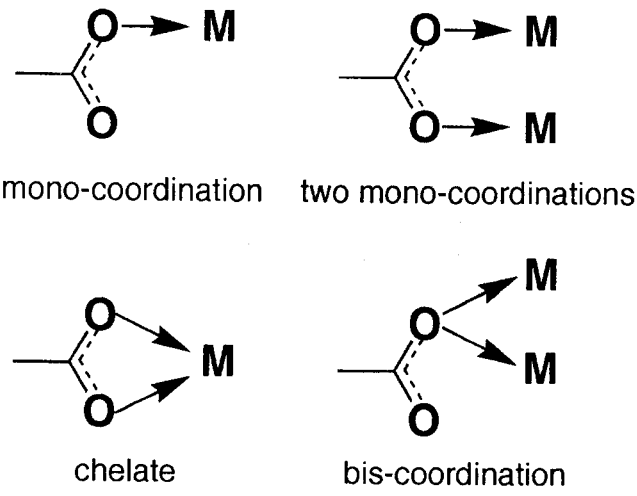

In this chapter, the author reports on a successful bond engineering of coordination polymers, $\{[MCu(2,4\text{-pydca})_2(H_2O)_4]\cdot 2H_2O\}_n$ (M = Co (**III-2**), Cu (**III-3**), Zn (**III-4**)), $[MCu(2,4\text{-pydca})_2(H_2O)_4]_n$ (M = Mn (**III-5**), Fe (**III-6**)), $\{[Cu(2,2'\text{-bpy})Cu(2,4\text{-pydca})_2]\cdot 3H_2O\}_n$

(**III-7**), and $[ZnCu(2,4\text{-pydca})_2(H_2O)_2(MeOH)_2]_n$ (**III-8**), from the combination of the metalloligand **III-1**·$2Et_3NH$ and various first-periodic transition metal ions or metal complex connector as the second building units (Scheme III.3). As expected, this metalloligand indicated the bonding selectivity for first periodic transition metal ions (Mn(II), Fe(II), Co(II), Cu(II), and Zn(II)), namely, control of bonding site could be realized. Also synthesized was coordination polymer of $[Ag_2Cu(2,4\text{-pydca})_2]_n$ (**III-9**), and their detailed structural features and magnetic susceptibilities were discussed.

Scheme III.3

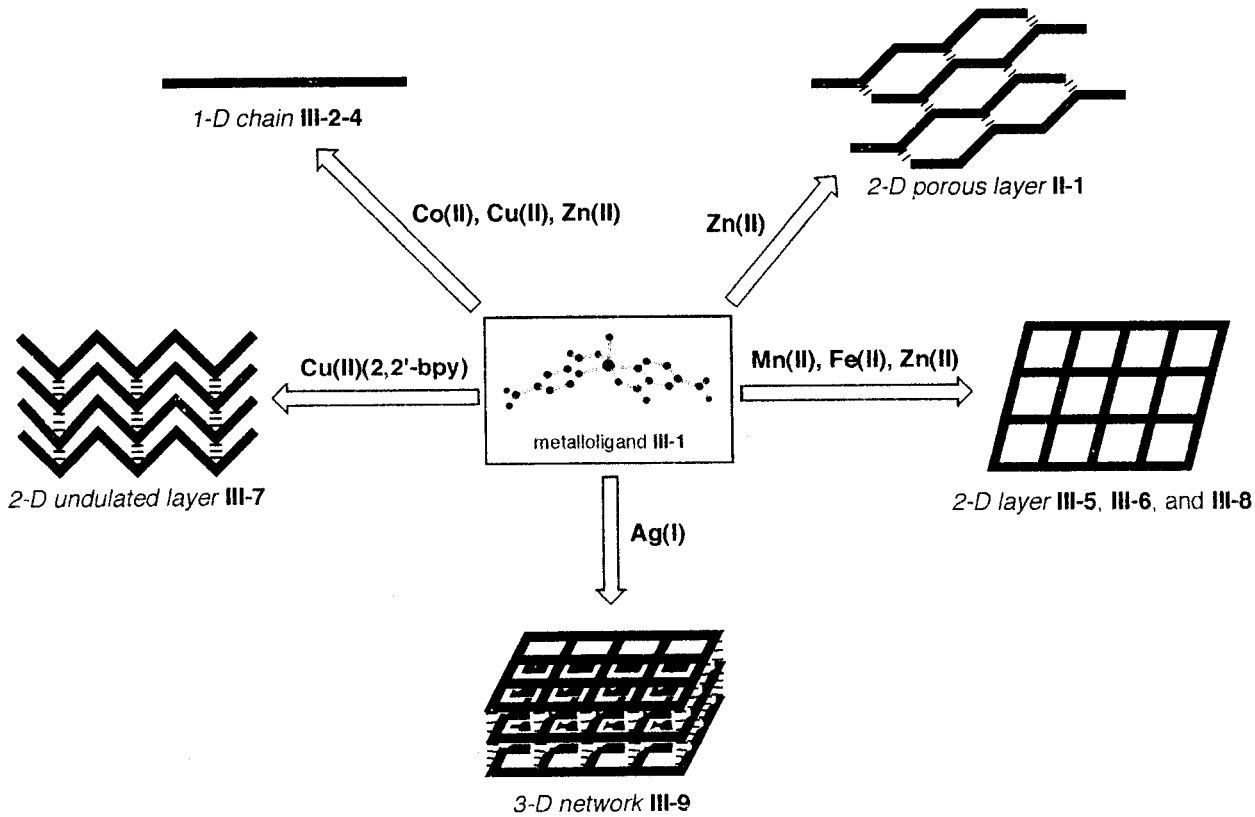

III. 2 Experimental

III. 2. 1 Physical Measurements

The physical measurements were performed as described in Chapter I.

III. 2. 2 Syntheses

Materials. $CuSO_4 \cdot 5H_2O$, $Cu(AcO)_2 \cdot H_2O$, $Zn(NO_3)_2 \cdot 6H_2O$, and triethylamine were obtained from Wako Co. 2,4-H_2pydca was purchased from Tokyo Kasei Industrial Co. $Co(BF_4)_2 \cdot 6H_2O$, $Fe(ClO_4)_2 \cdot 6H_2O$, and $AgBF_4$ were obtained from Aldrich Chemical Co. $MnSO_4 \cdot 5H_2O$ was obtained from Kanto Chemical Co. $\{[Cu(2,2'\text{-bpy})_2] \cdot 2Cl \cdot 6H_2O\}_n$ was prepared according to the literature.[31]

Synthesis of $[Cu(2,4\text{-Hpydca})_2(H_2O)_2]$ (III-1·2H). A methanol solution (300 mL) of 2,4-H_2pydca (3.34 g, 20.0 mmol) was added to an aqueous solution (50 mL) of $CuSO_4 \cdot 5H_2O$ (2.50 g, 10.0 mmol). The blue powder was collected by filtration, washed with methanol, and dried under vacuum for 1 h. Yield: 3.80 g (8.80 mmol, 88 %) Anal. Calcd for $C_{14}H_{12}CuN_2O_{10}$: C, 39.12; H, 2.35; N, 6.52. Found: C, 38.30; H, 2.78; N, 6.35. IR (KBr pellet): 3406 m, 1728 s, 1635 s, 1610 s, 1562 m, 1477 w, 1433 w, 1367 s, 1282 s, 1257 s, 1182 m, 1093 w, 1035 w, 997 w, 902 w, 873 w, 810 w, 765 w, 721 m, 686 m, 574 w, 530 w, 472 w cm^{-1}.

The single crystals suitable for X-ray analysis were prepared by the careful diffusion of a methanol solution of 2,4-H_2pydca into an aqueous solution of $CuSO_4 \cdot 5H_2O$.

Synthesis of $\{[Cu(2,4\text{-pydca})_2(H_2O)] \cdot 2Et_3NH\}$ (III-1·2Et$_3$NH). An excess triethylamine solution was added to a DMF suspension (30 mL) of **III-1**·2H (1.00 g, 2.31 mmol). To the resulting thick-blue solution was added an excess acetone solution. The blue powder was collected by filtration, washed with acetone, and dried under vacuum for 1 h. Yield: 1.37 g (2.22 mmol, 96 %) Anal. Calcd for $C_{26}H_{40}CuN_4O_9$: C, 50.68; H, 9.09; N, 6.54. Found: C, 50.46; H, 9.07; N, 6.31. IR (KBr pellet): 3379 mb, 2976 m, 2939 m, 2739 m, 2677 m, 2492 m, 1658 s,

1628 s, 1614 s, 1554 m, 1469 m, 1435 w, 1369 m, 1342 s, 1263 m, 1161 w, 1035 m, 825 w, 781 m, 734 m, 694 m cm^{-1}.

The single crystals suitable for X-ray analysis were prepared by the careful diffusion of an acetone solution into a DMF solution of **III-1**·2H and excess Et_3N.

Synthesis of $\{[CoCu(2,4\text{-pydca})_2(H_2O)_4]\cdot 2H_2O\}_n$ (III-2). An acetonitrile solution (20 mL) of $Co(BF_4)_2\cdot 6H_2O$ (218 mg, 0.640 mmol) was slowly diffused into an aqueous solution (20 mL) of **III-1**·$2Et_3NH$ (200 mg, 0.325 mmol). The bluish-purple crystals were obtained after a few weeks, washed with methanol, and dried in air. Yield: 58 mg (0.103 mmol, 32 %) Anal. Calcd for $C_{14}H_{18}CoCuN_2O_{14}$: C, 29.99; H, 3.24; N, 5.00. Found: C, 29.92; H, 3.18; N, 5.06. IR (KBr pellet): 3368 mb, 1645 s, 1616 s, 1558 m, 1477 w, 1392 m, 1336 s, 1257 m, 1095 w, 1035 w, 843 w, 773 m, 740 m, 690 m, 669 w, 574 w, 468 w cm^{-1}.

Synthesis of $\{[Cu_2(2,4\text{-pydca})_2(H_2O)_4]\cdot 2H_2O\}_n$ (III-3). A H_2O/methanol mixed solution (4 mL + 16 mL) of $Cu(AcO)_2\cdot H_2O$ (200 mg, 1.00 mmol) was slowly diffused into an aqueous solution (20 mL) of **III-1**·$2Et_3NH$ (616 mg, 1.00 mmol) at room temperature. After a week, the obtained blue crystals were filtered, washed with methanol, and dried in air. Yield: 98 mg (0.067 mmol, 17 %) Anal. Calcd for $C_{14}H_{18}Cu_2N_2O_{14}$: C, 29.74; H, 3.21; N, 4.95. Found: C, 30.17; H, 2.80; N, 5.02. IR (KBr pellet): 3373 mb, 1643 s, 1614 s, 1556 m, 1477 w, 1392 m, 1336 s, 1257 m, 1095 w, 1035 w, 841 w, 773 m, 740 m, 690 m, 584 w, 466 w cm^{-1}.

Synthesis of $\{[ZnCu(2,4\text{-pydca})_2(H_2O)_4]\cdot 2H_2O\}_n$ (III-4). A MeOH solution (10 mL) of $Zn(NO_3)_2\cdot 6H_2O$ (149 mg, 0.500 mmol) was slowly diffused into an aqueous solution (10 mL) of **III-1**·$2Et_3NH$ (308 mg, 0.500 mmol). After a few weeks, the obtained blue crystals were collected, washed with methanol, and dried in air. Yield: 240 mg (0.423 mmol, 85 %) Anal. Calcd for $C_{14}H_{18}CuN_2O_{14}Zn$: C, 29.64; H, 3.20; N, 4.94. Found: C, 29.63; H, 2.94; N, 4.94. IR (KBr pellet): 3350 mb, 1645 s, 1616 s, 1558 m, 1477 w, 1392 m, 1336 s, 1259 m, 1093 w, 1037 w, 881 w, 839 w, 775 m, 740 m, 690 m, 669 w, 617 w, 466 w cm^{-1}.

Synthesis of $[MnCu(2,4\text{-pydca})_2(H_2O)_4]_n$ (III-5). A H_2O/MeOH solution (4 mL + 16 mL) of $MnSO_4\cdot 5H_2O$ (242 mg, 1.00 mmol) was carefully diffused to an aqueous solution (20 mL) of **III-1**·$2Et_3NH$ (616 mg, 1 mmol). After a few weeks, the obtained purple crystals were

filtered, washed with methanol, and dried in air. Yield: 104 mg (0.200 mmol, 20 %) Anal. Calcd for $C_{14}H_{14}CuMnN_2O_{12}$: C, 32.29; H, 2.71; N, 5.38. Found: C, 31.86; H, 2.77; N, 5.30. IR (KBr pellet): 3383 mb, 3067 m, 1630 s, 1610 s, 1583 s, 1549 m, 1475 m, 1444 w, 1377 s, 1363 s, 1275 w, 1261 m, 1103 w, 1035 w, 825 w, 787 m, 733 m, 692 m, 569 w, 478 w cm^{-1}.

Synthesis of $[FeCu(2,4\text{-pydca})_2(H_2O)_4]_n$ (III-6). A MeOH solution (10 mL) of $Fe(ClO_4)_2 \cdot 6H_2O$ (182 mg, 0.500 mmol) was carefully diffused to an aqueous solution (10 mL) of **III-1**·$2Et_3NH$ (308 mg, 0.500 mmol). After a few weeks, the light-brown crystals were obtained with $Fe(OH)_2$. After filtration, the mixture was separated by hand, and crystals were washed with methanol, and dried in air. Yield: 62 mg (0.119 mmol, 24 %) Anal. Calcd for $C_{14}H_{14}CuFeN_2O_{12}$: C, 32.23; H, 2.71; N, 5.37. Found: C, 31.93; H, 2.70; N, 5.35. IR (KBr pellet): 3368 wb, 3211 wb, 3069 w, 1630 s, 1610 s, 1583 s, 1549 m, 1475 m, 1444 w, 1378 s, 1363 s, 1275 w, 1261 m, 887 w, 833 w, 787 m, 733 m, 713 m, 688 m, 572 w, 480 w cm^{-1}.

Synthesis of $\{[Cu(2,2'\text{-bpy})Cu(2,4\text{-pydca})_2]\cdot 3H_2O\}_n$ (III-7). A MeOH solution (20 mL) of $\{[Cu(2,2'\text{-bpy})_2]\cdot 2Cl\cdot 6H_2O\}$ (180 mg, 0.324 mmol) was added to a MeOH solution (20 mL) of **III-1**·$2Et_3NH$ (200 mg, 0.324 mmol). When resulting blue solution was allowed to stand for a day, the bluish-purple microcrystals were obtained, filtered, washed with methanol, and dried in air. Yield: 119 mg (0.178 mmol, 55 %) Anal. Calcd for $C_{24}H_{20}Cu_2N_4O_{11}$: C, 43.18; H, 3.021; N, 8.39. Found: C, 42.39; H, 2.93; N, 8.24. IR (KBr pellet): 3472 mb, 1643 s, 1608 s, 1556 m, 1471 m, 1448 w, 1383 m, 1342 s, 1273 w, 1261 m, 1157 w, 781 m, 772 m, 742 m, 731 w, 700 m, 667 w, 648 w, 445 w cm^{-1}.

The single crystals suitable for X-ray analysis were prepared by the careful diffusion of a MeOH solution of $\{[Cu(2,2'\text{-bpy})_2]\cdot 2Cl\cdot 6H_2O\}$ into a MeOH/ethyleneglycol mixed solution of **III-1**·$2Et_3NH$.

Synthesis of $[ZnCu(2,4\text{-pydca})_2(H_2O)_2(MeOH)_2]_n$ (III-8). The crystals suitable for X-ray analysis were prepared by the reaction of $Zn(NO_3)_2 \cdot 6H_2O$ with **III-1**·$2Et_3NH$ in a MeOH solution. Anal. Calcd for $C_{16}H_{18}CuN_2O_{12}Zn$: C, 34.36; H, 3.24; N, 5.01. Found: C, 34.30; H, 3.22; N, 5.08.

Synthesis of $[Ag_2Cu(2,4\text{-pydca})_2]_n$ (III-9). A MeOH solution (10 mL) of **III-1**·$2Et_3NH$ (154 mg, 0.250 mmol) was carefully diffused to an aqueous solution (10 mL) of $AgBF_4$ (98 mg, 0.500 mmol). After a few days, the obtained purple crystals were filtered, washed with methanol, and dried under vacuum for 1 hour. Yield: 133 mg (0.218 mmol, 87 %) Anal. Calcd for $C_{14}H_6Ag_2CuN_2O_8$: C, 27.59; H, 0.99; N, 4.60. Found: C, 27.21; H, 1.16; N, 4.53. IR (KBr pellet): 3445 mb, 1633 s, 1608 s, 1585 s, 1547 s, 1477 m, 1373 s, 1342 s, 1263 m, 1190 w, 1086 m, 1039 w, 951 w, 875 w, 829 w, 775 m, 736 m, 688 m, 437 w cm^{-1}.

III. 2. 3 X-Ray Structure Determination

Single crystals of all compounds were mounted on a glass fiber and coated with epoxy resin. For **III-1**·$2Et_3NH$, **III-2**, and **III-5-9**, all measurements were made on a Rigaku RAXIS-RAPID imaging plate diffractometer with graphite monochromated Mo-Kα radiation. For **III-1**·2H, all measurements were made on a Rigaku AFC7R diffractometer with graphite monochromated Mo-Kα radiation and a rotating anode generator. Cell constants and an orientation matrix for data collection were obtained from a least-squares refinement using the setting angles of 25 carefully centered reflections in the range $29.69 < 2\theta < 29.96$ °. For **III-3** and **III-4**, X-ray data collections were carried out by a Rigaku Mercury charge coupled device (CCD) system with graphite monochromated Mo-Kα radiation. For **III-1**·2H, the structure was solved by a direct method using the SHELXS86 program[32] and expanded using Fourier techniques.[33] For **III-1**·$2Et_3NH$ and **III-2-8**, the structures were solved by a direct method using the SIR92 program[34] and expanded using Fourier techniques.[33] For **III-9**, the structure was solved by heavy-atom Patterson methods using the PATTY program[35] and expanded using Fourier techniques.[33] In all complexes, the non-hydrogen atoms were refined anisotropically. All hydrogen atoms, which were placed in idealized positions, were included but not refined. In the only case of **III-1**·$2Et_3NH$, the H(19) (triethylammonium proton) was observed from a Fourier map and fixed. The refinements were carried out using full-matrix least squares techniques. Crystal data and details of the structure determinations are summarized in Table III.1. All calculations were performed using the teXsan[36] crystallographic software package of Molecular Structure Corporation.

Table III.1a. Crystallographic Data for $\{[Cu(2,4\text{-pydca})_2(H_2O)]\cdot 2Et_3NH\}$ (**III-1**·$2Et_3NH$), $[Cu(2,4\text{-Hpydca})_2(H_2O)_2]$ (**III-1**·2H), $\{[CoCu(2,4\text{-pydca})_2(H_2O)_4]\cdot 2H_2O\}_n$ (**III-2**), and $\{[Cu_2(2,4\text{-pydca})_2(H_2O)_4]\cdot 2H_2O\}_n$ (**III-3**).

compounds	**III-1**·$2Et_3NH$	**III-1**·2H	**III-2**	**III-3**
formula	$C_{26}H_{40}N_4CuO_9$	$C_{14}H_{12}N_2CuO_{10}$	$C_{14}H_{18}N_2CoCuO_{14}$	$C_{14}H_{18}N_2Cu_2O_{14}$
fw	616.17	431.80	560.78	565.39
crystal system	monoclinic	triclinic	monoclinic	monoclinic
a, Å	18.546(3)	10.146(6)	14.7281(9)	14.683(2)
b, Å	10.511(2)	11.319(6)	8.3905(4)	8.398(1)
c, Å	15.050(2)	7.218(3)	15.471(1)	15.4555(2)
α, deg		97.41(4)		
β, deg	95.404(4)	94.74(4)	93.643(2)	93.0221(4)
γ, deg		73.69(5)		
V, Å^3	2920.9(8)	788.0(7)	1907.9(2)	1903.2(2)
space group	*C2/c* (No.15)	$P\bar{1}$ (No.2)	$P2_1/a$ (No.14)	$P2_1/a$ (No.14)
Z	4	2	4	4
ρ(calcd), g·cm^{-3}	1.401	1.820	1.952	1.973
F(000)	1300.00	438.00	1136.00	1144.00
μ(Mo Kα), cm^{-1}	8.05	14.50	20.67	23.17
diffractometer	RAXIS-RAPID	AFC7R	RAXIS-RAPID	CCD
radiation (λ, Å)	0.71069	0.71069	0.71069	0.71069
temp., ℃	25	25	25	25
GOF	1.446	1.472	1.073	1.893
no. of obsd data	3279 (all data)	3416 (all data)	3983 (all data)	4049 (all data)
no. of variables	182	244	289	289
R^a ($I > 2.00\sigma(I)$, all data)	0.0359, 0.0386	0.0399, 0.0452	0.0410, 0.0640	0.0380, 0.0460
R_w^b ($I > 2.00\sigma(I)$, all data)	0.0537, 0.0545	0.0603, 0.0617	0.0531, 0.0586	0.0650, 0.0711

[a] $R = \Sigma\|\|Fo| - |Fc|\|/\Sigma|Fo|$. [b] $R_w = [(\Sigma w\,(|Fo| - |Fc|)^2/\Sigma wFo^2)]^{1/2}$.

Table III.1b. Crystallographic Data for $\{[ZnCu(2,4\text{-pydca})_2(H_2O)_4]\cdot 2H_2O\}_n$ (**III-4**), $[MnCu(2,4\text{-pydca})_2(H_2O)_4]_n$ (**III-5**), $[FeCu(2,4\text{-pydca})_2(H_2O)_4]_n$ (**III-6**), and $\{[Cu(2,2'\text{-bpy})Cu(2,4\text{-pydca})_2]\cdot 3H_2O\}_n$ (**III-7**).

compounds	**III-4**	**III-5**	**III-6**	**III-7**
formula	$C_{14}H_{18}N_2CuZnO_{14}$	$C_{14}H_{14}N_2CuMnO_{12}$	$C_{14}H_{12}N_2CuFeO_{12}$	$C_{24}H_{20}N_4Cu_2O_{11}$
fw	567.23	520.75	521.66	667.53
crystal system	monoclinic	triclinic	triclinic	orthorhombic
a, Å	14.779(2)	7.898(1)	7.7656(5)	35.954(2)
b, Å	8.364(2)	8.005(1)	7.9258(6)	56.323(2)
c, Å	15.4923(3)	7.580(1)	7.5144(5)	5.1710(2)
α, deg		97.325(4)	97.499(4)	
β, deg	93.8722(5)	90.874(7)	91.663(3)	
γ, deg		112.07(1)	112.495(4)	
V, Å^3	1910.7(3)	439.4(1)	422.08(5)	10471.4(8)
space group	$P2_1/a$ (No.14)	$P\bar{1}$ (No.2)	$P\bar{1}$ (No.2)	*Fdd2* (No.43)
Z	4	1	1	16
ρ(calcd), g·cm^{-3}	1.972	1.968	2.052	1.694
F(000)	1148.00	262.00	263.00	5408.00
μ(Mo Kα), cm^{-1}	24.51	20.02	21.95	16.94
diffractometer	CCD	RAXIS-RAPID	RAXIS-RAPID	RAXIS-RAPID
radiation (λ, Å)	0.71069	0.71069	0.71609	0.71069
temp., ℃	25	25	25	-40
GOF	1.407	1.188	1.432	0.891
no. of obsd data	3903 (all data)	1715 (all data)	1764 (all data)	3238 (all data)
no. of variables	289	139	139	371
R^a ($I > 2.00\sigma(I)$, all data)	0.0416, 0.0569	0.0466, 0.0756	0.0386, 0.0467	0.0444, 0.0568
R_w^b ($I > 2.00\sigma(I)$, all data)	0.0609, 0.0650	0.0556, 0.0622	0.0565, 0.0586	0.0538, 0.0579

[a] $R = \Sigma\||Fo| - |Fc|\|/\Sigma|Fo|$. [b] $R_w = [(\Sigma w\,(|Fo| - |Fc|)^2/\Sigma wFo^2)]^{1/2}$.

Table III.1c Crystallographic Data for $[ZnCu(2,4\text{-pydca})_2(H_2O)_2(MeOH)_2]_n$ (**III-8**) and $[Ag_2Cu(2,4\text{-pydca})_2]_n$ (**III-9**).

compound	**III-8**	**III-9**
formula	$C_{16}H_{18}CuN_2O_{12}Zn$	$C_{14}H_6Ag_2CuN_2O_8$
fw	559.25	609.49
crystal system	triclinic	triclinic
a, Å	7.5451(9)	8.7317(7)
b, Å	10.942(2)	8.7642(6)
c, Å	6.7415(8)	5.1250(5)
α, deg	98.482(5)	93.678(5)
β, deg	113.109(9)	99.508(3)
γ, deg	72.188(5)	108.496(2)
V, Å^3	487.1(1)	363.97(5)
space group	$P\bar{1}$ (No.2)	$P\bar{1}$ (No.2)
Z	1	1
ρ(calcd), g·cm^{-3}	1.906	2.780
F(000)	283.00	291.00
μ(MoKα), cm^{-1}	23.95	41.59
diffractometer	RAXIS-RAPID	RAXIS-RAPID
radiation (λ, Å)	0.71069	0.71069
temp., ℃	25	25
GOF	1.265	1.159
no. of obsd data	2002 (all data)	1562 (all data)
no. of variables	148	124
R^a (I > 2.00σ(I), all data)	0.0387, 0.0496	0.0290, 0.0317
$R_w{}^b$ (I > 2.00σ(I), all data)	0.0512, 0.0542	0.0400, 0.0414

[a] $R = \Sigma||Fo| - |Fc||/\Sigma|Fo|$. [b] $R_w = [(\Sigma w\,(|Fo| - |Fc|)^2/\Sigma wFo^2)]^{1/2}$.

III. 3 Results and Discussion

III. 3. 1 Preparation of a Soluble Metalloligand.

Reaction of Cu(II) ion with 2,4-H_2pydca ligand in an H_2O/MeOH solution affords a novel metalloligand **III-1**·2H, whose IR spectrum shows a ν(C=O) stretching band of the 4-COOH groups at 1728 cm^{-1} and $\nu_{as}(COO)/\nu_s(COO)$ ones of the 2-COO^- groups at 1653/1367 cm^{-1}. On the other hand, **III-1**·2Et_3NH represents only $\nu_{as}(COO)/\nu_s(COO)$ stretching bands at 1658, 1628/1369, 1342 cm^{-1}, indicating that all substituent groups take an anionic mode, COO^-. Therefore, more polar metalloligand **III-1**·2Et_3NH than **III-1**·2H is soluble in polar solvents such as H_2O, MeOH, and DMF. Moreover, the difference between the crystal packing forms of **III-1**·2H and **III-1**·2Et_3NH influences solubility (vide infra).

Table III.2. C-O Bond Distances, Difference, and Charge Type of 2- and 4-Carboxylates for **III-1**·2H and **III-1**·2Et_3NH.

Compounds		Bond lengths (Å)	Difference (Å)	Type (Charge)
III-1·2H	I	1.265(3), 1.240(3)	0.025	COO^- (delocalize)
	II	1.261(3), 1.240(3)	0.021	COO^- (delocalize)
	III	1.317(3), 1.207(3)	0.110	COOH (localize)
	IV	1.311(3), 1.202(4)	0.109	COOH (localize)
III-1·2Et_3NH	I	1.285(2), 1.210(2)	0.075	COO^- (localize)
	II	1.256(2), 1.215(2)	0.041	COO^- (delocalize)

III. 3. 2 Crystal Structures

III. 3. 2. 1 Crystal Structures of Metalloligands of [Cu(2,4-Hpydca)$_2$(H$_2$O)$_2$] (III-1·2H) and {[Cu(2,4-pydca)$_2$(H$_2$O)]·2Et$_3$NH} (III-1·2Et$_3$NH).

The four bonding modes of the metalloligand **III-1** are classified as follows. The two metalloligands (**III-1**·2H and **III-1**·2Et$_3$NH) and nine coordination polymers, **III-2-9** and **II-1**, are examined in relation to the metalloligand's multi-functionality. Regular coordination bonds are represented by CB-A (Coordination Bond) and weak coordination bonds by CB-B. Especially, in semi-chelating bonds, longer coordination bonds are indicated by CB-A'. All hydrogen bonds between the oxygen atoms of each carboxylate group and metal-coordinated solvent molecules are expressed by HB-X (X = A, B, C, •••) (Hydrogen Bond). Other hydrogen bonds between metal-coordinated and free solvents are not defined.

An ORTEP view around the Cu(II) center of **III-1**·2H is shown in Figure III.1(a) with a numbering scheme. The coordination environment of the Cu(II) center can be described as distorted elongated octahedral with two coordinated H$_2$O molecules in the axial position and the two nitrogen and the two oxygen donors of the chelating 2,4-Hpydca$^-$ ligands occupying the basal sites. The Cu(II) center is displaced on the basal oxygen and nitrogen array. The Cu-O(9) and Cu-O(10) bond lengths of 2.684(2) and 2.524(2) Å, respectively, are apparently longer than the 2.39(1) Å Cu-O bond found for the axially coordinated H$_2$O molecules in [Cu(pyrazinecarboxylate)$_2$(H$_2$O)$_2$][37] and similar to the corresponding value of 2.506(3) Å for {[Cu(pyridazin-1-ium-3.6-dicarboxylate)$_2$(H$_2$O)$_2$]·2H$_2$O}.[38] The planes of the two 2,4-Hpydca$^-$ ligands are canted *ca.* 16 ° with respect to each other. Each C-O bond distance of the 2-position in **III-1**·2H is similar, while each C-O bond distance of the 4-position is apparently different from each other (Table III.2), indicative of a COO$^-$ mode with delocalizing negative charge at the 2-position and a COOH mode at the 4-position. No coordination is observed for the COOH groups of the 4-position, which, however, form hydrogen bonds with coordinated H$_2$O molecules (HB-A : av. 2.590 Å) and 4-COOH units (HB-B : av. 2.952 Å) of another metalloligands. The coordination-free oxygen atoms of the 2-COO$^-$ groups also link to the coordinated H$_2$O molecules by hydrogen bonds (HB-C : av.

2.730 Å). As a result, a hydrogen bonding 3-D network is constructed as shown in Figure III.1(b). This complex scarcely solves in common solvents such as H_2O, alcohol, acetonitrile, DMF, $CHCl_3$, CH_2Cl_2, and diethylether, because of quasi 3-D polymer structure via three types of hydrogen bonds.

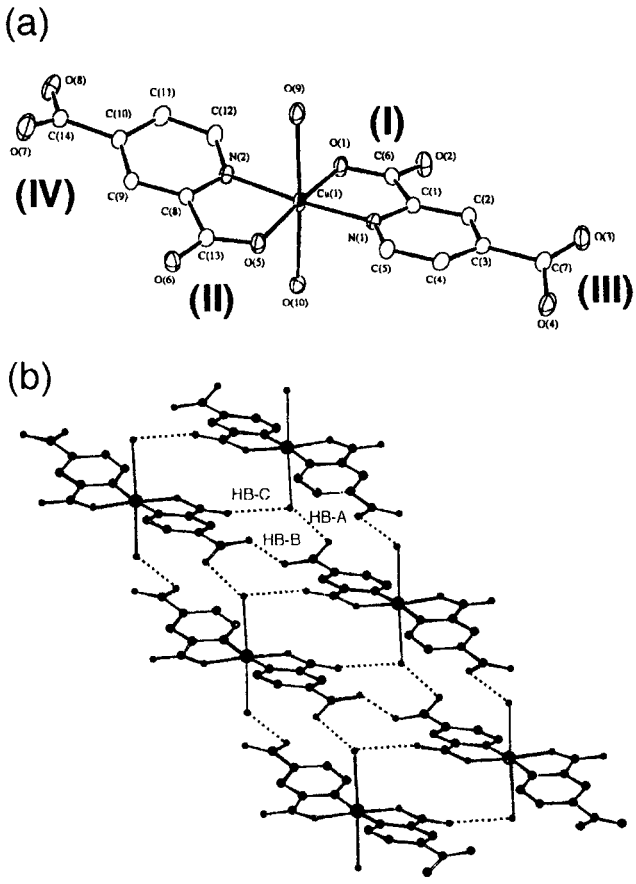

Figure III.1. (a) ORTEP drawing around a Cu(II) center of **III-1**·2H at the 30 % probability level. In regard to all figures except for Figure III.2(a), the hydrogen atoms are omitted for clarity. (b) View of the hydrogen bonding network of **III-1**·2H.

In order to decrease the hydrogen bonding interaction between the metalloligands, the author tried to deprotonate the 4-COOH groups of **III-1**·2H by using a Et_3N amine and succeeded in the synthesis of **III-1**·2Et_3NH. An ORTEP view around the Cu(II) center of **III-1**·2Et_3NH is shown in Figure III.2(a) with a numbering scheme. The Cu(II) ion is based on a distorted square-pyramidal environment with two nitrogen atoms of pyridines and two oxygen atoms of 2-COO^- groups in the

basal plane and one oxygen atom of H_2O at the apical site, which is apparently different from **III-1**·2H. The Cu-O(5) bond length of 2.141(2) Å is significantly shorter than the corresponding values of 2.204(3), 2.257(2), and 2.212(6) Å, which were found for the apical H_2O and EtOH molecules in the square-pyramidal complexes, $[Cu(hfacac)_2(H_2O)]$,[39] $\{[Cu(2\text{-methylpyrazine-5-carboxylate})_2(H_2O)_2]\cdot 3H_2O\}$,[17] and $[Cu(C_3F_7C(O)CHC(O)C_3F_7)_2(EtOH)]$,[40] respectively. However, the bond length is close to those of the 2.143(3) and 2.080(5) Å Cu-O bonds found for the apical-coordinated H_2O molecule in $[Cu(2\text{-quinolinecarboxylate})_2(H_2O)]$[41] and $\{[Cu(4\text{-amino-3,5,6-trichloropyridine-2-carboxylate})_2(H_2O)]\cdot 2H_2O\}$,[42] respectively, which have the distorted square-pyramidal environment. The Cu(II) center is displaced *ca.* 0.3 Å above the basal oxygen and nitrogen array. The planes of the two 2,4-pydca^{2-} ligands are canted *ca.* 38 °. Similar distortion was observed in complex $\{[Cu(2\text{-methylpyrazine-5-carboxylate})_2(H_2O)_2]\cdot 3H_2O\}$.[17] Each C-O bond distance of the 4-position is similar, indicative of COO^- modes with delocalized charge at the 4-position, while a negative charge of the 2-position localizes at the oxygen atom coordinating to the Cu(II) ion (see Table III.2), which affects the hydrogen bonding ability of 2-COO^- groups for coordinated H_2O molecules in a crystal. In the case of **III-1**·2H, coordination-free oxygen atoms of the 2-COO^- groups interact with protic hydrogen atoms of coordinated H_2O molecules, which leads to the delocalization of an anionic charge of 2-COO^-. On the other hand, corresponding oxygen atoms of **III-1**·2Et_3NH participate entirely in neither coordination nor hydrogen bonds, which displaces an anionic charge to the coordinated oxygen atoms. The nitrogen atom of the Et_3N molecule undergoes the protonation, which was confirmed by the X-ray diffraction analysis (N-H = 0.98 Å and O-H = 1.71 Å). No coordination is observed for the COO^- groups of the 4-position, which, however, give hydrogen bonds with coordinated H_2O molecules (HB-A : 2.679(2) Å) and free Et_3NH molecules (HB-B : 2.683(2) Å). In compared with **III-1**·2H, the coordination-free oxygen atoms of the 2-COO^- groups in the complex **III-1**·2Et_3NH afford no hydrogen bonding interaction. As a result, a hydrogen-bonding 1-D network is constructed as shown in Figure III.2(b). Therefore, this complex is soluble in H_2O, MeOH, and DMF, which is in contrast with complex **III-1**·2H.

The most important structural feature of **III-1**·$2Et_3NH$ is the presence of two free 2- and 4-carboxylate donors, which enables **III-1**·$2Et_3NH$ to be used as metalloligand that can be linked by other transition metals and yield novel bimetallic polymers.

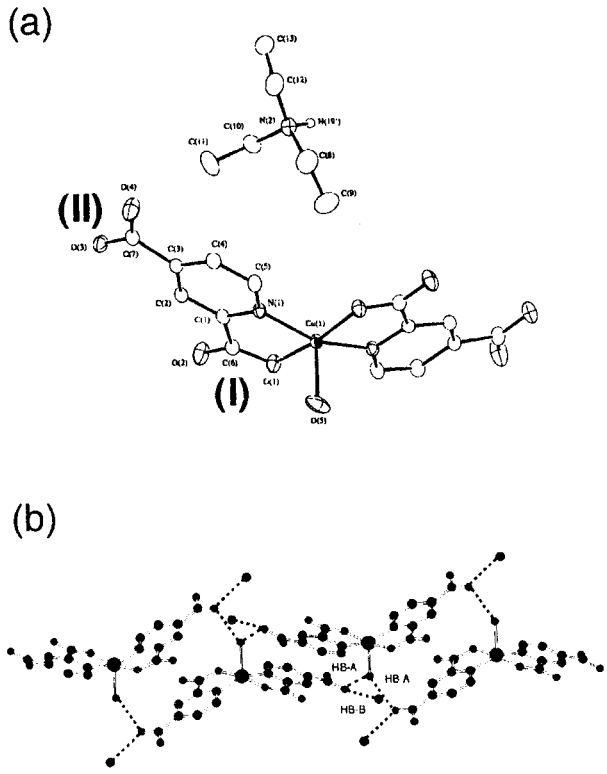

Figure III.2. (a) ORTEP drawing around a Cu(II) center of **III-1**·$2Et_3NH$ at the 30 % probability level. All hydrogen atoms except for Et_3NH are omitted for clarity. (b) View of the hydrogen-bonding network of **III-1**·$2Et_3NH$. The carbon atoms of Et_3NH are omitted for clarity.

VI. 3. 2. 2 Crystal Structures of 1-D Chain Polymers, $\{[MCu(2,4\text{-}pydca)_2(H_2O)_4]\cdot 2H_2O\}_n$ (M = Co (III-2), Cu (III-3), Zn (III-4)).

An ORTEP view around the metal centers of **III-2** is shown in Figure III.3(a) with a numbering scheme. In this 1-D polymer, the metalloligand **III-1** functions as a linear-type bridge. The coordination environment of each Cu(II) center consists of two oxygen donors and two nitrogen donors from 2,4-$pydca^{2-}$ chelating ligands and one H_2O oxygen donor. The distorted square

pyramidal geometry may be described as a basal plane associated with N(1), N(2), O(1), and O(5) from 2,4-pydca^{2-} ligands, having Cu-O and Cu-N bond lengths of av. 1.957 and 1.983 Å, respectively, with the apical position occupied by one H_2O oxygen donor O(9). The Cu-O(9) distance is 2.268(3) Å, which is remarkably long compared with 2.141(2) Å of **III-1**·2Et_3NH. On the other hand, the Co(II) center is based on a distorted square pyramidal environment with two oxygen donors of H_2O molecules (Co-O(H_2O) = av. 2.007 Å) and two oxygen donors of 4-carboxylate groups of metalloligands (Co-O(4-carboxylate) = av. 1.975 Å) in the basal plane and one oxygen donor of another H_2O molecule at the apical site (Co-O(12) = 2.155(3) Å). It is noteworthy that the coordination environment of **III-1** used as a building block is retained even in the extended structure.

In the solid state, as shown in Figure III.3(b), alternating Co(II) centers and **III-1** by 4-carboxylate bridges (CB-A : av. 1.975 Å) form a 1-D chain, in which each pyridine ring of the 2,4-pydca^{2-} ligands is parallel to each other. The intrachain Cu•••Co distance is *ca.* 8.80 Å, while the shortest interchain Cu•••Cu and Co•••Co distances are *ca.* 5.34 and 4.43 Å, respectively. The Co(II)-Cu(II) coordination polymer chains are bound to each other by interpolymer hydrogen bonds between Cu- or Co-coordinated H_2O molecules and oxygen atoms of 2-carboxylate groups (HB-A : 2.795(4) Å and HB-B : 2.879(4) Å for Cu-coordinated H_2O; HB-C : 2.724(4) Å for Co-coordinated H_2O), and between Co-coordinated H_2O molecules and oxygen atoms of 4-carboxylate groups (HB-D : 2.723(4) Å, HB-E : 2.680(4) Å), as shown in Figure III.3(c). The free H_2O molecules are located between the chains and linked by hydrogen bonds with coordinated H_2O molecules at the Co(II) ions and oxygen atoms of 2-/4-carboxylate, respectively (2.703-3.022 Å).

A series of isostructural coordination polymers could be obtained by using other metal(II) ions such as Cu(II) and Zn(II). Generally, the structures of the coordination polymers are quite sensitive to the M^{2+} ions employed, however, three similar coordination networks $\{[MCu(2,4\text{-pydca})_2(H_2O)_4]\cdot 2H_2O\}_n$ (M = Co (**III-2**), Cu (**III-3**), and Zn (**III-4**)) were successfully obtained in this case.

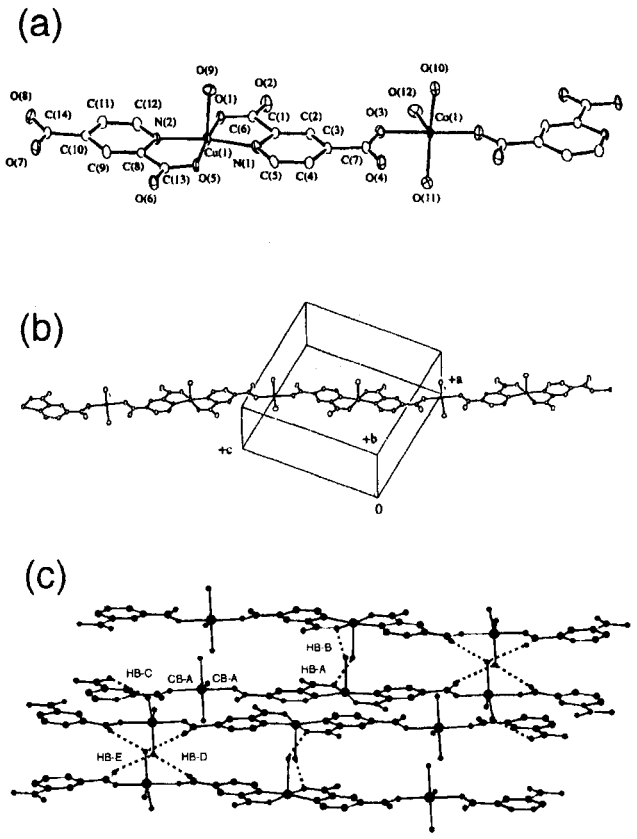

Figure III.3. (a) ORTEP drawing around Cu(II) and Co(II) centers of **III-2** at the 30 % probability level. (b) ORTEP view of the 1-D chain structure of **III-2** at the 30 % probability level. (c) View of the hydrogen-bonding network among the 1-D chains of **III-2**.

VI. 3. 2. 3 Crystal Structures of 2-D Polymers, $[MCu(2,4\text{-pydca})_2]_n$ (M = Mn (III-5), Fe (III-6)), $\{[Cu(2,2'\text{-bpy})Cu(2,4\text{-pydca})_2]\cdot 3H_2O\}_n$ (III-7), and $[ZnCu(2,4\text{-pydca})_2(H_2O)_2(MeOH)_2]_n$ (III-8).

Detailed crystal structure of **II-1** has been explained in Chapter II. In order to compare the bonding mode of the metalloligand **III-1** in **II-1** with those of other novel coordination polymers reported in this chapter, the author shows only bonding scheme around the metalloligand **III-1** in **II-1** again (Figure III.4). The 4-carboxylate groups of **III-1** bridge the Zn(II) ions by semi-chelating and mono-coordination modes (CB-A : av. 2.070 Å, CB-A' : 2.351(3) Å), and form the hydrogen bonds with Zn-coordinated H_2O molecules (HB-A : 2.665(4) Å). On the other hand, the 2-carboxylate groups of **III-1** are coordination-free but support the infinite 2-D framework by hydrogen bonds (HB-B : 2.818(4) Å) in addition to H_2O bridge between Zn(II) and Cu(II) ions. Each 2-D sheet is linked by other hydrogen bonds between Zn-coordinated H_2O molecules and the oxygen atoms of 2- or 4-carboxylate groups (HB-C : 2.744(4) Å, HB-D : 2.713(5) Å, HB-E : 2.764(4) Å).

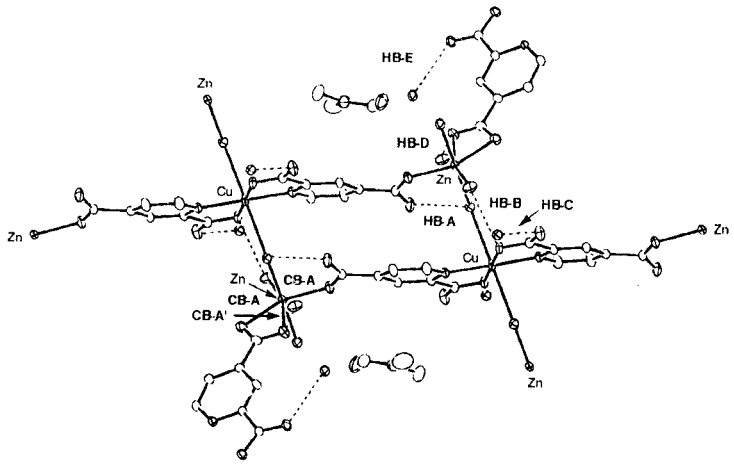

Figure III.4. ORTEP drawing of the bonding mode of **III-1** in **II-1**.

An ORTEP view around the metal centers of **III-5** is shown in Figure III.5(a) with a numbering scheme. In a crystal of **III-5**, the metalloligand **III-1** functions as a tetradentate bridge, which is in contrast to 1-D polymers **III-2-4**. Each Cu(II) atom resides on an inversion center in a 4

+ 2 pseudo-octahedral coordination sphere, with the equatorial sites occupied by two symmetry-equivalent chelating 2,4-pydca^{2-} ligands (Cu-O(1) = 1.936(3) Å and Cu-N(1) = 1.995(3) Å). The axial sites are occupied by the oxygen atoms of 4-carboxylate parts from the other symmetry-independent metalloligand moieties (Cu-O(4*) = 2.712(4) Å). On the other hand, the Mn(II) center is based on a distorted, slightly elongated octahedral environment with two oxygen donors of H_2O molecules (Mn-O(6) = 2.185(3) Å) and two oxygen donors of 2-carboxylate groups of the metalloligands (Mn-O(2) = 2.198(3) Å) in the basal plane and two oxygen donors of another H_2O molecules at the axial site (Mn-O(5) = 2.217(3) Å). The coordination environment of **III-1** used as a building block changes from distorted square pyramidal to elongated octahedral geometry by release of apical H_2O molecule and attack of carboxylate oxygen atoms, which is in contrast to those observed for **III-2-4**.

The 2-carboxylate groups of **III-1** bridge the Mn(II) ions (CB-A : 2.198(3) Å) to form a 1-D zigzag chain structure as shown in Figure III.5(b), in which the intrachain Cu•••Mn distance is *ca.* 5.15 Å. These chains are connected by two kinds of weak interactions: (i) weak coordination bond between the Cu(II) ions and the oxygen atoms at the 4-carboxylate (CB-B : 2.712(4) Å) and (ii) hydrogen bond between coordinated H_2O molecules at the Mn(II) centers and the oxygen atoms at the 4-carboxylate (HB-A 2.867(4) Å), resulting in a 2-D thick sheet-like structure as shown in Figures III.5(c) and III.5(d). The shortest interchain Cu•••Cu, Cu•••Mn, and Mn•••Mn distances are *ca.* 7.90, 8.01, and 7.90 Å, respectively. Each 2-D sheet is also linked by hydrogen bonds between coordinated H_2O molecules at the Mn(II) ions and oxygen atoms of 4-carboxylate (HB-B, -C, and -D : 2.827(4), 2.853(5), and 2.690(5) Å) (Figures III.5(c) and III.5(d)). The shortest intersheet Cu•••Mn distance is *ca.* 5.85 Å. A Fe(II)-Cu(II) mixed-metallic coordination polymer **III-6** is isostructural with **III-5**. The intrachain Cu•••Fe, interchain Cu•••Cu, Cu•••Fe, Fe•••Fe, and intersheet Cu•••Fe distances are *ca.* 5.09, 7.77, 7.81, 7.77, and 5.81 Å, respectively.

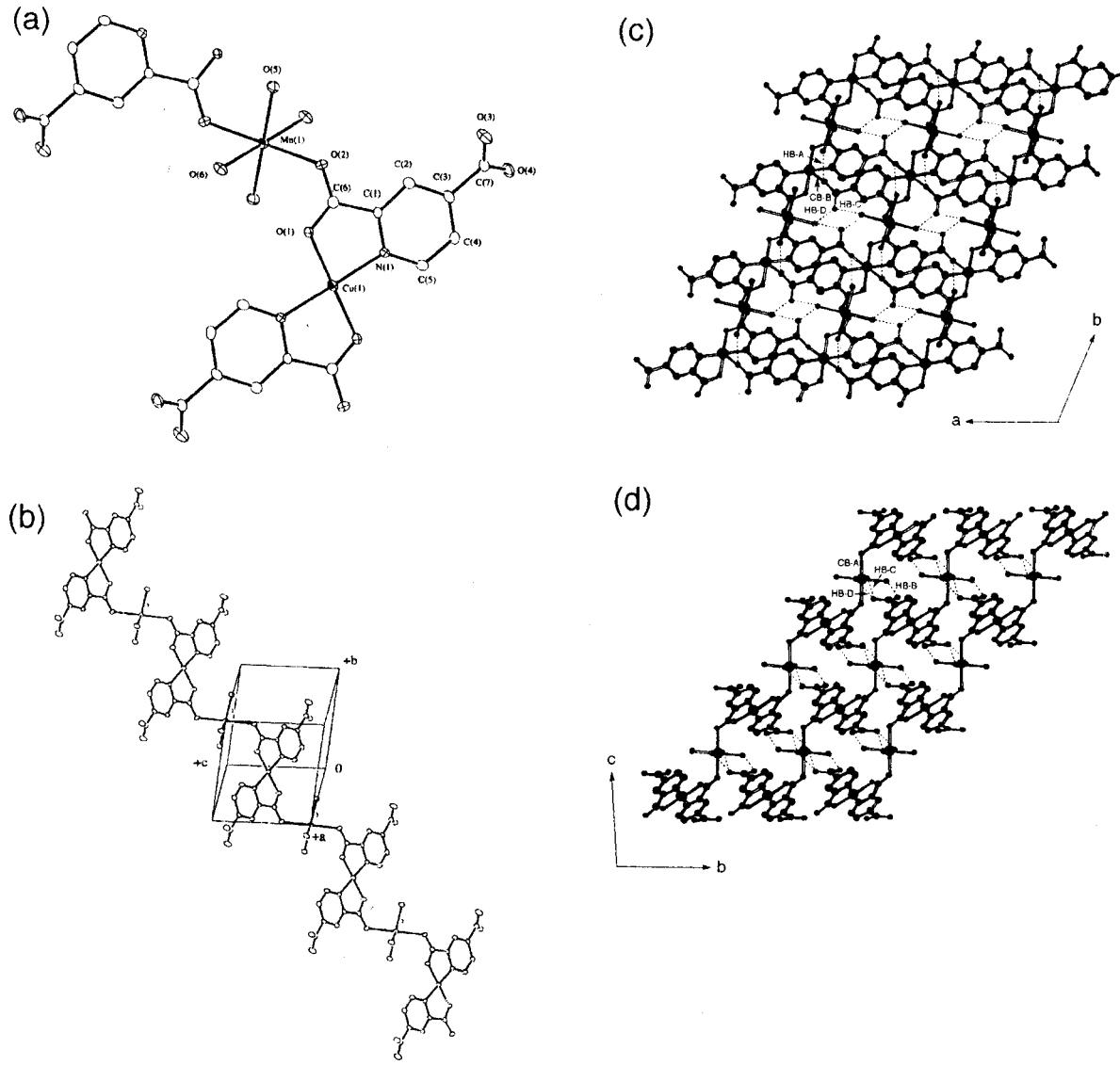

Figure III.5. (a) ORTEP drawing around Cu(II) and Mn(II) centers of **III-5** at the 30 % probability level. (b) ORTEP view of the 1-D zigzag chain structure of **III-5** at the 30 % probability level. (c and d) View of the hydrogen-bonding network among the 1-D chains of **III-5** along the *c*- (c) and *a*-axes (d).

An ORTEP view around the Cu(II) centers of **III-7** is shown in Figure III.6(a) with a numbering scheme. Although the metalloligand **III-1** in **III-7** also functions as the tetradentate bridge, its coordination mode is slightly different from those of **III-5** and **III-6**. In a crystal, there

are two kinds of Cu(II) ions. The coordination environment of each Cu(1) center consists of two oxygen donors and two nitrogen donors from 2,4-pydca^{2-} chelating ligands and two oxygen donors from 2-carboxylate parts of another ligands. The elongated octahedral geometry may be described as a basal plane associated with N(1), N(2), O(1), and O(5) from 2,4-pydca^{2-} ligands, having Cu-O and Cu-N bond lengths of av. 1.944 and 1.963 Å, respectively, with the axial positions occupied by two oxygen donors of O(2*) and O(6*) from 2-carboxylate parts of another ligands (Cu-O = av. 2.760 Å). Other (Cu(2)) has a pentagonal environment with two nitrogen donors from one 2,2'-bpy (Cu-N = av. 1.985 Å), one oxygen donor from 4-carboxylate of the metalloligand **III-1** (Cu(2)-O(8***) = 1.924(4) Å), and two oxygen donors from 4-carboxylate of another one by a semi-chelating mode (Cu(2)-O(3) = 2.608(5) Å and Cu(2)-O(4) = 1.933(5) Å).

The 4-carboxylate groups of **III-1** bridge Cu(2) ions in mono-coordination and semi-chelating modes (CB-A : av. 1.929 Å, CB-A' : 2.608(5) Å) to form a 1-D zigzag chain structure. The Cu(1)•••Cu(2)•••Cu(1) and Cu(2)•••Cu(1)•••Cu(2) angles are *ca.* 79 and 173 °, respectively. The intrachain Cu(1)•••Cu(2) distance is av. 8.75 Å. These zigzag chains are linked by weak coordination bonds between the Cu(1) ions and oxygen atoms of 2-carboxylate of neighboring metalloligands **III-1** (CB-B : av. 2.760 Å) to form a 2-D undulated sheet as shown in Figures III.6(b) and III.6(c). The interchain Cu(1)•••Cu(1) distance is *ca.* 5.17 Å, which is related to the antiferromagnetic interaction as mentioned in the section of magnetic properties. No bonding interaction is observed between the 2-D undulated sheets. The shortest intersheet Cu•••Cu bond distance (Cu(2)•••Cu(2)) is *ca.* 7.91 Å. The H_2O molecules are included between the 2-D sheets and coordinated to the oxygen atoms of the metalloligands **III-1** by hydrogen bonds (2.81-3.05 Å). In addition, the hydrogen-bonding interactions between free H_2O molecules are observed (2.76-3.03 Å). In analogy with **III-5** and **III-6**, the metalloligand **III-1** slightly changes its own geometry, while metal complex of $\{[Cu(2,2'\text{-bpy})_2]\cdot 2Cl\cdot 6H_2O\}$ loses one 2,2'-bpy ligand, generating a new metal complex connector, $[Cu(2,2'\text{-bpy})]^{2+}$, which affords free *cis*-coordination sites and directly influences the overall structural network.

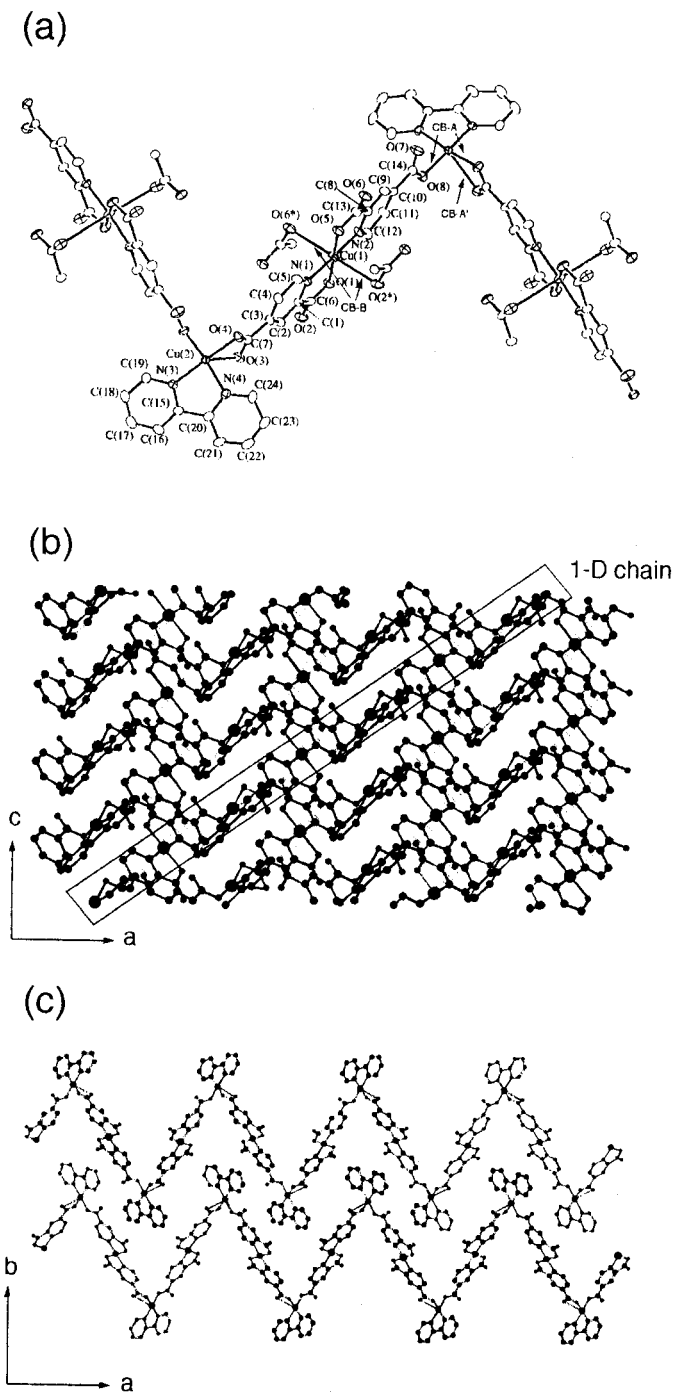

Figure III.6. (a) ORTEP drawing of the 1-D zigzag chain of **III-7** at the 30 % probability level. (b) View of the 2-D undulated sheet of **III-7** along the *b*- (b) and *c*-axes (c).

Metal complex connectors have an advantage to control a joint angle; coordination sites for no use can be blocked by chelating or macrocyclic ligands directly bound to a connector metal ion, and therefore, special sites remain for ligand. This "ligand-regulation" of a connector is quite useful. The $[Cu(2,2'\text{-bpy})]^{2+}$ connector is of great use to create 1-D zigzag chain structures with bipyridine derivatives.[43-47] Here, it should be noted that combination of the metalloligand with the metal complex connector could expand a structural diversity, because of their several independent components, that is, two metal ions, blocking ligand for metal complex connector, and bridging ligand for metalloligand. **III-7** is a first example with the framework constructed form metal complex connector and metalloligand.

A view around the metal centers of **III-8** is shown in Figure III.7(a). The Cu(II) ion lying on an inversion center is based on an elongated octahedral environment with two oxygen atoms of 2-carboxylate (1.918(2) Å) and two nitrogen atoms of pyridine (1.970(3) Å) in a chelating mode in the equatorial plane, and two oxygen atoms of 4-carboxylate of another metalloligands (2.883(3) Å) at the axial sites. On the other hand, the Zn(II) ion, which also lies on an inversion center, is based on an octahedral environment with two oxygen atoms of 4-carboxylate (2.074(2) Å), H_2O (2.116(3) Å), and MeOH (2.100(2) Å), at the *trans* position. Analogy to **III-5-7**, the coordination number of **III-1** used as a building block increases to six by removal of the capped H_2O molecule and attack of carboxylate oxygen atoms.

The metalloligand **III-1** bridges the Zn(II) ions (CB-A : Zn-O = 2.074(2) Å) to form a linear 1-D chain structure, in which a Cu-Zn-Cu angle is *ca.* 180 °. The intrachain distance of Cu-Zn is *ca.* 8.83 Å. These chains are linked by free oxygen atoms of 4-carboxylate, which weakly coordinate to Cu(II) ions (CB-B : Cu-O = 2.883(3) Å). In addition, the chains are connected between coordinated H_2O molecules at the Zn(II) centers and oxygen atoms of 2-carboxylate via hydrogen bonds (HB-A : 2.847(4) Å). These two connections create a 2-D network as illustrated in Figure III.7(b). Each 2-D sheet is linked by hydrogen bonds among the coordinated H_2O molecules at the Zn(II) centers and oxygen atoms of 2-carboxylate (HB-B : 2.709(3) Å) to form rhombic channels with a dimension of *ca.* 2 Å x 2 Å as shown in Figure III.7(c). These channels are filled with H_2O and MeOH molecules,

which coordinate to the Zn(II) centers. The coordinated MeOH molecules are also supported by hydrogen bonds with 4-carboxylate (HB-C : 2.671(4) Å).

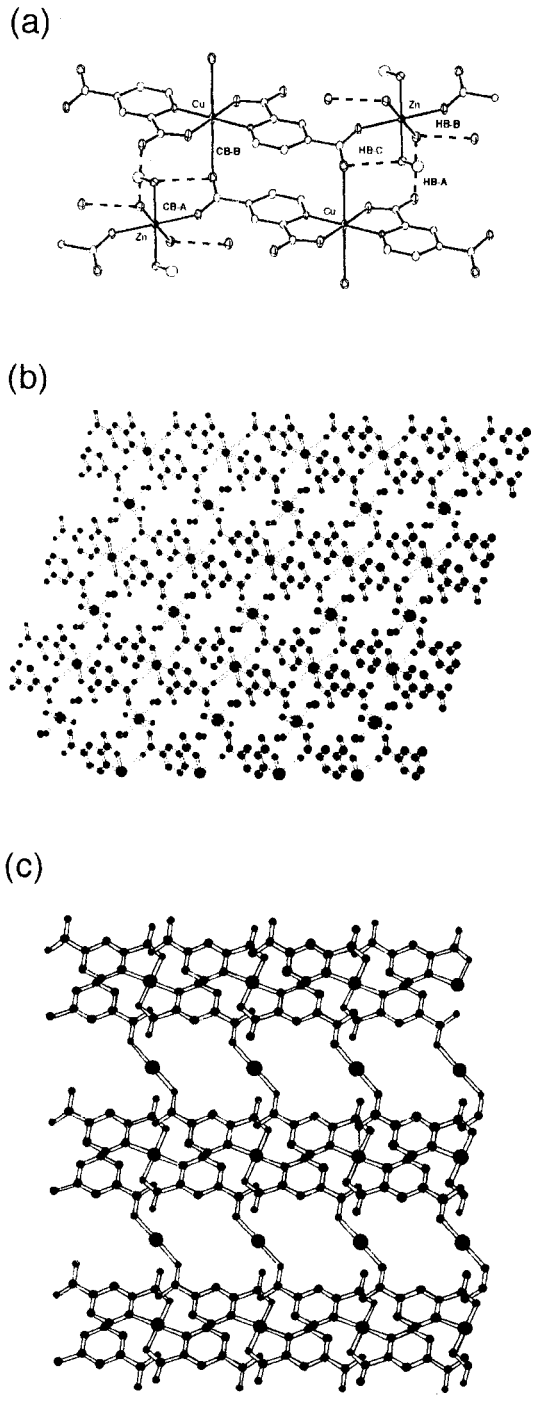

Figure III.7. (a) View of metal centers of **III-8**. The dotted line represents a hydrogen bond. (b) View of a 2-D network of **III-8** along the *c*-axis. (c) View of a microporous network of **III-8**. The coordinated H_2O and MeOH molecules are omitted for clarity.

III. 3. 2. 4 Crystal Structure of 3-D polymer $[Ag_2Cu(2,4\text{-pydca})_2]_n$ (III-9)

Figure III.8(a) with a numbering scheme shows an ORTEP view around the metal centers of **III-9**. The metalloligand **III-1** acts as a multidentate bridge, creating a 3-D network in this Ag compound. The coordination environment of each Cu(II) center consists of two oxygen donors and two nitrogen donors from 2,4-pydca^{2-} chelating ligands and two oxygen donors from 2-carboxylate parts of another ligands. The elongated octahedral geometry may be described as a basal plane associated with N(1) and O(1) from 2,4-pydca^{2-} ligands, having Cu-O and Cu-N bond lengths of 1.945(2) and 1.949(3) Å, respectively, with the axial positions occupied by two oxygen donors of O(2****) from 2-carboxylate parts of another ligands (Cu-O = 2.795(3) Å). On the other hand, the Ag(I) atoms create a dimer unit. Each Ag-Ag dimer is bound to six metalloligands **III-1** with four coordinated to dimer as mono-coordination (Ag-O(2-carboxylate) = 2.415(3) Å, Ag-O(4-carboxylate) = 2.713(3) Å), two as two mono-coordinations (Ag-O = av. 2.214 Å). The Ag-Ag bond distance is 2.8822(5) Å, which is slightly smaller than that in metallic silver (2.89 Å) and thus suggestive of a weak metal-metal interaction.[48] Analogy to **III-5-8**, the coordination number of **III-1** used as a building block increases to six by removal of the capped H_2O molecule and attack of carboxylate oxygen atoms.

The 4-carboxylate groups of **III-1** bridge the Ag_2 dimers (CB-A : av. 2.214 Å) to form a 1-D chain structure, in which the intrachain Cu•••Cu distance is *ca.* 16.60 Å. Furthermore, these chains are also connected by coordination bonds between the Ag(I) ions and the oxygen atoms at the 2-carboxylate (CB-B1 : 2.415(3) Å), forming a 2-D sheet as shown in Figure III.8(b). The shortest Cu•••Cu distance in the 2-D sheet is *ca.* 10.22 Å. These 2-D sheets are linked by weak interactions between one oxygen atom of 2-carboxylate and the Cu(II) ion (CB-B2 : 2.795(3) Å), and between one oxygen atom of 4-carboxylate and the Ag(I) ion (CB-B3 : 2.713(3) Å), affording a 3-D network as illustrated in Figure III.8(c). The shortest Cu•••Cu distance bridged by 2-carboxylate between neighboring 2-D sheets is *ca.* 5.12 Å, whose value is related to the antiferromagnetic interaction. The dimeric structures, formulated as $[Ag_2(\text{carboxylate-O,O'})_2]_n$, have been classified into four types,[49] and the dimer of complex **III-9** belongs to the typical type D classification.

Previously, a large number of hetero-metallic Cu-M coordination polymers bridged by organic ligands (MnCu,[4,8-14,22-25,27-29,50-52] FeCu,[53-60] CoCu,[2,6,26] ZnCu,[5,61] and AgCu[17,19,62,63]) have been reported. The author succeeded in systematic syntheses of a series of mixed-metallic coordination polymers mentioned above by utilizing only one multifunctional metalloligand **III-1**, which makes it possible to study on a coordination mode of the metalloligand for the second metal units in detail (vide infra).

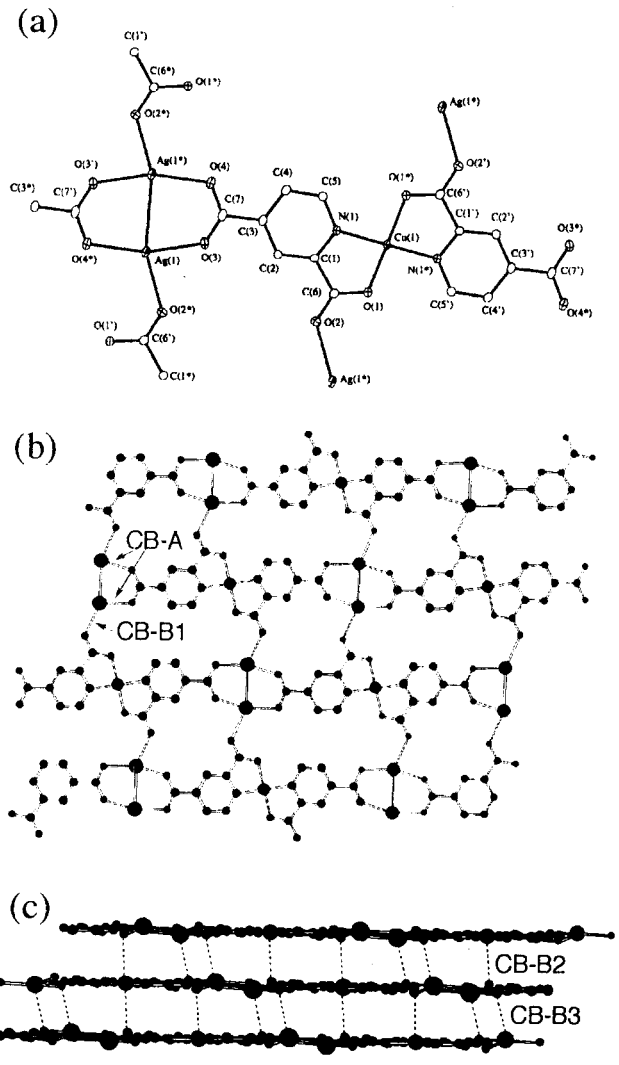

Figure III.8. (a) ORTEP drawing around Cu(II) and Ag(I) centers of **III-9** at the 30 % probability level. (b) View of the 2-D sheet of **III-9**. (c) View of the 3-D network of **III-9**.

III. 3. 3 Multi-Functional Property of Metalloligand with Several Characteristic Coordination Sites: Bond Engineering of Coordination Networks

As mentioned in introduction, the metalloligand **III-1** can give various coordination modes. In this chapter, six characteristic coordination modes of **III-1** were observed as shown in Scheme III.4. In 1-D coordination polymers **III-2-4**, **III-1** acts as a linear ligand such as 4,4'-bpy and its derivatives. **III-1** of 2-D porous polymer **II-1** takes a similar coordination mode to those of 1-D linear polymers **III-2-4**. However, existence of bridged H_2O molecules between metal centers affords 2-D sheet structure, supported by hydrogen-bonding interaction between coordinated H_2O molecules and 2-carboxylate groups. In 2-D polymers **III-5** and **III-6**, which are regarded as an analogue of that of 5,10,15,20-tetra(4-pyridyl)-21H,23H-porphyrin,[64] four oxygen atoms of each 2- and 4-carboxylate of **III-1** take the mono-coordination mode. The coordination mode of **III-1** in 2-D undulated polymer **III-7** is similar to those of **III-5** and **III-6**. The metal complex connector $[Cu(2,2'\text{-bpy})]^{2+}$ affords *cis*-coordination sites for the metalloligand, resulting to a 2-D undulated sheet. In 2-D polymer **III-8**, four oxygen atoms of only 4-carboxylate parts of **III-1** take the mono-coordination mode. This coordination mode can be regarded as the derivative of those of **III-5-7** as shown in Scheme III.4. In 3-D polymer **III-9**, two 2-carboxylate groups produce bis-coordination modes, while the oxygen atoms of 4-carboxylate ones yield mono- and bis-coordination modes. Moreover, in the case of **III-5-9**, central Cu(II) ions act as Lewis-acidic sites for 2- or 4-carboxylate groups of the neighboring metalloligands.

Lewis-acidic Cu(II) sites supplied from the metalloligand act in cooperation with the 2-carboxylate sites. In complexes, **III-5-7** and **III-9**, when the 2-carboxylate sites are coordinating to cationic, Lewis-acidic metal ions, the axial sites of the Cu(II) ions are occupied by anionic 2- or 4-carboxylate oxygen atoms of another metalloligands. This is possibly because the Cu(II) ion regulates its charge and electron balance by coordinated to anionic Lewis-basic parts: oxygen atoms of carboxylate groups. The 2-carboxylate sites are coordination-free and the 4-carboxylate ones are coordinating to the Cu(II) axial sites in the case of **III-8**. However, since Cu-O(4-carboxylate) bond

of **III-8** is very weak (CB-B : 2.883(3) Å) compared with those of **III-5-7** and **III-9**, the electrostatic and Lewis-basic effect given in the Cu(II) center may be small.

Scheme III.4

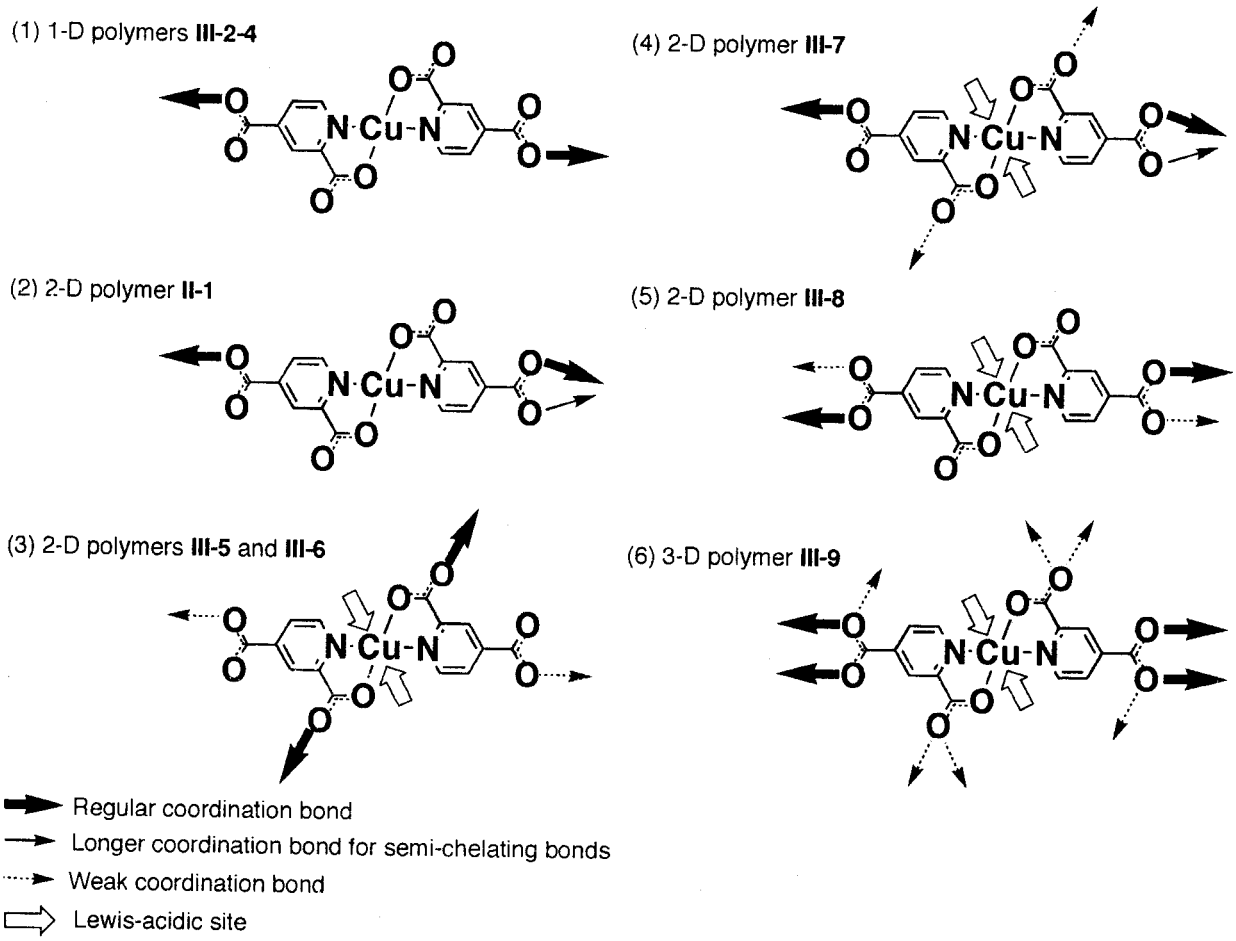

From these results, it is revealed that this metalloligand **III-1** can change its coordination patterns flexibly, with the aid of second metal units employed, and is a candidate for useful building units of novel coordination polymers having mixed-metals and various dimensions.

In order to control the bonding mode of the metalloligand, the author used divalent ions of the first periodic transition metal series (Mn(II), Fe(II), Co(II), Cu(II), and Zn(II)) as the second metal units. It is well-known that the stabilities of corresponding complexes of the divalent ions of the first periodic transition series, irrespective of the particular ligand involved, usually vary in the Irving-Williams order:[30]

Mn(II) < Fe(II) < Co(II) < Ni(II) < Cu(II) > Zn(II)

which is related to the electrostatic and covalent interactions, namely, the reciprocal of the ionic radius and the second ionisation potential, both of which increase monotonically throughout the series from Mn to Cu. Although Zn ion also has a higher ionisation potential and a lower radius than Ni and Co, the existence of an orbital stabilization, which generally increases the stability of Cu complexes, makes the order of Cu and Zn reversed.[30] In the case of the metalloligand **III-1**, the oxygen atoms of 4-carboxylate groups are more anionic and have a stronger coordination ability than those of 2-carboxylate ones which coordinate to the cationic and Lewis-acidic Cu(II) ion. Therefore, the author could easily predict the bonding selectivity of each carboxylate group for the first periodic transition metal units, that is, 2-carboxylate coordinating to Mn(II) and Fe(II) and 4-carboxylate to Cu(II) and Zn(II). As mentioned in above 'Crystal Structures' sections, the coordination bonds of the metalloligand **III-1** are mainly classified into two types: CB-A and CB-B. CB-A, which means a regular coordination bond, is given by 4-carboxylate groups for Co(II), Cu(II), and Zn(II) second metal units, and by 2-carboxylate ones for Mn and Fe ones. This tendency is good agreement with the Irving-Williams order. Consequently, the author succeeded in the bond engineering by utilizing the different coordination sites of the metalloligand **III-1**, and further rational, structural engineering by **III-1** will be carried out.

III. 3. 4 Magnetic Properties

The compounds, **III-2-7** and **III-9**, exhibit interesting magnetic behaviors, classified into two categories, that is, weak antiferromagnetic system (**III-2-4**, **III-7**, and **III-9**) and ferrimagnetic one (**III-5** and **III-6**).[65]

2-D polymers **III-5** and **III-6** afford 1-D mixed-metal chains bridged by 2-carboxylate, and the appearance of the ferrimagnetic interaction is anticipated. In practice, the $\chi_M T$ curves of **III-5** and **III-6** are similar to those of Mn(II)Cu(II) infinite bimetallic chain compounds previously reported[4,9,23,25,28], which show strong ferrimagnetic interactions. Figure III.9(a) shows a plot of the temperature dependence of $\chi_M T$. In **III-6**, the plots of $1/\chi_M$ *vs* T between 159 and 249 K obey the Curis-Weiss law with a negative Weiss constant of θ = - 1.2 K, indicating the presence of a weak

antiferromagnetic interaction. At 300 K, the $\chi_M T$ value is estimated to be 4.129 emu·K·mol^{-1}, which is in the range of values expected for a high spin Fe(II) ion and a Cu(II) ion. As the temperature is lowered, the $\chi_M T$ value gradually increases to the maximum of 4.171 emu·K·mol^{-1} at 249 K. On further lowering of the temperature, the $\chi_M T$ value gradually decreases to the minimum of 4.159 emu·K·mol^{-1} at 159 K, abruptly increases to a maximum of 6.144 emu·K·mol^{-1} at 5 K and sharply decreases to 4.062 emu·K·mol^{-1} at 2 K. This behavior is characteristic of a Fe(II)Cu(II) ordered bimetallic chain with an intrachain ferrimagnetic interaction on which interchain and/or intrasheet antiferromagnetic interaction is superimposed. Magnetization was measured as a function of the external magnetic field at 2 K (Figure III.9(b)). The magnetization much rapidly increases with increasing applied field in the range 0-1 T, then gradually in the range 1-5 T. The magnetization of **III-6** at 5 T is *ca.* 4.2 $N\beta$, which is apparently smaller than that of the expected value for a magnetically dilute two spin system (5 $N\beta$) due to the spin canting effect. As compared with a magnetization curve determined from the Brillouin function, the magnetization of **III-6** more rapidly increases until *ca.* 2 T, but in the range 2-5 T the value is smaller that that determined from the Brillouin function, which clearly indicates that the interchain and/or intrasheet antiferromagnetic interactions, and the intrachain ferrimagnetic interaction exist at 2 K.

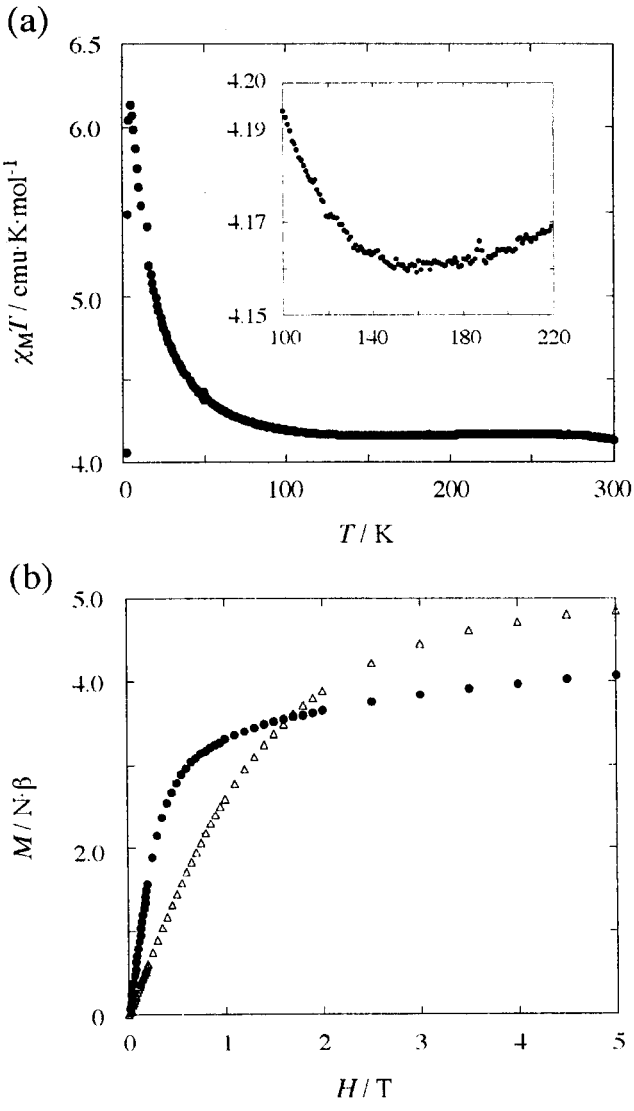

Figure III.9. Plots of the temperature dependence of $\chi_M T$ (a) and the magnetization as a function of the applied magnetic field at 2 K (b, closed circle) for **III-6**. Plot of a theoretical magnetization curve is represented by open triangles.

III. 4 Conclusion

By using a multi-functional metalloligand, [Cu(2,4-Hpydca)$_2$(H_2O)] (**III-1**·2Et_3NH), as the building block, bond engineering of novel coordination polymers with homo- and hetero-metals in the crystal has been predictably conducted and their crystal structures characterized. The combination of metalloligand with Co(II), Cu(II), and Zn(II) ions at the various conditions yielded 1-D coordination polymers, {[MCu(2,4-pydca)$_2$(H_2O)$_4$]·2H_2O}$_n$ (M = Co (**III-2**), Cu (**III-3**), Zn (**III-4**)), and 2-D ones of {[Cu(2,2'-bpy)Cu(2,4-pydca)$_2$]·3H_2O}$_n$ (**III-7**) and [ZnCu(2,4-pydca)$_2$(H_2O)$_2$(MeOH)$_2$]$_n$ (**III-8**), all of which have regular M-O bonds constructed from the 4-carboxylate donors. On the other hand, 2-D coordination polymers of [MCu(2,4-pydca)$_2$(H_2O)$_4$]$_n$ (M = Mn (**III-5**), Fe (**III-6**)) possess regular M-O bonds supplied from the 2-carboxylate donors. These results clearly indicate that the author beautifully succeeded in the bond engineering of coordination polymers. Also created was 3-D coordination polymer [Ag_2Cu(2,4-pydca)$_2$]$_n$ (**III-9**), in which both 2- and 4-carboxylate of **III-1** link to Ag2 dimers to form a 3-D network. During these reactions, the main body of the metalloligand used as a building block is almost retained, indicating of a very stable ligand. It should be noted that this metalloligand is good candidate for the construction of not only the mixed-metallic polymers but also novel framework topologies, because of a high flexibility for the coordination to several transition metal ions, in addition to the existence of Lewis-acidic metal sites. The author will anticipate this approach to be viable for the construction of desired coordination polymers, namely, 'crystal engineering'.

III. 5 References

(1) Sugimoto, K.; Kuroda-Sowa, T.; Maekawa, M.; Munakata, M. *J. Chem. Soc., Chem. Commun.* **1999**, 455-456.

(2) Chang, W.-K.; Sheu, S.-C.; Lee, G.-H.; Wang, Y.; Ho, T.-I.; Lin, Y.-C. *J. Chem. Soc., Dalton Trans.* **1993**, 687-694.

(3) Miah, M. A. A.; Phillips, D. J.; Rae, A. D. *Inorg. Chim. Acta* **1996**, *245*, 231-235.

(4) Gleizes, A.; Verdaguer, M. *J. Am. Chem. Soc.* **1984**, *106*, 3727-3737.

(5) Ruiz, R.; Julve, M.; Faus, J.; Lloret, F.; Muñoz, M. C.; Journaux, Y.; Bois, C. *Inorg. Chem.* **1997**, *36*, 3434-3439.

(6) Xu, D.; Gu, J.; Xu, L.; Liang, K.; Xu, Y. *Polyhedron* **1998**, *17*, 231-233.

(7) Tamaki, J.; Zhong, Z. J.; Matsumoto, N.; Kida, S.; Koikawa, M.; Achiwa, N.; Hashimoto, Y.; Okawa, H. *J. Am. Chem. Soc.* **1992**, *114*, 6974-6979.

(8) Pei, Y.; Kahn, O.; Sletten, J. *J. Am. Chem. Soc.* **1986**, *108*, 3143-3145.

(9) Pei, Y.; Kahn, O.; Sletten, J.; Renard, J.-P.; Georges, R.; Gianduzzo, J.-C.; Curely, J.; Xu, Q. *Inorg. Chem.* **1988**, *27*, 47-53.

(10) Kahn, O.; Pei, Y.; Verdaguer, M.; Renard, J. P.; Sletten, J. *J. Am. Chem. Soc.* **1988**, *110*, 782-789.

(11) Stumpf, H. O.; Ouahab, L.; Pei, Y.; Grandjean, D.; Kahn, O. *Science* **1993**, *261*, 447-449.

(12) Lloret, F.; Julve, M.; Ruiz, R.; Journaux, Y.; Nakatani, K.; Kahn, O.; Sletten, J. *Inorg. Chem.* **1993**, *32*, 27-31.

(13) Nakatani, K.; Sletten, J.; Halut-Desporte, S.; Jeannin, S.; Jeannin, Y.; Kahn, O. *Inorg. Chem.* **1991**, *30*, 164-171.

(14) Pei, Y.; Nakatani, K.; Kahn, O.; Sletten, J.; Renard, J. P. *Inorg. Chem.* **1989**, *28*, 3170-3175.

(15) Ciurtin, D. M.; Smith, M. D.; zur Loye, H.-C. *Inorg. Chim. Acta* **2001**, *324*, 46-56.

(16) Ciurtin, D. M.; Smith, M. D.; zur Loye, H.-C. *Chem. Commun.* **2002**, 74-75.

(17) Dong, Y.-B.; Smith, M. D.; zur Loye, H.-C. *Inorg. Chem.* **2000**, *39*, 1943-1949.

(18) Dong, Y.-B.; Smith, M. D.; zur Loye, H.-C. *Angew. Chem., Int. Ed. Engl.* **2000**, *39*, 4271-4273.

(19) Dong, Y.-B.; Smith, M. D.; zur Loye, H.-C. *Solid State Sci.* **2000**, *2*, 335-341.

(20) Dong, Y.-B.; Smith, M. D.; zur Loye, H.-C. *Solid State Sci.* **2000**, *2*, 861-870.

(21) Carlucci, L.; Ciani, G.; Porta, F.; Proserpio, D. M.; Santagostini, L. *Angew. Chem., Int. Ed. Engl.* **2002**, *41*, 1907-1911.

(22) Pei, Y.; Verdaguer, M.; Kahn, O. *J. Am. Chem. Soc.* **1986**, *108*, 7428-7430.

(23) Pei, Y.; Verdaguer, M.; Kahn, O.; Sletten, J.; Renard, J.-P. *Inorg. Chem.* **1987**, *26*, 138-143.

(24) Stumpf, H. O.; Pei, Y.; Kahn, O.; Sletten, J.; Renard, J. P. *J. Am. Chem. Soc.* **1993**, *115*, 6738-6745.

(25) Stumpf, H. O.; Pei, Y.; Ouahab, L.; Le Berre, F.; Codjovi, E.; Kahn, O. *Inorg. Chem.* **1993**, *32*, 5687-5691.

(26) Gulbrandsen, A.; Sletten, J.; Nakatani, K.; Pei, Y.; Kahn, O. *Inorg. Chim. Acta* **1993**, *212*, 271-279.

(27) Stumpf, H. O.; Ouahab, L.; Pei, Y.; Bergerat, P.; Kahn, O. *J. Am. Chem. Soc.* **1994**, *116*, 3866-3874.

(28) Baron, V.; Gillon, B.; Sletten, J.; Mathoniere, C.; Codjovi, E.; Kahn, O. *Inorg. Chim. Acta* **1995**, *235*, 69-76.

(29) Baron, V.; Gillon, B.; Cousson, A.; Mathonière, C.; Kahn, O.; Grand, A.; Öhrström, L.; Delley, B.; Bonnet, M.; Boucherle, J.-X. *J. Am. Chem. Soc.* **1997**, *119*, 3500-3506.

(30) Irving, H.; Williams, R. J. P. *J. Chem. Soc.* **1953**, 3192-3210.

(31) Hathaway, B. J.; Procter, I. M.; Slade, R. C.; Tomlinson, A. A. G. *J. Chem. Soc. A* **1969**, 2219-2224.

(32) Sheldrick, G. M. **1985**, In "Crystallographic Computing 3" (Eds G.M. Sheldrick, C. Kruger and R. Goddard) Oxford University Press, pp. 175-189.

(33) Beurskens, P. T.; Admiraal, G.; Beurskens, G.; Bosman, W. P.; de Gelder, R.; Israel, R.; Smits, J. M. M. **1994**, The DIRDIF-94 program system, Technical Report of the Crystallography Laboratory, University of Nijmegen, The Netherlands.

(34) Altomare, A.; Burla, M. C.; Camalli, M.; Cascarano, M.; Giacovazzo, C.; Guagliardi, A.; Polidori, G. *J. Appl. Cryst.* **1994**, *27*, 435.

(35) Beurskens, P. T.; Admiraal, G.; Beurskens, G.; Bosman, W. P.; de Gelder, R.; Israel, R.; Smits, J. M. M. **1994**, The DIRDIF-94 program system, Technical Report of the Crystallography Laboratory, University of Nijmegen, The Netherlands.

(36) Crystal Structure Analysis Package, Molecular Structure Corporation (1985 & 1999).

(37) Klein, C. L.; Majeste, R. J.; Trefonas, L. M.; O'Connor, C. J. *Inorg. Chem.* **1982**, *21*, 1891-1897.

(38) Sobanska, S.; Lagrenee, M.; Wignacourt, J.-P.; Holt, E. M. *Acta Cryst.* **1999**, *C55*, 553-555.

(39) Pinkas, J.; Huffman, J. C.; Baxter, D. V.; Chisholm, M. H.; Caulton, K. G. *Chem. Mater.* **1995**, *7*, 1589.

(40) Thompson, S. C.; Cole-Hamilton, D. J.; Gilland, D. C.; Hitchman, M. L.; Barnes, J. C. *Adc. Mater. Opt. Electron.* **1992**, *1*, 81.

(41) Haendler, H. M. *Acta Cryst.* **1986**, *C42*, 147-149.

(42) O'Reilly, E. J.; Smith, G.; Kennard, C. H. L.; White, A. H. *Aust. J. Chem.* **1983**, *36*, 183-190.

(43) Carlucci, L.; Ciani, G.; Gramaccioli, A.; Proserpio, D. M.; Rizzato, S. *CrystEngComm* **2000**, *29*, 1-10.

(44) Chen, C.; Xu, D.; Xu, Y.; Cheng, C. *Acta Cryst.* **1992**, *C48*, 1231-1233.

(45) Chawla, S. K.; Hundal, M. S.; Kaur, J.; Obrai, S. *Polyhedron* **2001**, *20*, 2105-2111.

(46) Park, H. W.; Sung, S. M.; Min, K. S.; Bang, H.; Suh, M. P. *Eur. J. Inorg. Chem.* **2001**, 2857-2863.

(47) Carlucci, L.; Ciani, G.; Proserpio, D. M.; Rizzato, S. *Chem. Commun.* **2001**, 1198-1199.

(48) Wu, D.-D.; Mak, T. C. W. *J. Chem. Soc., Dalton Trans.* **1995**, 2671-2678.

(49) Mak, T. C. W.; Yip, W.-H.; Kennard, C. H. L.; Smith, G.; O'Reilly, E. J. *Aust. J. Chem.* **1986**, *39*, 541-546.

(50) Gleizes, A.; Verdaguer, M. *J. Am. Chem. Soc.* **1981**, *103*, 7373-7374.

(51) Solans, X.; Font-Altaba, M.; Oliva, J.; Herrera, J. *Acta Cryst.* **1983**, *C39*, 435-438.

(52) Kim, J.; Lim, J. M.; Choi, Y.-K.; Do, Y. *Angew. Chem., Int. Ed. Engl.* **1996**, *35*, 998-1000.

(53) Morpurgo, G. O.; Mosini, V.; Porta, P.; Dessy, G.; Fares, V. *J. Chem. Soc., Dalton Trans.* **1980**, 1272-1276.

(54) Morpurgo, G. O.; Mosini, V.; Porta, P.; Dessy, G.; Fares, V. *J. Chem. Soc., Dalton Trans.* **1981**, 111-117.

(55) Kou, H.-Z.; Liao, D.-Z.; Cheng, P.; Jiang, Z.-H.; Yan, S.-P.; Wang, G.-L.; Yao, X.-K.; Wang, H.-G. *J. Chem. Soc., Dalton Trans.* **1997**, 1503-1506.

(56) Kou, H.-Z.; Wang, H.-M.; Liao, D.-Z.; Cheng, P.; Jiang, Z.-H.; Yan, S.-P.; Huang, X.-Y.; Wang, G.-L. *Aust. J. Chem.* **1998**, *51*, 661.

(57) Zou, J.; Hu, X.; Duan, C.; Xu, Z.; You, X. *Transition Met. Chem.* **1998**, *23*, 477.

(58) Gomez-Romero, P.; Jameson, G. B.; Borras-Almenar, J. J.; Escriva, E.; Coronado, E.; Beltran, D. *J. Chem. Soc., Dalton Trans.* **1988**, 2747-2751.

(59) Morgenstern-Badarau, I.; Laroque, D.; Bill, E.; Winkler, H.; Trautwein, A. X.; Robert, F.; Jeannin, Y. *Inorg. Chem.* **1991**, *30*, 3180-3188.

(60) Chen, Z. N.; Wang, J. L.; Qui, J.; Miao, F. M.; Tang, W. X. *Inorg. Chem.* **1995**, *34*, 2255-2257.

(61) Ogata, T.; Taga, T.; Osaki, K. *Bull. Chem. Soc. Jpn.* **1977**, *50*, 1680-1682.

(62) Brouca-Cabarrecq, C.; Marrot, B.; Mosset, A. *Acta Cryst.* **1996**, *C52*, 1903-1906.

(63) Krautscheid, H.; Emig, N.; Klaassen, N.; Seringer, P. *J. Chem. Soc., Dalton Trans.* **1998**, 3071-3077.

(64) Abrahams, B. F.; Hoskins, B. F.; Michail, D. M.; Robson, R. *Nature* **1994**, *369*, 727-729.

(65) In a series of 1-D polymers **III-2-4**, no strong interaction is observed in a measured temperature range, but very weak antiferromagnetic interactions are detected at low temperature in **III-2-4**. In 2-D polymer **III-7** and 3-D one **III-9**, Cu(II) chains bridged by 2-carboxylate groups of metalloligands, which are similar to those of **III-5** and **III-6**, exist in the crystals. However, since the Cu-O bond distance is very long (2.760 and 2.795 Å for **III-7** and **III-9**, respectively), only weak antiferromagnetic interaction represents.

Part 2

Porous Functionality of Coordination Polymers

A new methane adsorbent was synthesized from a coordination polymer. This material adsorbs the gas to a remarkable extent and opens up new dimensions for the study of inorganic–organic hybrid adsorbents based on coordination polymers. Find out more on the following pages.

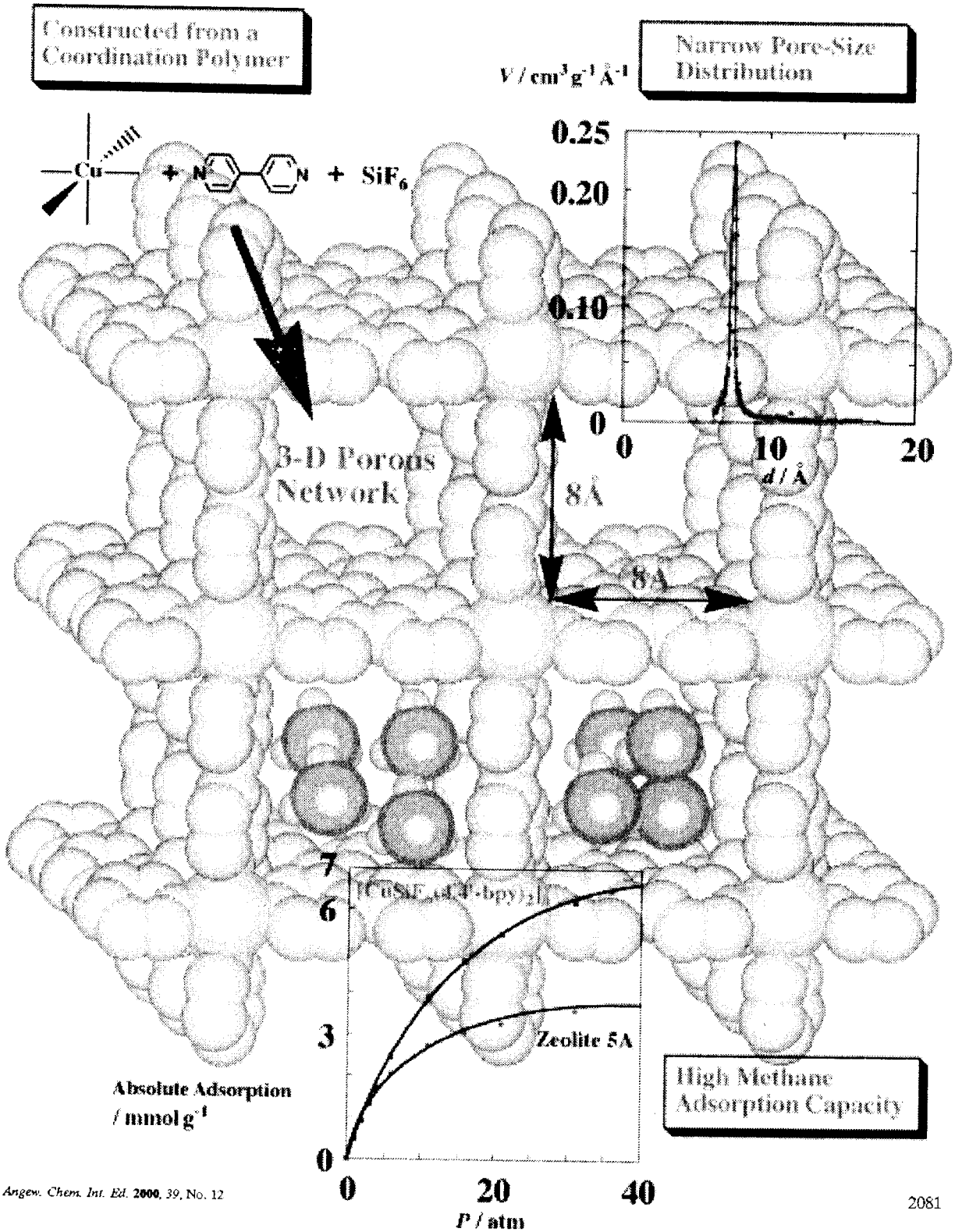

Chapter IV

New, Methane Adsorbents, Porous Coordination Polymers $\{[Cu(AF_6)(4,4'\text{-bpy})_2]\cdot 8H_2O\}_n$ (A = Si, Ge, and Ti)

Abstract: Creation of novel porous materials as adsorbents is an attractive research field for the purpose of storage and transport of natural gas. Porous coordination polymers can afford light materials with high porosity, and their channel shapes and sizes can be finely controlled by combining transition metals and organic bridging ligands. The author synthesized coordination polymers, $[Cu(AF_6)(4,4'\text{-bpy})_2]_n$ (A = Si (**IV-1**), Ge (**IV-2**), and Ti (**IV-3**)), each of which affords a stable, 3-D, microporous network. The channel size is *ca.* 8 Å × 8 Å along the *c*-axis and 6 Å × 2 Å along the *a*- or *b*-axes. **IV-1** has the specific surface area of 1337 $m^2 \cdot g^{-1}$ and the high CH_4 adsorption ability at ambient temperature and low pressure, which is superior to that of any zeolites, and thus opens up a new possibility for CH_4 storage materials.

IV. 1 Introduction

Natural gas (NG), the principal component of which is CH_4, has considerable advantages over conventional fuels, both from an environmental point of view and because of its natural abundance. For the purpose of its storage and transport, i.e., as a fuel vessel for vehicles, adsorbed natural gas (ANG) up to *ca.* 35 atm is a better alternative than compressed natural gas (CNG), and offers a very high potential for exploitation in both transport and large-scale applications. Therefore, development of the adsorbent is necessary to maximize CH_4 uptake per storage volume. One specific target in this regard is to produce new adsorbents that meet or exceed the performance established for low-pressure natural gas storage materials, that is, the development of materials with high porosity and well-controlled micropore geometry.

Nanoporous inorganic materials such as zeolites, metal phosphates, and activated carbons, have hitherto found a wide range of technological applications (for example, molecular sieves, desiccants, ion exchangers, and catalysts).[1-3] The relatively new field of microporous metallo-organic coordination polymers could give great potential for chemical and structural diversity, including the direct incorporation of catalytic sites. Until very recently, their synthesis suffered from general difficulties in the control of polymer dimensionality or framework stability. Low-dimensional coordination polymers can still show selective inclusion based on host-guest shape recognition,[4,5] but they lack framework integrity. Furthermore, although organic bridging ligands can be designed to make large voids, the resulting coordination polymers are easily badgered by lattice interpenetration or framework breakdown after the removal of guest molecules.

The author reports the syntheses, structure, and CH_4 gas adsorption properties of the highly porous coordination polymers $[Cu(AF_6)(4,4'\text{-bpy})_2]_n$ (A = Si (**IV-1**), Ge (**IV-2**), and Ti (**IV-3**)) as shown in Scheme IV.1. These polymers form a 3-D framework that creates large square pores (8 Å x 8 Å).

Scheme IV.1

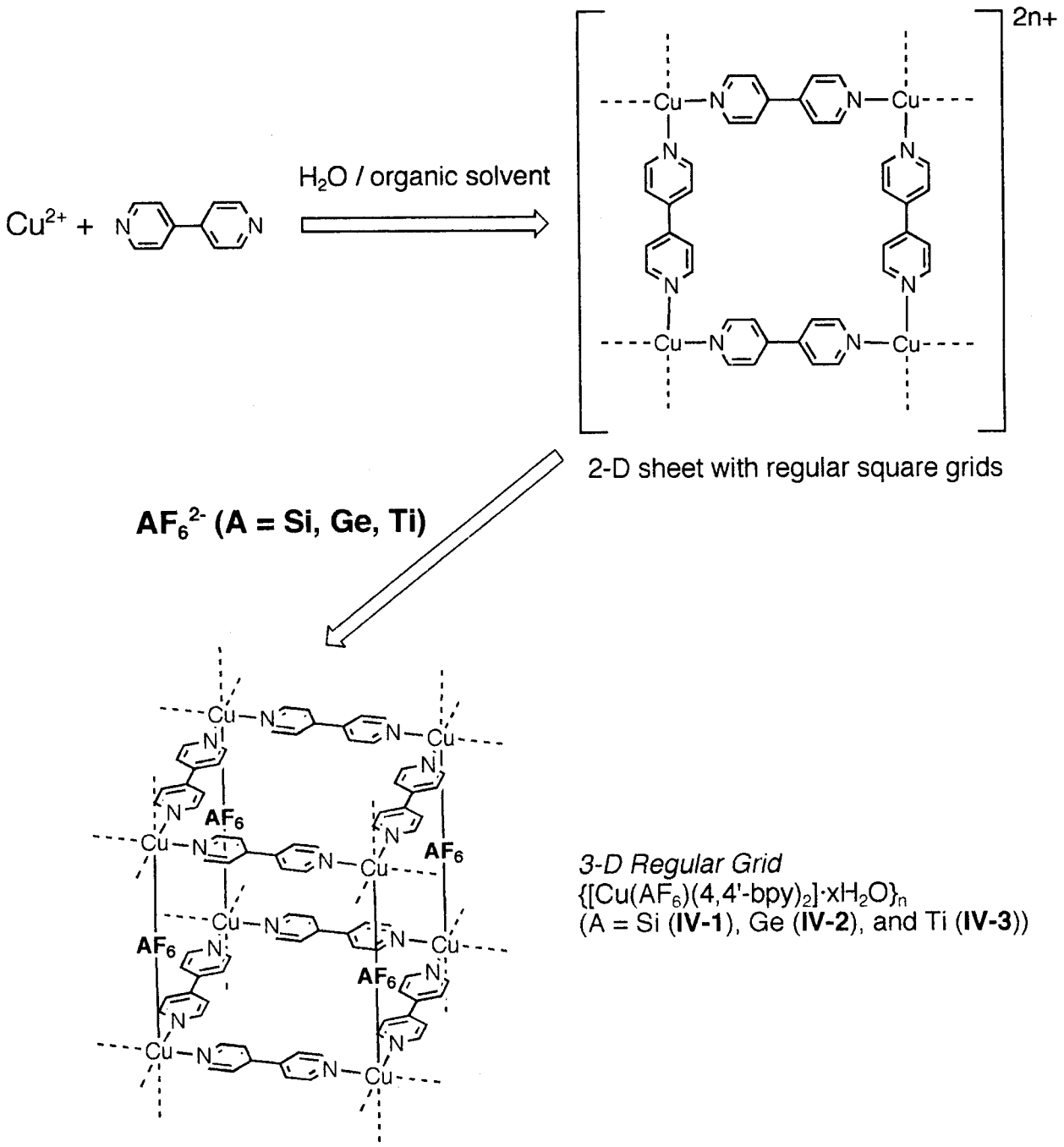

3-D Regular Grid
$\{[Cu(AF_6)(4,4'\text{-bpy})_2]\cdot xH_2O\}_n$
(A = Si (**IV-1**), Ge (**IV-2**), and Ti (**IV-3**))

IV. 2 Experimental

IV. 2. 1 Physical Measurements

The physical measurements were performed as described in Chapter I.

The adsorption isotherms of CH_4 gas on the sample were measured according to the reported procedure.[6,7] The apparatus was equipped with a Cahn R-100 electrobalance contained within a SUS steel pressure chamber that was connected with two separate lines for evacuation and adsorbate gas pressurization. After the sample was set in the apparatus, the solvated molecules in the channels were removed under reduced pressure at 298 K. The removal process was monitored by the change in weight. The CH_4 gas was dosed into the adsorption chamber, and then the change in weight of the sample was monitored. The entire adsorption isotherms at 298 K were determined by increasing the adsorbate gas pressure to a maximum of 36 atm. After the buoyancy was corrected to the obtained amount of the weight change the adsorbed amount was calculated. Zeolite 5A was purchased from Bayer Co. The adsorption isotherms of CH_4 gas were measured with the same method as for the sample. The adsorption properties of zeolites have been reported by L. Mentasty et al.,[8] and the CH_4 adsorption quantity (2.9 $mmol\cdot g^{-1}$ at 36 atm) of zeolite 5A was smaller than our experimental data (3.7 $mmol\cdot g^{-1}$ at 36 atm). The author used the higher CH_4 adsorption quantity as comparison data with the sample.

The adsorption isotherms of Ar gas were measured using ASAP 2000M volumetric adsorption equipment from Micromeritics, Norcross, GA.

IV. 2. 2 Syntheses

Materials. $Cu(BF_4)_2\cdot 6H_2O$, $(NH_4)_2SiF_6$, $(NH_4)_2GeF_6$, and $(NH_4)_2TiF_6$, were obtained from Aldrich Chemical Co. 4,4'-bpy was purchased from Tokyo Kasei Chemical Co. and Wako Co., respectively.

Synthesis of $\{[Cu(SiF_6)(4,4'\text{-bpy})_2]\cdot 8H_2O\}_n$ (IV-1·8H$_2$O). The compound of **IV-1**·8H$_2$O was synthesized as follows: a hot aqueous solution (20 mL) of $Cu(BF_4)_2\cdot xH_2O$ (266 mg, 1.12 mmol) and $(NH_4)_2SiF_6$ (199 mg, 1.12 mmol) was added to a hot ethyleneglycol solution

(40 mL) of 4,4'-bpy (350 mg, 2.24 mmol). The obtained purple microcrystals were filtered, washed with MeOH, and dried in air to give 579 mg of product (88 % yield). This compound easily released the guest H_2O molecules to form a partially dehydrated one. The crystals suitable for the X-ray analysis were obtained as follows: a EtOH solution of 4,4'-bpy was diffused to an aqueous solution of $Cu(BF_4)_2 \cdot xH_2O$ and $(NH_4)SiF_6$ in the straight glass tube. Purple crystals of **IV-1**$\cdot 8H_2O$ were obtained together with sky-blue crystals of **V-1** after a few weeks. The homogeneity of the powder sample was confirmed by comparison of the observed and calculated XRPD patterns obtained from the single-crystal data. Anal. Calcd for $\{[Cu(SiF_6)(4,4'\text{-bpy})_2] \cdot 4H_2O\}_n$ (**IV-1**$\cdot 4H_2O$): C, 40.71; H, 4.10; N, 9.50. Found: C, 40.81; H, 3.50; N, 9.27. IR (KBr pellet): 3412 bm, 3098 w, 3045 w, 1610 m, 1535 w, 1493 w, 1412 w, 1221 w, 1078 w, 995 w, 812 s, 742 s, 644 m, 482 s (cm^{-1}).

Synthesis of $\{[Cu(GeF_6)(4,4'\text{-bpy})_2] \cdot 8H_2O\}_n$ (IV-2$\cdot 8H_2O$). This compound was prepared in the procedure similar to that of **IV-1**$\cdot 8H_2O$ (65 % yield). Anal. Calcd for $\{[Cu(GeF_6)(4,4'\text{-bpy})_2] \cdot 4H_2O\}_n$ (**IV-2**$\cdot 4H_2O$): C, 37.85; H, 3.81; N, 8.83. Found: C, 37.52; H, 3.48; N, 8.42. IR (KBr pellet): 3410 bm, 3098 m, 3045 m, 1610 s, 1535 w, 1493 w, 1412 m, 1332 w, 1221 m, 1111 m, 1076 m, 1045 w, 1012 w, 812 s, 723 w, 642 m, 607 s, 470 w (cm^{-1}).

Synthesis of $\{[Cu(TiF_6)(4,4'\text{-bpy})_2] \cdot xH_2O\}_n$ (IV-3$\cdot xH_2O$). This compound was prepared in the procedure similar to that of **IV-1**$\cdot 8H_2O$. Anal. Calcd for $\{[Cu(TiF_6)(4,4'\text{-bpy})_2(H_2O)_2] \cdot 4H_2O\}_n$ (**IV-3**$\cdot 4H_2O$): C, 39.39; H, 3.97; N, 9.19. Found: C, 40.82; H, 3.81; N, 8.98.

IV. 2. 3 X-Ray Structure Determination

Single crystals of **IV-1**$\cdot 8H_2O$ and **IV-2**$\cdot 8H_2O$ were mounted on a glass fiber and coated with epoxy resin. In **IV-1**$\cdot 8H_2O$, X-ray data collections were carried out by a Rigaku Mercury charge coupled device (CCD) system with graphite monochromated Mo-Kα radiation. No adsorption correction was applied. In **IV-2**$\cdot 8H_2O$, all measurements were made on a Rigaku RAXIS-CS imaging plate diffractometer with graphite monochromated Mo-Kα radiation. Data were processed by the PROCESS-AUTO program package. A numerical adsorption correction using the program NUMABS was applied which resulted in transmission factors ranging from 0.80 to 0.85.

In **IV-1'**·$5H_2O$, all measurements were made on a Rigaku RAXIS-RAPID imaging plate diffractometer with graphite monochromated Mo-Kα radiation. A symmetry-related adsorption correction using the program ABSCOR was applied which resulted in transmission factors ranging from 0.46 to 0.88. The data were corrected for Lorentz and polarization effects. For **IV-1**·$8H_2O$ and **IV-2**·$8H_2O$, the structures were solved by a direct method using the SIR92 program[9] and expanded using Fourier techniques.[10] For **IV-1'**·$5H_2O$, the structure was solved by a direct method using the SHELXS-97 program[11] and expanded using Fourier techniques.[10] The non-hydrogen atoms were refined anisotropically. All hydrogen atoms, which were placed in idealized positions, were included but not refined. The refinements were carried out using full-matrix least squares techniques. Crystal data and details of the structure determinations are summarized in Table IV. 1. All calculations were performed using the teXsan[12] crystallographic software package of Molecular Structure Corporation.

Table IV.1. Crystallographic Data for $\{[Cu(AF_6)(4,4'\text{-bpy})_2]\cdot 8H_2O\}_n$ (A = Si (**IV-1**·$8H_2O$) and Ge (**IV-2**·$8H_2O$))

compound	**IV-1**·$8H_2O$	**IV-2**·$8H_2O$
formula	$C_{20}H_{32}CuF_6N_4O_8Si$	$C_{20}H_{32}CuF_6GeN_4O_8$
fw	662.12	706.62
crystal color	purple	purple
crystal system	tetragonal	tetragonal
a, Å	11.108(1)	11.0934(5)
c, Å	8.1107(9)	8.2070(6)
V, Å^3	1000.8(1)	1009.99(9)
space group	*P4/mmm* (No.123)	*P4/mmm* (No.123)
Z	1	1
ρ(calcd), g·cm^{-3}	1.098	1.162
F(000)	341.00	359.00
μ(Mo Kα), cm^{-1}	6.38	13.32
diffractometer	CCD	RAXIS-CS
radiation (γ, Å)	0.71069	0.71069
temp., °C	-50	-50
GOF	2.062	1.683
no. of obsd data	937 ($I > 2.00\sigma(I)$)	579 ($I > 2.00\sigma(I)$)
no. of variables	50	48
R^a ($I > 2.00\sigma(I)$, all data)	0.0557 ($I > 2.00\sigma(I)$)	0.0548, 0.0648
R_w^b ($I > 2.00\sigma(I)$, all data)	0.0502 ($I > 2.00\sigma(I)$)	0.0790, 0.0819

[a] $R = \Sigma\|\|Fo| - |Fc\|\|/\Sigma|Fo|$. [b] $R_w = [(\Sigma w\ (|Fo| - |Fc|)^2/\Sigma wFo^2)]^{1/2}$.

IV. 3 Results and Discussion

IV. 3. 1 Synthetic Approach to a 3-D Porous Network.

Although a number of porous coordination polymer have been hitherto synthesized, still lacking are examples of ones providing useful channels which are so robust that the framework is stably maintained even under a wide pressure region at ambient temperature. Since nature dislike vacuum, aim at creation of large channel faces with the following difficulties: (1) counter anions often occupy channel; (2) an interpenetrating network is readily formed; (3) a channel network is broken down on removal of guest molecules. Therefore, to establish the rational synthetic methodology is the most critical point for creation of porous coordination polymers. Generally, the network of coordination polymers with coordinated solvent molecules has low-dimensionality and often makes no channels. In this chapter, the Cu(II) ion and the AF_6^{2-} dianion (A = Si, Ge, and Ti) are selected as the building blocks for construction of a high-dimensional porous coordination polymer. The Cu(II) ion (d^9) is liable to undergo Jahn-Teller distortion, resulting in the weakly coordinated bond sites in the axial positions. Consequently, the AF_6^{2-} can coordinate to the Cu(II) ion more easily than water or other solvents. Since the AF_6^{2-} dianion can link the basic copper units sitting in each nearest-neighbor square-grid layer, the resulting 3-D framework is expected to be robust and free from the occupation of channels by free counter anions. Described herein is the successful synthesis of a porous coordination polymer by using Cu(II) and the AF_6^{2-} dianion.

IV. 3. 2 Crystal Structures of $\{[Cu(AF_6)(4,4'\text{-bpy})_2]\cdot 8H_2O\}_n$ (A = Si (IV-1·8H$_2$O) and Ge (IV-2·8H$_2$O)).

Figure IV.1(a) shows a coordination environment around a Cu(II) ion in **IV-2**·8H$_2$O. Four pyridyl nitrogen atoms of 4,4'-bpy ligands are coordinated to the Cu(II) ion. Association of two F atoms of the GeF_6^{2-} anions provides a (4+2) environment. The 4,4'-bpy ligands bridge Cu(II) ions to form a 2-D network of square grids. The layers are linked with GeF_6^{2-} anions by coordination bonds to give a 3-D structure without interpenetration (*3-D Regular Grid*). This network provides channels with dimensions of *ca.* 8 Å × 8 Å along the *c*-axis and *ca.* 6 Å × 2 Å along the *a*- and *b*-axes,

as shown in Figures IV.1(b) and IV.1(c), respectively.[13] The channels are filled with eight crystallization H_2O molecules per one Cu(II) ion. In this crystal, there are two types of hydrogen bonds of the H_2O molecules. Four H_2O molecules (type A) are hydrogen-bonded to the F atoms of the GeF_6^{2-} ions and the nearest-neighbor H_2O molecules. The remaining four H_2O molecules (type B) link the type A of H_2O molecules to form an octangle ring (Figure IV.1(d)). These rings are located between Cu-4,4'-bpy layers as illustrated in Figure IV.1(e), because of the preference of hydrophilic environment. The similar network has been obtained for $\{[Zn(SiF_6)(4,4'\text{-}bpy)_2]\cdot xDMF\}_n$,[14] which was synthesized from DMF/dioxane solution media. On the other hand, $\{[Zn(4,4'\text{-}bpy)_2(H_2O)_2]\cdot SiF_6\}_n$[15] was isolated from an aqueous media containing $ZnSiF_6$ and 4,4'-bpy, in which interpenetration of 2-D $[Zn(4,4'\text{-}bpy)_2(H_2O)_2]_n$ sheets afforded no channeling structure,. Reaction of $ZnSiF_6$ with azpy, which is longer ligand than 4,4'-bpy, in $EtOH/CH_2Cl_2$ media yielded a similar interpenetrated network, $\{[Zn(azpy)_2(H_2O)_2]\cdot SiF_6\cdot H_2O\}_n$.[16] The frameworks in the Zn(II)-bipyridine systems are sensitive to the solvent employed, whereas those in the Cu(II)-bipyridine systems are dependent on the dianion.

The crystal structure of **IV-1**$\cdot 8H_2O$ affords a similar 3-D porous network as **IV-2**$\cdot 8H_2O$. The Cu-N bond distance (2.008(5) Å) of **IV-2**$\cdot 8H_2O$ is essentially same as that in **IV-1**$\cdot 8H_2O$ (2.010(3) Å). On the other hand, the Cu-F distance (2.320(5) Å) of **IV-2**$\cdot 8H_2O$ is slightly shorter than that in **IV-1**$\cdot 8H_2O$ (2.357(3) Å).

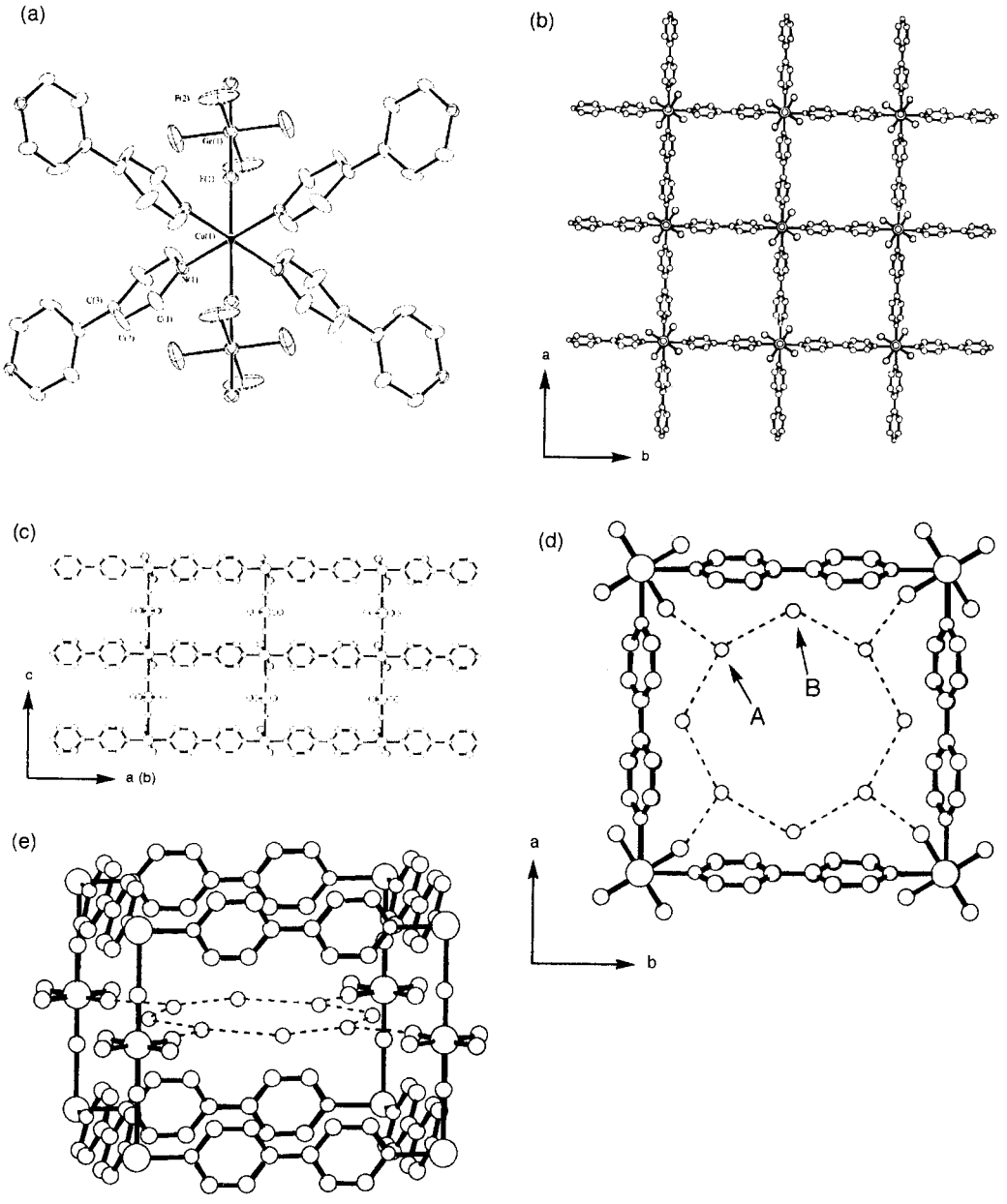

Figure IV.1. (a) ORTEP drawing around a Cu(II) center of **IV-2**·8H_2O at the 30 % probability level. The hydrogen atoms, disordered pyridine carbon atoms, and disordered fluoro atoms, are omitted for clarity. (b and c) View of the microporous network of **IV-2**·8H_2O along the *c*-axis (b) and *a*- or *b*-axes (c). The guest H_2O molecules, the hydrogen atoms, disordered pyridine carbon atoms, and disordered fluoro atoms, are omitted for clarity. (d and e) View of the 8-membered ring of guest H_2O molecules. The hydrogen atoms, disordered pyridine carbon atoms, and disordered fluoro atoms, are omitted for clarity.

IV. 3. 3 Framework Stability.

The stability of porous networks was studied by XRPD measurements and thermal gravimetric analyses (TGA). The XRPD pattern can be reproduced by simulation based on the single-crystal data with no crystallized water molecules. The TGA data of **IV-1**·xH_2O reveal that the guest H_2O molecules are removed until *ca.* 100 ℃ and the decomposition of the porous framework is observed up to *ca.* 150 ℃ as illustrated in Figure IV.2(a). The XRPD pattern of **IV-1**·xH_2O was measured at 100 ℃ under vacuum. The good agreement of the peaks in both simulation (Figure IV.3(a)) and observed pattern (Figure IV.3(b)) demonstrates that the porous network is retained in the absence of any guest molecules in the channels. Similar results were observed in **IV-2**·xH_2O as illustrated in Figures IV.2(b), IV.3(c), and IV.3(d). Further evidence for the stability of the framework was obtained by heating the solvated crystals **IV-1**·8H_2O at 80 ℃ for a 1 hour, which had no effect on either their morphology or crystallinity. The cell parameters obtained are unaltered relative to those found for the unheated solvated crystals, illustrating the robustness of the framework in the absence of guest molecules.[17] This heated sample $\{[Cu(SiF_6)(4,4'\text{-bpy})_2]\cdot 5H_2O\}_n$ (**IV-1'**·5H_2O) includes 5 moles of H_2O molecules per 1 mole of the Cu(II) atom. This is because moisture in the atmosphere promote readsorption of H_2O in the vacant channels. The readsorbed H_2O molecules are also located in SiF_6^{2-} layers and incorporated in a linear fashion along the *a*- and *b*-axes.

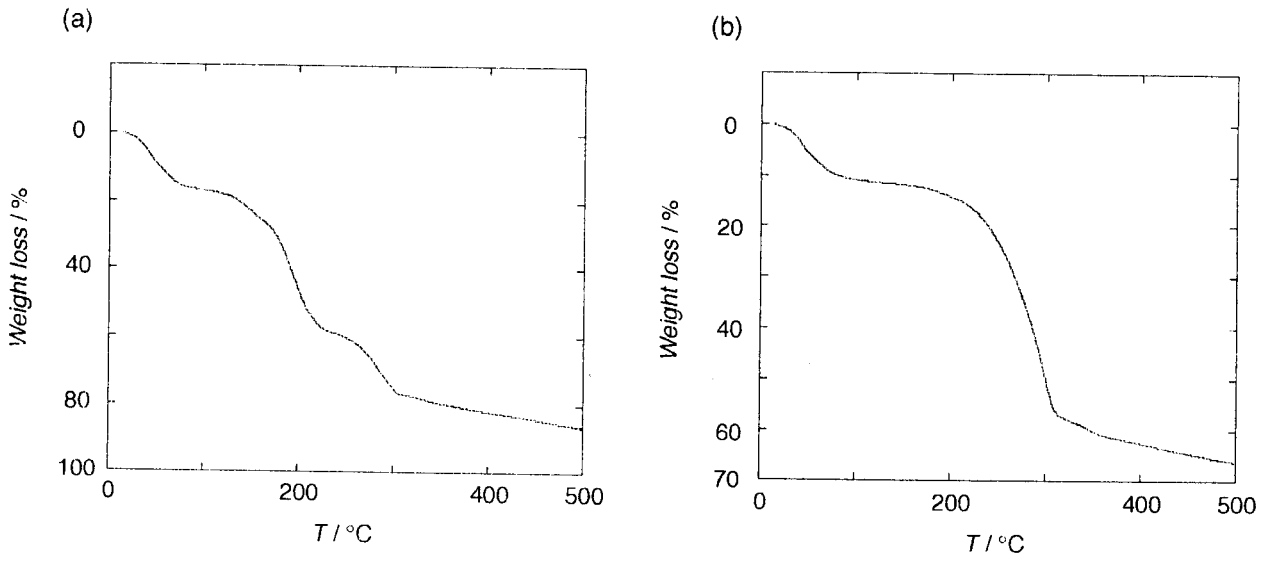

Figure IV.2. Thermogravimetric analysis data for **IV-1**·xH_2O and **IV-2**·xH_2O.

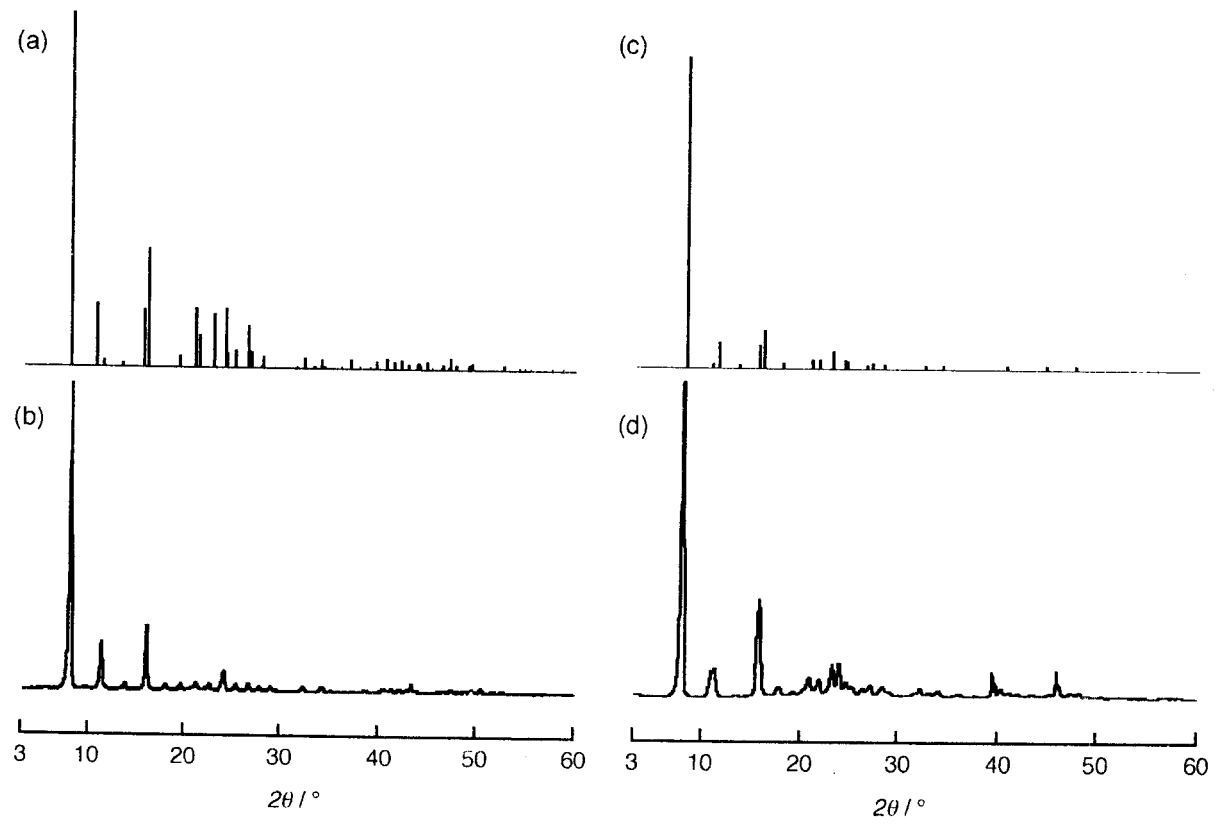

Figure IV.3. Simulated XRPD pattern upon removal of the water molecules from the single crystal model (a and c) and the observed pattern under reduced pressure at 100 ℃ (b and d) of **IV-1**·xH_2O and **IV-2**·xH_2O, respectively.

IV. 3. 4 Adsorption Properties

The 3-D porous coordination polymers **IV-1**, **IV-2**, and **IV-3** are useful for adsorbent of several gases. For **IV-1**, the Ar adsorption experiment was carried out in the relative pressure range from 10^{-6} to 1 at -185.7 ℃ (Figure IV.4(a)). This compound shows a typical isotherm of type I, indicative of a typical microporous one. The isotherm displays a rapid rise at low relative pressure followed by a monotonously increasing curve. This is attributed to the uniform micropore, characteristic of metal-organic frameworks. The micropore filling of vapors is well described by the following Dubinin-Radushkevich (DR) equation :

$$[\ln(W_0/W)]^{1/2} = (RT/\beta E_0)(\ln P_0 - \ln P) \quad \text{(eq-1)}$$

Here the parameters, W and W_0, are the amount of adsorption at P/P_0 and the pore volume, respectively. βE_0 is the adsorption potential, in which β and E_0 are the affinity coefficient and characteristic adsorption energy, respectively. The DR plot is almost linear in the higher P/P_0 region, giving the micropore volume W_0 = 379 Ncc·g^{-1} and βE_0 = 10.3 kJ·mol^{-1}. Furthermore, the βE_0 leads to the isosteric heat of adsorption $q_{st,\ \phi=1/e}$ at the fractional filling of *1/e* by the equation :

$$q_{st,\ \phi=1/e} = \Delta H_v + \beta E_0 \quad \text{(eq-2)},$$

where ΔH_v is the heat of vaporization of bulk liquid. The $q_{st,\ \phi=1/e}$ value is 16.8 kJ·mol^{-1}, whose value is comparable with those of porous coordination polymers $[Cu(dicarboxylate)]_n$ (dicarboxylate = fumarate, terephthalate, and *trans*-1,4-cyclohexanedicarboxylate).[18]

The surface area and pore size distribution of **IV-1** were calculated from Ar gas adsorption at -185.7 ℃ according to the BET equation and Horvath-Kawazoe (HK) method,[19] respectively. The differential pore volume plot, represented by the HK method, shows a single sharp peak around 8 Å as shown in Figure IV.4(b). This compound possesses a quite uniform square pore (8 Å × 8 Å), which is in fairly good agreement with the crystallographic structure. This plot also exhibits that Ar

molecules cannot pass through the rectangular pore (6 Å × 2 Å) at -185.7 ℃ because of the larger diameter of Ar. The specific surface area from Ar adsorption is calculated to be 1337 $m^2 \cdot g^{-1}$.

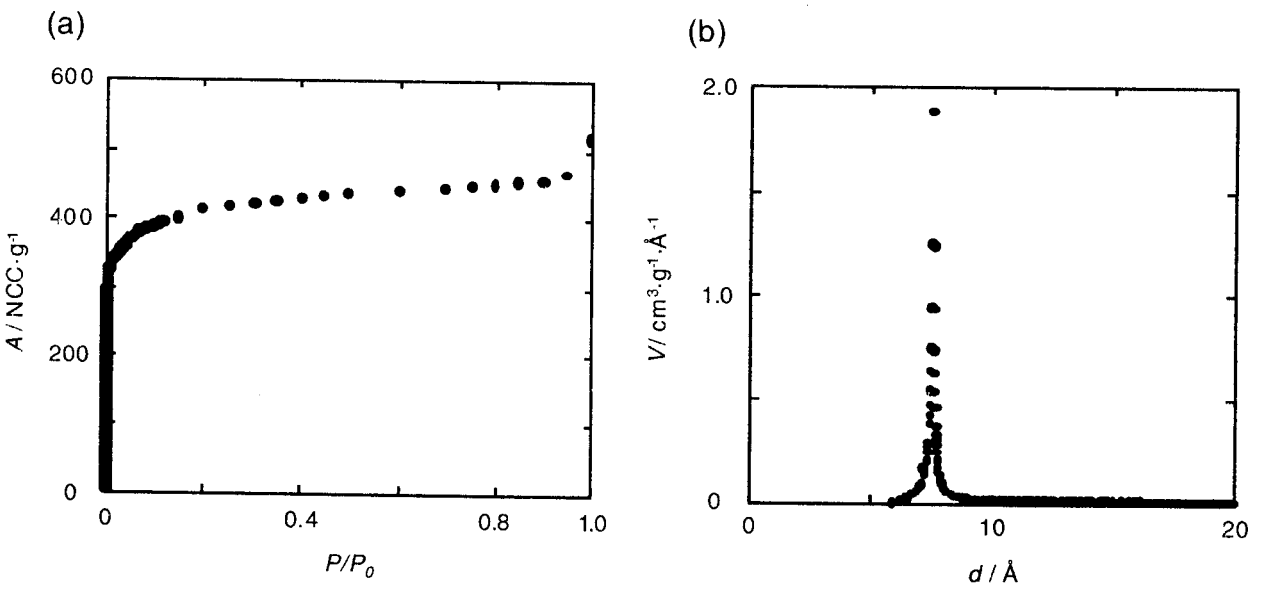

Figure IV.4. (a) Adsorption isotherms of **IV-1** obtained with an Ar gas in the relative pressure range from 10^{-6} to 1 at -185.7 ℃ (*A* = absolute adsorption ($Ncc \cdot g^{-1}$)). (b) Horvath-Kawazoe Differential Pore Volume Plot of **IV-1**. Only one sharp peak at about 8 Å is observed, indicating that the regular size of microporous channels is opened.

The CH_4 adsorption experiments of **IV-1**, **IV-2**, and **IV-3** were also carried out in comparison with zeolite 5A, which has the highest CH_4 adsorption capacity in zeolites.[6-8] Figure IV.5 shows the isotherms for the CH_4 adsorption in the pressure range between 1 and 36 atm at 25 ℃. The CH_4 adsorption quantity at high pressure in **IV-1** (*ca.* 146 $Ncc \cdot g^{-1}$ at 36 atm) is much larger than that of zeolite 5A (*ca.* 83 $Ncc \cdot g^{-1}$ at 36 atm). At 36 atm, the density of CH_4 adsorbed in **IV-1** for micropore volume is 0.21 $g \cdot ml^{-1}$. The density of the compressed CH_4 gas at 27 ℃ and 280 atm (0.16 $g \cdot ml^{-1}$) is almost the same as that of **IV-1** at 25 ℃ and 36 atm, indicative of a concentration effect by strong micropore filling in the cavities. The high-pressure adsorption of supercritical CH_4 in the micropore field has been studied with the following extended DR equation,[20,21]

$$[\ln(W_L/W)]^{1/2} = (RT/\beta E_0)(\ln P_{0q} - \ln P) \quad \text{(eq-3)}$$

Here the parameters, W_L and P_{0q}, are the inherent micropore volume and the saturated vapor pressure of the quasi-vaporized supercritical CH_4, respectively. The large inherent micropore volume, W_L, of 224 Ncc·g^{-1} is obtained from the Langmuir plot. This isotherm is well explained by this extended DR equation. The obtained parameters, βE_0 and P_{0q}, are 8.0 kJ·mol^{-1} and 284 atm, respectively. The similar porous compounds **IV-2** and **IV-3** to **IV-1** also adsorb a large amount of the CH_4 gas (*ca.* 134 Ncc·g^{-1} for **IV-2** and *ca.* 110 Ncc·g^{-1} for **IV-3** at 36 atm). The obtained parameters, W_L, βE_0, and P_{0q}, are 212 Ncc·g^{-1}, 8.0 kJ·mol^{-1}, 290 atm for **IV-2**, and 168 Ncc·g^{-1}, 8.0 kJ·mol^{-1}, 265 atm for **IV-3**, respectively, comparable to those of **IV-1**. The $q_{st,\ \phi=1/e}$ value of 16.2 kJ·mol^{-1}, calculated from the eq-2, is similar to those of activated carbon (17.6 kJ·mol^{-1}),[22] activated carbon fibers (17-18 kJ·mol^{-1}),[20] and the porous coordination polymer $[Cd_2(NO_3)_4(azpy)_3]_n$ (16.3 kJ·mol^{-1}) (azpy = 4,4'-azopyridine).[23] On the other hand, the $q_{st,\ \phi=1/e}$ values of **IV-1** and **IV-2** are apparently smaller than that of $[Co(NCS)_2(azpy)_2]_n$ (20.2 kJ·mol^{-1}),[23] because the interpenetrating coordination polymer $[Co(NCS)_2(azpy)_2]_n$ affords very small channels (*ca.* 3 Å × 3 Å) and has a deeper potential well than **IV-1** and **IV-2**.

Micropore filling of Ar, N_2, and supercritical CH_4, is physical adsorption enhanced by the micropore field and has greater heat of adsorption than typical physical adsorption on the flat surface by several kJ·mol^{-1}. Therefore, the enhancement of the micropore filling strongly depends on the micropore width and shape. As mentioned above, coordination polymers can easily afford a nano-order size of channels by crystal engineering, potentially being a good candidate for a new adsorbent.

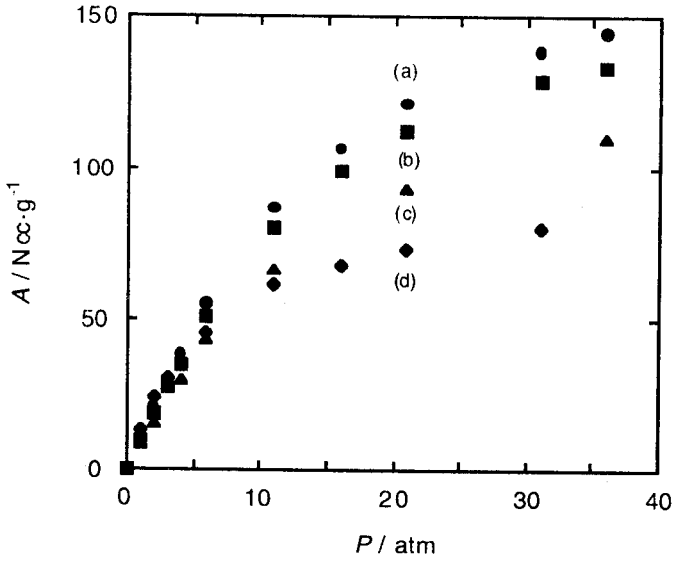

Figure IV.5. Adsorption isotherms of (a) **IV-1**, (b) **IV-2**, (c) **IV-3**, and (d) zeolite 5A, obtained with a CH_4 gas between 1 and 36 atm at 25 ℃ (A = absolute adsorption ($Ncc\cdot g^{-1}$)).

IV. 4 Conclusion

By using the AF_6^{2-} dianions (A = Si, Ge, and Ti) as a bridging unit for the Cu(II) ion, the author succeeded in synthesizing coordination polymers, $[Cu(AF_6)(4,4'\text{-bpy})_2]_n$ (A = Si (**IV-1**), Ge (**IV-2**), and Ti (**IV-3**)), which afford a stable, 3-D, microporous network. The channel size is *ca.* 8 Å x 8 Å along the *c*-axis and *ca.* 6 Å x 2 Å along the *a*- or *b*-axes. These compounds show the high adsorption ability for the CH_4 gas (second generation compounds), illustrating that van der Waals mechanism operates well in the case of microporous coordination polymers. It is worth noting that the selection of AF_6^{2-} anions in the Cu(II)/4,4'-bpy system is of significance for the construction of 3-D porous networks.

IV. 5 References

(1) Corma, A. *Chem. Rev.* **1997**, *97*, 2373-2419.

(2) Ozin, G. A.; Kuperman, A.; Stein, A. *Angew. Chem., Int. Ed. Engl.* **1989**, *28*, 359-376.

(3) Hölderich, W.; Hesse, M.; Naumann, F. *Angew. Chem., Int. Ed. Engl.* **1988**, *27*, 226-246.

(4) Yaghi, O. M.; Li, G.; Li, H. *Nature* **1995**, *378*, 703-706.

(5) Yaghi, O. M.; Davis, C. E.; Li, G.; Li, H. *J. Am. Chem. Soc.* **1997**, *119*, 2861-2868.

(6) Zhang, S.-Y.; Talu, O.; Hayhurst, D. T. *J. Phys. Chem.* **1991**, *95*, 1722-1726.

(7) Zuech, J. L.; Hines, A. L.; Sloan, E. D. *Ind. Eng. Chem. Process Des. Dev.* **1983**, *22*, 172-174.

(8) Mentasty, L.; Woestyn, A. M.; Zgrablich, G. *Adsorp. Sci. Technol.* **1994**, *11*, 123-133.

(9) Altomare, A.; Burla, M. C.; Camalli, M.; Cascarano, M.; Giacovazzo, C.; Guagliardi, A.; Polidori, G. *J. Appl. Cryst.* **1994**, *27*, 435.

(10) Beurskens, P. T.; Admiraal, G.; Beurskens, G.; Bosman, W. P.; de Gelder, R.; Israel, R.; Smits, J. M. M. **1994**, The DIRDIF-94 program system, Technical Report of the Crystallography Laboratory, University of Nijmegen, The Netherlands.

(11) Sheldrick, G. M.; **1997**, Program for the Solution of Crystal Structures. University of Goettingen, Germany.

(12) Crystal Structure Analysis Package, Molecular Structure Corporation (1985 & 1999).

(13) Hereafter the channel dimensions are calculated by considering overlapping spheres with van der Waals radii.

(14) Subramanian, S.; Zaworotko, M. J. *Angew. Chem., Int. Ed. Engl.* **1995**, *34*, 2127-2129.

(15) Gable, R. W.; Hoskins, B. F.; Robson, R. *Chem. Commun.* **1990**, 1667-1668.

(16) Carlucci, L.; Ciani, G.; Proserpio, D. M. *New J. Chem.* **1998**, 1319-1321.

(17) The heated single crystal **IV-1'**$\cdot 5H_2O$ was analyzed at -100 ℃: Tetragonal, space group *P4/mmm* with a = 11.0449(6) Å, c = 8.055(1) Å, V = 982.6(1) Å^3, Z = 1, ρ(calcd) = 1.027 g·cm^{-3}, $F(000)$ = 311.00, μ(Mo Kα) = 6.40 cm^{-1}, no. of obsd data = 447, no. of variables = 44, R (I > 2.00σ(I), all data) = 0.1231, 01529, R_w (I > 2.00σ(I), all data) = 0.1557, 0.1609, GOF = 2.250.

(18) Seki, K.; Takamizawa, S.; Mori, W. *Chem. Lett.* **2001**, 122-123.

(19) Horvath, G.; Kawazoe, K. *J. Chem. Engineer. Jpn.* **1983**, *16*, 470-475.

(20) Kaneko, K.; Murata, K.; Shimizu, K.; Camara, S.; Suzuki, T. *Langmuir* **1993**, *9*, 1165-1167.

(21) Kaneko, K.; Murata, K. *Adsorption* **1997**, *3*, 197-208.

(22) Agarwal, R. K.; Schwarz, J. A. *J. Colloid Interface Sci.* **1989**, *130*, 137-145.

(23) Kondo, M.; Shimamura, M.; Noro, S.; Minakoshi, S.; Asami, A.; Seki, K.; Kitagawa, S. *Chem. Mater.* **2000**, *12*, 1288-1299.

Chapter V

Framework Engineering by Anions and Dynamic Anion-Exchange Properties of Cu(II)/4,4'-bpy Coordination Polymers

Abstract: Combination of framework-builder (Cu(II) ion and 4,4'-bpy ligand) and framework-regulator (AF_6 type anions; A = Si, Ge, and P) provides a series of novel porous coordination polymers. When compounds **IV-1-3** were immersed in water, a conversion of 3-D networks (**IV-1-3**) to interpenetrated ones $\{[Cu(4,4'\text{-bpy})_2(H_2O)_2]\cdot AF_6\}_n$ (A = Si (**V-1**), Ge (**V-2**), and Ti (**V-3**)) (*2-D Interpenetration*) took place. This 2-D interpenetrated network **V-1** shows unique dynamic anion-exchange properties, which accompany drastic structural conversions. When a PF_6^- monoanion instead of AF_6^{2-} dianions was used as the framework-regulator with another co-counter anions (coexistent anions), porous coordination polymers with various types of frameworks, $\{[Cu_2(4,4'\text{-bpy})_5(H_2O)_4]\cdot\text{anions}\cdot 2H_2O\cdot 4EtOH\}_n$ (anions = $4PF_6^-$ (**V-4**·$2H_2O$·4EtOH), $2PF_6^- + 2ClO_4^-$ (**V-5**·$2H_2O$·4EtOH)) (*2-D Double-Layer*), $\{[Cu_2(PF_6)(NO_3)(4,4'\text{-bpy})_4]\cdot 2PF_6\cdot 2H_2O\}_n$ (**V-6**·$2PF_6$·$2H_2O$) (*3-D Undulated Grid*), $\{[Cu(PF_6)(4,4'\text{-bpy})_2(MeCN)]\cdot PF_6\cdot 2MeCN\}_n$ (**V-7**·2MeCN) (*2-D Grid*), and $\{[Cu(4,4'\text{-bpy})_2(H_2O)_2]\cdot PF_6\cdot BF_4\}_n$ (**V-8**) (*2-D Grid*), were obtained, where the three modes of PF_6^- anions are observed. **V-6**·$2PF_6$·$2H_2O$ has rare PF_6^- bridges. The PF_6^- and NO_3^- monoanions alternately link to the Cu(II) centers in the undulated 2-D sheets of $[Cu(4,4'\text{-bpy})_2]_n$ to form a 3-D porous network. The free PF_6^- anions are included in the channels. **V-7**·2MeCN affords both free and terminal-bridged PF_6^- anions. **V-4**·$2H_2O$·4EtOH, **V-5**·$2H_2O$·4EtOH, and **V-8** bear free PF_6^- anions. All of the anion in **V-4**·$2H_2O$·4EtOH and **V-5**·$2H_2O$·4EtOH are freely located in the channels constructed from a host network. Interestingly, these Cu(II) frameworks are rationally controlled by counter anions and selectively converted to other ones.

V. 1 Introduction

Coordination polymers having flexible or rigid microporous channels are of great interest due to their unique properties such as physical gas adsorption,[1-15] chemical adsorption,[2,6,16-20] ion-exchange,[21-24] heterogeneous catalysis,[25-27] and so on. The porous coordination polymers have advantages to provide not only light materials with high porosity but also desirable regular networks. Werner complexes,[28] Prussian blue compounds,[29-31] and Hofmann clathrates and their derivatives[32] are widely known as porous materials that can reversibly adsorb small molecules. There are also numerous examples of porous organic frameworks that are sustained by hydrogen bonds.[33-38] Previously, our laboratory has defined the porous compounds in the three categories.[39] The first generation compounds afford microporous channels with guest molecules, which are destroyed by the removal of all guest molecules. The second ones have rigid vacant channels formed after the removal of guest molecules. The third ones bear flexible channels, which change their own frameworks responding to an external physical stimulus, such as pressure and light, and a chemical stimulus by guest molecules. A large number of dicarboxylate- or tricarboxylate-bridged porous coordination polymers have been hitherto synthesized and investigated about their porous functions.[1-5,13,14,18-20,40] These carboxylate-bridged porous coordination polymers tend to provide rigid framework because of the two site-binding mode of anionic carboxylate groups, therefore classified as the second generation compounds. Recently, several coordination polymers have been prepared, where these frameworks change reversibly on removal/clathration of guest molecules or anions.[20,40-45] The porous coordination polymers of 4,4'-bpy have relatively flexible frameworks based on the single site-binding of neutral pyridyl groups, potentially affording the third generation compounds evolving from the second generation ones.[7,22,25] On this background, the author has challenged to develop a new type of coordination polymer chemistry of 4,4'-bpy. Recent synthetic chemistry of coordination polymers has so far been mainly focused on transition metal ions and co-ligands. This is because frameworks owe to topology and geometry of both ligands and metal cations. In this sense, a pair of a metal and a

ligand is regarded as a framework-builder. In addition, the author noted counter anions, which have not only a role to neutralize overall charge in the solid but also to regulate frameworks, therefore this anion is called a framework-regulator. As shown in Scheme V.1, AF_6^{2-} (A = Si, Ge, and Ti) and PF_6^- anions are utilized, resulting in a key for construction, interconversion, and restoration of frameworks.

Scheme V.1

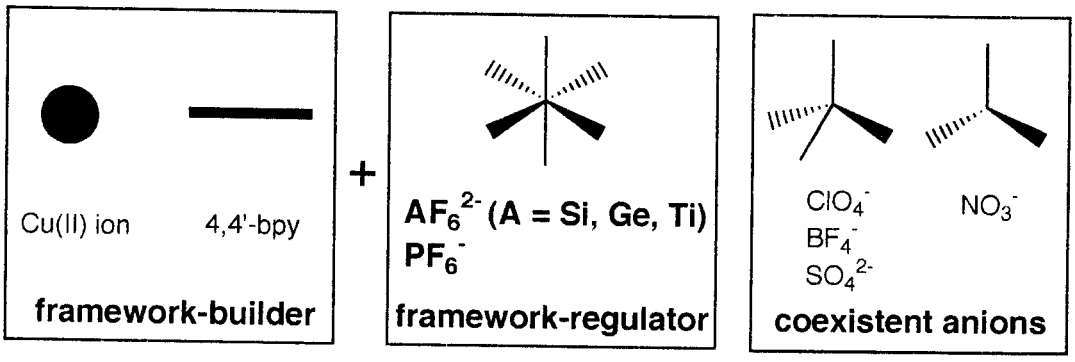

Cu(II) complexes could be relevant for crystal engineering by framework-builder/-regulator, liable to undergo Jahn-Teller effect, resulting in a (4+2) coordination. In the presence of 4,4'-bpy ligand, the AF_6 anions tend to sit the axial sites of the Cu(II) ion. By utilizing this tendency, the control of the framework by anions could be carried out. Moreover, the author introduced additional coexistent anions such as NO_3^-, BF_4^-, ClO_4^-, and SO_4^{2-} (Scheme V.1), which afford various shapes (tetrahedral or trigonal), sizes, charges (mono- or di-anion), and coordinate atoms (O or F), in the PF_6^- system to closely study about the influence of the counter anion in the Cu/4,4'-bpy system.

In this chapter, the author obtained the following porous coordination polymers, $\{[Cu(4,4'\text{-bpy})_2(H_2O)_2]\cdot AF_6\}_n$ (A = Si (**V-1**), Ge (**V-2**), and Ti (**V-3**)) (*2-D Interpenetration*), $\{[Cu_2(4,4'\text{-bpy})_5(H_2O)_4]\cdot anions\cdot 2H_2O\cdot 4EtOH\}_n$ (anions = $4PF_6^-$ (**V-4**·$2H_2O$·4EtOH), $2PF_6^-$ + $2ClO_4^-$ (**V-5**·$2H_2O$·4EtOH)) (*2-D Double-Layer*), $\{[Cu_2(PF_6)(NO_3)(4,4'\text{-bpy})_4]\cdot 2PF_6\cdot 2H_2O\}_n$ (**V-6**·$2PF_6$·$2H_2O$) (*3-D Undulated Grid*), $\{[Cu(PF_6)(4,4'\text{-bpy})_2(MeCN)]\cdot PF_6\cdot 2MeCN\}_n$ (**V-7**·2MeCN) (*2-D Grid*), and $\{[Cu(4,4'\text{-bpy})_2(H_2O)_2]\cdot PF_6\cdot BF_4\}_n$ (**V-8**) (*2-D Grid*), which were

crystallographically characterized and investigated about porous functions. In these complexes, 3-D network of **V-6**·2PF_6·2H_2O is the second generation compound. A conversion of 3-D networks (**IV-1-3**) to interpenetrated networks (**V-1-3**) took place in being immersed in water. **V-1** shows unprecedented dynamic anion-exchange properties and is classified as the third generation compound. When the PF_6^- anion was used together with coexistent anions in the reaction with the Cu(II) ion and 4,4'-bpy, various types of porous networks were constructed as shown in Scheme V.2. In these PF_6^- complexes, only **V-6**·2PF_6·2H_2O affords a 3-D porous framework, in which 2-D undulated layers of $[Cu(4,4'\text{-bpy})_2]_n$ are bridged by PF_6^- and NO_3^- anions alternately. Other coordination polymers (**V-4**·2H_2O·4EtOH, **V-5**·2H_2O·4EtOH, **V-7**·2MeCN, and **V-8**) represent 2-D porous networks, but their detailed structures are clearly different from each other. This observation of the coexistent effect of counter anions is first example.

Scheme V.2

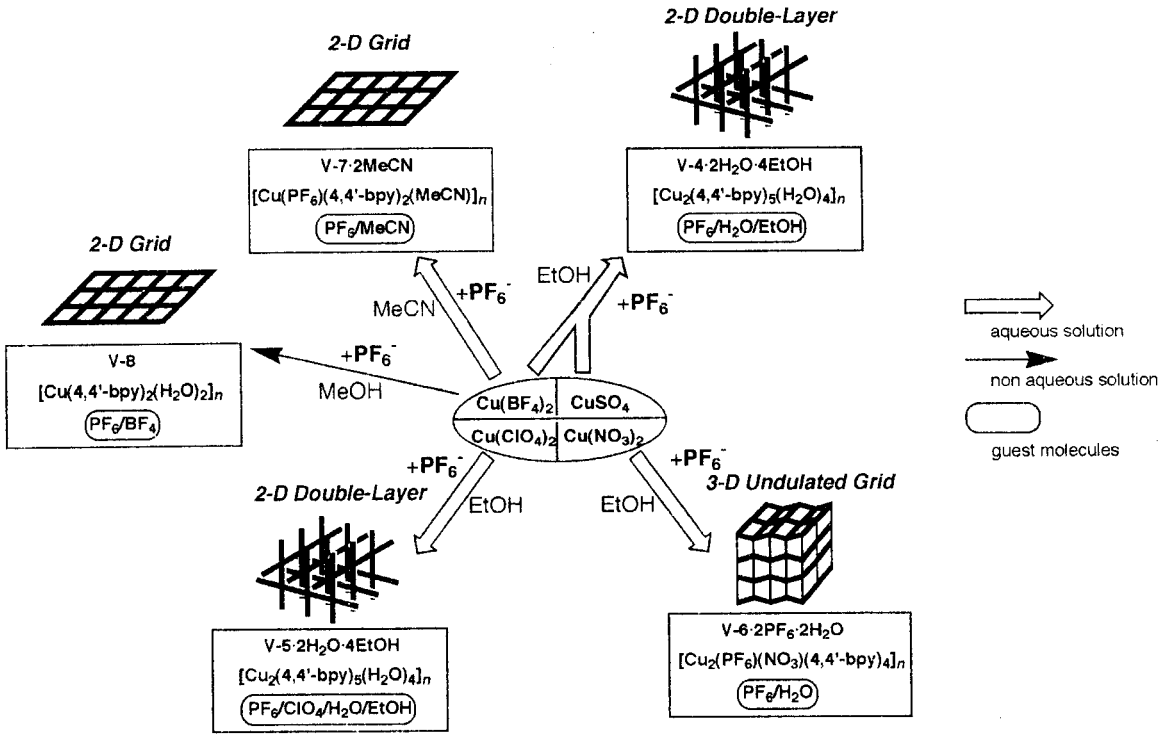

V. 2 Experimental

V. 2. 1 Physical Measurements

The physical measurements were performed as described in Chapter I.

V. 2. 2 Syntheses

Materials. $CuSO_4 \cdot 5H_2O$, $Cu(NO_3)_2 \cdot 3H_2O$, NH_4PF_6, and $(NH_4)_2SO_4$ were obtained from Wako Co. 4,4'-Bpy was purchased from Tokyo Kasei Industrial Co. $Cu(BF_4)_2 \cdot xH_2O$, $(NH_4)_2SiF_6$, $(NH_4)_2GeF_6$, and $(NH_4)_2TiF_6$, were obtained from Aldrich Chemical Co. $Cu(ClO_4)_2 \cdot 6H_2O$ was obtained from Kanto Chemical Co.

Synthesis of $\{[Cu(4,4'\text{-}bpy)_2(H_2O)_2]\cdot SiF_6\}_n$ (V-1). The compound of **V-1** was synthesized as follows: a hot aqueous solution (10 mL) of $Cu(BF_4)_2 \cdot xH_2O$ (237 mg, 1.00 mmol) and $(NH_4)_2SiF_6$ (178 mg, 1.00 mmol) was added to a hot aqueous solution (10 mL) of 4,4'-bpy (312 mg, 2.00 mmol). Color of the resultant suspension was purple and gradually changed to sky-blue. The obtained sky-blue powder was filtered, washed with acetone, and dried in air to give the microcrystals (yield; 362 mg, 61 %). The crystals suitable for the X-ray analysis were obtained by the same method as **IV-1**$\cdot 8H_2O$. The homogeneity of the powder sample was confirmed by comparison of the observed and calculated XRPD patterns obtained from the single-crystal data. This powder sample contains guest H_2O molecules, because of the presence of a vacant space generated by a slight defect of the overall structure. Anal. Calcd for $\{[Cu(4,4'\text{-}bpy)_2(H_2O)_2]\cdot SiF_6\cdot 2.3H_2O\}_n$ (**V-1**$\cdot 2.3H_2O$): C, 40.34; H, 4.16; N, 9.41. Found: C, 40.36; H, 3.78; N, 9.42. IR (KBr pellet): 3441 bm, 3109 w, 3088 w, 1635 w, 1612 s, 1537 w, 1493 w, 1415 m, 1223 m, 1068 m, 1014 w, 852 m, 812 m, 748 s, 690 s, 671 m, 642 m, 617 m, 480 m, 462 m (cm^{-1}).

Synthesis of $\{[Cu(4,4'\text{-}bpy)_2(H_2O)_2]\cdot GeF_6\}_n$ (V-2). This compound was prepared in the procedure similar to that of **V-1** (62 % yield). Anal. Calcd for $\{[Cu(4,4'\text{-}bpy)_2(H_2O)_2]\cdot GeF_6\cdot 2.7H_2O\}_n$ (**V-2**$\cdot 2.7H_2O$): C, 37.12; H, 3.96; N, 8.66. Found: C, 37.00; H, 3.58; N, 8.66. IR (KBr pellet): 3426 bm, 3111 w, 1637 w, 1610 s, 1537 w, 1493 w, 1415 m, 1323 w, 1223 w, 1068 m, 1014 w, 850 w, 812 m, 731 w, 679 w, 625 m, 603 s, 563 s, 470 w (cm^{-1}).

Synthesis of $\{[Cu(4,4'\text{-bpy})_2(H_2O)_2]\cdot TiF_6\}_n$ (V-3) This compound was prepared in the procedure similar to that of **V-1** (66 % yield). Anal. Calcd for $\{[Cu(4,4'\text{-bpy})_2(H_2O)_2]\cdot TiF_6\cdot 1.3H_2O\}_n$ (**V-3**$\cdot 3H_2O$): C, 40.25; H, 3.59; N, 9.42. Found: C, 40.22; H, 3.81; N, 9.38. IR (KBr pellet): 3366 bm, 3106 w, 3083 w, 1645 w, 1609 s, 1536 m, 1490 m, 1413 m, 1322 w, 1221 m, 1067 m, 1012 w, 850 w, 813 m, 730 w, 680 m, 637 m, 526 s, 470 m (cm^{-1}).

Synthesis of $\{[Cu_2(4,4'\text{-bpy})_5(H_2O)_4]\cdot 4PF_6\cdot 2H_2O\cdot 4EtOH\}_n$ (V-4$\cdot 2H_2O\cdot 4EtOH$). An EtOH solution (10 mL) of 4,4'-bpy (390 mg, 2.50 mmol) was diffused to an aqueous solution (10 mL) of $Cu(BF_4)_2\cdot xH_2O$ (237 mg, 1.00 mmol) and NH_4PF_6 (326 mg, 2.00 mmol) in the straight glass tube. Purple single crystals of **V-4**$\cdot 2H_2O\cdot 4EtOH$ were obtained after a few days, and collected. They were washed with EtOH, and dried in air (yield 85 mg, 10 %). The crystals of **V-4**$\cdot 2H_2O\cdot 4EtOH$ were also obtained together with sky-blue crystals of $\{[Cu(SO_4)(4,4'\text{-bpy})(H_2O)_3]\cdot 2H_2O\}_n$ (**V-9**$\cdot 2H_2O$) by using $CuSO_4\cdot 5H_2O$ as a starting material. This compound easily released guest H_2O and EtOH molecules to form a desolvated one. Anal. Calcd for $\{[Cu_2(4,4'\text{-bpy})_5(H_2O)_4]\cdot 4PF_6\cdot 2EtOH\}_n$ (**V-4**$\cdot 2EtOH$): C, 39.26; H, 3.66; N, 8.48. Found: C, 38.72; H, 3.47; N, 8.47. IR (KBr pellet): 3395 w, 3117 w, 1684 w, 1616 m, 1539 w, 1493 w, 1425 m, 1226 w, 1076 m, 1022 w, 1001 w, 843 s, 814 s, 738 w, 669 w, 646 w, 639 w, 557 s (cm^{-1}).

Synthesis of $\{[Cu_2(4,4'\text{-bpy})_5(H_2O)_4]\cdot 2PF_6\cdot 2ClO_4\cdot 2H_2O\cdot 4EtOH\}_n$ (V-5$\cdot 2H_2O\cdot 4EtOH$). An EtOH solution (10 mL) of 4,4'-bpy (390 mg, 2.50 mmol) was diffused to an aqueous solution (10 mL) of $Cu(ClO_4)_2\cdot 6H_2O$ (370 mg, 1.00 mmol) and NH_4PF_6 (326 mg, 2.00 mmmol) in the straight glass tube. Purple single crystals of **V-5**$\cdot 2H_2O\cdot 4EtOH$ were obtained after a few days, and collected. They were washed with EtOH, and dried in air (yield; 131 mg, 17 %). This compound readily released the guest H_2O and EtOH molecules to form a desolvated one. Anal. Calcd for $\{[Cu_2(4,4'\text{-bpy})_5(H_2O)_4]\cdot 2PF_6\cdot 2ClO_4\cdot 2EtOH\}_n$ (**V-5**$\cdot 2EtOH$): C, 41.55; H, 3.87; N, 8.97. Found: C, 41.02; H, 3.68; N, 9.09. IR (KBr pellet): 3422 w, 3113 w, 1616 m, 1558 w, 1539 w, 1491 w, 1423 w, 1224 w, 1115 m, 1076 m, 843 s, 814 s, 738 w, 669 m, 648 m, 625 m, 557 m (cm^{-1}).

Synthesis of $\{[Cu_2(PF_6)(NO_3)(4,4'\text{-bpy})_4]\cdot 2PF_6\cdot 2H_2O\}_n$ (V-6$\cdot 2PF_6\cdot 2H_2O$). An EtOH

solution (20 mL) of 4,4'-bpy (312 mg, 2.00 mmol) was diffused to an aqueous solution (20 mL) of $Cu(NO_3)_2 \cdot 3H_2O$ (242 mg, 1.00 mmol) and NH_4PF_6 (326 mg, 2 mmol) at the 1:2 ratio in the straight glass tube. Purple single crystals were obtained after a few days, and collected. They were washed with EtOH, and dried in air (yield; 150 mg, 23 %). They are available for the single crystal X-ray structure determination. According to the single crystal structure, it contains only PF_6^- anions as metal-free counter anions in the channels. In the case of a large scale preparation, partial replace of the NO_3^- anions occurs for the free PF_6^- anions, and therefore, the ratio of PF_6^- and NO_3^- anions in the elemental analysis is different from that of **V-6**$\cdot 2PF_6 \cdot 2H_2O$. When a NO_3^- anion, with a smaller volume than that of PF_6^-, is included in the channel, an additional EtOH molecule is clathrated to occupy a vacant space of the channel. The XRPD pattern of the sample with mixed free counter anions is in agreement with the simulated pattern obtained from the X-ray crystal analysis of **V-6**$\cdot 2PF_6 \cdot 2H_2O$, indicating the formation of the similar 3-D network. Anal. Calcd for $\{[Cu_2(PF_6)(NO_3)(4,4'\text{-bpy})_4] \cdot 1.4PF_6 \cdot 0.6NO_3 \cdot 2H_2O \cdot 1.2EtOH\}_n$ (**V-6**$\cdot 1.4PF_6 \cdot 0.6NO_3 \cdot 2H_2O \cdot 1.2EtOH$): C, 39.47; H, 3.37; N, 10.42. Found: C, 39.55; H, 3.11; N, 10.44. IR (KBr pellet): 3421 bw, 3308 bw, 3113 w, 1705 w, 1645 w, 1616 m, 1537 w, 1495 w, 1421 m, 1385 m, 1348 m, 1321 m, 1228 w, 1107 w, 1070 w, 1020 w, 843 s, 738 w, 673 w, 646 m, 557 m (cm^{-1}).

Synthesis of $\{[Cu(PF_6)(4,4'\text{-bpy})_2(MeCN)] \cdot PF_6 \cdot 2MeCN\}_n$ (V-7·2MeCN). An MeCN solution (10 mL) of 4,4'-bpy (312 mg, 2.00 mmol) was diffused to an aqueous solution (10 mL) of $Cu(BF_4)_2 \cdot xH_2O$ (237 mg, 1.00 mmol) and NH_4PF_6 (326 mg, 2.00 mmol) in the straight glass tube. Purple single crystals of **V-7**·2MeCN were obtained after a few days, and collected. They were washed with MeCN, and dried in air (yield; 132 mg, 17 %). This compound readily released guest MeCN molecules and adsorbed *ca.* 3 molecules of H_2O in the atmosphere to form a hydrated one $\{[Cu(PF_6)(4,4'\text{-bpy})_2(MeCN)] \cdot PF_6 \cdot 3H_2O\}_n$ (**V-7**$\cdot 3H_2O$). Anal. Calcd for $\{[Cu(PF_6)(4,4'\text{-bpy})_2(MeCN)] \cdot PF_6 \cdot 3H_2O\}_n$ (**V-7**$\cdot 3H_2O$): C, 34.73; H, 3.31; N, 9.20. Found: C, 34.37; H, 2.85; N, 9.21. IR (KBr pellet): 3431 bw, 1956 w, 1616 m, 1539 w, 1496 w, 1423 m, 1224 m, 1074 m, 1020 w, 839 s, 810 s, 738 w, 646 m, 557 m (cm^{-1}).

Synthesis of $\{[Cu(4,4'\text{-bpy})_2(H_2O)_2] \cdot PF_6 \cdot BF_4\}_n$ (V-8). A MeOH solution (10 mL) of

4,4'-bpy (312 mg, 2.00 mmol) was diffused to a MeOH solution (10 mL) of $Cu(BF_4)_2 \cdot xH_2O$ (237 mg, 1.00 mmol) and NH_4PF_6 (326 mg, 2.00 mmol) in the straight glass tube. Purple single crystals were obtained after a few days, and collected. They were washed with MeOH, and dried in air (yield; 144 mg, 22 %). Anal. Calcd for $\{[Cu(4,4'\text{-bpy})_2(H_2O)_2] \cdot PF_6 \cdot BF_4\}_n$ (**V-8**): C, 37.32; H, 3.13; N, 8.70. Found: C, 37.37; H, 2.99; N, 8.88. IR (KBr pellet): 3437 bm, 3118 w, 1645 w, 1616 s, 1539 w, 1496 w, 1423 m, 1230 m, 1076 m, 1045 m, 976 w, 844 s, 819 s, 729 w, 648 w, 557 m, 482 w (cm^{-1}).

Synthesis of $\{[Cu(SO_4)(4,4'\text{-bpy})(H_2O)_3] \cdot 2H_2O\}_n$ (V-9·2H$_2$O). A MeOH solution (10 mL) of 4,4'-bpy (156 mg, 1.00 mmol) was added to an aqueous solution (10 mL) of $CuSO_4 \cdot 5H_2O$ (250 mg, 1.00 mmol). The obtained sky-blue powder was filtered, washed with H_2O and MeOH, and dried under vacuum for 2 hours to give the microcrystals (yield; 363 mg, 89 %). The homogeneity of the powder sample was confirmed by comparison of the observed XRPD pattern with calculated one obtained from the single-crystal data reported previously.[46] Anal. Calcd for $\{[Cu(SO_4)(4,4'\text{-bpy})(H_2O)_3] \cdot 2H_2O\}_n$ (**V-9**·2H$_2$O): C, 29.59; H, 4.47; N, 6.90. Found: C, 29.77; H, 3.81; N, 6.82. IR (KBr pellet): 3422 bs, 1610 m, 1535 w, 1493 w, 1417 w, 1223 m, 1107 s, 1076 m, 1043 m, 968 w, 812 m, 723 w, 669 w, 646 m, 617 m, 472 w (cm^{-1}).

Synthesis of $\{[Cu(4,4'\text{-bpy})_2(H_2O)_2] \cdot 2PF_6\}_n$ (V-10). This compound was obtained by the anion-exchange reaction with **V-1**. An excess amount of NH_4PF_6 was added to **V-1** in an aqueous solution. After three days, a solution color changed from sky-blue to purple, and the resultant precipitate was filtered, washed with H_2O and acetone, and dried under vacuum for 2 hours. Anal. Calcd for $\{[Cu(4,4'\text{-bpy})_2(H_2O)_2] \cdot 2PF_6\}_n$ (**V-10**): C, 34.23; H, 2.87; N, 7.98. Found: C, 34.58; H, 2.54; N, 7.65. IR (KBr pellet): 3443 bw, 1616 m, 1539 w, 1496 w, 1423 w, 1327 w, 1226 w, 1074 w, 1020 w, 843 s, 814 m, 736 w, 648 w, 555 m, 505 w (cm^{-1}).

Synthesis of $\{[Cu(ClO_4)_2(4,4'\text{-bpy})(H_2O)_2] \cdot 4,4'\text{-bpy}\}_n$ (V-11). To a hot aqueous solution (10 mL, 50 °C) of 4,4'-bpy (312 mg, 2.00 mmol) was added an aqueous solution (20 mL, 50 °C) of $Cu(ClO_4) \cdot 6H_2O$ (371 mg, 1.00 mmol). The obtained pale purplish-blue powder was obtained, washed with acetone, and dried under vacuum for 15 hours (yield; 534 mg, 87 %).

The homogeneity of the powder sample was confirmed by comparison of the observed XRPD pattern with calculated one obtained from the single-crystal data reported previously. [47] IR (KBr pellet): 3374 bm, 3046 w, 1599 m, 1534 w, 1491 w, 1412 m, 1324 w, 1221 w, 1143 s, 1111 s, 1086 s, 994 w, 940 w, 810 m, 724 w, 627 m cm^{-1}.

V. 2. 3 X-Ray Structure Determination

A single crystal for each compound was mounted on a glass fiber and coated with epoxy resin. For **V-1**, **V-4**·$2H_2O$·4EtOH, and **V-5**·$2H_2O$·4EtOH, X-ray data collections were carried out by a Rigaku Mercury diffractometer with graphite monochromated Mo-Kα radiation. For **V-2**, all measurements were made on a Rigaku RAXIS-CS with graphite monochromated Mo-Kα radiation. In compound **V-3**, data collections were carried on a Rigaku AFC7R automated diffractometer with a graphite monochromated Mo-Kα radiation. Unit cell constants were obtained from a least-squares refinement using the setting angles of 25 well-centered reflections in the ranges $22.95 < 2\theta < 29.83$ °. Azimuthal scans of several reflections indicated no need for an adsorption correction. For **V-6**·$2PF_6$·$2H_2O$ and **V-7**·2MeCN, all measurements were made on a Rigaku RAXIS-RAPID imaging plate diffractometer with graphite monochromated Mo-Kα radiation. For **V-2** and **V-4-7**, structures were solved by a direct method using the SIR92 program[48] and expanded using Fourier techniques.[49] For **V-1** and **V-3**, the structures were solved by a direct method using the MITHRIL90 program[50] and expanded using Fourier techniques.[49] In all complexes, except **V-4**·$2H_2O$·4EtOH, the non-hydrogen atoms were refined anisotropically. In **V-4**·$2H_2O$·4EtOH, two carbon and one oxygen atoms of one EtOH molecule were fixed. All hydrogen atoms, which were placed in idealized positions, were included but not refined. The refinements were carried out using full-matrix least squares techniques. Crystal data and details of the structure determinations are summarized in Table V.1. Unfortunately, the author could not obtain single crystals with a good quality for compounds **V-4**·$2H_2O$·4EtOH and **V-5**·$2H_2O$·4EtOH, and the data of the X-ray analysis were poorer than others. All calculations were performed using the teXsan[51] crystallographic software package of Molecular Structure Corporation.

Table V.1a. Crystallographic Data for $\{[Cu(4,4'\text{-bpy})_2(H_2O)_2]\cdot AF_6\}_n$ (A = Si (**V-1**), Ge (**V-2**), and Ti (**V-3**)) and $\{[Cu_2(4,4'\text{-bpy})_5(H_2O)_4]\cdot 4PF_6\cdot 2H_2O\cdot 4EtOH\}_n$ (**V-4**·$2H_2O$·4EtOH).

compoounds	**V-1**	**V-2**	**V-3**	**V-4**·$2H_2O$·4EtOH
formula	$C_{20}H_{20}N_4CuF_6O_2Si$	$C_{20}H_{20}N_4CuF_6GeO_2$	$C_{20}H_{20}CuF_6N_4O_2Ti$	$C_{29}H_{38}N_5CuF_{12}O_5P_2$
fw	554.03	598.53	573.84	890.12
crystal system	tetragonal	tetragonal	tetragonal	orthorhombic
a, Å	11.080(2)	11.1835(6)	11.301(1)	45.47(1)
b, Å				20.523(8)
c, Å	16.0239(7)	15.876(2)	15.733(2)	8.229(3)
V, Å^3	1967.3(5)	1985.6(3)	2009.3(4)	7679(4)
space group	*P4/ncc* (No. 130)	*P4/ncc* (No. 130)	*P4/ncc* (No.130)	*Aba2* (No. 41)
Z	4	4	4	8
ρ(calcd), g·cm^{-3}	1.870	2.002	1.897	1.540
F(000)	1124.00	1196.00	1156.00	3632.00
μ(Mo Kα), cm^{-1}	12.57	26.69	15.40	7.54
diffractometer	CCD	RAXIS-CS	AFC7R	CCD
radiation (λ, Å)	0.71069	0.71069	0.71069	0.71069
temp., °C	25	25	25	-50
GOF	1.831	1.210	1.064	2.694
no. of obsd data	1022 (all data)	1097 (all data)	570 (I > 2.00σ(I))	4052 (all data)
no. of variables	81	81	81	461
R^a (I > 2.00σ(I), all data)	0.0501, 0.0591	0.0530, 0.1129	0.0423	0.1009, 0.1143
$R_w{}^b$ (I > 2.00σ(I), all data)	0.0751, 0.0786	0.0550, 0.0640	0.0703	0.1289, 0.1307

[a] $R = \Sigma||Fo| - |Fc||/\Sigma|Fo|$. [b] $R_w = [(\Sigma w\,(|Fo| - |Fc|)^2/\Sigma wFo^2)]^{1/2}$.

Table V.1b. Crystallographic Data for $\{[Cu_2(4,4'\text{-bpy})_5(H_2O)_4]\cdot 2PF_6\cdot 2ClO_4\cdot 2H_2O\cdot 4EtOH\}_n$ (**V-5**·$2H_2O$·4EtOH), $\{[Cu_2(PF_6)(NO_3)(4,4'\text{-bpy})_4]\cdot 2PF_6\cdot 2H_2O\}_n$ (**V-6**·$2PF_6$·$2H_2O$), and $\{[Cu(PF_6)(4,4'\text{-bpy})_2(MeCN)]\cdot PF_6\cdot 2MeCN\}_n$ (**V-7**·2MeCN).

compoounds	**V-5**·$2H_2O$·4EtOH	**V-6**·$2PF_6$·$2H_2O$	**V-7**·2MeCN
formula	$C_{29}H_{38}N_5CuClF_6O_9P$	$C_{40}H_{36}N_9Cu_2F_{18}O_5P_3$	$C_{26}H_{25}N_7CuF_{12}P_2$
fw	844.61	1284.77	789.00
crystal system	orthorhombic	monoclinic	monoclinic
a, Å	44.870(10)	22.184(2)	11.1611(6)
b, Å	20.292(5)	15.313(1)	13.1786(7)
c, Å	8.170(2)	11.1085(8)	22.1972(2)
β, deg		93.704(3)	92.569(3)
V, Å^3	7439(3)	3765.7(5)	3261.7(2)
space group	*Aba2* (No. 41)	*C2/m* (No. 12)	*P2$_1$/c* (No. 14)
Z	8	2	4
ρ(calcd), g·cm^{-3}	1.508	1.133	1.607
F(000)	3472.00	1288.00	1588.00
μ(Mo Kα), cm^{-1}	7.88	7.08	8.67
diffractometer	CCD	RAXIS-RAPID	RAXIS-RAPID
radiation (λ, Å)	0.71069	0.71069	0.71069
temp., °C	-50	25	-50
GOF	2.756	1.610	1.849
no. of obsd data	4098 (all data)	4155 (all data)	6431 (all data)
no. of variables	470	197	433
R^a (I > 2.00σ(I), all data)	0.0978, 0.1086	0.0615, 0.0767	0.0724, 0.0938
R_w^b (I > 2.00σ(I), all data)	0.1272, 0.1288	0.0812, 0.0841	0.0914, 0.0963

[a] $R = \Sigma||Fo| - |Fc||/\Sigma|Fo|$. [b] $R_w = [(\Sigma w (|Fo| - |Fc|)^2/\Sigma wFo^2)]^{1/2}$.

V. 3 Results and Discussion

V. 3. 1 Crystal Structures

V. 3. 1. 1 Crystal Structures of $\{[Cu(4,4'\text{-bpy})_2(H_2O)_2]\cdot AF_6\}_n$ (A = Si (V-1), Ge (V-2), and Ti (V-3)).

An ORTEP view around a Cu(II) center of **V-1** is shown in Figure V.1(a) with numbering scheme. The Cu(II) atom has an elongated octahedral environment with four nitrogen atoms of 4,4'-bpy ligands in the equatorial plane and two oxygen atoms of H_2O molecules in the axial sites. The Cu(II) centers are bridged by 4,4'-bpy ligands to form a 2-D sheet having square grids with corner angles of *ca.* 89 and 91 ° as shown in Figure V.1(b). Each 2-D sheet lying in (a-b)c and (b-a)c planes affords a perpendicularly-interpenetration mode (*2-D Interpenetration*) to make microporous channels with dimensions of *ca.* 2 Å × 2 Å along the *c*-axis (Figures V.1(c) and V.1(d)). These channels are filled by free SiF_6^{2-} dianions, which interact with the coordinated H_2O molecules by hydrogen bonds (2.702(3) Å). The complexes **V-2** and **V-3** also afford similar networks to **V-1**, which is confirmed by the X-ray crystallographic determination. The hydrogen bond lengths between AF_6^{2-} (A = Ge and Ti) and coordinated H_2O molecule in **V-2** and **V-3** are 2.686(4) and 2.665(4) Å, respectively, relevant for a size of AF_6 anions. These compounds are isostructural with the Zn(II) compounds reported previously.[52]

An interesting feature of these complexes is that the 3-D structures of **IV-1-3** (*3-D Regular Grid*) are transformed into the 2-D interpenetrated structures of **V-1-3** (*2-D Interpenetration*), respectively, in the solid phase. When solid sample of **IV-1-3** was immersed in H_2O, the color changed from purple to sky-blue. The IR measurements show that A-F (A = Si, Ge, and Ti) stretching bands of the sky-blue sample have the different frequency from those of the purple sample (from 742 to 748 cm^{-1} for Si, from 607 to 563 cm^{-1} for Ge, and from 570 to 526 cm^{-1} for Ti). Moreover, the XRPD patterns of the sky-blue powder are in good agreement with the simulated patterns calculated from the crystallographic data of **V-1-3**, clearly indicating that the 3-D porous coordination polymers, **IV-1-3**, are transformed into the 2-D interpenetrated networks, **V-1-3**.

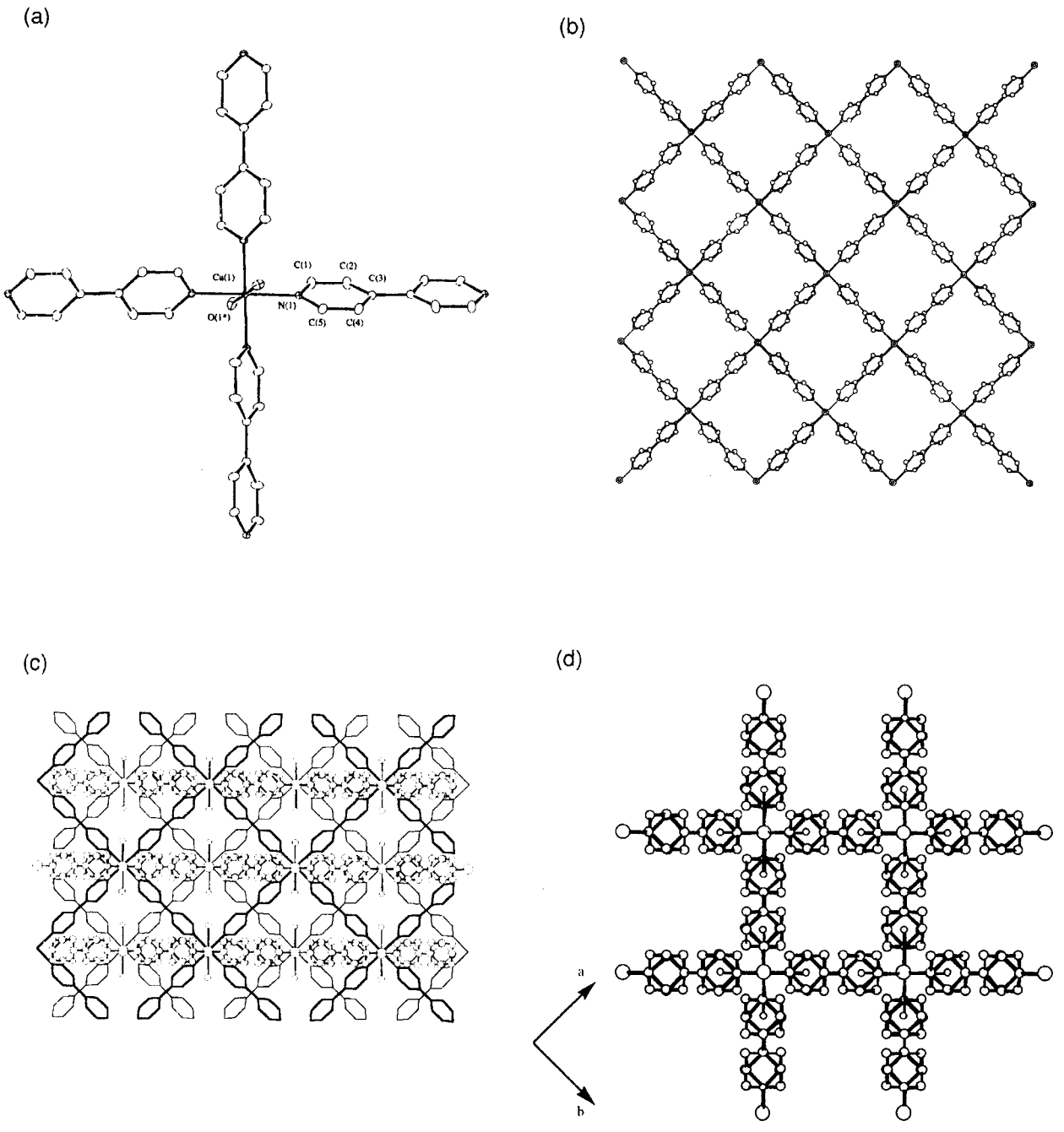

Figure V.1. (a) ORTEP drawing around a Cu(II) center of **V-1** at the 30 % probability level. In regard to all figures, the hydrogen atoms are omitted for clarity. (b) View of a 2-D network of **V-1** along the ab vector. (c) View of the interpenetration mode of **V-1** along the ab vector. The two types of 2-D layers lying parallel and perpendicular to the paper plane are represented by the stick and cylindrical bond models, respectively. The counter SiF_6^{2-} anions are omitted for clarity. (d) View showing the micropore cross section of the network of **V-1** along the *c*-axis. The counter SiF_6^{2-} anions are omitted for clarity.

V. 3. 1. 2 Crystal Structures of $\{[Cu_2(4,4'\text{-bpy})_5(H_2O)_4]\cdot anions\cdot 2H_2O\cdot 4EtOH\}_n$ (anions = $4PF_6^-$ (V-4·2H$_2$O·4EtOH); anions = $2PF_6^-$ and $2ClO_4^-$ (V-5·2H$_2$O·4EtOH)).

An ORTEP view around Cu(II) centers of **V-5**·2H$_2$O·4EtOH is illustrated in Figure V.2(a) with numbering scheme. The Cu(II) center has an elongated distorted octahedral environment with four 4,4'-bpy nitrogen atoms in the equatorial plane, and two oxygen atoms of the H_2O molecules in the axial sites. There are three modes of the coordination for the 4,4'-bpy ligands as illustrated in Figure V.2(a). One is an infinite bridging mode (A), which links two Cu(II) atoms to form a linear chain. Another is a chain-chain bridging mode (B), which links the nearest-neighbor two chains. Interestingly, the 4,4'-bpy ligands (mode B) ligate these linear chains in a different direction (dihedral angle = *ca.* 44 °) as shown in Figures V.2(b) and V.2(c), resulting in a 2-D thick layer. The other is a terminal coordination mode (C), which is in a trans position to the mode B ligand. These three modes of the 4,4'-bpy afford an unprecedented 2-D structure (*2-D Double-Layer*) as illustrated in Figure V.2(d). This type of network is a first example in the 4,4'-bpy system,[53] although similar 2-D thick networks $[M_2(NO_3)_4(4,4'\text{-bpy})_3]_n$ (M = Co, Ni, Zn) have been found.[7,54,55] $[M_2(NO_3)_4(4,4'\text{-bpy})_3]_n$ networks afford a dihedral angle of *ca.* 60 ° between bridged 1-D chains, but an obvious difference is that the two NO_3^- anions ligate to the metal centers instead of terminal 4,4'-bpy ligands in **V-5**·2H$_2$O·4EtOH. Therefore, stacking forms of these 2-D thick layers are apparently different from each other: the tongue-and-groove type stacking is seen for $[M_2(NO_3)_4(4,4'\text{-bpy})_3]_n$ while the π–π stacking of terminal 4,4'-bpy ligands for **V-5**·2H$_2$O·4EtOH.

Each 2-D thick layer assembles by π-π stacking interactions between the mode C of the 4,4'-bpy to form a channeling network along the *c*-axis as shown in Figure V.2(e) and Scheme V.3. The shortest C•••C separation, plane-plane angle, and angle between the ring normal of the pyridine plane and the ring-centroid vector, are *ca.* 3.37 Å, 30 °, and 11 °, respectively.[56] Similar π-π interaction has been reported in other 4,4'-bpy complex.[57] In this crystal, there are two kinds of channels. One (A') is defined by two 4,4'-bpy (mode C) ligands and two 2-D thick layers, and its channel size is *ca.* 7 Å × 3 Å. Another (B') forms within the 2-D thick layer, and

its size is *ca.* 6 Å × 6 Å. In the complex **V-5**·2H_2O·4EtOH, all PF_6^- anions are located in the channels A', and all ClO_4^- ones are located in the channels B'. The guest H_2O and EtOH molecules are also included in the channels and no bonding interactions with the host network are observed. The crystal structure of **V-4**·2H_2O·4EtOH is similar to that of **V-5**·2H_2O·4EtOH.

Scheme V.3

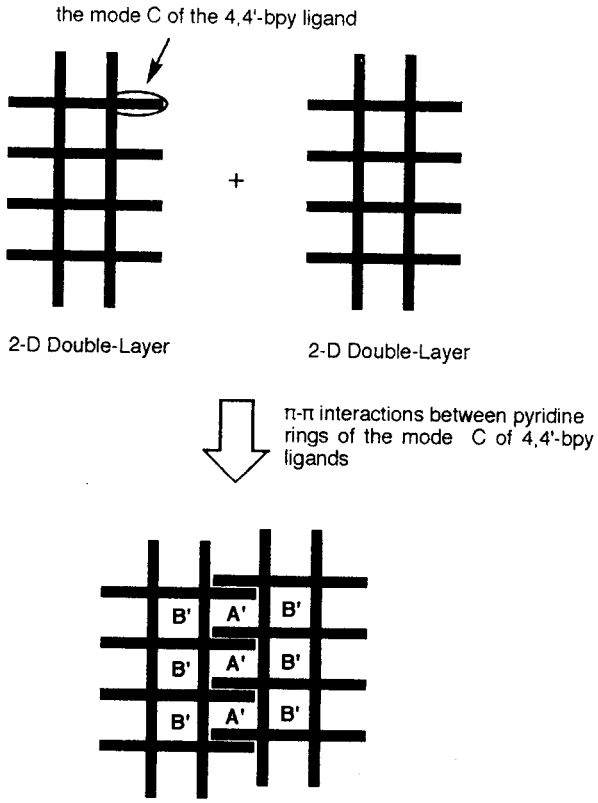

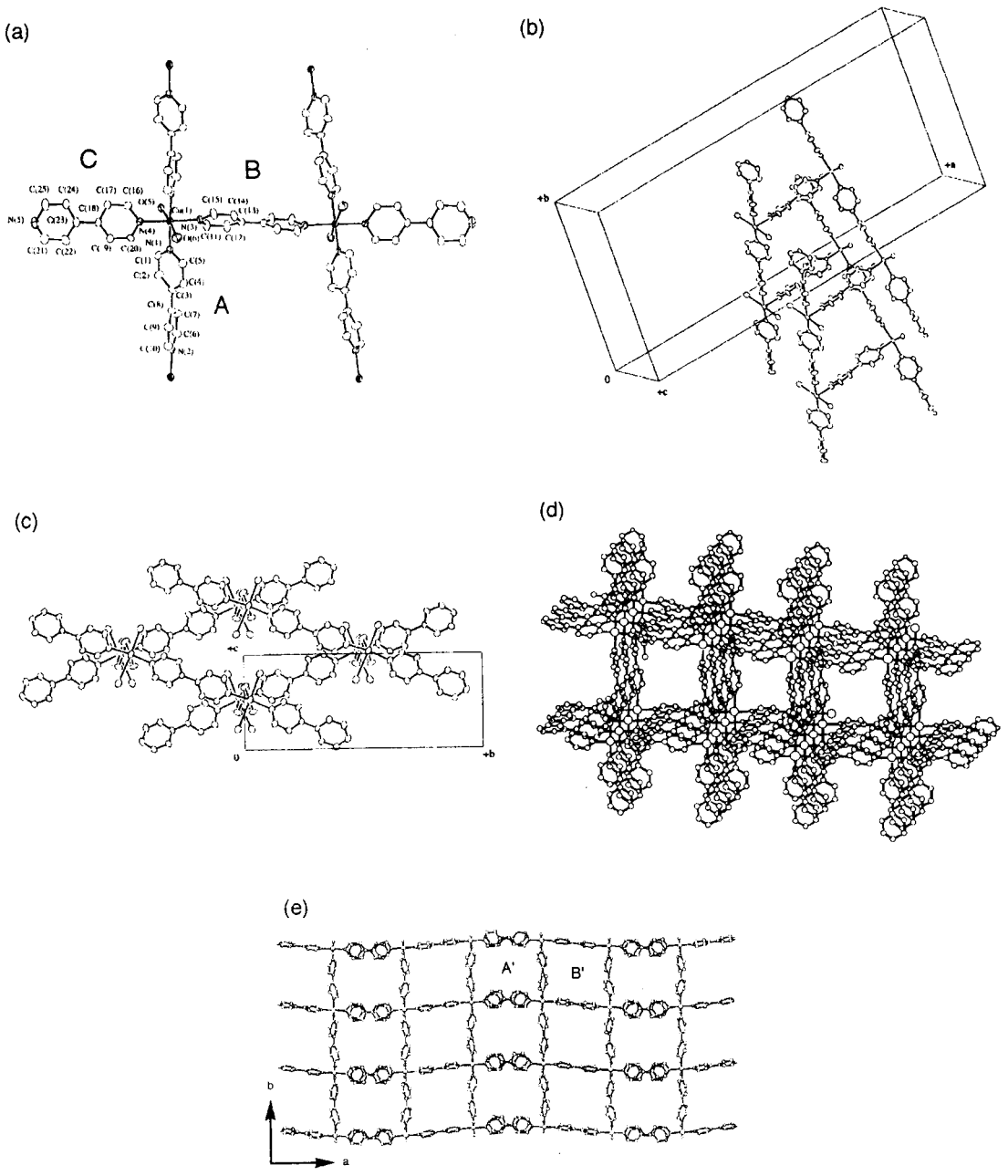

Figure V.2. (a) ORTEP drawing around Cu(II) centers of **V-5**·2H_2O·4EtOH at the 30 % probability level. (b and c) ORTEP view of the 4,4'-bpy ligands (mode B) bridging neighboring 1-D chains of **V-5**·2H_2O·4EtOH at the 30 % probability level. The mode B of the 4,4'-bpy is directed to the *a*-axis. The mode C of the 4,4'-bpy (only b) are omitted for clarity. (d) View of the 2-D thick network of **V-5**·2H_2O·4EtOH. (e) View showing the micropore cross section of the network of **V-5**·2H_2O·4EtOH along the *c*-axis. The counter PF_6^- and ClO_4^- anions, guest H_2O and EtOH molecules, are omitted for clarity.

V. 3. 1. 3 Crystal Structure of $\{[Cu_2(PF_6)(NO_3)(4,4'\text{-bpy})_4]\cdot 2PF_6\cdot 2H_2O\}_n$ (V-6·2PF$_6$·2H$_2$O).

An ORTEP view around a Cu(II) center of **V-6**·2PF$_6$·2H$_2$O is shown in Figure V.3(a) with numbering scheme. The Cu(II) atom has an elongated distorted octahedral environment with four 4,4'-bpy nitrogen atoms in the equatorial plane, and one oxygen atom of the NO_3^- anion and one fluoro atom of the PF_6^- one in the axial sites. The Cu-F distance (2.676(4) Å) is far longer than the Cu-O distance (2.320(5) Å), indicative of a weak coordination ability of the PF_6^- anion. Interestingly, the Cu-F distance of **V-6**·2PF$_6$·2H$_2$O is longer than those of **IV-1**·8H$_2$O (2.357(3) Å) and **IV-2**·8H$_2$O (2.320(5) Å), exhibiting that the interaction of Cu^{2+}•••F could be modulated for infinite networks even though the principal origin is electrostatic.

The 4,4'-bpy ligands bridge Cu(II) ions to form a 2-D network of rhombus grids with the corner angles of *ca.* 86 ° and 94 ° as shown in Figure V.3(b). The layers are linked alternately with NO_3^- and PF_6^- anions by coordination bonds to give a 3-D structure without interpenetration (*3-D Undulated Grid*). Since the Cu•••Cu bridging distances of NO_3^- and PF_6^- anions are different from each other (Cu•••NO_3•••Cu distance = 6.807 Å; Cu•••PF_6•••Cu distance = 8.506 Å), the 2-D sheets of $[Cu(4,4'\text{-bpy})_2]_n$ undulate as shown in Figure V.3(c). This network provides channels with dimensions of *ca.* 7 Å × 7 Å along the *b*-axis, *ca.* 6 Å × 3 Å along the *c*-axis, and *ca.* 6 Å × 2 Å along the *a*-axis as shown in Figures V.3(b-d). The 3-D network of **V-6**·2PF$_6$·2H$_2$O is very similar to those of **IV-1**·8H$_2$O and **IV-2**·8H$_2$O, but the remarkable difference is the valence of the counter anions. In **IV-1**·8H$_2$O and **IV-2**·8H$_2$O, the 2-D sheets are bridged by the dianions (SiF_6^{2-} or GeF_6^{2-}) to form a neutral 3-D network. On the other hand, the 2-D sheets of **V-6**·2PF$_6$·2H$_2$O are linked by the monoanions (NO_3^- and PF_6^-) to afford a cationic 3-D network of $[Cu_2(PF_6)(NO_3)(4,4'\text{-bpy})_4]_n^{n+}$. Thus, the additional metal-free anions PF_6^- are contained in the channels, which are located near the bridging NO_3^- anions, and the effective channel sizes are *ca.* 4 Å × 3 Å along the *b*-axis and *ca.* 3 Å × 3 Å along the *c*-axis. As a result, 3 moles of PF_6^- and 1 mole of NO_3^- per 1 mole of **V-6**·2PF$_6$·2H$_2$O exist in the crystal. The IR stretching bands of both PF_6^- and NO_3^- anions are observed, consistent with the structure. The guest H$_2$O molecules sit in the channels with the distance of av. 4.00 Å for the bridging PF_6^-

anions. No bonding interaction is observed between the 3-D network and H_2O molecules. It is worth nothing that **V-6**·$2PF_6$·$2H_2O$ is a first example that has a mixed-pillar structure.

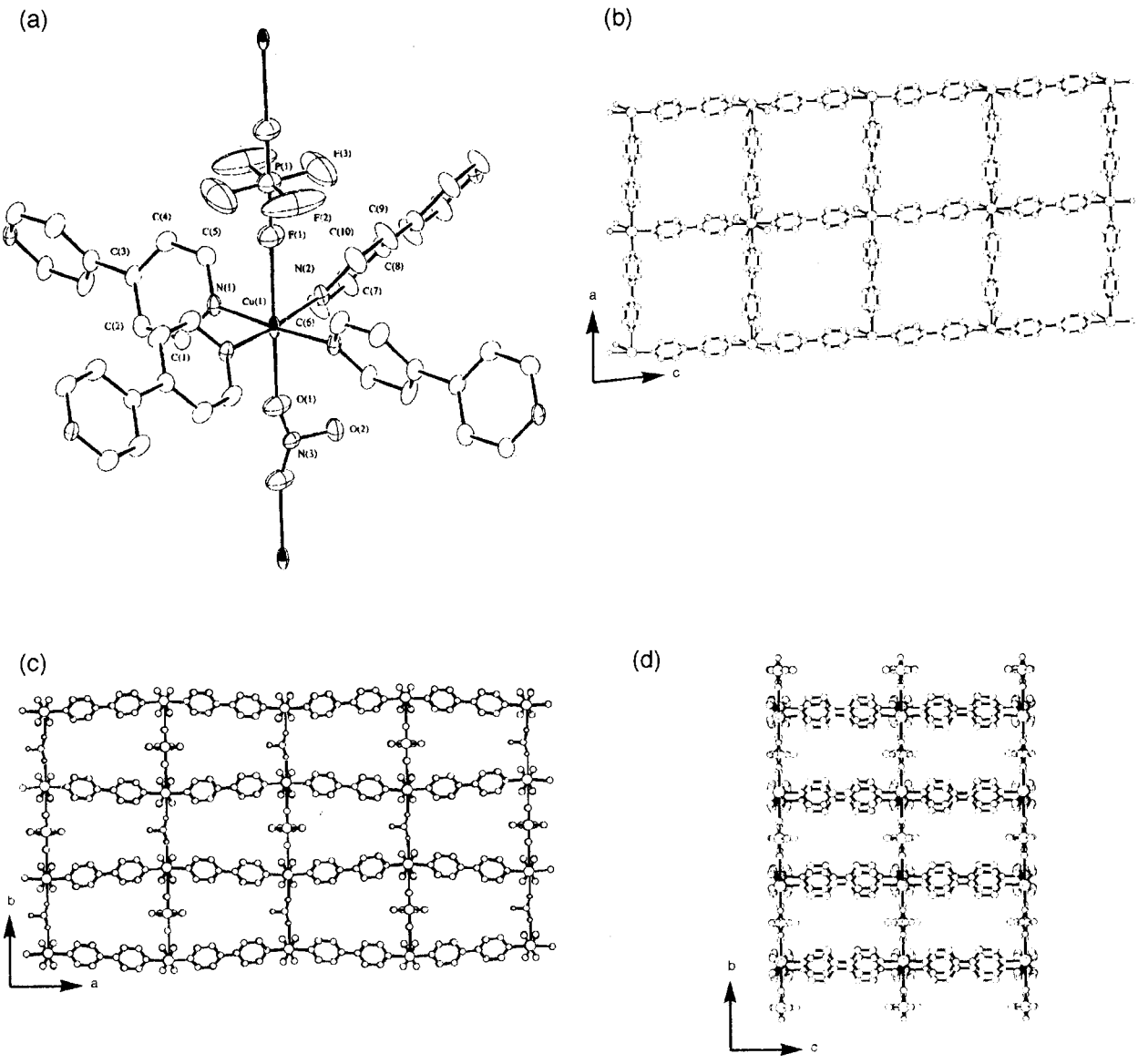

Figure V.3. (a) ORTEP drawing around a Cu(II) center of **V-6**·$2PF_6$·$2H_2O$ at the 30 % probability level. (b-d) View of the microporous network of **V-6**·$2PF_6$·$2H_2O$ along the *b*- (b), *c*- (c), and *a*-axes. The counter PF_6^- anions and guest H_2O molecules are omitted for clarity.

V. 3. 1. 4 Crystal Structure of $\{[Cu(PF_6)(4,4'\text{-bpy})_2(MeCN)]\cdot PF_6\cdot 2MeCN\}_n$ (V-7·2MeCN)

An ORTEP view around a Cu(II) center of **V-7**·2MeCN is shown in Figure V.4(a) with numbering scheme. The Cu(II) atom has an elongated distorted octahedral environment with four 4,4'-bpy nitrogen atoms in the equatorial plane, and one nitrogen atom of the MeCN and one fluoro atom of the PF_6^- in the axial sites. The Cu-F distance (2.583(3) Å) of **V-7**·2MeCN is apparently shorter than that of **V-6**·$2PF_6$·$2H_2O$ (2.676(4) Å), associated with the terminal coordination mode of the PF_6^- anion.

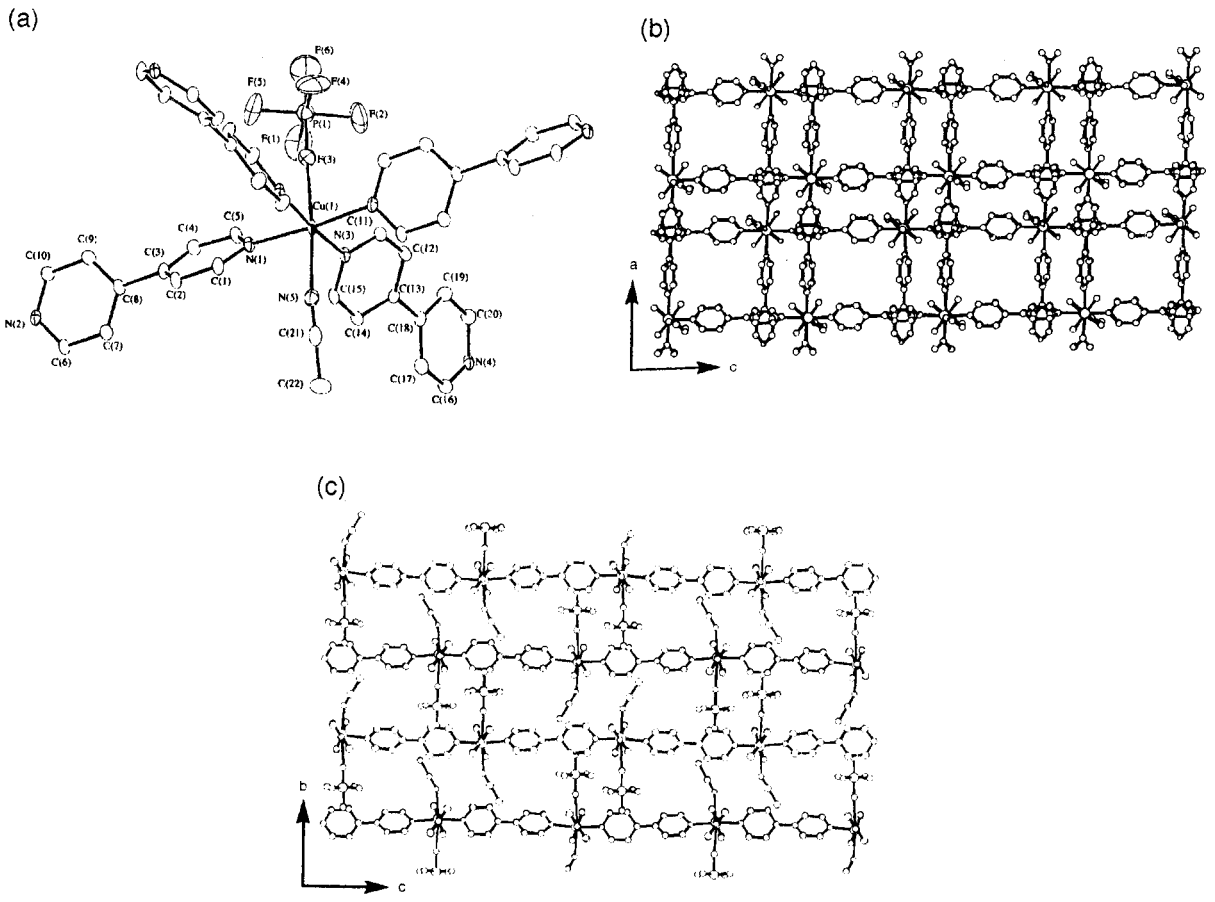

Figure V.4. (a) ORTEP drawing around a Cu(II) center of **V-7**·2MeCN at the 30 % probability level. (b and c) View of the microporous network of **V-7**·2MeCN along the *b*- (b) and *a*- (c) axes. The counter PF_6^- anions and guest MeCN molecules are omitted for clarity.

The 4,4'-bpy ligands bridge Cu(II) ions to form a 2-D network of rhombus grids with the corner angles of *ca.* 87 ° and 93 °. No significant bonding interactions are observed between the 2-D sheets except for a short F•••F contact with the distance (2.879(8) Å) of coordinated PF_6^- anions in the neighboring sheets. The F•••F contact is comparable to that of an F_2 solid,[58] implying the presence of a weak interaction between the 2-D sheets. These layers mutually slide to form small channels with dimensions of *ca.* 3 Å × 4 Å along the *b*-axis and *ca.* 3 Å × 2 Å along the *a*-axis as shown in Figures V.4(b) and V.4(c). These channels are filled with free PF_6^- anions, which show no interactions with the host network. Two free guest MeCN molecules are located between the 2-D layers and in the channels, respectively.

V. 3. 2 Participation of PF_6^- Anion in Frameworks

Three types of participation of PF_6^- anion are observed in the frameworks. The first is coordination-free type, which is a usual phenomenon for coordination polymers containing PF_6^- anions reported so far. The second is bridging type, which is first observed in complex **V-6**·$2PF_6$·$2H_2O$. The third is terminal coordination type (**V-7**·2MeCN), whose examples are still sparse to date.[59-61] PF_6^- anion has poor coordination ability for usual transition metal ions, hardly providing complexes with a direct bond between a metal atom and a fluorine atom. In the case of Cu(II) complexes, which undergo Jahn-Teller distortion and give a (4+2) coordination environment, PF_6^- anions could occupy the axial sites of the Cu(II) ion. This finding in **V-6**·$2PF_6$·$2H_2O$ indicates that the PF_6^- anion is also effective for the construction of the 3-D porous network as well as AF_6^{2-} (A = Si, Ge, and Ti) ones in the Cu(II)/4,4'-bpy system. The evaluation of the porous properties is mentioned below.

V. 3. 3 Coexistent Effect of Counter Anions in Porous Coordination Polymers Containing PF_6^- Anions

For the synthesis $Cu(PF_6)_2$ could not be utilized because it was not commercially available. Therefore, the mixture of NH_4PF_6 with appropriate Cu salt such as $Cu(ClO_4)_2$·$6H_2O$, $CuSO_4$·$5H_2O$, $Cu(BF_4)_2$·xH_2O, and $Cu(NO_3)_2$·$3H_2O$, was used as a starting salt. The frameworks

of obtained complexes are considerably dependent on the combination of anions. A summary is shown in Scheme V.2. When $Cu(ClO_4)_2 \cdot 6H_2O$ and NH_4PF_6 were employed in the reaction with 4,4'-bpy ligand in a H_2O/EtOH solution, the cationic coordination polymer, **V-5**$\cdot 2H_2O \cdot 4$EtOH, containing both ClO_4^- and PF_6^- anions at the 1:1 ratio was selectively obtained. The coexistence of counter anions is checked by the IR measurement, which shows the peaks of both 1115 and 843 cm^{-1} assigned to stretching bonds of ClO_4^- and PF_6^-, respectively. On the other hand, a combination of $Cu(BF_4)_2 \cdot xH_2O$ or $CuSO_4 \cdot 5H_2O$ with NH_4PF_6 in a H_2O/EtOH solution afforded isostructural cationic coordination polymer **V-4**$\cdot 2H_2O \cdot 4$EtOH. In this compound, only PF_6^- anions are clathrated in the channels, in contrast to the case of $Cu(ClO_4)_2 \cdot 6H_2O$. When the $Cu(NO_3)_2 \cdot 3H_2O$ and NH_4PF_6 were used in a H_2O/EtOH solution, the cationic 3-D coordination polymer **V-6**$\cdot 2PF_6 \cdot 2H_2O$ containing both NO_3^- and PF_6^- anions at the 1:3 ratio was formed. Interestingly, both bridged and free PF_6^- anions occur at the 1:2 ratio. A combined action of solvent molecules and anions was observed in the PF_6^-/BF_4^- system. Both MeCN and PF_6^- anion are coordinated to Cu(II) atoms to give a 2-D coordination polymer **V-7**$\cdot 2$MeCN with both terminal-coordinated and free PF_6^- anions. On the other hand, **V-8** forms preferentially in the absence of MeCN. On the basis, the combination of anions in a certain solvent provides a variety of infinite frameworks even for simple Cu(II) ion and 4,4'-bpy system, indicating that the framework is designable and controllable. Crystalline frameworks depending on single-anion have so far been reported,[62-68] and in addition, the finding on framework-transformation by the combination of anions makes crystal engineering by anions promising.

V. 3. 4 Framework Stability

In porous compounds, only **V-7**$\cdot 2$MeCN showed the replacement of three H_2O from two MeCN, resulting in **V-7**$\cdot 3H_2O$. Therefore, the author examined the framework stability of this replaced one in detail. For **V-7**$\cdot 3H_2O$, the TGA data show three steps of weight loss. First, at the region of r.t.- 70 °C **V-7**$\cdot 3H_2O$ loses three H_2O molecules. Immediately, the coordinated MeCN molecule is released from host network between 70 °C and 127 °C, and the decomposition of host network is observed up to 200 °C. The elemental analysis, IR, and TGA measurements

reveal that guest MeCN molecules of the complex **V-7**·2MeCN are easily replaced by H_2O molecules in the atmosphere. The XRPD pattern of this replaced complex **V-7**·3H_2O was measured as shown in Figure V.5, and the good agreement of peaks in both simulation and observed patterns at r.t. demonstrates that the porous network is retained after the replacement by H_2O molecules in the atmosphere.

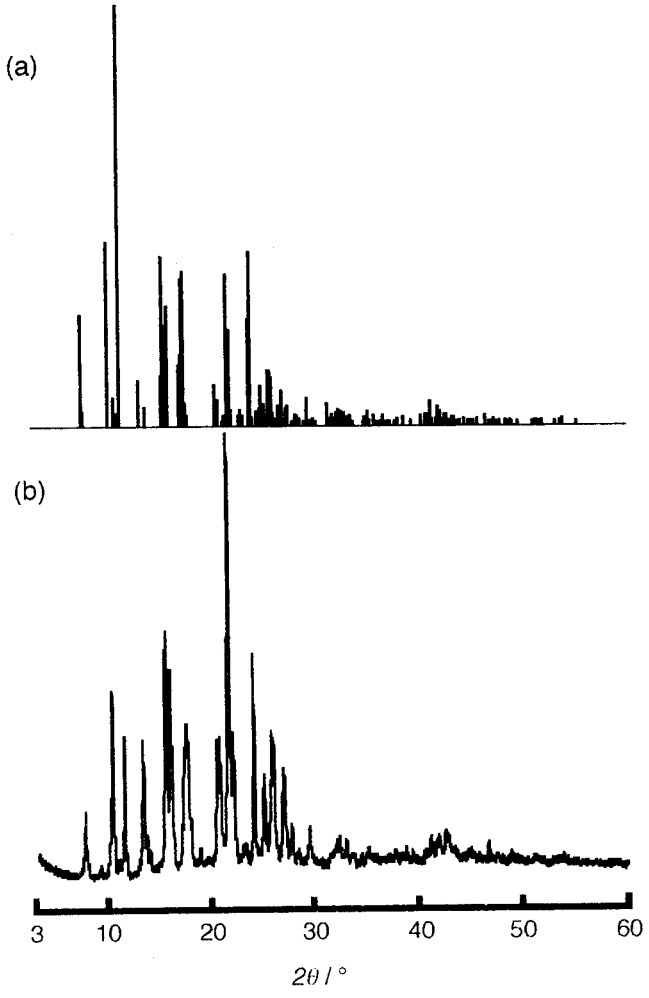

Figure V.5. Simulated XRPD pattern from (a) the single crystal model of **V-7**·2MeCN and (b) the observed pattern at r.t. of **V-7**·3H_2O.

V. 3. 5 Gas Adsorption Properties of 3-D Porous Coordination Polymer (V-6·1.4PF_6·0.6NO_3)

The 3-D cationic porous coordination polymer **V-6**·1.4PF_6·0.6NO_3 contains small channels (*ca.* 4 Å × 3 Å and *ca.* 3 Å × 3 Å). The N_2 adsorption and desorption measurements of **V-6**·1.4PF_6·0.6NO_3 were carried out in the relative pressure range from 10^{-6} to 0.9 at -196 °C (Figure V.6). The adsorption isotherm shows a typical isotherm of type I for microporous compounds. The rapid rise at low relative pressure followed by a monotonously increasing curve indicates a uniform micropore. From the equations (eq-1) and (eq-2) appeared in Chapter IV, the values of W_0 = 146 Ncc·g^{-1}, βE_0 = 10.1 kJ·mol^{-1}, and $q_{st.\ \phi=1/e}$ = 15.7 kJ·mol^{-1}, are estimated. The value of the specific surface area of **V-6**·1.4PF_6·0.6NO_3, which is calculated from the BET equation, is 559 m^2·g^{-1}. On the other hand, the desorption isotherm does not trace the adsorption one any more, instead, showing a constant value until a low relative pressure. At this stage, the author guesses that this hysteresis causes a blocking effect of free counter anions (PF_6^- and NO_3^-) to adsorbed N_2 gas.

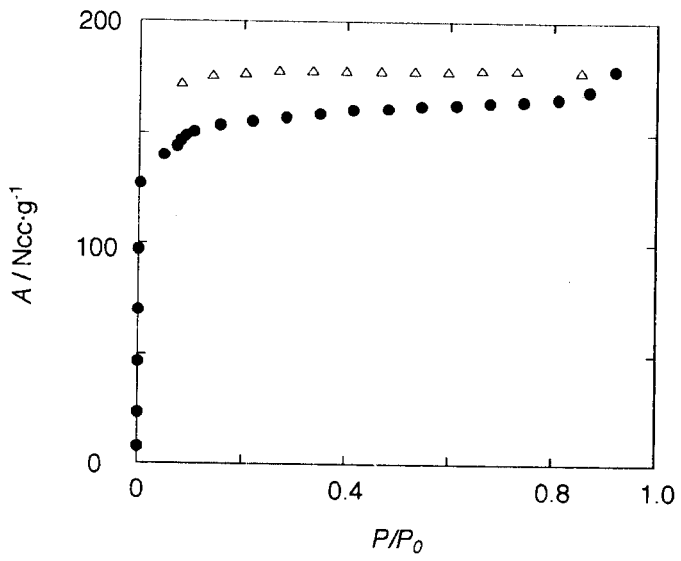

Figure V.6. N_2 adsorption (filled circles) and desorption (open triangles) isotherms of **V-6**·1.4PF_6·0.6NO_3 in the relative pressure range from 10^{-6} to 0.9 at -196 °C (A = absolute adsorption (Ncc·g^{-1})).

This dried sample also adsorbs a small amount of the CH_4 gas (*ca.* 31 Ncc·g^{-1} at 36 atm) as illustrated in Figure V.7. The parameters obtained from the Langmuir plot and the extended DR equation (eq-3), W_L, βE_0, and P_{0q}, are 35 Ncc·g^{-1}, 8.8 kJ·mol^{-1}, and 146 atm, respectively. The $q_{st,\ \phi=1/e}$ value of 17.0 kJ·mol^{-1} is comparable with those of **IV-1-3**.

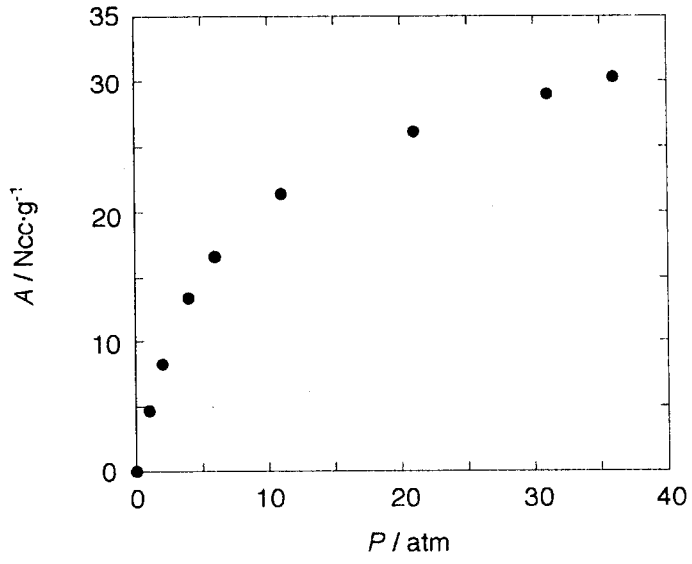

Figure V.7 Adsorption isotherm of **V-6**·1.4PF_6·0.6NO_3 obtained with a CH_4 gas between 1 and 36 atm at 25 °C (*A* = absolute adsorption (Ncc·g^{-1})).

V. 3. 6 Crystal Engineering by Anions for Cu(II)/4,4'-bpy Frameworks

The framework construction and conversion accompanied by anion-exchange are listed in Scheme V.4.

Several anion-exchangeable porous coordination polymers have so far been reported,[21-24] in which the microporous frameworks are maintained during the anion-exchange, so called the second generation compounds. The anion-exchange properties of **V-1-3** were investigated, illustrating the third generation system.[39]

Scheme V.4

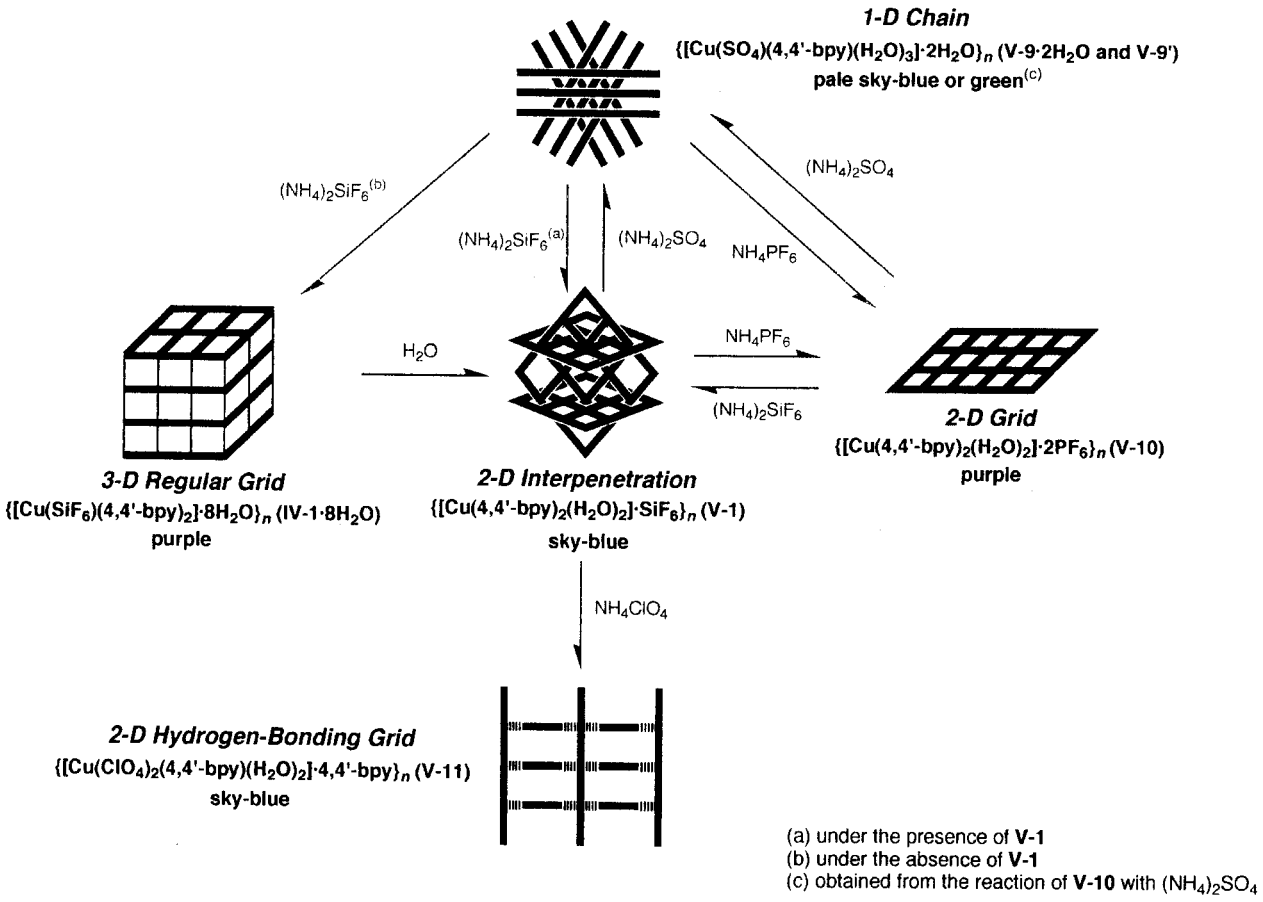

Microcrystals of **V-1** were immersed in a $(NH_4)_2GeF_6$ (excess) solution for a few days. Although the color of the compound unchanged, the IR spectrum clearly shows decrease in intensity of SiF_6^{2-} bands (748 and 480 cm^{-1}) and increase in that of a GeF_6^{2-} band (561 cm^{-1}), indicating that the compound partially underwent the anion-exchange.[69] This compound maintains crystallinity during the anion-exchange process as illustrated by sharp peaks observed in the XRPD pattern, which is in a good agreement with that of an original sample **V-1** as shown in Figure V.8. The complete exchange of the counter anion is not attained. This is possibly because the GeF_6^{2-} anion is larger than SiF_6^{2-} and is readily trapped in the channel near the surface by a strong hydrogen bonding interaction with coordinated H_2O molecules. Therefore, interpenetration into a deeper region of the anion is prevented. Indeed, no anion-exchange from GeF_6^{2-} to SiF_6^{2-} occurred in **V-2**.

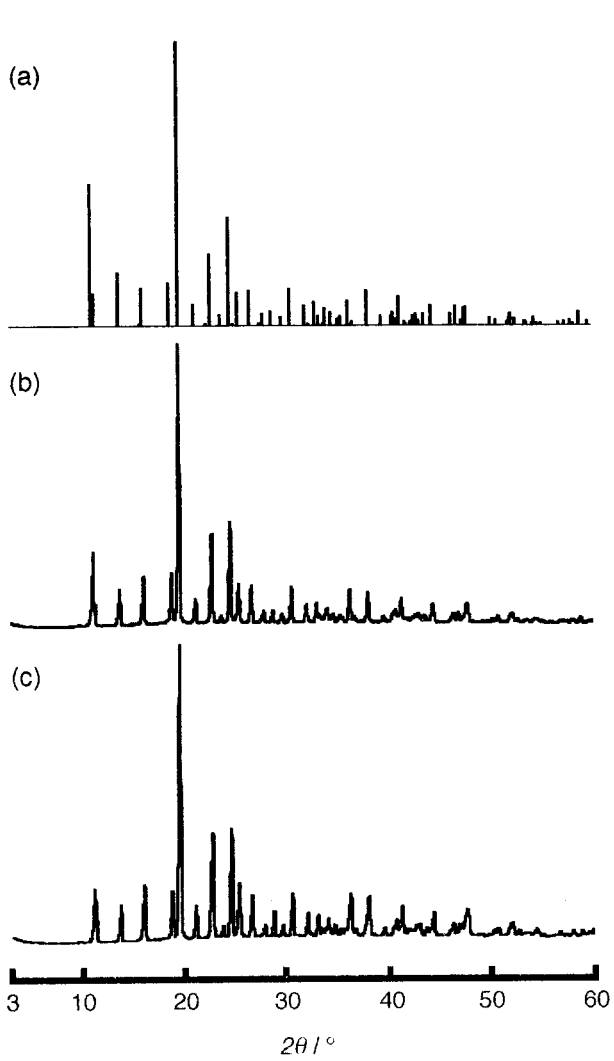

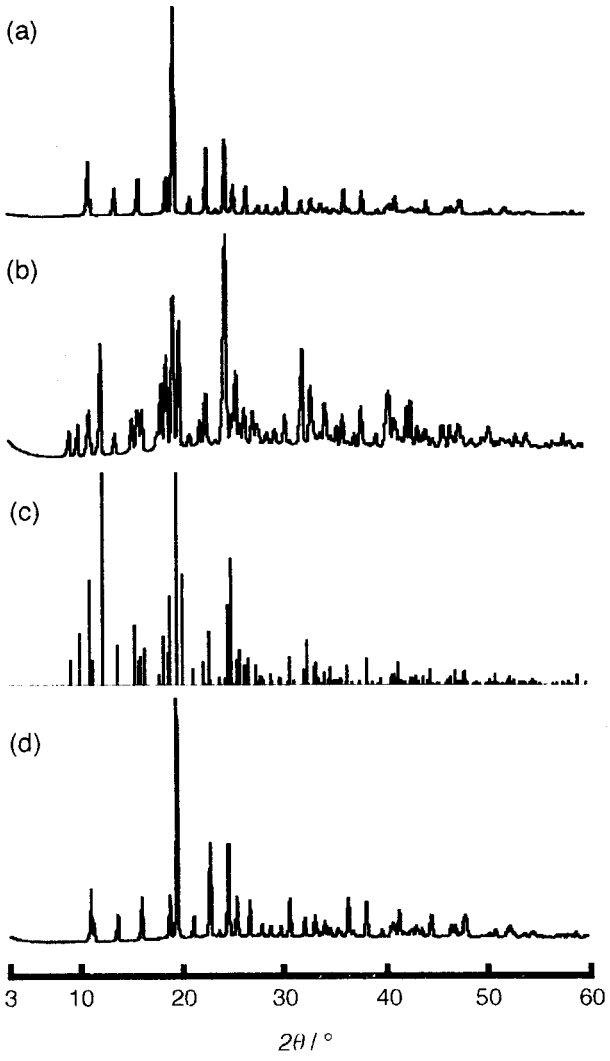

Figure V.8 (left). XRPD patterns of **V-1** ((a) simulation and (b) observed patterns) and (c) solid obtained by immersing **V-1** in a H_2O solution containing excess amount of $(NH_4)_2GeF_6$.

Figure V.9 (right). XRPD patterns of (a) **V-1**, (b) solid obtained by immersing **V-1** in a H_2O solution containing excess amount of $(NH_4)_2SO_4$, (c) superposition of **V-1** and **V-9**·$2H_2O$ (simulation patterns), and (d) solid obtained by immersing the partially exchanged sample in a H_2O solution containing the 4,4'-bpy ligand and excess amount of $(NH_4)_2SiF_6$.

On the other hand, intriguing phenomena were observed in the case of SO_4^{2-}, PF_6^-, and ClO_4^- anions. When SO_4^{2-} dianion was employed for microcrystals of **V-1**, the color changed from sky-blue to pale sky-blue. The phenomenon was monitored by EA, IR, and XRPD measurements. The compound appears to maintain crystallinity during the anion-exchange process as illustrated by sharp peaks in the XRPD pattern but the peak pattern is different from that of the initial sample of **V-1.** This is well demonstrated in Figures V.9(a) and V.9(b), indicating that the initial compound is transformed to a new type of network including SO_4^{2-} instead of SiF_6^{2-}. Surprisingly, the XRPD pattern of the resultant compound is quite similar to that of 1-D polymer $\{[Cu(SO_4)(4,4'\text{-bpy})(H_2O)_3]\cdot 2H_2O\}_n$ (**V-9**·$2H_2O$) reported previously.[46] This is shown in Figures V.9(b) and V.9(c). **V-9**·$2H_2O$ affords linear 1-D chain structures of $[Cu(SO_4)(4,4'\text{-bpy})(H_2O)_3]_n$, which form layers parallel to the *ab*-plane and stacking along the *c*-axis. Adjacent layers are rotated by 60 ° to produce triangle cavities with dimensions of *ca.* 3 Å. The SO_4^{2-} dianions, which weakly interact with Cu(II) ions, and free H_2O molecules occupy these triangle channels. The elemental analysis indicates that the ratio of starting **V-1** and resultant **V-9**·$2H_2O$ is *ca.* 3 : 7.[70] The complete conversion under the condition was not attained. Furthermore, when the mixture was immersed in a H_2O solution containing 4,4'-bpy and excess amount of $(NH_4)_2SiF_6$, microcrystals of only **V-1** came back as illustrated in Figure V.9(d).

Interestingly, when the pure sample of **V-9**·$2H_2O$ was immersed in a H_2O solution containing 4,4'-bpy and excess amount of $(NH_4)_2SiF_6$, the color immediately changed from pale sky-blue to purple, indicative of the quick transformation to the 3-D network **IV-1** as illustrated in Figures 10(b) and 10(c). The IR data reveal that the position of a SiF_6^{2-} band (741 cm^{-1}) is similar to that of **IV-1**·$4H_2O$, and the XRPD pattern of the resultant compound is in good agreement with that of **IV-1**·$8H_2O$ as shown in Figure V.10(c). This result is apparently different from that of the mixed compounds of **V-1** and **V-9**·$2H_2O$. Further stirring of this suspension causes a conversion of the 3-D network of **IV-1** into the 2-D interpenetrated one of **V-1** as illustrated in Figure 10(d). Similar phenomenon was observed by using the $(NH_4)_2GeF_6$ dianion instead of $(NH_4)_2SiF_6$ one as shown in Figure V.11.[71] On the basis, the structural transformation from **V-9**·$2H_2O$ to **IV-1** (or **IV-2**) first occurs, then finally **V-1** (or **V-2**) is

completed by use of SO_4^{2-}/SiF_6^{2-} (or GeF_6^{2-}) anion system.

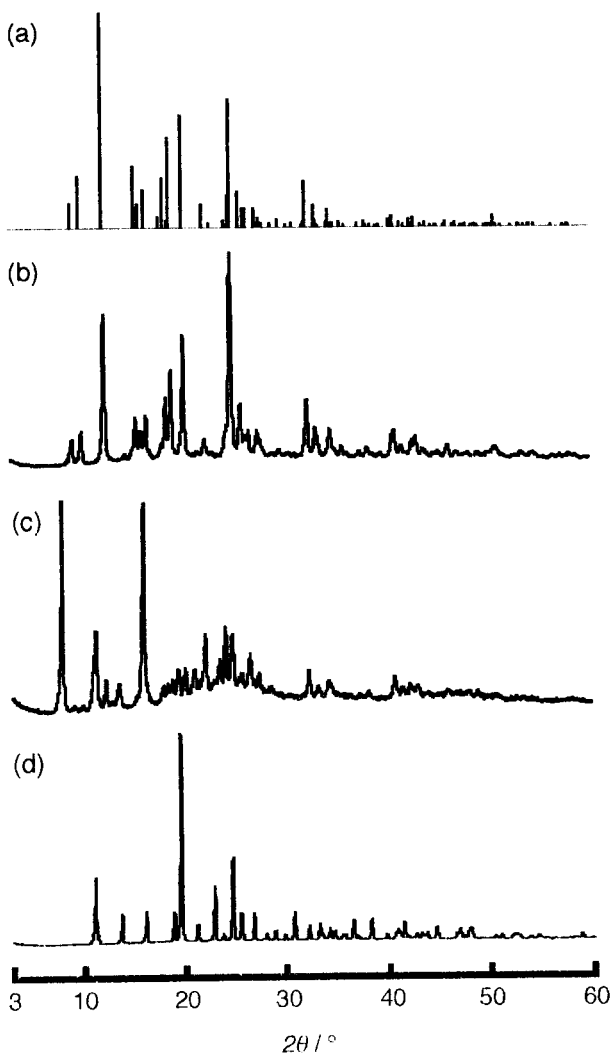

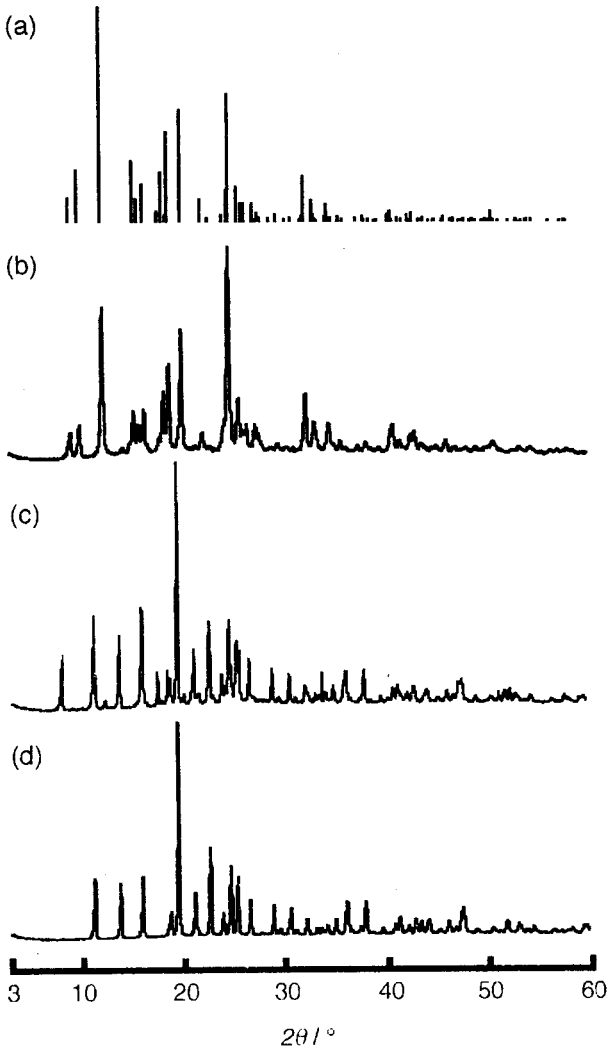

Figures V.10 (left) and V.11 (right). XRPD patterns of pure **V-9**·$2H_2O$ ((a) simulation and (b) observed patterns), (c) purple or bluish-purple solid immediately obtained by immersing pure **V-9**·$2H_2O$ in a H_2O solution containing the 4,4'-bpy ligand and excess amount of $(NH_4)_2SiF_6$ or $(NH_4)_2GeF_6$, respectively, and (d) sky-blue solid obtained by long immersing pure **V-9**·$2H_2O$ in a H_2O solution containing the 4,4'-bpy ligand and excess amount of $(NH_4)_2SiF_6$ or $(NH_4)_2GeF_6$.

It is worth noting that PF_6^- and ClO_4^- anions also promote a framework transformation, whose phenomenon was monitored by EA, IR, and XRPD measurements. In Scheme V.4, the treatment of **V-1** with NH_4PF_6 solution afforded $\{[Cu(4,4'\text{-bpy})_2(H_2O)_2]\cdot 2PF_6\}_n$ (**V-10**), clearly showing the disappearance of intense SiF_6^{2-} bands (748 and 480 cm^{-1}) of **V-1** and the appearance of an equally intense PF_6^- band (843 cm^{-1}). Concomitantly, the color of the compound turned from sky-blue to purple. Compound **V-10** represents a XRPD pattern with rather broad peaks, clearly different from the original one as illustrated in Figures V.12(a) and V.12(b). The broad XRPD pattern also indicates that each layer stacks randomly, namely, non-interpenetrating structure. The 2-D interpenetrated framework of **V-1** was well reproduced by immersing **V-10** in aqueous solution with excess amount of $(NH_4)_2SiF_6$ (Figure V.12(c)). In this sense, the transformation is reversible.

When ClO_4^- anion was employed for microcrystals of **V-1**, the color almost unchanged. However, resulting compound clearly shows the disappearance of intense SiF_6^{2-} bands (748 and 480 cm^{-1}) of **V-1** and the appearance of an equally intense ClO_4^- band (1109 and 627 cm^{-1}). Furthermore, the compound appears to maintain crystallinity during the anion-exchange process as illustrated by sharp peaks in the XRPD pattern but the peak pattern is apparently different from that of the initial sample of **V-1.** This is well demonstrated in Figures V.13(a) and V.13(b), indicating that the initial compound is transformed to a new type of network including ClO_4^- instead of SiF_6^{2-}. Surprisingly, the XRPD pattern of the resultant compound is quite similar to that of 2-D hydrogen-bonding network $\{[Cu(ClO_4)_2(4,4'\text{-bpy})(H_2O)_2]\cdot 4,4'\text{-bpy}\}_n$ (**V-11**) reported previously.[47] This is shown in Figures V.13(b) and V.13(c). **V-11** affords linear 1-D chain structures of $[Cu(ClO_4)_2(4,4'\text{-bpy})(H_2O)_2]_n$, which are linked by hydrogen bonds with free 4,4'-bpy ligands ($O(H_2O)$-N(free 4,4'-bpy) = 2.653(5) Å). The ClO_4^- anions weakly coordinate to Cu(II) ions (Cu-O = 2.414(4) Å).

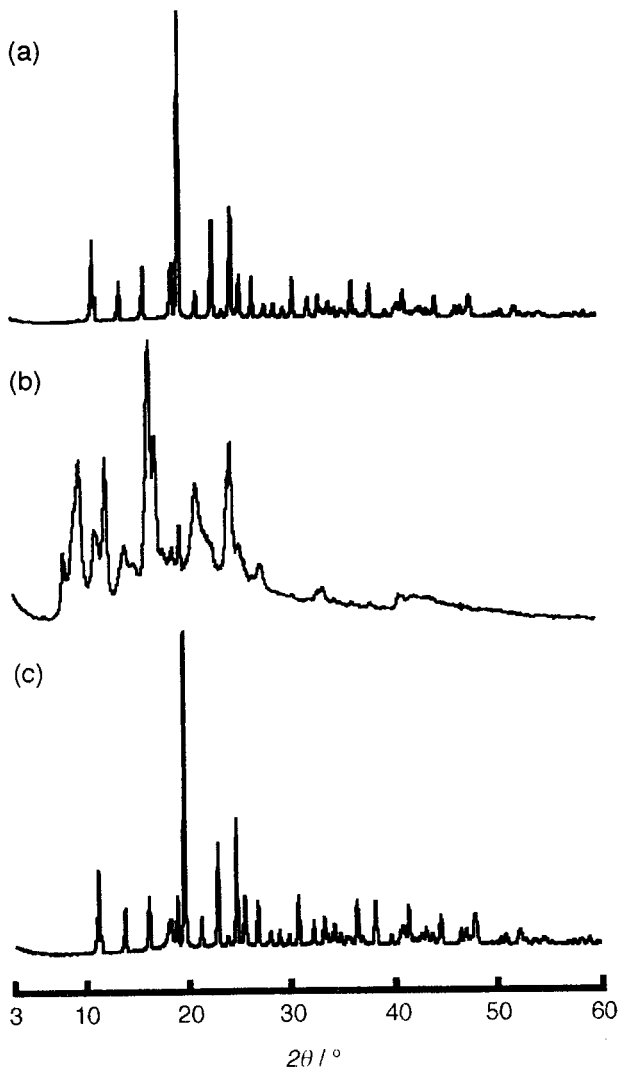

Figure V.12 (left). XRPD patterns of (a) **V-1**, (b) solid obtained by immersing **V-1** in a H_2O solution containing excess amount of NH_4PF_6, and (c) solid obtained by immersing the exchanged sample in a H_2O solution containing excess amount of $(NH_4)_2SiF_6$.

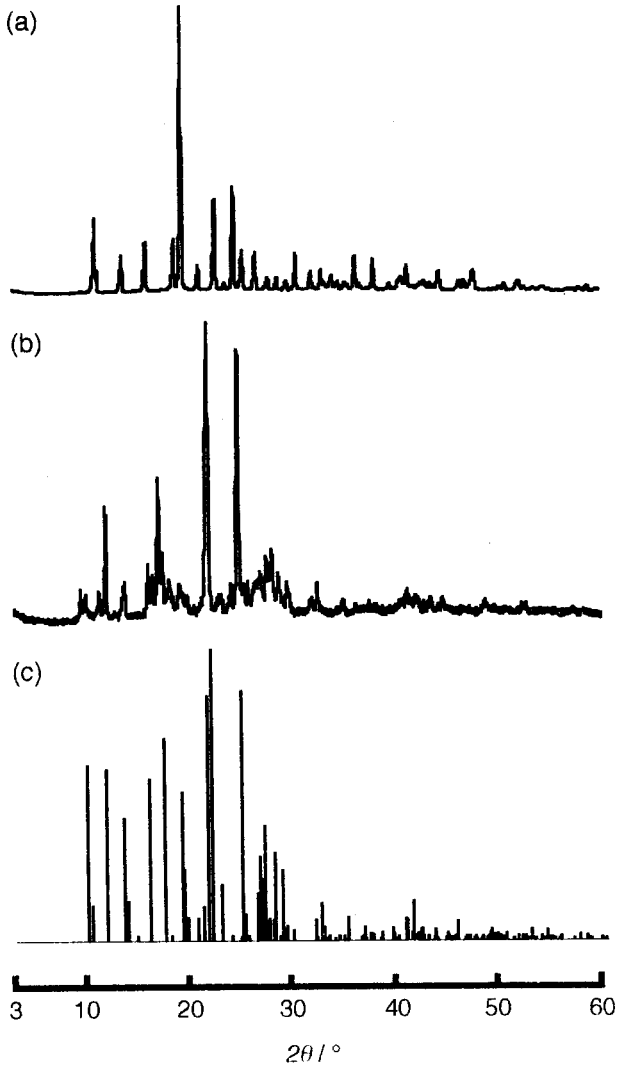

Fiugre V.13 (right). XRPD patterns of (a) **V-1**, (b) solid obtained by immersing **V-1** in a H_2O solution containing excess amount of NH_4ClO_4, and (c) simulation pattern of **V-11**.

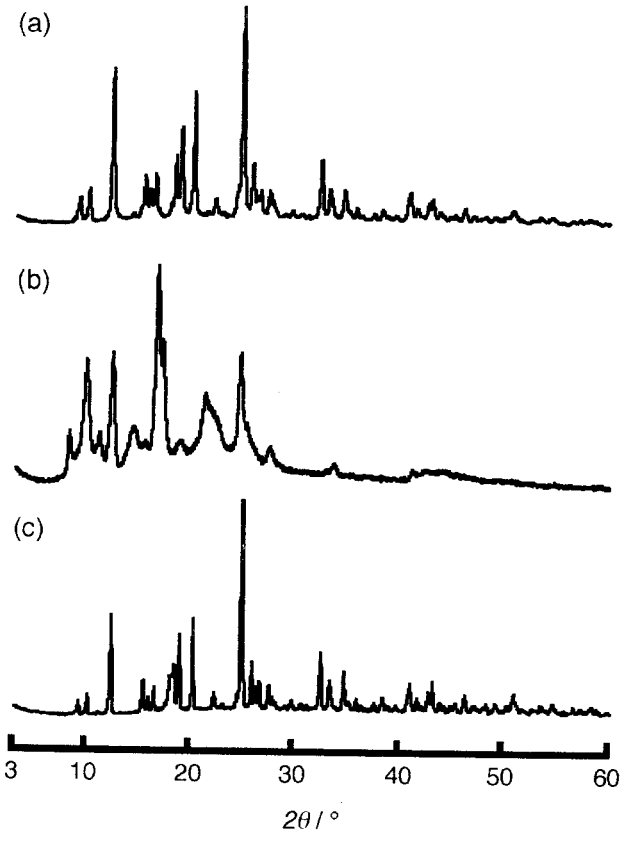

Figure V.14. XRPD patterns of (a) pure **V-9**·$2H_2O$, (b) solid obtained by immersing **V-9**·$2H_2O$ in a H_2O solution containing the 4,4'-bpy ligand and excess amount of NH_4PF_6, and (c) solid obtained by immersing **V-10** in a H_2O solution containing excess amount of $(NH_4)_2SO_4$.

As illustrated in Figure V.14, a reversible transformation between **V-9**·$2H_2O$ and **V-10**, accompanying the anion exchange, was also observed. When the pure sample of **V-9**·$2H_2O$ was immersed in a H_2O solution with the 4,4'-bpy ligand and an excess amount of NH_4PF_6, the compound **V-10** was obtained. In contrast, when **V-10** was immersed in a H_2O solution with an excess amount of $(NH_4)_2SO_4$, the resultant solid, **V-9'**, was green and different from **V-9**·$2H_2O$ (pale sky-blue). The IR measurement of **V-9'** shows the disappearance of the intense PF_6^- band (843 cm^{-1}) and the appearance of an equally intense SO_4^{2-} band (1107 cm^{-1}). The EA and XRPD measurements reveal that the structure of **V-9'** is quite similar to **V-9**·$2H_2O$, representing a 1-D chain structure. Compound **V-10** formed again when **V-9'** was immersed in a H_2O solution with the 4,4'-bpy ligand and an excess amount of NH_4PF_6. The difference of the color in **V-9**·$2H_2O$

and **V-9'** is probably due to the difference of a strength of a Cu-O (SO_4) bond. Each Cu(II) ion in **V-9**·$2H_2O$ has a distorted octahedral environment with two nitrogen atoms of 4,4'-bpy ligands (2.044 and 2.049 Å) and two oxygen atoms of H_2O molecules (1.952 and 1.976 Å) in the basal plane, and one oxygen atom of a H_2O molecule (2.207 Å) and one oxygen atom of a SO_4^{2-} dianion (2.673 Å) in the axial sites. The UV-VIS spectra show that the d-d transition of the Cu(II) ion in **V-9'** (green) appears at a higher energy (703 nm) than that of **V-9**·$2H_2O$ (sky-blue) (712 nm), associated with the different mode in coordination of SO_4^{2-} between **V-9'** and **V-9**·$2H_2O$.

Scheme V.5

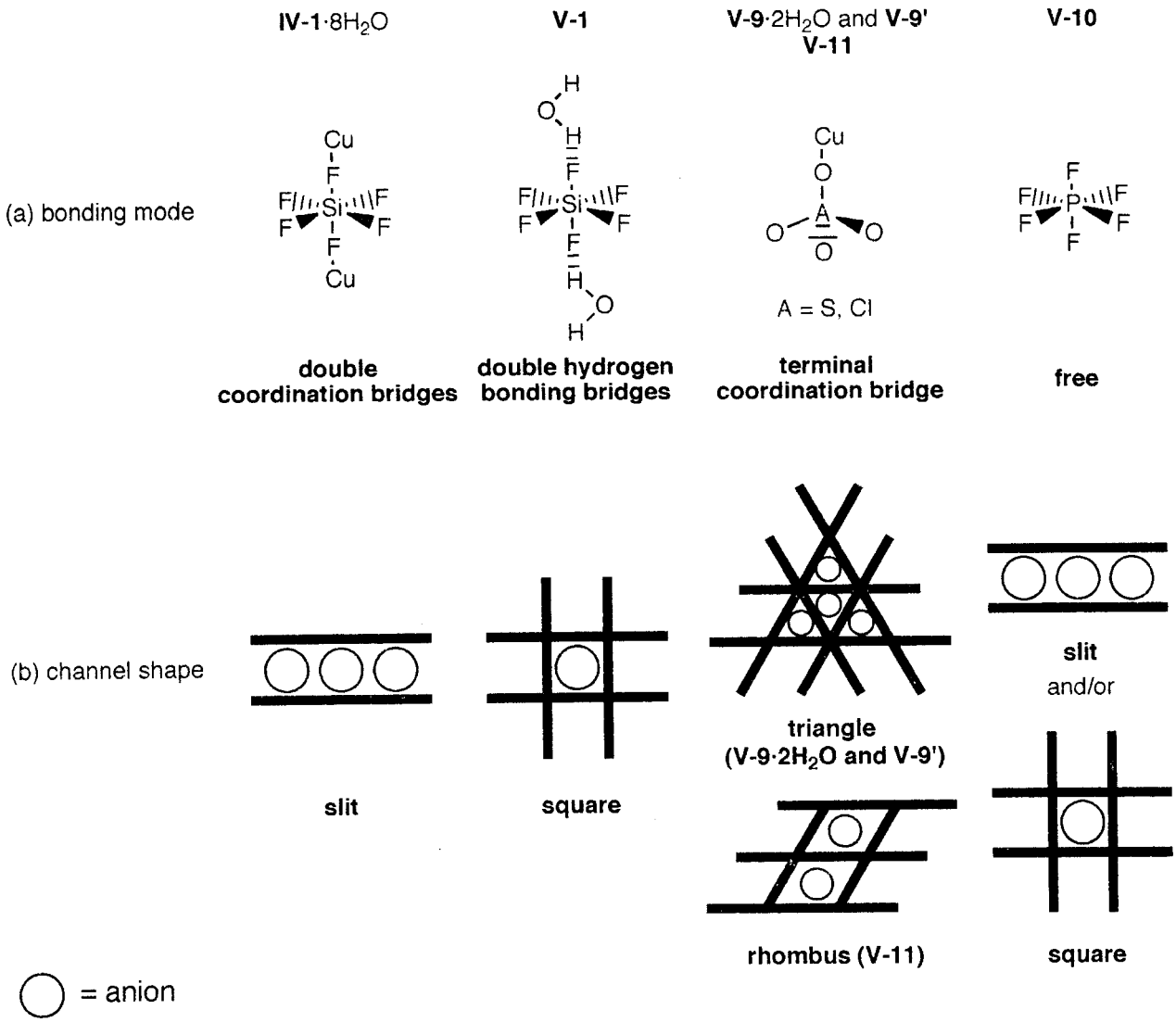

On the other hand, when **V-2** or **V-3** was immersed in aqueous solution in the presence of excess amount of $(NH_4)_2SiF_6$, NH_4PF_6, NH_4NO_3, or $(NH_4)_2SO_4$, no anion-exchange occurred. This is associated with the sizes of GeF_6^{2-} and TiF_6^{2-} anions: the anions are too large to go through the small channel windows (*ca.* 2 Å × 2 Å). Moreover, hydrogen bonds with coordinated H_2O molecules may support the strong trap of GeF_6^{2-} and TiF_6^{2-} anions to the channels.

The reversible structural conversions induced by anions in this chapter are unique and useful for framework design. Recently, one example has been reported,[42] in which the structural conversions happen by slight movement of CN substituent groups of the ligand. In contrast, the anion-exchange in this work shows drastic reversible structural transformations among the 3-D network **IV-1**·$8H_2O$, the 2-D interpenetrated framework **V-1**, the 1-D chain **V-9**·$2H_2O$ and **V-9'**, the 2-D non-interpenetrating framework **V-10**, and 2-D hydrogen-bonding framework **V-11**, with Cu-N (4,4'-bpy) bond formation and cleavage. These four types of complexes incorporate the anions in different modes as shown in Scheme V.5. The SiF_6^{2-} dianions in **IV-1**·$8H_2O$ become incorporated between the Cu(II) centers by coordination bonds, while the SiF_6^{2-} ones in **V-1** are not coordinated to the Cu(II) ions but are linked with coordinated H_2O molecules by hydrogen bonds. The SO_4^{2-} dianions in **V-9**·$2H_2O$ and **V-9'**, and the ClO_4^- anions in **V-11**, are ligated to the Cu(II) ions by coordination bonds in the monodentate fashion. The PF_6^- anions in **V-10** are probably coordination-free, because each Cu(II) center is coordinatively saturated by four nitrogen atoms of 4,4'-bpy ligands and two oxygen atoms of H_2O molecules. Furthermore, it is worth noting that these Cu-4,4'-bpy polymers can incorporate counter anions (SiF_6^{2-}, PF_6^-, ClO_4^-, and SO_4^{2-}) with various sizes and charges by changing the overall structures, in a sense, the author can regard as an anion receptor having flexible Cu(II)-4,4'-bpy frameworks. These results also reveal that the structures in the Cu(II)-4,4'-bpy system considerably depend on counter anions, which are, therefore, regarded as the framework-regulator.

In the anion-exchange process observed in this chapter, not only the micropore width and shape but also the electrostatic affinity between Cu(II) ions and counter anions are important factors governing the drastic structural transformation. In addition, the competition for the Cu(II) sites between counter anions and coordinated guest molecules (H_2O molecule in this case)

makes a behavior of the anion-exchange fruitful.

V. 4 Conclusion

Based on combination of Cu(II) ion and 4,4'-bpy, a variety of coordination polymer frameworks were created by using the framework-regulator AF_6 anions. The obtained frameworks are *2-D Interpenetration* (**V-1-3**), *2-D Double-Layer* (**V-4**·$2H_2O$·4EtOH and **V-5**·$2H_2O$·4EtOH), *3-D Undulated Grid* (**V-6**·$2PF_6$·$2H_2O$), and *2-D Grid* (**V-7**·2MeCN and **V-8**). The 3-D porous coordination polymer **V-6**·$2PF_6$·$2H_2O$ affords rigid microporous channels with dimensions of *ca.* 4 Å × 3 Å and 3 Å × 3 Å. This compound shows the adsorption ability for N_2 and CH_4 gas (second generation compound), indicating that the selection of PF_6^- anion as the framework-regulator in the Cu(II)/4,4'-bpy system is of significance for the construction of 3-D porous networks as well as the case of AF_6^{2-} (A = Si, Ge, and Ti). Interestingly, the 3-D networks, **IV-1-3**, suitable for the gas adsorption (second generation compounds) are transformed into the 2-D interpenetrated networks **V-1-3** suitable for the anion-exchange in the presence of H_2O (third generation compounds). The 2-D interpenetrating network **V-1** shows unprecedented unique anion-exchange properties, in which the drastic structural conversion in the process of the anion-exchange occurs. This finding contains a basic concept for an anion sensor based on spectroscopic properties, characteristic of color change, and implies that the 4,4'-bpy-bridged porous coordination polymers are suitable for the construction of not only the second generation compounds but also the third generation ones. When the PF_6^- as the framework-regulator was employed with coexistent anions, various types of porous coordination networks depending on coexistent anions (ClO_4^-, BF_4^-, NO_3^-, and SO_4^{2-}) were obtained as shown in Scheme V.2, in which novel types of frameworks with mixed anions were created (**V-5**·$2H_2O$·4EtOH, **V-6**·$2PF_6$·$2H_2O$, and **V-8**). In particular, **V-6**·$2PF_6$·$2H_2O$ has a rare mixed-pillar structure. All the structures strongly depend on counter anions with the aid of guest solvents.

V. 5 References

(1) Yaghi, O. M.; Li, G.; Li, H. *Nature* **1995**, *378*, 703-706.

(2) Eddaoudi, M.; Li, H.; Yaghi, O. M. *J. Am. Chem. Soc.* **2000**, *122*, 1391-1397.

(3) Li, H.; Eddaoudi, M.; Groy, T. L.; Yaghi, O. M. *J. Am. Chem. Soc.* **1998**, *120*, 8571-8572.

(4) Li, H.; Eddaoudi, M.; O'Keeffe, M.; Yaghi, O. M. *Nature* **1999**, *402*, 276-279.

(5) Reineke, T. M.; Eddaoudi, M.; O'Keeffe, M.; Yaghi, O. M. *Angew. Chem., Int. Ed. Engl.* **1999**, *38*, 2590-2594.

(6) Chui, S. S.-Y.; Lo, S. M.-F.; Charmant, J. P. H.; Orpen, A. G.; Williams, I. D. *Science* **1999**, *283*, 1148-1150.

(7) Kondo, M.; Yoshitomi, T.; Seki, K.; Matsuzaka, H.; Kitagawa, S. *Angew. Chem., Int. Ed. Engl.* **1997**, *36*, 1725-1727.

(8) Kondo, M.; Okubo, T.; Asami, A.; Noro, S.; Yoshitomi, T.; Kitagawa, S.; Ishii, T.; Matsuzaka, H.; Seki, K. *Angew. Chem., Int. Ed. Engl.* **1999**, *38*, 140-143.

(9) Kondo, M.; Shimamura, M.; Noro, S.; Minakoshi, S.; Asami, A.; Seki, K.; Kitagawa, S. *Chem. Mater.* **2000**, *12*, 1288-1299.

(10) Mori, W.; Inoue, F.; Yoshida, K.; Nakayama, H.; Takamizawa, S.; Kishita, M. *Chem. Lett.* **1997**, 1219-1220.

(11) Nukada, R.; Mori, W.; Takamizawa, S.; Mikuriya, M.; Handa, M.; Naono, H. *Chem. Lett.* **1999**, 367-368.

(12) Takamizawa, S.; Mori, W.; Furihata, M.; Takeda, S.; Yamaguchi, K. *Inorg. Chim. Acta* **1998**, *283*, 268-274.

(13) Seki, K.; Takamizawa, S.; Mori, W. *Chem. Lett.* **2001**, 122-123.

(14) Seki, K.; Takamizawa, S.; Mori, W. *Chem. Lett.* **2001**, 332-333.

(15) Li, D.; Kaneko, K. *Chem. Phys. Lett.* **2001**, *335*, 50-56.

(16) Yaghi, O. M.; Li, H.; Groy, T. L. *J. Am. Chem. Soc.* **1996**, *118*, 9096-9101.

(17) Yaghi, O. M.; Davis, C. E.; Li, G.; Li, H. *J. Am. Chem. Soc.* **1997**, *119*, 2861-2868.

(18) Li, H.; Davis, C. E.; Groy, T. L.; Kelley, D. G.; Yaghi, O. M. *J. Am. Chem. Soc.* **1998**, *120*, 2186-2187.

(19) Reineke, T. M.; Eddaoudi, M.; Fehr, M.; Kelley, D.; Yaghi, O. M. *J. Am. Chem. Soc.* **1999**, *121*, 1651-1657.

(20) Choi, H. J.; Lee, T. S.; Suh, M. P. *Angew. Chem., Int. Ed. Engl.* **1999**, *38*, 1405-1408.

(21) Yaghi, O. M.; Li, H. *J. Am. Chem. Soc.* **1995**, *117*, 10401-10402.

(22) Yaghi, O. M.; Li, H. *J. Am. Chem. Soc.* **1996**, *118*, 295-296.

(23) Yaghi, O. M.; Li, H.; Groy, T. L. *Inorg. Chem.* **1997**, *36*, 4292-4293.

(24) Hoskins, B. F.; Robson, R. *J. Am. Chem. Soc.* **1990**, *112*, 1546-1554.

(25) Fujita, M.; Kwon, Y. J.; Washizu, S.; Ogura, K. *J. Am. Chem. Soc.* **1994**, *116*, 1151-1152.

(26) Sawaki, T.; Dewa, T.; Aoyama, Y. *J. Am. Chem. Soc.* **1998**, *120*, 8539-8640.

(27) Seo, J. S.; Whang, D.; Lee, H.; Jun, S. I.; Oh, J.; Jeon, Y. J.; Kim, K. *Nature* **2000**, *404*, 982-986.

(28) Barrer, R. M. In *Molecular Sieves*; Meier, W. M., Utyyerhoeven, J. B., Eds.; ACS Advances in Chemistry Series 121; American Chemical Society: Washington, DC, 1974; p 1.

(29) Wilde, R. E.; Ghosh, S. N.; Marshall, B. J. *Inorg. Chem.* **1970**, *9*, 2512-2516.

(30) Buser, H. J.; Schwarzenbach, D.; Petter, W.; Ludi, A. *Inorg. Chem.* **1977**, *16*, 2704-2710.

(31) Dunbar, K. R.; Heintz, R. A. *Prog. Inorg. Chem.* **1997**, *45*, 283-391.

(32) Iwamoto, T. In *Inclusion Compounds*; Atwood, J. L., Davies, J. E. D., MacNicol, D. D., Eds.; Oxford: New York, 1991; Vol. 5, p 177.

(33) Endo, K.; Sawaki, T.; Koyanagi, M.; Kobayashi, K.; Masuda, H.; Aoyama, Y. *J. Am. Chem. Soc.* **1995**, *117*, 8341-8352.

(34) Endo, K.; Koike, T.; Sawaki, T.; Hyashida, O.; Masuda, H.; Aoyama, Y. *J. Am. Chem. Soc.* **1997**, *119*, 4117-4122.

(35) Dewa, T.; Endo, K.; Aoyama, Y. *J. Am. Chem. Soc.* **1998**, *120*, 8933-8940.

(36) Dewa, T.; Aoyama, Y. *Chem. Lett.* **2000**, 854-855.

(37) Dewa, T.; Saiki, T.; Imai, Y.; Endo, K.; Aoyama, Y. *Bull. Chem. Soc. Jpn.* **2000**, *73*, 2123-2127.

(38) Tanaka, T.; Endo, K.; Aoyama, Y. *Chem. Lett.* **2000**, 1424-1425.

(39) Kitagawa, S.; Kondo, M. *Bull. Chem. Soc. Jpn.* **1998**, *71*, 1739-1753.

(40) Kepert, C. J.; Prior, T. J.; Rosseinsky, M. J. *J. Am. Chem. Soc.* **2000**, *122*, 5158-5168.

(41) Soldatov, D. V.; Ripmeester, J. A.; Shergina, S. I.; Sokolov, I. E.; Zanina, A. S.; Gromilov, S. A.; Dyadin, Y. A. *J. Am. Chem. Soc.* **1999**, *121*, 4179-4188.

(42) Min, K. S.; Suh, M. P. *J. Am. Chem. Soc.* **2000**, *122*, 6834-6840.

(43) Min, K. S.; Suh, M. P. *Chem. Eur. J.* **2001**, *7*, 303-313.

(44) Tabares, L. C.; Navarro, J. A. R.; Salas, J. M. *J. Am. Chem. Soc.* **2001**, *123*, 383-387.

(45) Jung, O.-S.; Kim, Y. J.; Lee, Y.-A.; Park, J. K.; Chae, H. K. *J. Am. Chem. Soc.* **2000**, *122*, 9921-9925.

(46) Hagrman, D.; Hammond, R. P.; Haushalter, R.; Zubieta, J. *Chem. Mater.* **1998**, *10*, 2091-2100.

(47) Chen, X. M.; Tong, M. L.; Luo, Y. J.; Chen, Z. N. *Aust. J. Chem.* **1996**, *49*, 835-838.

(48) Altomare, A.; Burla, M. C.; Camalli, M.; Cascarano, M.; Giacovazzo, C.; Guagliardi, A.; Polidori, G. *J. Appl. Cryst.* **1994**, *27*, 435.

(49) Beurskens, P. T.; Admiraal, G.; Beurskens, G.; Bosman, W. P.; de Gelder, R.; Israel, R.; Smits, J. M. M. **1994**, The DIRDIF-94 program system, Technical Report of the Crystallography Laboratory, University of Nijmegen, The Netherlands.

(50) Gilmore, C. J.; **1990**, MITHRIL - an integrated direct methods computer program. University of Glasgow, Scotland.

(51) Crystal Structure Analysis Package, Molecular Structure Corporation (1985 & 1999).

(52) Gable, R. W.; Hoskins, B. F.; Robson, R. *Chem. Commun.* **1990**, 1667-1668.

(53) Hagrman, P. J.; Hagrman, D.; Zubieta, J. *Angew. Chem., Int. Ed. Engl.* **1999**, *38*, 2638-2684.

(54) Power, K. N.; Hennigar, T. L.; Zaworotko, M. J. *New J. Chem.* **1998**, 177-181.

(55) Kepert, C. J.; Rosseinsky, M. J. *Chem. Commun.* **1999**, 375-376.

(56) Janiak, C. *J. Chem. Soc., Dalton Trans.* **2000**, 3885-3896.

(57) Tong, M.-L.; Lee, H.-K.; Chen, X.-M.; Huang, R.-B.; Mak, T. C. W. *J. Chem. Soc., Dalton Trans.* **1999**, 3657-3659.

(58) Greenwood, N. N.; Earnshaw, A. *Chemistry of the Elements (Second edition)*; Butterworth-Heinemann: Oxford, 2001, p 803.

(59) Yamamoto, Y.; Aoki, K.; Yamazaki, H. *Inorg. Chim. Acta* **1983**, *68*, 75-78.

(60) Dartiguenave, M.; Dartiguenave, Y.; Mari, A.; Guitard, A.; Olivier, M. J.; Beauchamp, A. L. *Can. J. Chem.* **1988**, *66*, 2386-2394.

(61) Honeychuck, R. V.; Hersh, W. H. *Inorg. Chem.* **1989**, *28*, 2869-2886.

(62) Withersby, M. A.; Blake, A. J.; Champness, N. R.; Hubberstey, P.; Li, W. S.; Schröder, M. *Angew. Chem., Int. Ed. Engl.* **1997**, *36*, 2327-2329.

(63) Hirsch, K. A.; Wilson, S. R.; Moore, J. S. *Inorg. Chem.* **1997**, *36*, 2960-2968.

(64) Carlucci, L.; Ciani, G.; Macchi, P.; Proserpio, D. M.; Rizzato, S. *Chem. Eur. J.* **1999**, *5*, 237-243.

(65) Wu, H.-P.; Janiak, C.; Rheinwald, G.; Hang, H. *J. Chem. Soc., Dalton Trans.* **1999**, 183-190.

(66) Janiak, C.; Uehlin, L.; Wu, H.-P.; Klüfers, P.; Piotrowski, H.; Scharmann, T. G. *J. Chem. Soc., Dalton Trans.* **1999**, 3121-3131.

(67) Blake, A. J.; Champness, N. R.; Cooke, P. A.; Nicolson, J. E. B.; Wilson, C. *J. Chem. Soc., Dalton Trans.* **2000**, 3811-3819.

(68) Brooks, N. R.; Blake, A. J.; Champness, N. R.; Cunningham, J. W.; Hubberstey, P.; Teat, S. J.; Wilson, C.; Schröder, M. *J. Chem. Soc., Dalton Trans.* **2001**, 2530-2538.

(69) Anal. Calcd for $\{[Cu(4,4'\text{-bpy})_2(H_2O)_2]\cdot 0.2SiF_6\cdot 0.8GeF_6\cdot 0.6H_2O\}_n$: C, 40.01; H, 3.56; N, 9.33. Found: C, 39.85; H, 3.63; N, 9.36.

(70) Anal. Calcd for $(\mathbf{V\text{-}1})_{0.28}(\mathbf{V\text{-}9}\cdot 2H_2O)_{0.72}$: C, 34.37; H, 4.18; N, 8.02. Found: C, 34.21; H, 3.74; N, 8.06.

(71) The partially exchanged compound $(\mathbf{V\text{-}2})_x(\mathbf{V\text{-}9}\cdot 2H_2O)_{1-x}$ was not obtained from the reaction of **V-2** with excess amount of $(NH_4)_2SO_4$. Therefore, the author prepared the partially exchanged compound artificially (the molar ratio, **V-2** : **V-9**$\cdot 2H_2O$ = 3 : 7).

Chapter VI

Effective Interpenetration and π-π Interaction for Construction of Azpy-Containing Coordination Networks: Syntheses, Crystal Structures, and Microporous Functionalities with Soft Dynamic Channels

Abstract: New ten azpy-containing coordination polymers, $\{[Mn(NO_3)_2(azpy)(H_2O)_2]\cdot 2EtOH\}_n$ (**VI-1**·2EtOH) (*1-D linear chain*), $\{[Cd(azpy)_3(H_2O)_2]\cdot 2PF_6\cdot azpy\}_n$ (**VI-2**) (*1-D fishbone-type chain*), $\{[M_2(azpy)_6(H_2O)_5]\cdot 4PF_6\cdot azpy\cdot H_2O\}_n$ (M = Ni (**VI-3**), Zn (**VI-4**)) (*1-D defective zigzag chain*), $\{[Ag(azpy)]\cdot PF_6\}_n$ (**VI-5**) (*1-D linear chain*), $\{[Mn(NCS)_2(azpy)(MeOH)_2]\cdot azpy\}_n$ (**VI-6**) (*1-D linear chain*), $\{[Mn(NCS)_2(azpy)_2]\cdot azpy\}_n$ (**VI-7**) (*2-D square sheet*), $\{[Ni(NCS)_2(azpy)_2]\cdot 3toluene\}_n$ (**VI-8**·3toluene) (*2-D rhombic sheet*), and $\{[Ni_2(NCS)_4(azpy)_4]\cdot alcohol\}_n$ (alcohol = MeOH (**VI-9**·MeOH), EtOH (**VI-9**·EtOH)) (*2-D interpenetrating sheet*), have been synthesized and structurally characterized. **VI-1-6** show three types of 1-D chain structures. **VI-7** forms a 2-D sheet with square grids and takes a non-interpenetrating structure, which creates microporous channels with dimensions of *ca.* 5 Å x 3 Å along the *a*-axis. These channels are including free guest azpy molecules. Also **VI-8**·3toluene represents 2-D non-interpenetrating, rhombic sheets (*ca.* 9 Å x 9 Å), between which guest toluene molecules are incorporated. On the other hand, **VI-9**·MeOH and **VI-9**·EtOH afford perpendicularly interpenetrating structures of rhombic 2-D sheets, resulting in small microporous channels with dimensions of *ca.* 2 Å x 2 Å along the *c*-axis. These channels are filled with guest alcohol molecules (MeOH and EtOH). It should be noted that the interpenetration and π-π interaction play an important role in the framework stability of azpy-containing coordination polymers. The TGA data and XRPD patterns reveal that **VI-9**·MeOH and **VI-9**·EtOH retain their channel networks after the removal of guest molecules, while non-interpenetrating network of **VI-7** destroys with a release of guest azpy molecules. **VI-9** shows N_2 and CH_4 adsorption activity for the microporous channels, despite of a larger size of the N_2 (3 Å) and CH_4 (4 Å) than that of the

channel window (2 Å), which clearly indicates that this interpenetrating network has soft dynamic channels, namely, new type of third-generation microporous compounds.

VI. 1 Introduction

4,4'-bpy derivatives with appropriate spacers such as $-CH_2-CH_2-$ (bpetha),[1-6] -CH=CH- (bpethe),[2,7-10] -C≡C- (bpethy),[11-14] -N=N- (azpy),[2,13,15-22] -Ph- (bpb),[23,24] -Ph-Ph- (bpbp),[24-27] and so on (Scheme VI. 1), are used instead of simple 4,4'-bpy ligand for the aim of the construction of functional coordination polymers in recent years. The author noted the 4,4'-azopyridine (azpy) ligand as a new building block because of unique functionalities compared with 4,4'-bpy as mentioned in Chapter I. In addition to affording a longer metal-metal distance than 4,4'-bpy, the azpy ligand has redox- and optical-active properties introduced by -N=N- group. Furthermore, it is readily expected that azpy ligand conjugated by the azo group prefers a π-π interaction. In this chapter, the author reports on preparing and crystallographically characterizing new ten azpy-containing coordination polymers, $\{[Mn(NO_3)_2(azpy)(H_2O)_2]\cdot 2EtOH\}_n$ (**VI-1**·2EtOH) (*1-D linear chain*), $\{[Cd(azpy)_3(H_2O)_2]\cdot 2PF_6\cdot azpy\}_n$ (**VI-2**) (*1-D fishbone-type chain*), $\{[M_2(azpy)_6(H_2O)_5]\cdot 4PF_6\cdot azpy\cdot H_2O\}_n$ (M = Ni (**VI-3**), Zn (**VI-4**)) (*1-D defective zigzag chain*), $\{[Ag(azpy)]\cdot PF_6\}_n$ (**VI-5**) (*1-D linear chain*), $\{[Mn(NCS)_2(azpy)(MeOH)_2]\cdot azpy\}_n$ (**VI-6**) (*1-D linear chain*), $\{[Mn(NCS)_2(azpy)_2]\cdot azpy\}_n$ (**VI-7**) (*2-D square sheet*), $\{[Ni(NCS)_2(azpy)_2]\cdot 3toluene\}_n$ (**VI-8**·3toluene) (*2-D rhombic sheet*), and $\{[Ni_2(NCS)_4(azpy)_4]\cdot alcohol\}_n$ (alcohol = MeOH (**VI-9**·MeOH), EtOH (**VI-9**·EtOH)) (*2-D interpenetrating sheet*) (Scheme VI.2). In these compounds, **VI-1**·2EtOH, **VI-7**, **VI-8**·3toluene, **VI-9**·MeOH, and **VI-9**·EtOH, strongly capture guest molecules by π-π and/or micropore filling interactions into their microporous channels. The microporous stability and functionality are examined in detail.

Scheme VI.1

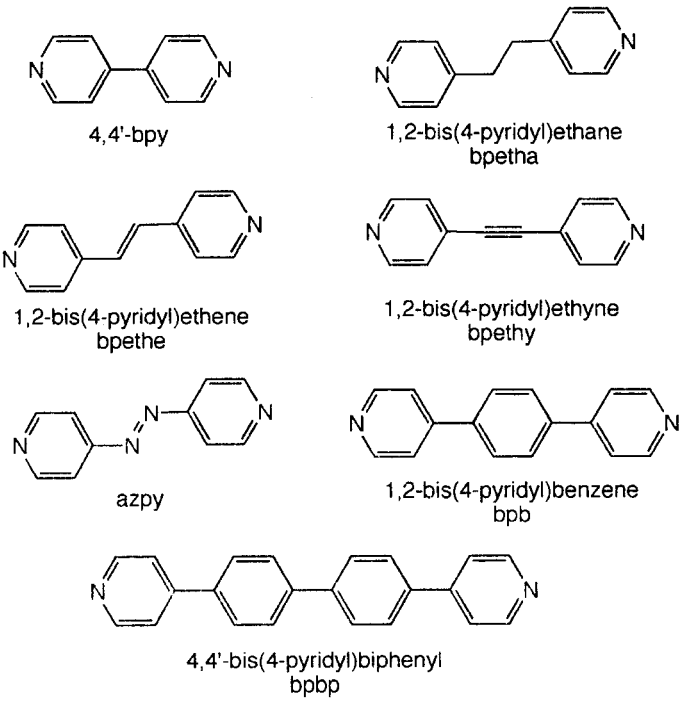

Scheme VI.2

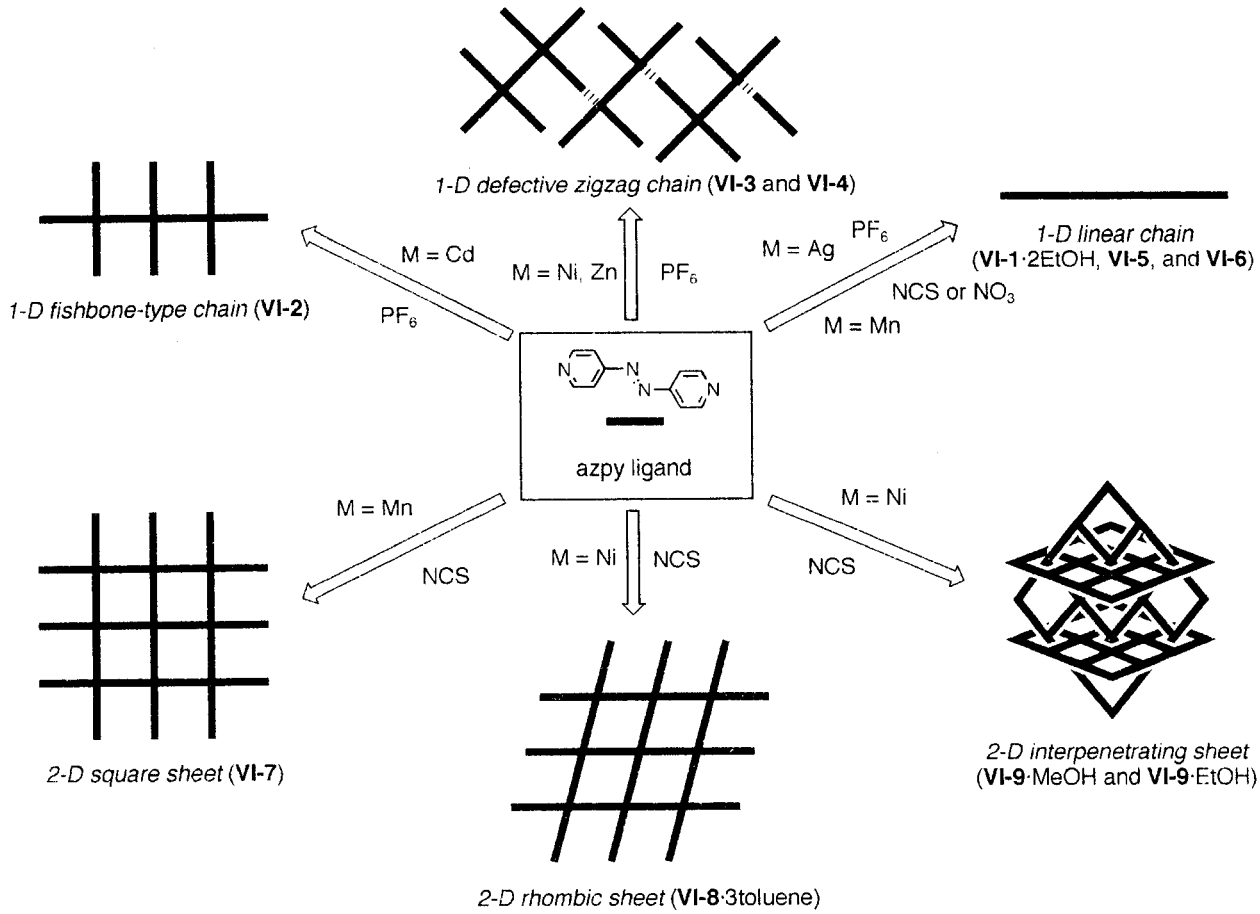

VI. 2 Experimental

VI. 2. 1 Physical Measurements

The physical measurements were performed as described in Chapter 1.

VI. 2. 2 Syntheses

Materials. $Cd(ClO_4)_2 \cdot nH_2O$, $Zn(BF_4)_2 \cdot H_2O$, $Mn(ClO_4)_2 \cdot 6H_2O$, and $AgPF_6$ were obtained from Aldrich Chemical Co. $Mn(NO_3) \cdot 6H_2O$, $Ni(ClO_4)_2 \cdot 6H_2O$, and KPF_6 were purchased from Kanto Chemical Co. NH_4SCN and NH_4PF_6 were obtained from Wako Co. Azpy was prepared according to the literature method.[28,29]

Synthesis of $\{[Mn(NO_3)_2(azpy)(H_2O)_2] \cdot 2EtOH\}_n$ (VI-1·2EtOH). An EtOH solution (20 mL) containing azpy (0.75 g, 4.0 mmol) was added to an acetone solution (20 mL) containing $Mn(NO_3)_2 \cdot 6H_2O$ (0.57 g, 2.0 mmol). The solution was filtered and allowed to stand for 3 days. Orange crystals obtained were collected by filtration, washed with EtOH, and dried under reduced pressure for 2 hours. This compound easily eliminated guest EtOH molecules to give a desolvated compound. Yield: 0.31 g (0.78 mmol, 39 %). Anal. Calcd for $C_{10}H_{12}MnN_6O_8$: C, 30.09; H, 3.03; N, 21.05. Found: C, 29.11; H, 2.93; N, 21.05. IR (KBr pellet): 3420 m, 3109 w, 3084 w, 3057 m, 3036 w, 1601 s, 1568 w, 1493 m, 1383 s, 1288 w, 1228 w, 1008 m, 846 s, 837 m, 825 m, 569 s, 542 m, 528 m cm^{-1}.

Synthesis of $\{[Cd(azpy)_3(H_2O)_2] \cdot 2PF_6 \cdot azpy\}_n$ (VI-2). An EtOH solution (10 mL) of azpy (0.100 g, 0.543 mmol) was added to an aqueous solution (10 mL) containing a mixture of $Cd(ClO_4)_2 \cdot nH_2O$ (0.089 g, 0.272 mmol) and KPF_6 (0.150 g, 0.815 mmol) at room temperature. As the resulting red solution was allowed to stand for 1 day, the obtained red crystals were collected by filtration, washed with EtOH, and dried under reduced pressure for 2 hours. Yield: 0.067 g (0.057 mmol, 21 %). Anal. Calcd for $C_{40}H_{36}CdF_{12}N_{16}O_2P_2$: C, 40.88; H, 3.09; N, 19.07. Found: C, 40.88; H, 3.05; N, 18.98. IR (KBr pellet): 2926 w, 1603 m, 1595 m, 1570 w, 1414 m, 1223 w, 1053 w, 1012 w, 871 m, 839 s, 740 w, 571 w, 557 m, 544 w, 522 w cm^{-1}.

Syntheses of $\{[M_2(azpy)_6(H_2O)_5]\cdot 4PF_6\cdot azpy\cdot H_2O\}_n$ (M = Ni (VI-3), Zn (VI-4)). An EtOH solution (10 mL) of azpy (0.100 mg, 0.543 mmol) was added to an aqueous solution (10 mL) containing a mixture of $Ni(ClO_4)_2\cdot 6H_2O$ (0.100 g, 0.272 mmol) or $Zn(BF_4)_2\cdot H_2O$ (0.070 g, 0.272 mmol) and NH_4PF_6 (0.089 g, 0.543 mmol) at room temperature. As the resulting red solution was allowed to stand for a few days, the obtained red crystals were collected by filtration, washed with EtOH, and dried under reduced pressure for 2 hours. Yield: 0.119 g (0.057 mmol, 72 %) (**VI-3**) and 0.080 g (0.038 mmol, 49 %) (**VI-4**). Anal. Calcd for $C_{70}H_{68}Ni_2F_{24}N_{28}O_6P_4$ (**VI-3**): C, 40.14; H, 3.27; N, 18.72. Found: C, 40.31; H, 3.24; N, 18.92. IR (KBr pellet): 3079 bm, 1598 m, 1571 m, 1492 w, 1417 m, 1324 w, 1226 m, 1191 w, 1106 w, 1049 m, 1014 m, 842 s, 738 m, 573 m, 557 m, 545 m, 527 m cm^{-1}. Anal. Calcd for $C_{70}H_{68}Zn_2F_{24}N_{28}O_6P_4$ (**VI-4**): C, 39.88; H, 3.25; N, 18.60. Found: C, 40.24; H, 3.27; N, 18.89. IR (KBr pellet): 3078 bm, 1596 m, 1571 m, 1535 w, 1417 m, 1324 w, 1226 m, 1191 w, 1050 w, 1013 m, 841 s, 737 w, 572 m, 557 m, 544 m, 526 m cm^{-1}.

Synthesis of $\{[Ag(azpy)]\cdot PF_6\}_n$ (VI-5). An EtOH solution (10 mL) of azpy (100 mg, 0.543 mmol) was added to an aqueous solution (10 mL) of $AgPF_6$ (137 mg, 0.543 mmol) at room temperature. The obtained pale-orange powder was filtered, washed with EtOH, and dried under reduced pressure for 5 hours. Anal. Calcd for $C_{10}H_8AgF_6N_4P$: C, 27.48; H, 1.85; N, 12.82. Found: C, 27.76; H, 2.14; N, 13.51. IR (KBr pellet): 3117 w, 3057 w, 1604 m, 1568 w, 1496 w, 1427 m, 1232 w, 1062 w, 1030 w, 889 m, 831 s, 738 w, 669 w, 576 w, 555 m, 526 w cm^{-1}.

Single crystals suitable for X-ray analysis were prepared by the careful diffusion of an EtOH solution of azpy into an aqueous solution containing $AgPF_6$. The homogeneity of the bulk product of each compound was confirmed by comparison of the observed and calculated powder diffraction patterns obtained from single crystal data.

Synthesis of $\{[Mn(NCS)_2(azpy)(MeOH)_2]\cdot azpy\}_n$ (VI-6). A MeOH solution (20 mL) of azpy (0.184 g, 1.00 mmol) was slowly added to a MeOH solution (20 mL) containing the mixture of $Mn(ClO_4)_2\cdot 6H_2O$ (0.181 g, 0.50 mmol) and NH_4SCN (0.114 g, 1.50 mmol) at room temperature. The obtained orange powder was filtered, washed with MeOH, and dried under

reduced pressure for 2 hours. Yield: 0.176 g (0.292 mmol, 58 %). Anal. Calcd for $C_{24}H_{24}MnN_{10}O_2S_2$: C, 47.76; H, 4.01; N, 23.21. Found: C, 47.24; H, 3.82; N, 23.18. IR (KBr pellet): 2993 w, 2744 w, 2549 w, 2067 s, 1597 m, 1567 w, 1456 w, 1412 m, 1320 w, 1222 w, 1048 w, 1028 m, 1007 m, 956 w, 835 m, 738 w, 663 w, 569 w, 543 w, 525 w, 477 w, 422 w cm^{-1}.

Single crystals suitable for X-ray analysis were prepared by the slow evaporation of a mixture of $Mn(ClO_4)_2 \cdot 6H_2O$, NH_4SCN, and azpy in MeOH/toluene solution. The homogeneity of the bulk product of the compound was confirmed by comparison of the observed and calculated powder diffraction patterns obtained from single crystal data.

Synthesis of $\{[Mn(NCS)_2(apzy)_2]\cdot azpy\}_n$ (VI-7). An EtOH solution (100 mL) of azpy (0.184 g, 1.00 mmol) was slowly added to an aqueous solution (100 mL) containing the mixture of $Mn(ClO_4)_2 \cdot 6H_2O$ (0.120 g, 0.33 mmol) and NH_4SCN (0.051 g, 0.67 mmol) at room temperature. As the resulting red solution was allowed to stand for a few weeks, the obtained red crystals were collected by filtration, washed with EtOH, and dried under reduced pressure for 2 hours. Yield: 0.035 g (0.048 mmol, 15 %). The reason of a low yield of **VI-7** is that this complex dissolves in ethanol. Anal. Calcd for $C_{32}H_{24}MnN_{14}S_2$: C, 53.11; H, 3.34; N, 27.10. Found: C, 53.00; H, 3.41; N, 27.00. IR (KBr pellet): 3040 w, 2042 s, 1599 s, 1566 m, 1489 w, 1414 m, 1323 w, 1248 w, 1221 m, 1051 w, 1008 m, 989 w, 976 w, 854 m, 844 m, 569 m, 544 w, 526 w, 486 w cm^{-1}.

Synthesis of $\{[Ni(NCS)_2(azpy)_2]\cdot 3toluene\}_n$ (VI-8·3toluene). Single crystals suitable for X-ray analysis were prepared by the careful diffusion of a MeOH solution containing $Ni(ClO_4)_2 \cdot 6H_2O$ and NH_4SCN into a toluene solution of azpy. The red crystals were obtained after a few weeks. Unfortunately, pure product of **VI-8**·3toluene was not isolated due to the coexistence of other low-crystalline product.

Syntheses of $\{[Ni_2(NCS)_4(azpy)_4]\cdot alcohol\}_n$ (alcohol = MeOH (VI-9·MeOH), EtOH (VI-9·EtOH)). A MeOH or EtOH solution (20 mL) of azpy (0.368 g, 2.00 mmol) was added to an aqueous solution (20 mL) containing a mixture of $Ni(ClO_4)_2 \cdot 6H_2O$ (0.365 g, 1.00 mmol) and NH_4SCN (0.152 g, 2.00 mmol) at room temperature. The obtained orange

powder was collected by filtration, washed with MeOH or EtOH, and dried under reduced pressure for 3 hours. Guest alcohol molecules were released by drying, and host networks easily adsorbed H_2O molecules in the atmosphere. Yield: 0.516 g (0.47 mmol, 93 %). Anal. Calcd for $C_{45}H_{36}Ni_2N_{20}OS_4$ (**VI-9**·H_2O): C, 47.85; H, 3.10; N, 25.36. Found: C, 47.73; H, 3.24; N, 25.04. IR (KBr pellet): 3472 w, 3101 w, 3074 w, 2069 s, 1603 m, 1570 m, 1489 w, 1415 m, 1321 w, 1226 m, 1190 w, 1049 w, 1016 w, 846 m, 806 w, 572 m, 549 w, 532 w, 484 w cm^{-1}.

Single crystals of **VI-9**·MeOH and **VI-9**·EtOH suitable for X-ray analysis were prepared by the careful diffusion of a MeOH or EtOH solution of azpy into an aqueous solution containing $Ni(ClO_4)_2 \cdot 6H_2O$ and NH_4SCN. The homogeneity of the bulk product was confirmed by comparison of the observed and calculated powder diffraction patterns obtained from single crystal data.

VI. 2. 3 X-Ray Structure Determination

For **VI-9**·MeOH and **VI-9**·EtOH, suitable crystals were sealed in glass capillary. For other compounds, suitable crystals were mounted on a glass fiber and coated with epoxy resin. In compounds, **VI-1**·2EtOH, **VI-2**, **VI-7**, and **VI-9**·EtOH, data collections were carried on a Rigaku AFC7R automated diffractometer fitted with a monochromatic Mo-Kα radiation source. Unit cell constants were obtained from a least-squares refinement using the setting angles of 25 well-centered reflections in the ranges $40.28 < 2\theta < 46.60$ ° for **VI-1**·2EtOH, $29.70 < 2\theta < 29.99$ ° for **VI-2**, $29.06 < 2\theta < 29.90$ ° for **VI-7**, and $25.16 < 2\theta < 29.57$ ° for **VI-9**·EtOH. In **VI-2**, azimuthal scans of several reflections indicated no need for an adsorption correction. In **VI-1**·2EtOH, **VI-7**, and **VI-9**·EtOH, an empirical adsorption correction based on azimuthal scans of several reflections was applied. In compounds, **VI-3**, **VI-4**, **VI-6**, and **VI-8**·3toluene, all measurements were made on a Rigaku RAXIS-CS imaging plate diffractometer with graphite monochromated Mo-Kα radiation. A numerical adsorption correction using the program NUMABS was applied. The data were corrected for Lorentz and polarization effects. In compound **VI-9**·MeOH, all measurements were made on a Rigaku RAXIS-RAPID imaging plate diffractometer with graphite monochromated Mo-Kα radiation. A symmetry-related adsorption correction using the program ABSCOR[30] was

applied. The data were corrected for Lorentz and polarization effects. In compound **VI-5**, all measurements were made on a Rigaku RAXIS-IV imaging plate diffractometer with graphite monochromated Mo-Kα radiation. An adsorption correction was not applied. The data were corrected for Lorentz and polarization effects. For **VI-1**·2EtOH, **VI-2**, **VI-3**, and **VI-5**, the structures were solved by a direct method using the SIR92 program[31] and expanded using Fourier techniques.[32] For **VI-6** and **VI-8**·3toluene, the structures were solved by a direct method using the SIR97 program[33] and expanded using Fourier techniques.[32] For **VI-7** and **VI-9**·EtOH, the structures were solved by a direct method using the SHELXS86 program[34] and expanded using Fourier techniques.[32] For **VI-9**·MeOH, the structure was solved by a direct method using the MITHRIL90 program[35] and expanded using Fourier techniques.[32] In compounds, **VI-1**·2EtOH, **VI-2**, **VI-5-7**, and **VI-9**·MeOH, the non-hydrogen atoms were refined anisotropically. In the case of **VI-3** and **VI-4**, some oxygen and carbon atoms of disordered H_2O and azpy molecules, respectively, were refined isotropically. In **VI-8**·3toluene, observed were two crystallographically independent toluene molecules, one of which was disordered and therefore fixed. Another one was refined isotropically. In the case of **VI-9**·EtOH, the carbon and oxygen atoms of an EtOH molecule were fixed. In all complexes except for **VI-1**·2EtOH and **VI-6**, all hydrogen atoms, which were placed in idealized positions, were included but not refined. In **VI-1**·2EtOH, all hydrogen atoms were refined isotropically. In **VI-6**, a hydrogen atom of a hydroxy group of MeOH was refined isotropically. The refinements were carried out using full-matrix least squares techniques. Crystal data and details of the structure determinations are summarized in Table VI. 1. All calculations were performed using the teXsan[36] crystallographic software package of Molecular Structure Corporation.

Table VI. 1a. Crystallographic Data for $\{[Mn(NO_3)_2(azpy)(H_2O)_2]\cdot 2EtOH\}_n$ (**VI-1**·2EtOH), $\{[Cd(azpy)_3(H_2O)_2]\cdot 2PF_6\cdot azpy\}_n$ (**VI-2**), $\{[Ni_2(azpy)_6(H_2O)_5]\cdot 4PF_6\cdot azpy\cdot H_2O\}_n$ (**VI-3**), and $\{[Zn_2(azpy)_6(H_2O)_5]\cdot 4PF_6\cdot azpy\cdot H_2O\}_n$ (**VI-4**).

compounds	**VI-1**·2EtOH	**VI-2**	**VI-3**	**VI-4**
formula	$C_{14}H_{24}MnN_6O_{10}$	$C_{40}H_{36}N_{16}CdF_{12}O_2P_2$	$C_{70}H_{68}N_{28}F_{24}Ni_2O_6P_4$	$C_{70}H_{68}N_{28}F_{24}O_6P_4Zn_2$
fw	491.32	1175.17	2094.75	2108.11
crystal system	monoclinic	triclinic	triclinic	triclinic
a, Å	24.488(4)	11.808(8)	11.6622(7)	11.7176(5)
b, Å	11.868(3)	12.625(8)	17.6438(8)	17.682(2)
c, Å	7.636(4)	9.614(7)	10.6097(7)	10.6794(9)
α, deg		98.29(6)	105.045(1)	105.064(1)
β, deg	91.39(3)	100.83(7)	89.998(2)	89.693(4)
γ, deg		116.79(5)	83.138(4)	82.992(4)
V, Å^3	2218(1)	1212(1)	2092.1(2)	2119.1(3)
space group	*C2/c* (No.15)	$P\bar{1}$ (No.2)	$P\bar{1}$ (No.2)	$P\bar{1}$ (No.2)
Z	4	1	1	1
ρ(calcd), g·cm^{-3}	1.471	1.609	1.663	1.652
F(000)	1020.00	590.00	1064.00	1068.00
μ(Mo Kα), cm^{-1}	6.56	6.17	6.50	7.64
diffractometer	AFC7R	AFC7R	RAXIS-CS	RAXIS-CS
radiation (λ, Å)	0.71069	0.71069	0.71069	0.71069
temp., ℃	25	25	-180	-180
GOF	3.272	1.206	1.748	2.145
no. of obsd data	2093 ($I > 3.00\sigma(I)$)	5494 (all data)	7741 (all data)	8093 (all data)
no. of variables	167	368	666	671
R[a] ($I > 2.00\sigma(I)$, all data)	0.0371 ($I > 3.00\sigma(I)$)	0.0346, 0.0371	0.0802, 0.1069	0.0591, 0.0641
R_w[b] ($I > 2.00\sigma(I)$, all data)	0.0393 ($I > 3.00\sigma(I)$)	0.0493, 0.0501	0.0886, 0.0944	0.0835, 0.0846

[a] $R = \Sigma\|\|Fo| - |Fc|\|/\Sigma|Fo|$. [b] $R_w = [(\Sigma w\,(|Fo| - |Fc|)^2/\Sigma w Fo^2)]^{1/2}$.

Table VI.1b. Crystallographic Data for $\{[Ag(azpy)]\cdot PF_6\}_n$ (**VI-5**), $\{[Mn(NCS)_2(azpy)(MeOH)_2]\cdot azpy\}_n$ (**VI-6**), $\{[Mn(NCS)_2(azpy)_2]\cdot azpy\}_n$ (**VI-7**), and $\{[Ni(NCS)_2(azpy)_2]\cdot 3toluene\}_n$ (**VI-8**·3toluene).

compounds	**VI-5**	**VI-6**	**VI-7**	**VI-8**·3toluene
formula	$C_{10}H_8N_4AgF_6P$	$C_{24}H_{24}NMnO_2S_2$	$C_{32}H_{24}N_{14}MnS_2$	$C_{43}H_{40}N_{10}Ni_1S_2$
fw	437.03	603.58	723.69	819.68
crystal system	monoclinic	monoclinic	monoclinic	monoclinic
a, Å	8.281(2)	7.1502(2)	11.593(2)	13.6831(6)
b, Å	13.264(1)	17.0859(7)	13.641(2)	20.656(1)
c, Å	13.406(4)	11.9412(5)	22.511(2)	16.3573(8)
β, deg	107.51(2)	93.272(2)	101.40(1)	110.346(2)
V, Å^3	1404.3(5)	1456.46(9)	3489.8(8)	4334.7(3)
space group	$P2_1/c$ (No. 14)	$P2_1/c$ (No. 14)	$P2/n$ (No.13)	$C2/c$ (No. 15)
Z	4	2	4	4
ρ(calcd), g cm^{-3}	2.067	1.376	1.377	1.256
F(000)	848.00	622.00	1484.00	1712.00
μ(Mo Kα), cm^{-1}	16.13	6.36	5.43	5.86
diffractometer	RAXIS-IV	RAXIS-CS	AFC7R	RAXIS-CS
radiation (λ, Å)	0.71069	0.71069	0.71069	0.71069
temp., ℃	25	-100	25	-100
GOF	1.872	1.518	1.382	1.833
no. of obsd data	2407 (all data)	3148 (all data)	6780 (all data)	4541 (all data)
no. of variables	200	182	465	187
R^a (I > 2.00σ(I), all data)	0.0693, 0.0721	0.0360, 0.0399	0.0617, 0.1030	0.0889, 0.1288
R_w^b (I > 2.00σ(I), all data)	0.0977, 0.0995	0.0557, 0.0574	0.0776, 0.0864	0.1087, 0.1157

[a] $R = \Sigma||Fo| - |Fc||/\Sigma|Fo|$. [b] $R_w = [(\Sigma w (|Fo| - |Fc|)^2/\Sigma wFo^2)]^{1/2}$.

Table VI.1c. Crystallographic Data for $\{[Ni_2(NCS)_4(azpy)_4]\cdot MeOH\}_n$ (**VI-9**·MeOH) and $\{[Ni_2(NCS)_4(azpy)_4]\cdot EtOH\}_n$ (**VI-9**·EtOH).

compound	**VI-9**·MeOH	**VI-9**·EtOH
formula	$C_{45}H_{36}N_{20}Ni_2OS_4$	$C_{46}H_{38}N_{20}Ni_2OS_4$
fw	1118.55	1132.58
crystal system	orthorhombic	orthorhombic
a, Å	18.099(1)	18.129(6)
b, Å	31.056(2)	31.109(8)
c, Å	19.387(1)	19.39(1)
V, Å^3	10897(1)	10937(7)
space group	*Ccca* (No. 68)	*Ccca* (No. 68)
Z	8	8
ρ(calcd), g·cm^{-3}	1.363	1.376
F(000)	4592.00	4656.00
μ(Mo Kα), cm^{-1}	8.98	8.96
diffractometer	RAXIS-RAPID	AFC7R
radiation (λ, Å)	0.71069	0.71069
temp., ℃	25	25
GOF	0.998	1.393
no. of observns	5648 (all data)	4707 (all data)
no. of variables	332	318
R^a (I > 2.00σ(I), all data)	0.0439, 0.0789	0.0751, 0.1928
R_w^b (I > 2.00σ(I), all data)	0.0534, 0.0622	0.0975, 0.1194

[a] $R = \Sigma\|Fo| - |Fc\|/\Sigma|Fo|$. [b] $R_w = [(\Sigma w\ (|Fo| - |Fc|)^2/\Sigma wFo^2)]^{1/2}$.

VI. 3 Results and Discussion

VI. 3. 1 Crystal Structures

VI. 3. 1. 1 Crystal Structure of $\{[Mn(NO_3)_2(azpy)(H_2O)_2]\cdot 2EtOH\}_n$ (VI-1·2EtOH).

An ORTEP view of the Mn(II) center of **VI-1**·2EtOH is shown in Figure VI. 1(a) with numbering scheme, where the metal sits on the crystallographic inversion center. The Mn(II) center is based on a distorted octahedral environment with two pyridine nitrogen donors, two nitrate oxygen donors, and two water molecules, in which each ligand occupies the *trans* position. The nitrate anions ligate to the Mn(II) atom as a monodentate fashion. In the coordination octahedron, all the *trans*-L-Mn-L bond angles are crystallographically linear, and all the *cis*-L-Mn-L angles are slightly deviated from 90 ° (81-99 °).

Scheme IV.3

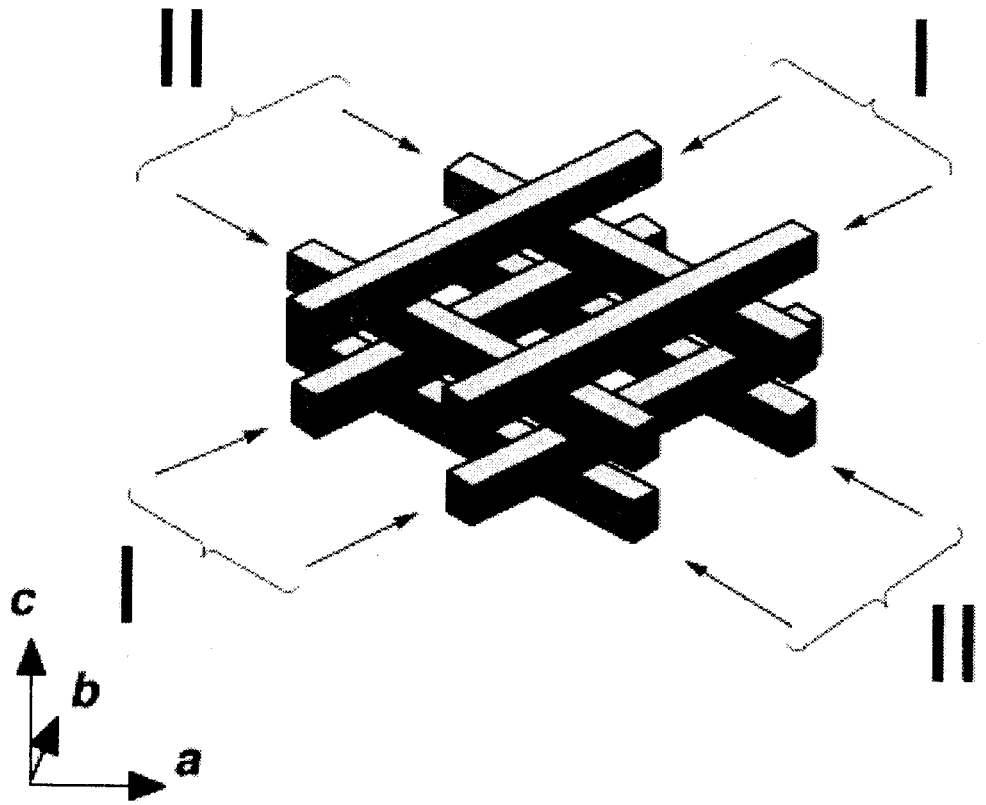

All azpy ligands are in a *trans* form, which is also the case for other coordination polymers reported in this chapter. Each azpy ligand links two Mn(II) centers (Mn•••Mn = *ca.* 13.6 Å) to form an infinite *1-D linear chain* in the *ab* plane (Figure VI. 1(b)). The two pyridine rings of the azpy ligand are almost coplanar and parallel to the *ab* plane. The *trans*-O(1)-Mn(1)-O(1*) and *trans*-O(4)-Mn(1)-O(4*) vectors bend by 36.6 ° and 45.3 ° to the *ab* plane, respectively. As shown in Scheme VI.3 and Figure VI. 1(c), the chains, oriented at the angle of 26 ° to the *a*-axis, form a flat parallel array I, while the other neighboring array II exists, whose chains are oriented by -26 ° to the *a*-axis. The chains of the arrays I and II are linked by hydrogen bonds between the terminal oxygen atoms of the coordinated nitrate and water molecules (N-O = *ca.* 2.7 and 3.2 Å), resulting in formation of a 3-D network, which is described as a *log-cabin* structure (Figures VI. 1(c) and VI. 1(d)). This framework creates hydrophobic large channels along the *c*-axis with dimensions of about 8 Å × 8 Å (Figure VI. 11(d)), which are filled with two ethanol molecules per Mn(II) atom. The two ethanol molecules are hydrogen-bonded to each other to form a dimer structure. In addition, the dimer units are connected by hydrogen bonds to give a 1-D chain in the channel. These guest ethanol molecules are not hydrogen-bonded to the host network.

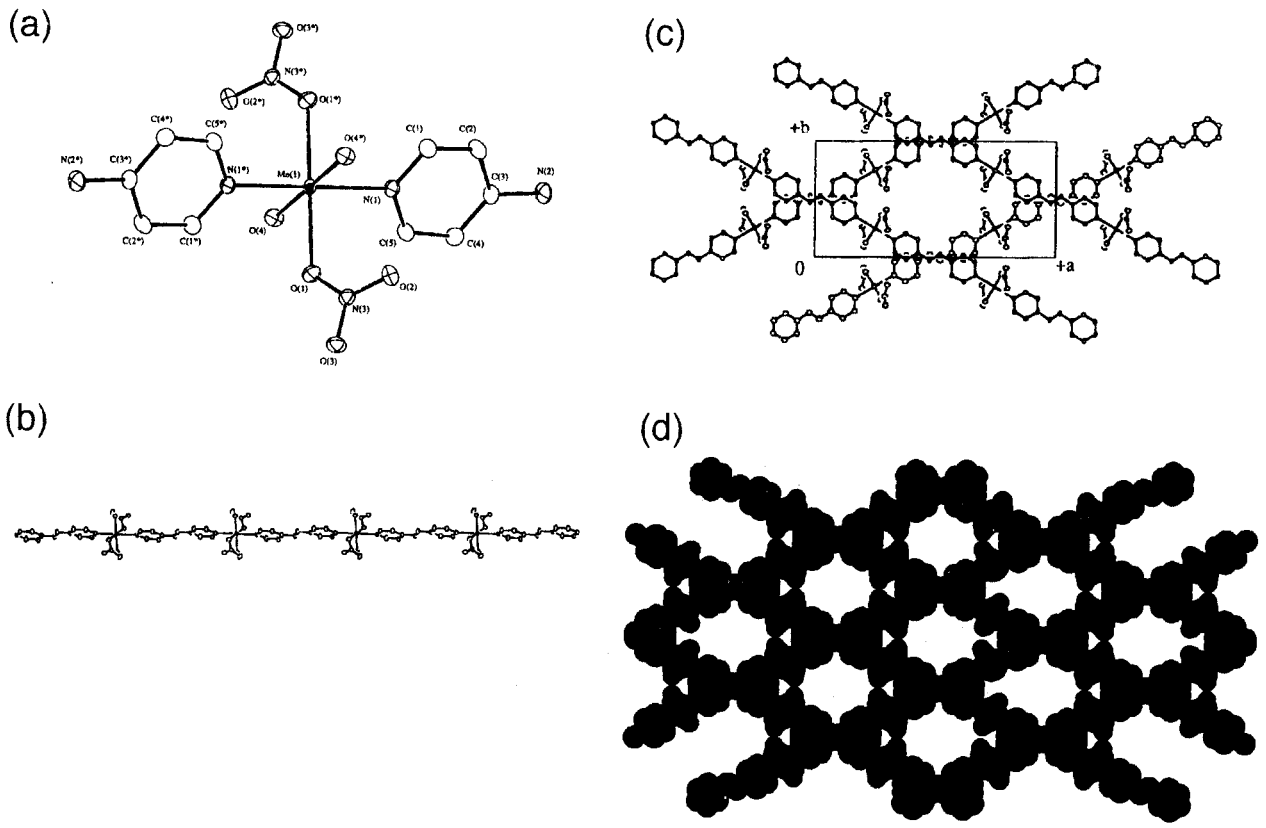

Figure VI.1 (a) ORTEP drawing around the Mn(II) center of **VI-1**·2EtOH at the 30 % probability level. In regard to all figures, the hydrogen atoms are omitted for clarity. (b) ORTEP drawing of a *1-D linear chain* structure of **VI-1**·2EtOH. (c) The stacking form of $[Mn(NO_3)_2(azpy)(H_2O)_2]_n$ chains of **VI-1**·2EtOH along the *c*-axis. (d) A space-filling model of a *log-cabin* structure of **VI-1**·2EtOH along the *c*-axis, indicating the aspect of large channel structure. The EtOH molecules are omitted for clarity.

VI. 3. 1. 2 Crystal Structure of $\{[Cd(azpy)_3(H_2O)_2]\cdot 2PF_6\cdot azpy\}_n$ (VI-2)

An ORTEP view around the Cd(II) center of **VI-2** is shown in Figure VI.2(a) with numbering scheme, where the metal site is on the crystallographic inversion center. The Cd(II) ion has a shortened octahedral environment with four azpy nitrogen atoms in the basal plane, and two H_2O oxygen atoms in the axial sites.

There are three types of association modes for the azpy ligand in the crystal. One is a bridging type (A), which links two Cd(II) centers. The second is a terminal-coordination type (B), which coordinates to Cd(II) centers via one of the two pyridine N atoms. These two types of azpy ligands make a *1-D fishbone-type chain* as shown in Figure VI.2(b). The fishbone-type chain motif is a rare structure, and some examples, $\{[Cd(4,4'\text{-bpy})_3(H_2O)_2]\cdot 2ClO_4\cdot 2H_2O\}_n$,[37] $\{[M(NCS)_2(4,4'\text{-bpy})(azpy)_2]\cdot H_2O\}_n$ (M = Ni,[19] Mn[38]), $\{[Co_2^{II}Co^{III}(nta)_2(azpy)_4(H_2O)_6][Co^{II}Co^{III}(nta)_2(azpy)_2(H_2O)_2]\cdot 4H_2O\}_n$ (nta = nitrilotriacetate),[39] and $[Cu(2,3\text{-pzdca})(4\text{-pia})_2]_n$ (2,3-pzdca = pyrazine-2,3-dicarboxylate, 4-pia = 4-pyridylisonicotinamide),[40] have been reported. The intrachain distance of the Cd•••Cd pair is *ca.* 11.8 Å. Moreover, coordination-free N atoms of type B azpy ligands interact with the coordinated H_2O molecules of neighboring chains via hydrogen bonds (2.747(3) Å) to afford a 2-D sheet network as illustrated in Figure VI.2(c), in which type B azpy ligands take a double-bridging mode and an effective π-π interaction between the pyridine rings of azpy B is observed (shortest distance : 3.31 Å). The third type of azpy molecule in the crystal is non-coordinated one (C), which links the coordinated H_2O molecules between the 2-D layers at intervals of two sheets via hydrogen bonds (2.760(3) Å) to form a 3-D network (Figure VI.2(d)). Three independent 3-D networks interpenetrate to each other. Free PF_6^- anions are included in a void space and no bonding interaction with the host network is observed. A short F•••F contact with the distances (2.81(3) and 3.08(2) Å), whose values are comparable to that of a F_2 solid,[41] in neighboring PF_6^- anions indicates the presence of a weak interaction.

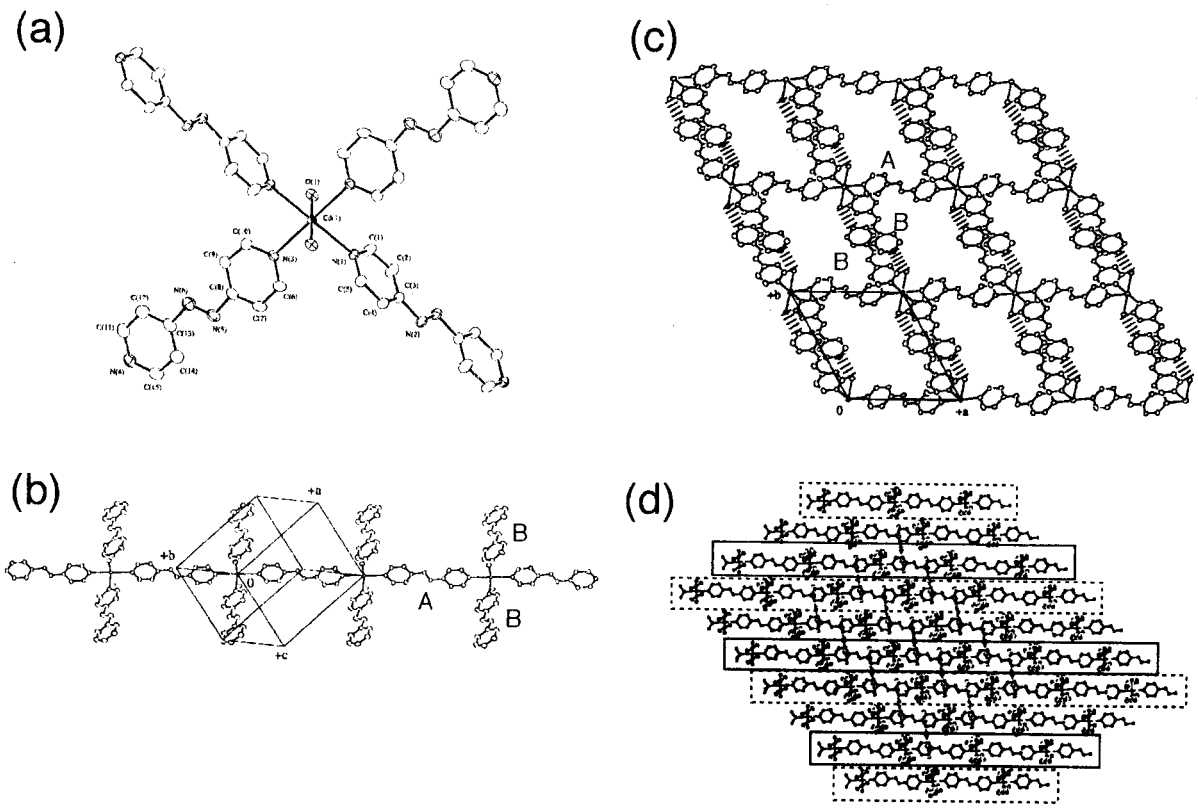

Figure VI.2. ORTEP view of (a) a Cd(II) center, (b) a *1-D fishbone-type chain*, (c) a 2-D hydrogen bonding sheet along the *c*-axis, and (d) a 3-D network of **VI-2** at the 30 % probability level. Hashed bonds indicate hydrogen-bonding interaction.

VI. 3. 1. 3 Crystal Structures of $\{[M_2(azpy)_6(H_2O)_5]\cdot 4PF_6\cdot azpy\cdot H_2O\}_n$ (M = Ni (VI-3), Zn (VI-4)).

Figure VI.3(a) shows an ORTEP view around the Ni(II) center of **VI-3**. **VI-4** is isostructural with **VI-3**. As shown in Scheme VI.2, **VI-3** affords a unique *1-D defective zigzag chain* structure, which is a first structural motif. Although only one crystallographically independent Ni(II) center exists, there are two kinds of Ni(II) circumstances in a crystal because one coordination site of the Ni(II) center is shared by two different molecules (H_2O and azpy) in 0.5 occupancy (Figure VI.3(a)). One (Ni1) has a distorted octahedral geometry with three nitrogen atoms of terminal-coordinating azpy ligands in a facial position and two oxygen atoms of H_2O molecules and one nitrogen atom of a bridging azpy ligand. Another (Ni2) also affords a similar coordination circumstance to the Ni1 center, but one of terminal-coordinated azpy ligands is replaced by a H_2O molecule.

In the crystal, the four kinds of azpy ligands are present. The first type is terminal-coordination one, A and A', each of which is located in a *cis*-position. The azpy A and A' are located in the *trans* position of bridging azpy ligand and coordinated H_2O molecule, respectively. The second type is bridging one (B), which links neighboring Ni(II) centers to form a Ni-Ni dimer as illustrated in the left of Figure VI.3(b). The third type is also terminal-coordination one (C), but this ligand takes a disorder form at the two independent positions. Such a disorder was observed when the single-crystal X-ray diffraction was measured at very low temperature (-180 °C), which clearly indicates that the type C of the azpy ligand is not located in the central position of two Ni(II) centers but essentially exists in the two independent positions. Moreover, large electron density around the N(11) atom was observed and defined as a Ni-coordinated H_2O molecule (N(11)-O(4) distance = 0.616(9) Å), which is consistent with the interpretation of the disorder mentioned above. Therefore, three types of Ni-Ni dimers bridged by the azpy ligand B are defined as shown in Scheme VI.4. These Ni-Ni dimers are randomly bridged by hydrogen bonds between the coordination-free nitrogen atoms of azpy (C) and the oxygen atoms of H_2O molecules (2.73(2) Å) to form a 1-D zigzag chain as illustrated in the right of Figure VI.3(b). The author calls this unique structure *1-D defective zigzag chain*. Each 1-D chain is linked by several hydrogen-bonding and π-π interactions. Free azpy

ligand (fourth type D) bridges two coordinated H_2O molecules of neighboring *1-D defective zigzag chains* (2.710(5) Å), and free nitrogen atoms of terminal-coordinating azpy ligands (A and A') interact with coordinated H_2O molecules (2.757(5) Å). Moreover, the π-π interaction between the type A azpy ligands is observed (shortest distance : 3.12 Å). As a result, two independent hydrogen-bonding 3-D frameworks, which doubly interpenetrate, are constructed as shown in Figure VI.3(c). Free H_2O molecules are hydrogen-bonded with coordinated H_2O molecules (2.63(3) Å). PF_6^- anions are included in a vacant space and interact with coordinated H_2O molecules (2.832(5) Å).

Scheme VI.4

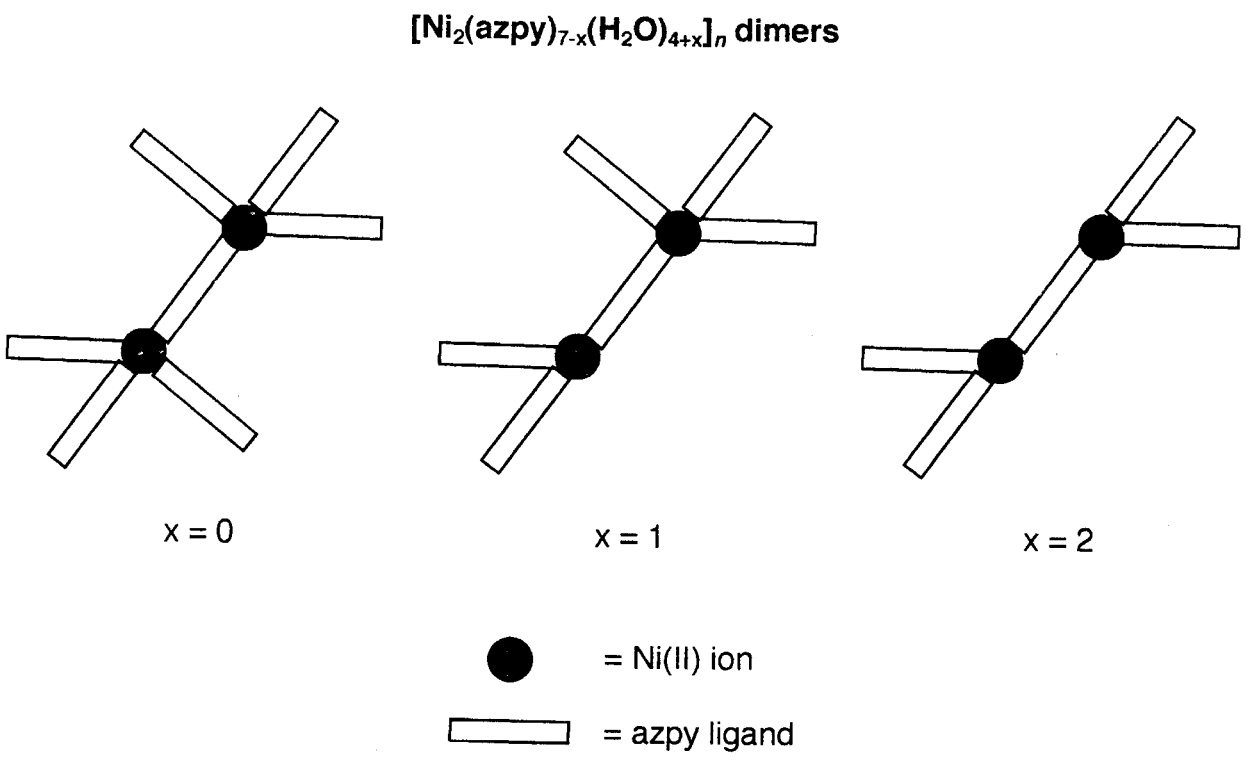

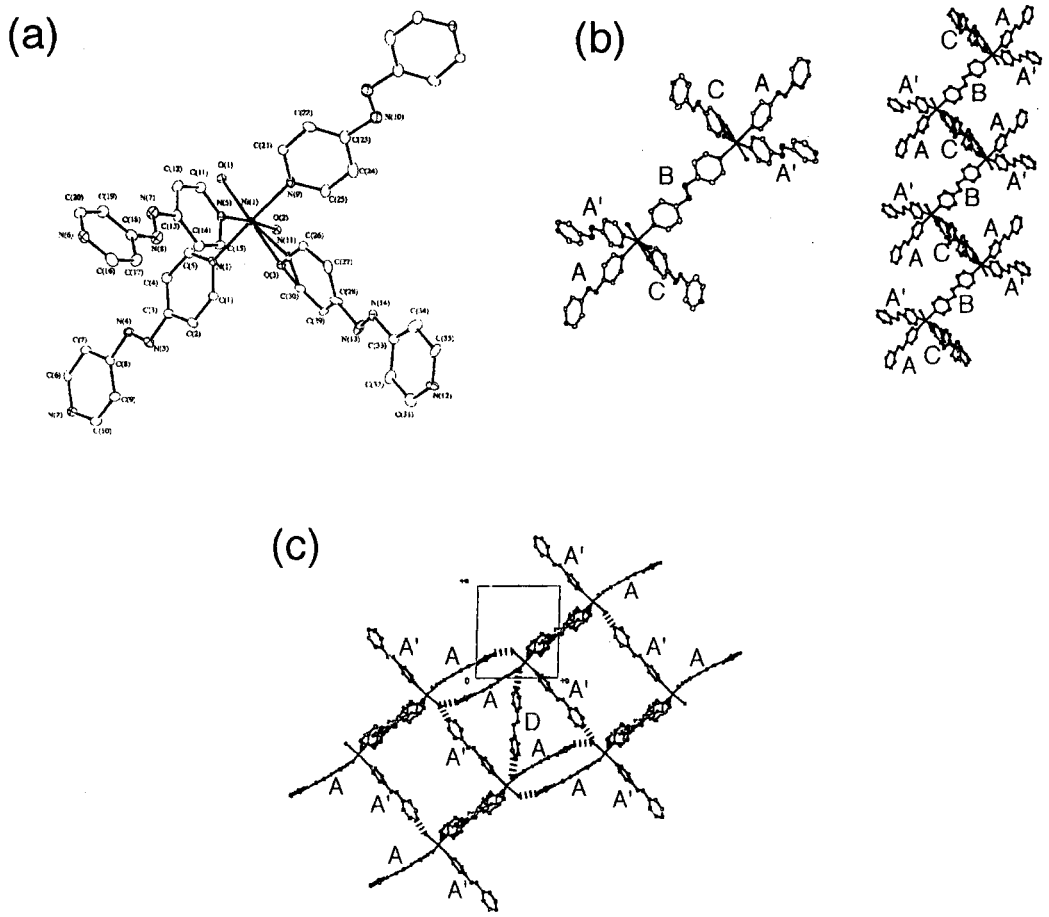

Figure VI.3. ORTEP view of (a) one Ni(II) center, (b, left) a Ni(II) dimer, (b, right) a *1-D defective zigzag chain*, and (c) one 3-D hydrogen bonding network along the *b*-axis of **VI-3** at the 30 % probability level. Hashed bonds indicate hydrogen-bonding interaction.

VI. 3. 1. 4 Crystal Structure of $\{[Ag(azpy)]\cdot PF_6\}_n$ (VI-5).

Figure VI.4(a) shows an ORTEP drawing of a 1-D chain of **VI-5** with numbering scheme. The Ag(I) has two coordination sites occupied with two azpy ligands. The Ag-N bond distances (2.133(6) and 2.167(7) Å) are similar to those of related 1-D Ag(I)-bipyridine complexes.[12,42-44] The N-Ag-N angle is almost linear (178.9(2) °). Each Ag atom is linked by azpy ligands to form a *1-D linear chain* structure along the *b*-axis (Figures VI.4(a) and VI.4(b)). The PF_6^- anions are weakly coordinated to the Ag(I) atoms in the terminal mode with distance of 2.847(7) Å. Observed are π-π interactions between the chains (shortest distance : 3.30 Å) as shown in Figure VI.4(c). A large number of coordination polymers with Ag(I) and bipyridine-type ligands have been hitherto reported.[12,16,42-49] The Ag(I) ion is liable to afford two (linear) or four (tetrahedral) coordination sites. The former gives 1-D chain structures such as linear[16,43,44,47,49] and helical[42,45] types. The latter affords a 2-D sheet,[46] a ladder,[12] and a 3-D diamond network.[48]

VI. 3. 1. 5 Crystal Structure of $\{[Mn(NCS)_2(azpy)(MeOH)_2]\cdot azpy\}_n$ (VI-6).

An ORTEP drawing of a Mn(II) center of **VI-6** with numbering scheme is illustrated in Figure VI.5(a), where the metal site is on the crystallographic inversion center. The Mn(II) center is based on a distorted elongated octahedral environment with two thiocyanate nitrogen donors and two methanol molecules in the basal plane, and two pyridine nitrogen donors in the axial sites. Each ligand occupies the *trans* position. The C-N-Mn bond of NCS^- ligands is bent from 180° (168.5(1) °). The N-C-S bond angle is almost linear (179.5(2) °).

There are two types of association modes for the azpy ligand in the crystal. One is a coordination type, which shows direct bridge between the Mn(II) centers to form a *1-D linear chain* with the Mn•••Mn separation of *ca.* 13.6 Å. The other is a hydrogen-bonding type, and bridges the coordinated MeOH ligands in the nearest neighbor chains to form a Mn-(MeOH)-azpy-(MeOH)-Mn link (O(MeOH)-N(py) = 2.691(2) Å). The Mn•••Mn distance between the 1-D chains is *ca.* 17.1 Å. The two pyridine rings in each type of azpy ligand are planer. The zigzag chain of Mn-(MeOH)-azpy-(MeOH)-Mn affords a hydrogen-bonding undulated 2-D structure (Figure VI.5(b)). These 2-

D sheets assemble by π-π interactions between coordinated and hydrogen-bonding azpy ligands (shortest distance : 3.25 Å) as illustrated in Figure VI.5(c).

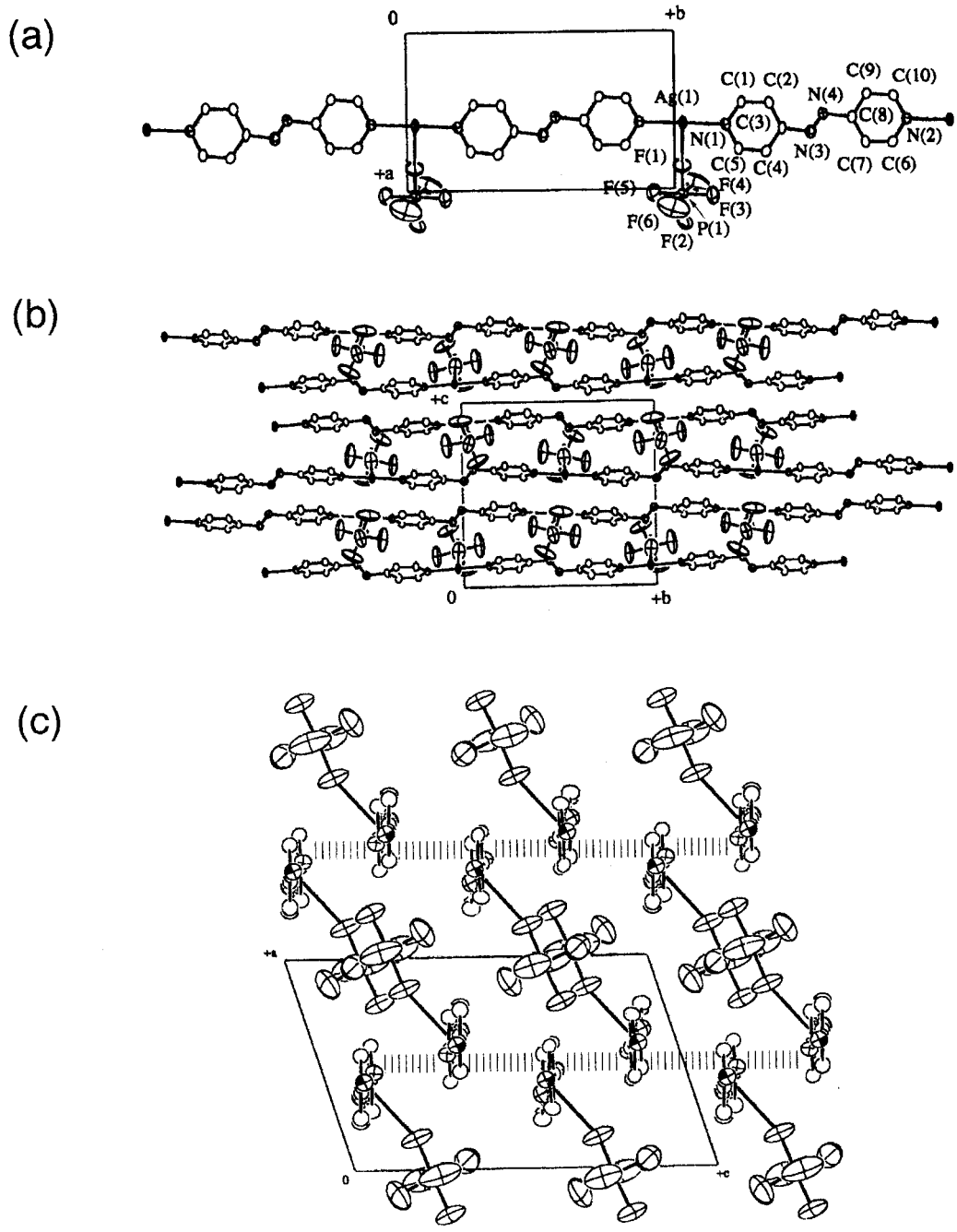

Figure VI.4. ORTEP view of (a) a *1-D linear chain* structure along the *c*-axis and (b and c) assembling structures along the *a*- and *b*-axes of **VI-5** at the 30 % probability level. Hashed bonds indicate π-π interaction.

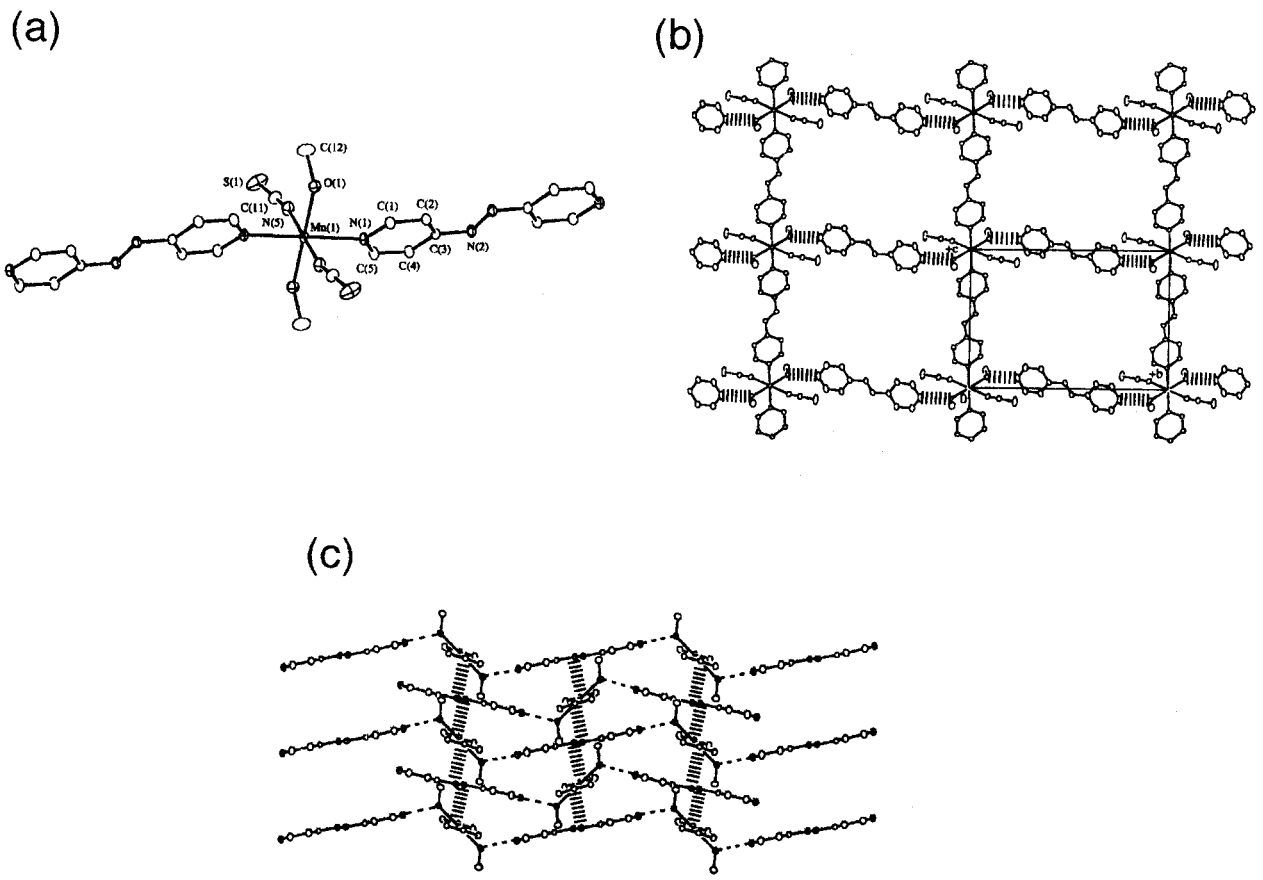

Figure VI.5. (a and b) ORTEP view of (a) a Mn(II) center and (b) a 2-D hydrogen-bonding undulated sheet along the *a*-axis of **VI-6** at the 30% probability level. Hashed bonds indicate hydrogen-bonding interaction. (c) ORTEP view of a stacking form of 2-D hydrogen-bonding undulated sheets of **VI-6** at the 30% probability level. The NCS anions are omitted for clarity. Dashed and Hashed bonds indicate hydrogen-bonding and π-π interactions.

VI. 3. 1. 6 Crystal Structure of $\{[Mn(NCS)_2(apzy)_2]\cdot azpy\}_n$ (VI-7).

There are two crystallographically independent Mn(II) centers, each circumstance of which is very similar. Figure VI.6(a) shows an ORTEP view of one Mn(II) center of **VI-7**. Each Mn(II) center has a shortened octahedral geometry with four pyridine nitrogen atoms and two *trans* thiocyanato nitrogen atoms. The C-N-Mn bonds of NCS^- ligands are bent from 180 °(av. 159.0 °). The N-C-S bond angles are almost linear (av. 179.4 °). Each Mn(II) center is linked by azpy ligands to yield a *2-D square sheet* with large grids (*ca.* 10 Å x 9 Å) and the corner angles of about 88 ° and 92 °as illustrated in Figure VI.6(b). As shown in Figure VI.6(b), the framework of **VI-7** contains two types of azpy molecules; one is almost perpendicular to the sheet, the other, whose azo group is disorderd, is twisted by about 52 °to the sheet. These two types of azpy molecules are alternately arranged in the infinite chains in the 2-D network. Because the sheets mutually slip to the channel direction, resulting channels afford a smaller rectangular shape (ca. 5 Å x 3 Å) along the *a*-axis as shown in Figure VI.6(c). These rectangular channels include free azpy molecules, which undergo π-π interactions with coordinated azpy ligands (shortest distance : 3.36 Å). Though several examples of azpy-containing coordination polymers affording 2-D grid network were previously reported,[13,15,18,21,22] many of them afford the interpenetration structure. This compound **VI-7** forms the non-interpenetration structure in spite of the large grid (*ca.* 10 Å x 9 Å), because of the template effect of free azpy ligands incorporated by the π-π interaction. The similar effect is also found in $\{[Cd(NO_3)_2(azpy)_2]\cdot azpy\}_n$.[18]

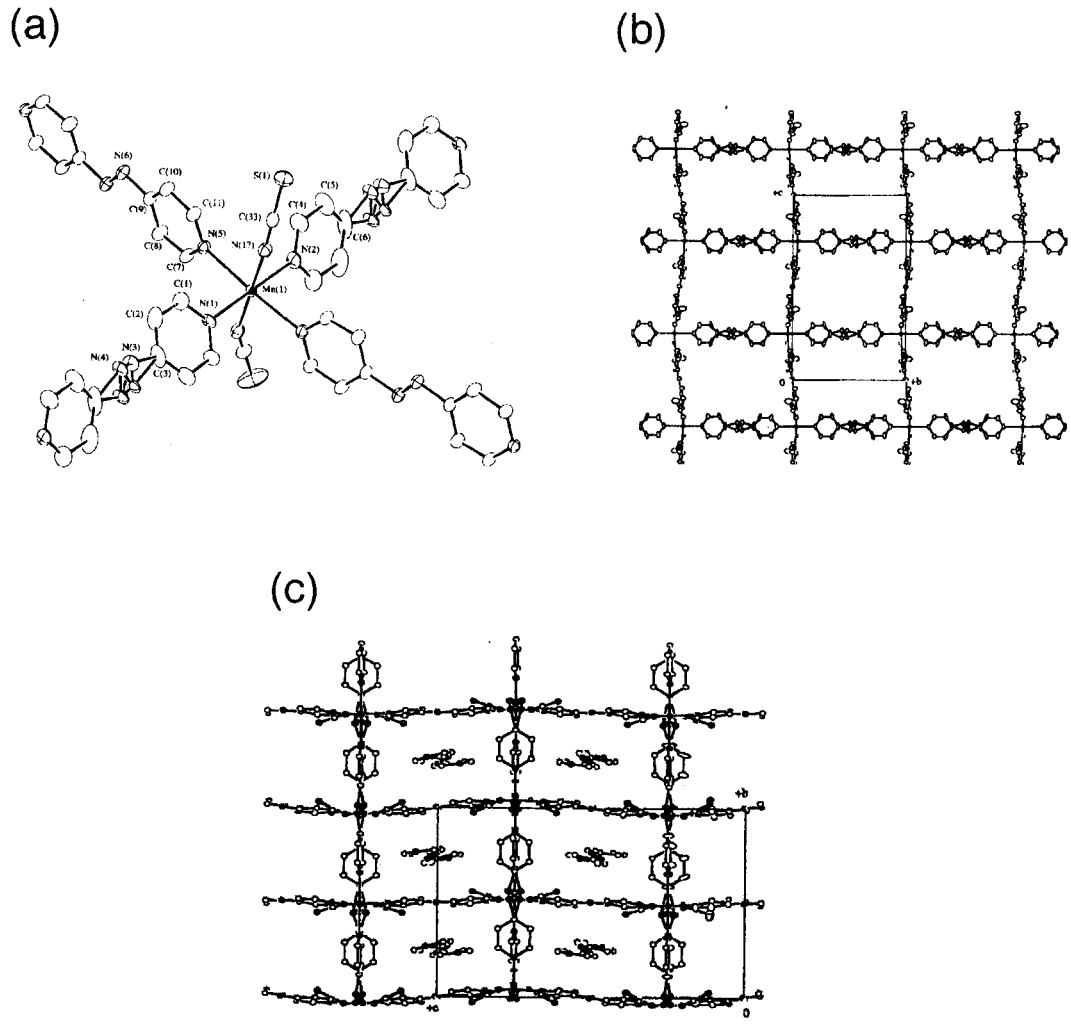

Figure VI. 6. ORTEP view of (a) one Mn(II) center, (b) a *2-D square sheet* structure along the *a*-axis, and (c) a microporous network along the *a*-axis of **VI-7** at the 30% probability level.

VI. 3. 1. 7 Crystal Structure of $\{[Ni(NCS)_2(azpy)_2]\cdot 3toluene\}_n$ (VI-8·3toluene).

Figure VI.7(a) represents an ORTEP drawing of a Ni(II) center of **VI-8**·3toluene. The Ni(II) center has a shortened octahedral geometry with four nitrogen atoms of azpy ligands in the basal plane and two nitrogen atoms of NCS anions at the axial sites. The C-N-Ni bond of NCS^- ligands is bent from 180 ° (166.1(5) °). The N-C-S bond angle is almost linear (178.8(5) °). The azpy ligands bridge the Ni(II) centers to form a *2-D rhombic sheet* with the corner angles of *ca.* 76 and 103 ° as illustrated in Figure VI.7 (b). Each sheet takes non-interpenetration mode in spite of a large grid size (*ca.* 9 Å x 9 Å). Because the sheets mutually slip to the channel direction, no microporous channels are observed in the perpendicular direction to the sheet. However, guest toluene molecules are filled between the 2-D layers as shown in Figure VI.7(c) (channel size : *ca.* 7 Å x 1 Å, 2 Å x 1 Å, and 5 Å x 2 Å, along the *c*-axis, *b*-axis, and (b-c) vector, respectively) and relate with host azpy ligands by π-π (shortest distance : 3.36 Å) and CH-π (shortest C-C distance : 3.64 Å) interactions.

VI. 3. 1. 8 Crystal Structures of $\{[Ni_2(NCS)_4(azpy)_4]\cdot alcohol\}_n$ (alcohol = MeOH (VI-9·MeOH), EtOH (VI-9·EtOH)).

In **VI-9**·MeOH, there are two crystallographically independent Ni(II) centers, the circumstances of which are very similar. Figure VI.8(a) shows an ORTEP view of one Ni(II) center of **VI-9**·MeOH. **VI-9**·EtOH is isostructural with **VI-9**·MeOH. Each Ni(II) center has a shortened octahedral geometry with four pyridine nitrogen atoms and two *trans* thiocyanato nitrogen atoms. The Ni-N (pyridine) distances of **VI-9**·MeOH are slightly shorter than those of $[Ni(NCS)_2(4,4'\text{-bpy})_2]_n$ (av. 2.148 Å).[50] The C-N-Ni bonds of NCS^- ligands are bent from 180° (av. 155.1 °). The N-C-S bond angles are almost linear (av. 178.9 °). Each Ni(II) center is linked by azpy ligands to yield a 2-D sheet with large rhombic grids (about 9 Å x 8 Å) and the corner angles of about 86° and 94° (Figure VI.8(b)). As shown in Figure VI.8(b), the framework of **VI-9**·MeOH contains two types of azpy molecules; one is parallel to the sheet, the other is perpendicular to the sheet. These two types of azpy molecules are alternately arranged in the infinite chains in the 2-D network. The 2-D sheets encounter perpendicular interpenetration (*2-D interpenetrating sheet*), giving rise to tightly

held 3-D structure as shown in Figure VI.8(c). In spite of the interpenetration, this network creates small channels with window dimensions of *ca.* 2 Å x 2 Å along the *c*-axis, which include MeOH molecules. Although these channel windows are smaller than a MeOH molecule, MeOH molecules can be remove without a breakdown of channels as shown in TGA, XRPD, and gas adsorption results as mentioned below. This reason is probably that the interpenetrating 2-D sheets are vibrating and therefore the channel windows temporarily expand. Rhombic 2-D sheets were also reported in $\{[Zn(4,4'\text{-bpy})_2(H_2O)_2]\cdot SiF_6\}_n$[51] and $\{[Zn(azpy)_2(H_2O)_2]\cdot SiF_6\cdot H_2O\}_n$,[15] which also show the interpenetrating structure.

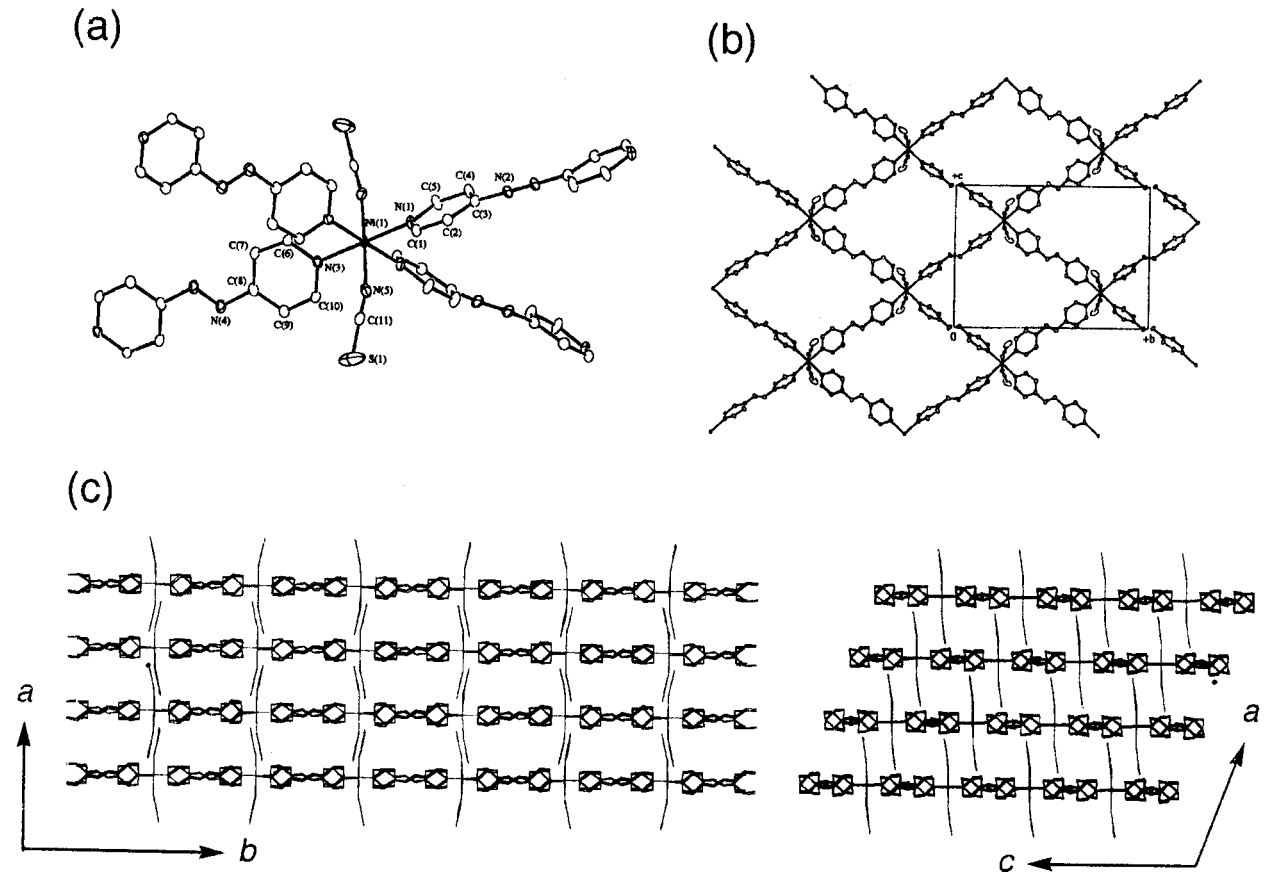

Figure VI.7. (a and b) ORTEP view of (a) a Ni(II) center and (b) a *2-D rhombic sheet* along the *a*-axis of **VI-8**·3toluene at the 30% probability level. (c) Perspective views of the stacking form along the *c*- (left) and *b*-axes (right) of **VI-8**·3toluene. The guest toluene molecules are omitted for clarity.

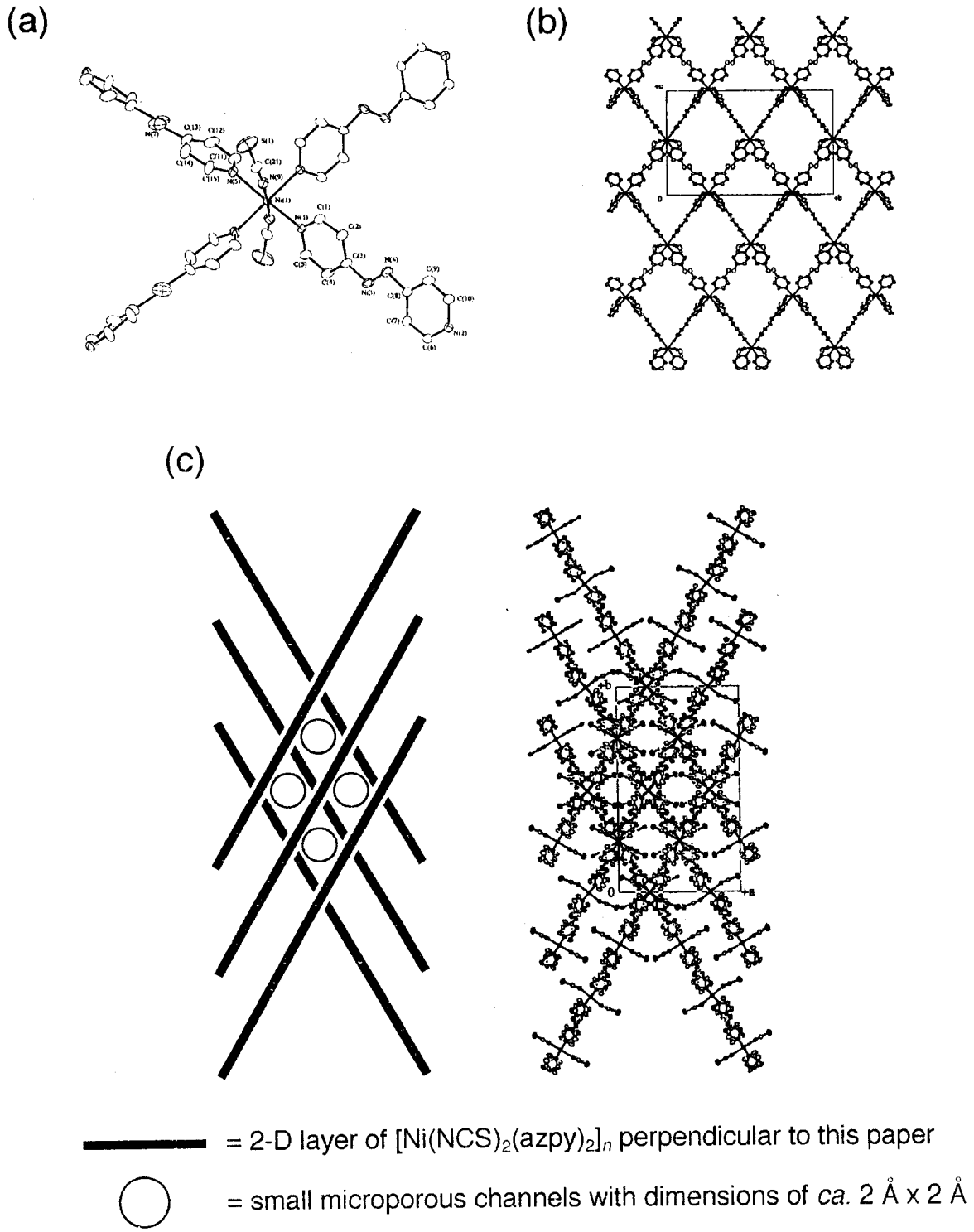

Figure VI.8. ORTEP view of (a) one Ni(II) center, (b) a 2-D sheet structure along the *a*-axis, and (c) a microporous network along the *c*-axis of **VI-9**·MeOH at the 30% probability level. The guest MeOH molecules are omitted for clarity.

VI. 3. 2 Characteristic Feature of Coordination Polymers with Azpy Ligand.

The number of coordination polymers containing the azpy ligand is appreciably less than that containing the 4,4'-bpy ligand, despite a first manuscript of azpy complexes has been reported in 1969.[52] In first report, several coordination polymers containing Co(II), Ni(II), and Cu(II) metal ions were prepared, but detailed crystal structures were not represented. Ciani et al. have first reported on the crystal structures of azpy-containing coordination polymers in 1998, and total 38 azpy-containing coordination polymers, in which those reported in this chapter are included, have been synthesized and crystallographically characterized (Table VI.2). When coordination networks of these polymers are investigated in detail, two interesting features are observed.

First, as shown in Table VI.2, the 2-D sheet and 3-D diamondoid structures tend to take the interpenetrating network in order to compensate a labile empty space. Exceptional cases are found in $\{[Cd(NO_3)_2(azpy)_2]\cdot azpy\}_n$,[18] $\{[Mn(NCS)_2(azpy)_2]\cdot azpy\}_n$ (**VI-7**), $\{[Cu(azpy)_2(H_2O)_2]\cdot 2ClO_4\cdot 2EtOH\}_n$,[16] $\{[Fe(NCS)_2(azpy)_2]\cdot 3H_2O\}_n$,[21] and $\{[Ni(NCS)_2(azpy)_2]\cdot 3toluene\}_n$ (**VI-8**·3toluene). $\{[Cd(NO_3)_2(azpy)_2]\cdot azpy\}_n$[18] and **VI-7** incorporate guest azpy molecules by a π-π interaction with the host network instead of the interpenetration. $\{[Cu(azpy)_2(H_2O)_2]\cdot 2ClO_4\cdot 2EtOH\}_n$[16] has coordinated H_2O and free ClO_4 molecules, both of which function as the hydrogen bonding sites and, therefore, stabilize a parallel stack of 2-D sheets. The 2-D grid of $\{[Fe(NCS)_2(azpy)_2]\cdot 3H_2O\}_n$[21] is stabilized by the incorporate of the NCS anions in neighboring sheets. **VI-8**·3toluene shows remarkable π-π and CH-π interactions between host networks and guest toluene molecules, which prevents the interpenetration.

Second, the azpy ligand in the network is liable to undergo the π-π interaction due to the expanded conjugation between pyridine rings, as mentioned in Introduction. In the case of 1-D polymers, the π-π interactions between the host azpy-chains are frequently observed (Table VI.2). One exceptional case is the 1-D chains of $\{[M(NCS)_2(azpy)(MeOH)_2]\cdot azpy\}_n$ (M = Fe,[21] Mn (**VI-6**)), bridging azpy ligands of which interact with guest azpy molecules by the π-π interaction. $\{[M_2(NO_3)_4(azpy)_3]\cdot x(guest)\}_n$ (M = Cd(II), Co(II))[13,18,22] is a rare example, in which π-π

interactions between 2-D host networks are observed, because of the triply interpenetration of the undulated sheets.

Table VI.2a. Summary of Azpy-Containing Coordination Polymers.

	π-π interaction	interpenetration
(I) 1-D compounds		
(a) $\{[Cd(azpy)_3(H_2O)_2]\cdot 2PF_6.azpy\}_n$	host-host	
(b) $\{[M_2(azpy)_6(H_2O)_5]\cdot 4PF_6\cdot azpy\cdot H_2O\}_n$ (M = Ni, Zn)	host-host	
(c) $\{[Ag(azpy)]\cdot PF_6\}_n$	host-host	
(d) $\{[Mn(NO_3)_2(azpy)(H_2O)_2]\cdot 2EtOH\}_n$	host-host	
(e) $\{[Ag(azpy)]\cdot NO_3\cdot MeOH\}_n$	host-host	
(f) $\{[M(NCS)_2(azpy)(MeOH)_2]\cdot azpy\}_n$ (M = Fe, Mn)	host-guest	
(g) $\{[M(NCS)_2(azpy)_2(4,4'\text{-bpy})]\cdot H_2O\}_n$ (M = Co, Mn)	host-host	
(h) $\{[Cu(CF_3SO_3)(2,2'\text{-bpy})(azpy)(H_2O)]\cdot CF_3SO_3\}_n$	host-host	
(i) $\{[Cu(2,2'\text{-bpy})(azpy)(H_2O)]\cdot 2NO_3\cdot H_2O\}_n$	host-host	
(j) $[HgI_2(azpy)]_n$	host-host	
(k) $\{[Co_2^{II}Co^{III}(nta)_2(azpy)_4(H_2O)_6][Co^{II}Co^{III}(nta)_2(azpy)_2(H_2O)_2]\cdot 4H_2O\}_n$	host-host	
(l) $\{[Cu(azpy)(H_2O)_4][Cu_2(nta)_2(azpy)]\cdot 6H_2O\}_n$	host-host	
(II) 2-D compounds		
(a) $\{[Mn(NCS)_2(azpy)_2]\cdot azpy\}_n$	host-guest	0-fold
(b) $\{[Ni(NCS)_2(azpy)_2]\cdot 3toluene\}_n$	host-guest	0-fold
(c) $\{[Ni_2(NCS)_4(azpy)_4]\cdot alcohol\}_n$ (alcohol = MeOH, EtOH)		perpendicular
(d) $\{[Co_2(NO_3)_4(azpy)_3]\cdot Me_2CO\cdot 3H_2O\}_n$		double inclined
(e) $\{[M_2(NCS)_4(azpy)_4]\cdot EtOH\}_n$ (M = Co, Fe)		perpendicular
(f) $\{[Cd(NO_3)_2(azpy)_2]\cdot azpy\}_n$	host-guest	0-fold

Table VI.2b. Summary of Azpy-Containing Coordination Polymers.

	π-π interaction	interpenetration
(II) 2-D compounds (continuance)		
(g) $\{[Cd_2(NO_3)_4(azpy)_3]\cdot 2Me_2CO\}_n$	host-host	3-fold
(h) $\{[Cu(azpy)_2(H_2O)_2]\cdot 2NO_3\cdot 2H_2O\}_n$		perpendicular
(i) $\{[Cu(azpy)_2(H_2O)_2]\cdot 2ClO_4\cdot 2EtOH\}_n$		0-fold
(j) $\{[Fe(NCS)_2(azpy)_2]\cdot 3H_2O\}_n$		0-fold
(k) $\{[Ni(NO_3)_2(azpy)_2]_2[Ni_2(NO_3)_4(azpy)_3]\cdot 4CH_2CL_2\}_n$		inclined
(l) $\{[M(azpy)_2(H_2O)_2]\cdot SiF_6\cdot H_2O\}_n$ (M = Zn, Cd)		perpendicular
(m) $\{[Co_2(NO_3)_4(azpy)_3]\cdot CH_2Cl_2\}_n$	host-host	3-fold
(n) $\{[Cd_2(NO_3)_4(azpy)_3]\cdot CH_2Cl_2\cdot 2H_2O\}_n$	host-host	3-fold
(o) $\{[Co_2(NO_3)_4(azpy)_3]\cdot CH_2Cl_2\}_n$		3-fold
(p) $\{[Zn_2(SO_4)_2(azpy)_2(H_2O)_3]\cdot 0.5azpy\}_n$	host-guest	0-fold
(q) $\{[Co(NCS)_2(azpy)_2]\cdot 1/4EtOH\cdot 1/2H_2O\}_n$		inclined
(r) $\{[Cu_3(nta)_2(azpy)_2(H_2O)_2]\cdot 6H_2O\}_n$	host-host	0-fold
(III) 3-D compounds		
(a) $\{[Cu(azpy)_2]\cdot ClO_4\}_n$		5-fold
(b) $\{[Cu(azpy)_2]\cdot BF_4\}_n$		5-fold

nta = nitrilotriacetate

VI. 3. 3 Crystal Engineering of Non-Interpenetrating Porous Network with Azpy Ligand

As mentioned above, 2-D or 3-D azpy-containing coordination polymers tend to create the interpenetrating network. Therefore, it is difficult to make large microporous channels or cavities. Although coordination polymers with guest azpy molecules into microporous channels have been reported previously and in this chapter ($\{[Mn(NCS)_2(azpy)_2]\cdot azpy\}_n$ (**VI-7**), $\{[Cd(NO_3)_2(azpy)_2]\cdot azpy\}_n$,[18] and $\{[Zn_2(SO_4)_2(azpy)_2(H_2O)_3]\cdot 0.5azpy\}_n$[17]), it is very difficult to remove the guest molecules without framework destruction as mentioned below. The author attempted to create the non-interpenetrating network by utilizing the feature that the azpy ligand is liable to undergo the π-π interaction: the use of aromatic small guest molecules such as benzene or toluene as a solvent. This synthetic strategy afforded a novel porous coordination polymer **VI-8**·3toluene incorporating aromatic toluene molecules by π-π and CH-π interactions. The computed free void of this compound is 53 %, whose value is so far the largest of those of previously reported azpy-containing coordination polymers and comparable to those (*ca.* 50 %) of highly porous coordination polymers $[M(AF_6)_2(4,4'\text{-bpy})_2]$ (M = Zn, A = Si;[53,54] M = Cu, A = Si;[54,55] M = Cu, A = Ge[56]), some of which exhibit the high surface area and the CH_4 adsorption capacity at room temperature and low pressure.[55,56]

VI. 3. 4 Stability of the Frameworks

In order to examine the stability of the channels in the absence of guest molecules, TGA and XRPD measurements of **VI-1**, **VI-7**, and **VI-9**·H_2O were carried out. The sample was heated to 500 ℃ at the rate of 5 ℃/min under N_2. The TGA data for **VI-1** show two steps of weight loss as shown in Figure VI.9(a). In the first region of r.t.-80 ℃, **VI-1** loses two coordinated H_2O molecules (observed 10.9 %, calculated 9.0 %). On further heating, **VI-1** shows a decomposition of $[Mn(NO_3)_2(azpy)]_n$ between 210 and 315 ℃. The TGA data of **VI-7** show two steps of weight loss as shown in Figure VI.9(b). In the first region of 160-240 ℃, **VI-7** loses concurrently one guest azpy molecule and one coordinated azpy molecule (observed 49.33 %, calculated 50.80 %). On further heating, **VI-7** loses another coordinated azpy molecule (observed 27.83 %, calculated

25.41 %) between 300 and 400 ℃. It is revealed that free azpy molecules are removed at about 100 ℃ from a result of TGA. This high removal temperature of the including guest azpy molecules in compound **VI-7** is attributable to the cooperation effect of micropore filling and π-π interactions between channel walls and guest azpy molecules. Unfortunately, since guest azpy molecules in channels were removed along with coordinated azpy molecules, the forming of vacant channels was impossible. The TGA data for **VI-9**·H_2O show three steps of weight loss as shown in Figure VI.9(c). In the first region of 20-150 ℃, **VI-9**·H_2O loses guest H_2O molecule (observed 2.43 %, calculated 1.63 %). On further heating, **VI-9**·H_2O loses two azpy molecules (observed 31.82 %, calculated 33.35 %) between 200 and 284 ℃. Finally, **VI-9**·H_2O loses another azpy molecules (observed 35.96 %, calculated 33.35 %) between 330 and 430 °C.

In order to obtain the information of structures produced by removal of guest molecules, XRPD patterns of **VI-1** and **VI-9**·H_2O were measured. As illustrated in Figure VI.10(a), the observed XRPD diagram of **VI-1** at an ambient condition shows slightly different peak pattern with the simulated powder pattern upon removal of the EtOH molecules from the single crystal model of **VI-1**·2EtOH, indicative of the slight exchange of the host framework of **VI-1** in the absence of included EtOH molecules. Figure VI.10(b) shows the XRPD patterns of **VI-9**·H_2O at 150 ℃ with a simulated pattern based of the single-crystal data with no crystallized MeOH molecules. TG data reveal that the guest H_2O molecules are wholly removed at 150 °C. The good agreement of the peaks in both diagrams demonstrates that the porous network is kept in this phase, indicating that the network is retained in the absence of any guest molecules in the channels.

From the results of the structural information, EA, IR, TGA, and XRPD measurements, it is revealed that the channel windows constructed from the interpenetrating framework in **VI-9** must expand and contract without the decomposition, because of easy removal of larger original guest molecules (MeOH and EtOH) than the channel window. This phenomenon was also checked by following experimental of gas adsorption measurements.

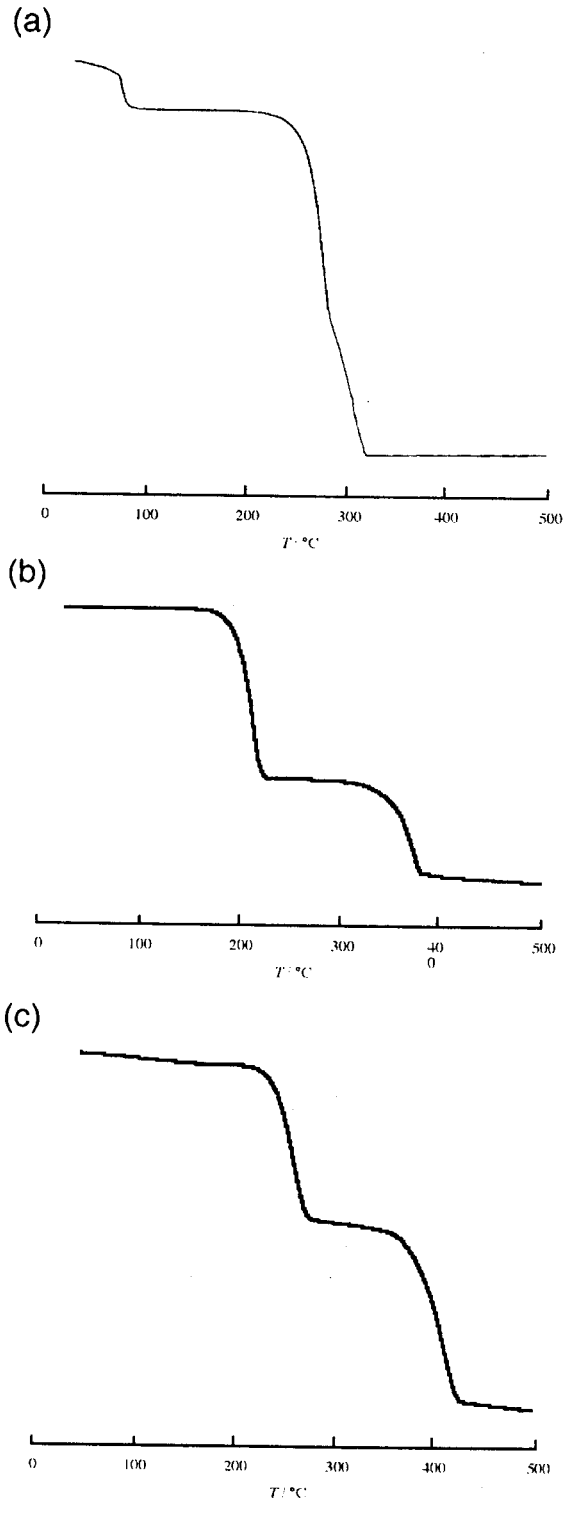

Figure VI.9. Thermogravimetric analysis data for (a) **VI-1**, (b) **VI-7**, and (c) **VI-9**·H_2O.

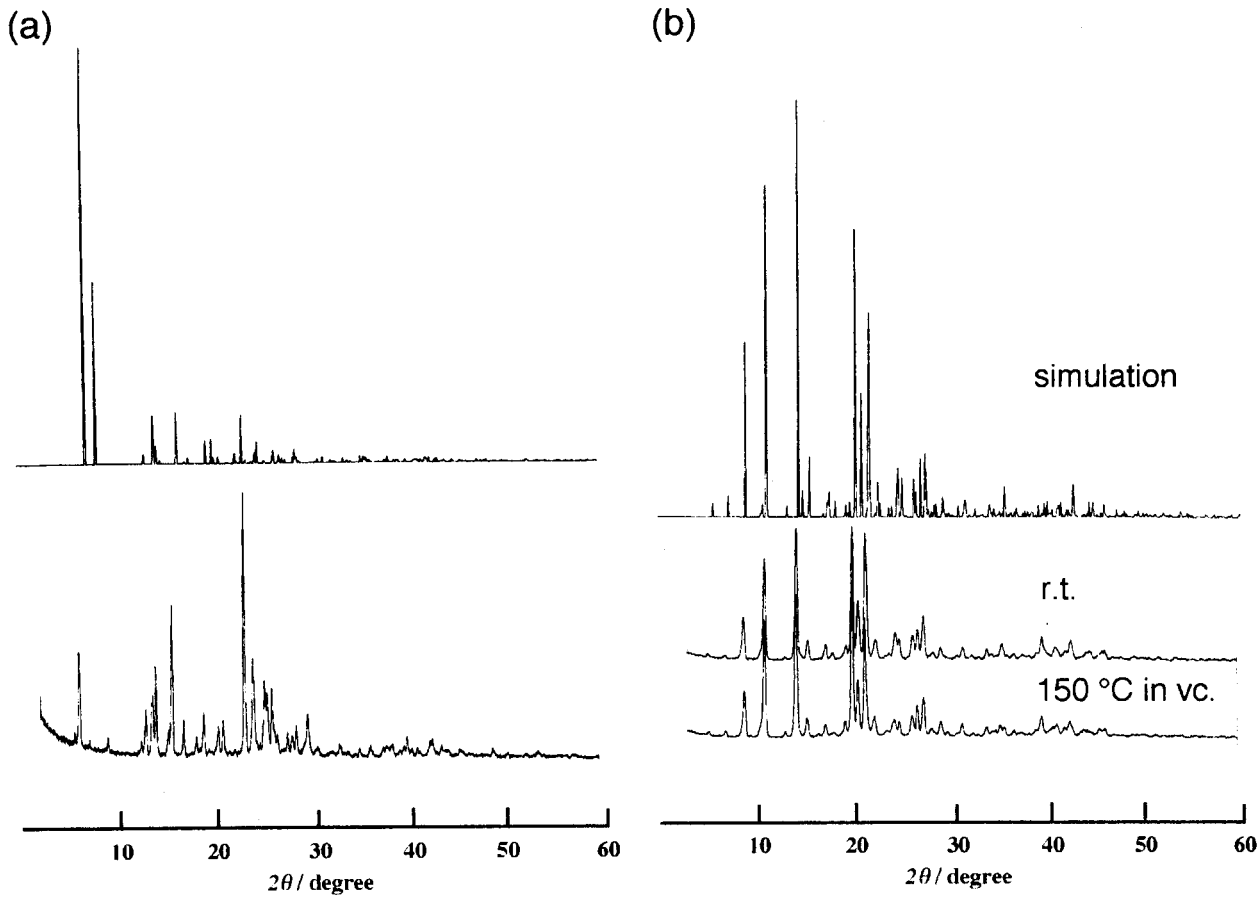

Figure VI.10. (a) Simulated XRPD pattern upon removal of the EtOH molecules from the single crystal model of **VI-1**·2EtOH (top) and the observed pattern of **VI-1** at r.t. (bottom). (b) Simulated XRPD pattern upon removal of the MeOH molecules from the single crystal model of **VI-9**·MeOH (top) and the observed pattern of **VI-9**·H_2O at r.t. (middle) and 150 °C (bottom).

VI. 3. 5 Gas Adsorption Properties

Gas adsorption is one of the most typical functionalities of the porous materials. The adsorption measurements were carried out after the sample was dried under reduced pressure at 80 ℃ in order to remove the guest molecules in the channels.

The adsorption isotherm of N_2 to **VI-9** at -196 ℃ indicates no uptake into the micropores at all (BET surface area = 22 $m^2 \cdot g^{-1}$), indicating that the channel size of **VI-9** (2 Å × 2 Å) is not enough to incorporate N_2 molecules (3 Å). On the other hand, **VI-9** adsorbs a N_2 gas at 25 ℃ with a type I curve in the IUPAC classification as shown in Figure VI.11(a).

The adsorption isotherm of CH_4, whose size (4 Å) is also larger than that of the micropore window, to **VI-9** in the pressure range between 1 and 69 atm at 25 ℃ shows a type I curve in the IUPAC classification as shown in Figure VI.11(b). About 25 Ncc of CH_4 are adsorbed per 1.0 g of desolvated sample of **VI-9** at 69 atm. The high-pressure adsorption of supercritical CH_4 in the micropore field has been studied by the extended Dubinin-Radushkevich (DR) equation (eq-3), which is represented in the Chapter IV. The inherent micropore volume, W_L, is determined by the Langmuir plot. The isotherms of **VI-9** are well explained by this equation. The obtained parameters, W_L (Ncc·g^{-1}), the adsorption energy βE_0 (kJ·mol^{-1}), and the saturated vapor pressure of the quasi-vaporized supercritical methane P_{0q} (atm), are 22, 10.1, and 63.9, respectively. Furthermore, the βE_0 value leads to isosteric heat of adsorption $q_{st,\phi=1/e}$ at the fractional filling of 1/e. The $q_{st,\phi=1/e}$ of **VI-9** (18.27 kJ·mol^{-1}) is larger than those (16.25-17.04 kJ·mol^{-1}) of Cu-dicarboxylate porous polymers having larger micropores (7-11 Å),[57] which clearly indicates the increase in attractive interaction between CH_4 molecules and the micropore surface.

Although the size of N_2 (3 Å) is smaller than that of CH_4 (4 Å), no N_2 gas is adsorbed into the micropore at -196 °C, which is associated with a framework vibration in addition of the effect of a slow diffusion at low temperature. At low temperature, the lattice vibration of the interpenetrating framework in **VI-9** is inhibited, and therefore the size of the channel window is almost constant. On the other hand, the channel window can expand in the size at room temperature. The author defines this interpenetrating framework **VI-9** as new soft dynamic microporous materials, namely, third-generation compounds.[58]

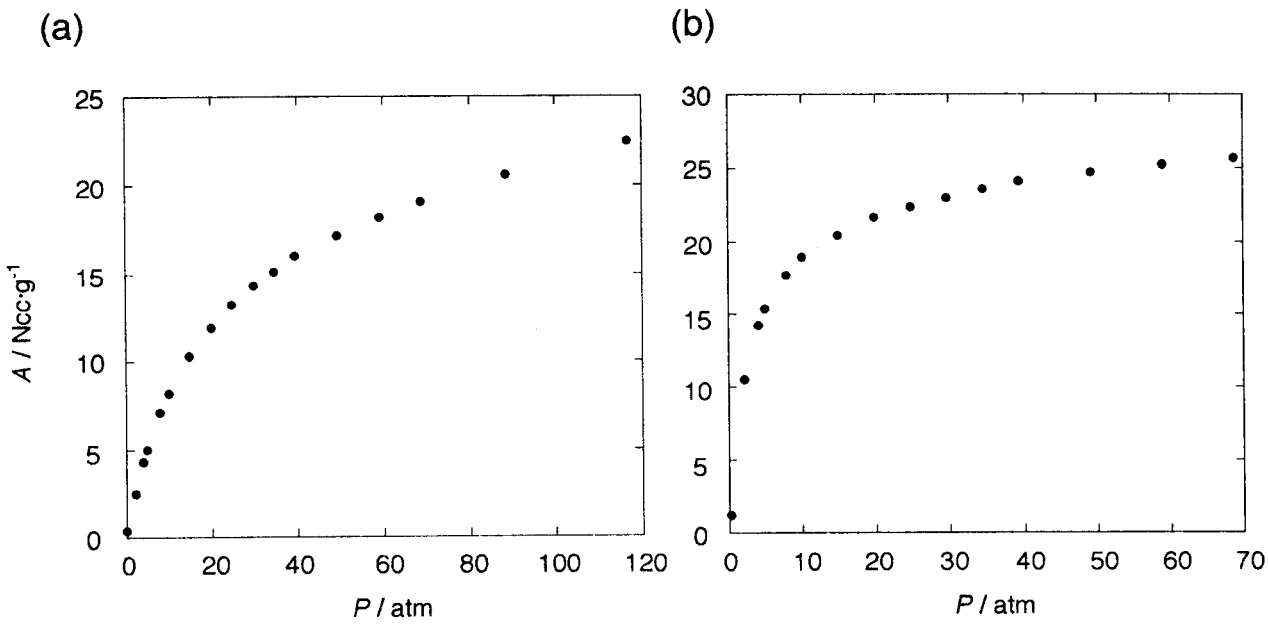

Figure VI.11. The adsorption isotherms of (a) N_2 and (b) CH_4 in **VI-9** at 25 °C.

VI. 3. 6 Classification of Porous Materials

Our laboratory has previously refined the third-generation compound as three categories as shown in General Introduction.[59]

1) The "recoverable collapsing" framework (type I): the framework in this species collapses due to the close-packing force on removal of the guest molecules; however, it regenerates under the initial conditions.[59-64]

2) The " guest-induced transformation" framework (type II): this framework has the property that structural shifts in the network are induced by the simultaneous exchanging of guest molecules.[56,65-67]

3) The "guest-induced reformation" framework (type III): this framework has the property that removal of guest molecules makes a structural change in the network; however, it reverts to the original structure under the initial conditions.[59,68,69]

Interestingly, the coordination polymer **VI-9** belongs to neither of above three categories. **VI-9** shows no structural change before and after the desorption of guest molecules. However, the channel windows must apparently spread and contract to release and incorporate larger guest molecules than the size of the window. Therefore, the author defines a new type of soft dynamic coordination polymer, that is, "guest-induced vibrating" framework (type IV) (Scheme VI.5). To our knowledge, only one example of $[Ni_2(NO_3)_4(4,4'\text{-bpy})_3]$ shows such a type IV adsorption /desorption system.[70]

Scheme VI.5

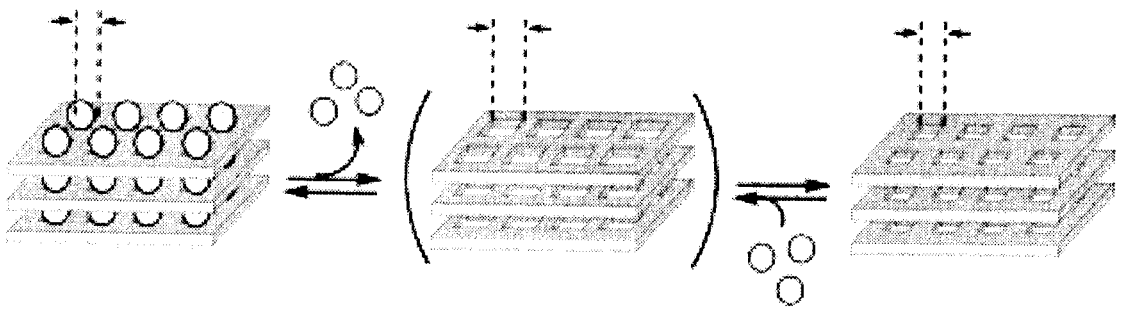

Guest-Induced Vibrating

VI. 4 Conclusion

Novel ten coordination polymers, $\{[Mn(NO_3)_2(azpy)(H_2O)_2]\cdot 2EtOH\}_n$ (**VI-1**·2EtOH) (*1-D linear chain*), $\{[Cd(azpy)_3(H_2O)_2]\cdot 2PF_6\cdot azpy\}_n$ (**VI-2**) (*1-D fishbone-type chain*), $\{[M_2(azpy)_6(H_2O)_5]\cdot 4PF_6\cdot azpy\cdot H_2O\}_n$ (M = Ni (**VI-3**), Zn (**VI-4**)) (*1-D defective zigzag chain*), $\{[Ag(azpy)]\cdot PF_6\}_n$ (**VI-5**) (*1-D linear chain*), $\{[Mn(NCS)_2(azpy)(MeOH)_2]\cdot azpy\}_n$ (**VI-6**) (*1-D linear chain*), $\{[Mn(NCS)_2(azpy)_2]\cdot azpy\}_n$ (**VI-7**) (*2-D square sheet*), $\{[Ni(NCS)_2(azpy)_2]\cdot 3toluene\}_n$ (**VI-8**·3toluene) (*2-D rhombic sheet*), and $\{[Ni_2(NCS)_4(azpy)_4]\cdot alcohol\}_n$ (alcohol = MeOH (**VI-9**·MeOH), EtOH (**VI-9**·EtOH)) (*2-D interpenetrating sheet*), have been newly constructed from combinations of corresponding metal salts and the azpy ligand. Their solid-state structures were characterized by the X-ray diffraction measurements. In these compounds, **VI-1**·2EtOH, **VI-7**, **VI-8**·3toluene, **VI-9**·MeOH, and **VI-9**·EtOH, have microporous channels with several dimensions and sizes. The structure of **VI-1**·2EtOH affords 1-D linear chains, each of which is linked by hydrogen bonds to form a 3-D *log-cabin* type network with micropores, which include guest EtOH molecules. **VI-7** affords large channels with dimensions of about 5 Å x 3 Å along the *a*-axis, in which guest azpy molecules are filled. This compound **VI-7** makes the non-interpenetration structure in spite of the large channel, because of the template effect of free azpy ligands. **VI-8**·3toluene gives the non-interpenetrating 2-D sheets, between which toluene molecules are encapsulated by π-π and CH-π interactions. On the other hand, the 2-D networks of **VI-9**·MeOH and **VI-9**·EtOH form the interpenetrating structures with channels, which are filled with solvated alcohol molecules, with dimensions of about 2 Å x 2 Å along the *c*-axis. The porous network of **VI-9** is maintained after the removal of guest alcohol molecules and the stable channels can adsorb the CH_4 and N_2 gas, whose sizes are apparently larger that that of the original channel window, indicative of the construction of new soft dynamic micropore, "guest-induced vibrating" framework.

VI. 5 References

(1) Carlucci, L.; Ciani, G.; Proserpio, D. M.; Rizzato, S. *J. Chem. Soc., Dalton Trans.* **2000**, 3821-3827.

(2) Carlucci, L.; Ciani, G.; Gramaccioli, A.; Proserpio, D. M.; Rizzato, S. *CrystEngComm* **2000**, *29*, 1-10.

(3) Günes, B.; Soylu, H.; Özbey, S.; Tufan, Y.; Karacan, N. *Acta Cryst.* **1996**, *C52*, 2425-2427.

(4) Kondo, M.; Shimamura, M.; Noro, S.; Kimura, Y.; Uemura, K.; Kitagawa, S. *J. Solid State Chem.* **2000**, *152*, 113-119.

(5) Moon, M.; Kim, I.; Lah, M. S. *Inorg. Chem.* **2000**, *39*, 2710-2711.

(6) Niel, V.; Muñoz, M. C.; Gaspar, A. B.; Galet, A.; Levchenko, G.; Real, J. A. *Chem. Eur. J.* **2002**, *8*, 2446-2453.

(7) Li, D.; Kaneko, K. *J. Phys. Chem. B* **2000**, *104*, 8940-8945.

(8) Lu, J. Y.; Runnels, K. A.; Norman, C. *Inorg. Chem.* **2001**, *40*, 4516-4517.

(9) Maekawa, M.; Sugimoto, K.; Kuroda-Sowa, T.; Suenaga, Y.; Munakata, M. *J. Chem. Soc., Dalton Trans.* **1999**, 4357-4362.

(10) Real, J. A.; Andrés, E.; Muñoz, M. C.; Julve, M.; Granier, T.; Bousseksou, A.; Varret, F. *Science* **1995**, *268*, 265-267.

(11) Brandys, M.-C.; Puddephatt, R. J. *Chem. Commun.* **2001**, 1508-1509.

(12) Carlucci, L.; Ciani, G.; Proserpio, D. M. *Chem. Commun.* **1999**, 449-450.

(13) Carlucci, L.; Ciani, G.; Proserpio, D. M. *J. Chem. Soc., Dalton Trans.* **1999**, 1799-1804.

(14) Dong, Y.-B.; Layland, R. C.; Pschirer, N. G.; Smith, M. D.; Bunz, U. H. F.; Loye, H.-C. Z. *Chem. Mater.* **1999**, *11*, 1413-1415.

(15) Carlucci, L.; Ciani, G.; Proserpio, D. M. *New J. Chem.* **1998**, 1319-1321.

(16) He, C.; Zhang, B.-G.; Duan, C.-Y.; Li, J.-H.; Meng, Q.-J. *Eur. J. Inorg. Chem.* **2000**, 2549-2554.

(17) Kondo, M.; Shimamura, M.; Noro, S.; Yoshitomi, T.; Minakoshi, S.; Kitagawa, S. *Chem. Lett.* **1999**, 285-286.

(18) Kondo, M.; Shimamura, M.; Noro, S.; Minakoshi, S.; Asami, A.; Seki, K.; Kitagawa, S. *Chem. Mater.* **2000**, *12*, 1288-1299.

(19) Li, B.; Liu, H.; Xu, Y.; Chen, J.; Xu, Z. *Chem. Lett.* **2001**, 902-903.

(20) Moliner, N.; Muñoz, M. C.; Real, J. A. *Inorg. Chem. Commun.* **1999**, *2*, 25-27.

(21) Noro, S.; Kondo, M.; Ishii, T.; Kitagawa, S.; Matsuzaka, H. *J. Chem. Soc., Dalton Trans.* **1999**, 1569-1574.

(22) Withersby, M. A.; Blake, A. J.; Champness, N. R.; Cooke, P. A.; Hubberstey, P.;

Schröder, M. *New J. Chem.* **1999**, *23*, 573-575.

(23) Biradha, K.; Fujita, M. *J. Chem. Soc., Dalton Trans.* **2000**, 3805-3810.

(24) Biradha, K.; Fujita, M. *Chem. Commun.* **2001**, 15-16.

(25) Biradha, K.; Hongo, Y.; Fujita, M. *Angew. Chem., Int. Ed. Engl.* **2000**, *39*, 3843-3845.

(26) Biradha, K.; Hongo, Y.; Fujita, M. *Angew. Chem., Int. Ed. Engl.* **2002**, *41*, 3395-3398.

(27) Biradha, K.; Fujita, M. *Chem. Commun.* **2002**, 1866-1867.

(28) Brown, E. V.; Granneman, G. R. *J. Am. Chem. Soc.* **1975**, *97*, 621-627.

(29) Campbell, N.; Henderson, A. W.; Taylor, D. *J. Chem. Soc.* **1953**, 1281-2185.

(30) Higashi, T. **1995**, Program for Adsorption Correction, Rigaku Corporation, Tokyo, Japan.

(31) Altomare, A.; Burla, M. C.; Camalli, M.; Cascarano, M.; Giacovazzo, C.; Guagliardi, A.; Polidori, G. *J. Appl. Cryst.* **1994**, *27*, 435.

(32) Beurskens, P. T.; Admiraal, G.; Beurskens, G.; Bosman, W. P.; de Gelder, R.; Israel, R.; Smits, J. M. M. **1994**, The DIRDIF-94 program system, Technical Report of the Crystallography Laboratory, University of Nijmegen, The Netherlands.

(33) Altomare, A.; Burla, M. C.; Camalli, M.; Cascarano, G. I.; Giacovazzo, C.; Guagliardi, A.; Moliterni, A. G. G.; Polidori, G.; Spagna, R. *J. Appl. Cryst.* **1999**, *32*, 115-119.

(34) Sheldrick, G. M. **1985**, In "Crystallographic Computing 3" (Eds G.M. Sheldrick, C. Kruger and R. Goddard) Oxford University Press, pp. 175-189.

(35) Gilmore, C. J.; **1990**, MITHRIL - an integrated direct methods computer program. University of Glasgow, Scotland.

(36) Crystal Structure Analysis Package, Molecular Structure Corporation (1985 & 1999).

(37) Huang, S. D.; Xiong, R.-G. *Polyhedron* **1997**, *16*, 3929-3939.

(38) Li, B.; Yin, G.; Cao, H.; Liu, Y.; Xu, Z. *Inorg. Chem. Commun.* **2001**, *4*, 451-453.

(39) Li, B.; Liu, H.; Xu, Y.; Yin, G.; Chen, J.; Xu, Z. *Chem. Lett.* **2001**, 214-215.

(40) Kondo, M.; Asami, A.; Chang, H.-C.; Kitagawa, S. *Cryst. Eng.* **1999**, *2*, 115-122.

(41) Greenwood, N. N.; Earnshaw, A. *Chemistry of the Elements (Second edition)*; Butterworth-Heinemann: Oxford, 2001, p 803.

(42) Tong, M.-L.; Chen, X.-M.; Ye, B. H.; Ng, S. W. *Inorg. Chem.* **1998**, *37*, 5278-5281.

(43) Withersby, M. A.; Blake, A. J.; Champness, N. R.; Hubberstey, P.; Li, W. S.; Schröder, M. *Angew. Chem., Int. Ed. Engl.* **1997**, *36*, 2327-2329.

(44) Robinson, F.; Zaworotko, M. J. *J. Chem. Soc., Chem. Commun.* **1995**, 2413-2414.

(45) Carlucci, L.; Ciani, G.; Gudenberg, D. W. V.; Proserpio, D. M. *Inorg. Chem.* **1997**, *36*, 3812-3813.

(46) Schauer, C. L.; Matwey, E.; Fowler, F. W.; Lauher, J. W. *J. Am. Chem. Soc.* **1997**, *119*, 10245-10246.

(47) Blake, A. J.; Champness, N. R.; Khlobystov, A. N.; Lemenovskii, D. A.; Li, W. S.; Schröder, M. *Chem. Commun.* **1997**, 1339-1340.

(48) Carlucci, L.; Ciani, G.; Proserpio, D. M.; Sironi, A. *Chem. Commun.* **1994**, 2755-2756.

(49) Yaghi, O. M.; Li, H. *J. Am. Chem. Soc.* **1996**, *118*, 295-296.

(50) Zhang, Y.; Jianmin, L.; Wei, D.; Nishiura, M.; Imamoto, T. *Chem. Lett.* **1999**, 195-196.

(51) Gable, R. W.; Hoskins, B. F.; Robson, R. *Chem. Commun.* **1990**, 1667-1668.

(52) Beadle, P. J.; Goldstein, M.; Goodgame, D. M. L.; Grzeskowiak, R. *Inorg. Chem.* **1969**, *8*, 1490-1493.

(53) Subramanian, S.; Zaworotko, M. J. *Angew. Chem., Int. Ed. Engl.* **1995**, *34*, 2127-2129.

(54) Zaworotko, M. J. *Angew. Chem., Int. Ed. Engl.* **2000**, *39*, 3052-3054.

(55) Noro, S.; Kitagawa, S.; Kondo, M.; Seki, K. *Angew. Chem., Int. Ed. Engl.* **2000**, *39*, 2082-2084.

(56) Noro, S.; Kitaura, R.; Kondo, M.; Kitagawa, S.; Ishii, T.; Matsuzaka, H.; Yamashita, M. *J. Am. Chem. Soc.* **2002**, *124*, 2568-2583.

(57) Seki, K.; Mori, W. *J. Phys. Chem. B* **2002**, *106*, 1380-1385.

(58) Kitagawa, S.; Kondo, M. *Bull. Chem. Soc. Jpn.* **1998**, *71*, 1739-1753.

(59) Uemura, K.; Kitagawa, S.; Kondo, M.; Fukui, K.; Kitaura, R.; Chang, H.-C.; Mizutani, T. *Chem. Eur. J.* **2002**, *8*, 3587-3600.

(60) Min, K. S.; Suh, M. P. *Chem. Eur. J.* **2001**, *7*, 303-313.

(61) Tabares, L. C.; Navarro, J. A. R.; Salas, J. M. *J. Am. Chem. Soc.* **2001**, *123*, 383-387.

(62) Choi, H. J.; Lee, T. S.; Suh, M. P. *Angew. Chem., Int. Ed. Engl.* **1999**, *38*, 1405-1408.

(63) Pan, L.; Woodlock, E. B.; Wang, X.; Zheng, C. *Inorg. Chem.* **2000**, *39*, 4174-4178.

(64) Li, H.; Davis, C. E.; Groy, T. L.; Kelley, D. G.; Yaghi, O. M. *J. Am. Chem. Soc.* **1998**, *120*, 2186-2187.

(65) Min, K. S.; Suh, M. P. *J. Am. Chem. Soc.* **2000**, *122*, 6834-6840.

(66) Jung, O.-S.; Kim, Y. J.; Lee, Y.-A.; Park, J. K.; Chae, H. K. *J. Am. Chem. Soc.* **2000**, *122*, 9921-9925.

(67) Jung, O.-S.; Kim, Y. J.; Lee, Y.-A.; Chae, H. K.; Jang, H. G.; Hong, J. *Inorg. Chem.* **2001**, *40*, 2105-2110.

(68) Beauvais, L. G.; Shores, M. P.; Long, J. R. *J. Am. Chem. Soc.* **2000**, *122*, 2763-2772.

(69) Kiritsis, V.; Michaelides, A.; Skoulika, S.; Golhen, S.; Ouahab, L. *Inorg. Chem.* **1998**, *37*, 3407-3410.

(70) Cussen, E. J.; Claridge, J. B.; Rosseinsky, M. J.; Kepert, C. J. *J. Am. Chem. Soc.* **2002**, *124*, 9574-9581.

General Conclusion

The author investigated the rational syntheses ("crystal engineering") and characterization of the coordination polymers toward the new functional materials, which involve the microporous property, dynamic phenomenon of the frameworks, and their multiple functionalities. The author also studied on the correlation between crystal structures and functions.

In Chapter I, several Fe(II) coordination polymers synthesized by the reaction of Fe(II) salts with linear azpy or 4,4'-bpy ligands were described. It is noteworthy that the control of the spin-crossover phenomenon was achieved by the structural transformation induced by the release of the coordinated solvent molecules.

In Chapter II, the development of new synthetic method of porous coordination polymer was carried out. The utilization of a metalloligand is a good candidate for the construction of porous coordination polymers that may afford fascinating properties derived from uncoordinated metal sites in channel wall: chemical adsorption and heterogeneous catalysis.

In Chapter III, described were rational design and bond engineering of coordination polymers by a Cu(II) metalloligand, whose bonding selectivity for first periodic transition metal ions (Mn(II), Fe(II), Co(II), Cu(II), and Zn(II)) was predictably controlled, following to an Irving-Williams order. Furthermore, the structural results clearly demonstrate that the metalloligand has a variety of coordination modes, depending on second metal ion units employed.

In Chapter IV, newly synthesized were 3-D highly porous coordination polymers, which showed the high CH_4 adsorption ability at ambient temperature and low pressure, and were superior to that of any zeolites, and thus opened up a new possibility for CH_4 storage materials.

In Chapter V, the crystal engineering by anions and dynamic porous functionalities were described. It was revealed that several Cu(II) coordination polymers tend to encounter an attack for their axial sites by coordinate anions or solvents because of the Jahn-Teller effect, which made it possible to regulate the framework.

In Chapter VI, the azpy-containing coordination polymers were studied on their structures

and microporous properties. It should be noted that the interpenetration and π-π interaction played an important role in the framework stability of coordination polymers with rich π-conjugated azpy ligand. Furthermore, new type of third-generation microporous compound, "guest-induced vibrating" framework, was observed in the interpenetrating network.

In summary, total 37 coordination polymers, several compounds of which have microporous channels or cavities, have been synthesized and characterized. In this thesis, the author principally showed the three topics, that is, (1) microporous functionalities, (2) dynamic structural transformation, and (3) rational synthetic strategy toward "crystal engineering". These three factors were closely related to each other.

On the basis of these results, the author has a future look for possibility of coordination polymers toward next materials.

Multi-functionality generated from the combination of individual properties such as magnetism, conductivity, nonlinear optics, optical properties, microporosity, spin transition, and so on, is one of an important topic in the area of chemistry because anticipated are the control of one properties by changing another property and the enhancement of each property by cooperative interaction. Although light-induced exited state spin trapping (LIESST) is a representative example of such a multi-functionality, other multi-functionalities are little observed and, therefore, little studied to date. The regulation of spin-crossover phenomenon by entrance and exit of guest molecules mentioned in Chapter I should be also categorized in one of the multi-functionality.

Now, man can consider that crystal engineering for coordination polymers would be achieved soon, and then a next challenge is to exploit coordination polymers in nano-level. Even at present, great numbers of coordination polymers are found as powder and/or crystal. Indeed, the human society requires other figurations such as film and fiber for useful application.

All dynamic coordination polymers change their own frameworks by chemical stimuli such as neutral guest molecules and counter anions, while the examples of corresponding polymers regulated by physical stimuli such as electric or magnetic field and light are almost nothing. The author defines such coordination polymers as a new type of dynamic framework: fourth-generation

compound, which may give an unprecedented property, for instance, that the trap and release of guest molecules are controlled by physical stimuli.

The functional coordination polymers have being occupying an important position in compounds that afford not only simple usefulness but also improvement of many of life for human.

List of Publications

General Introduction
"6.2.2. Infinite Systems"
Kitagawa, S.; Noro, S.
Comprehensive Coordination Chemistry -II: From Biology to Nanotechnology, **2003**, in press.

Part 1

Chapter I
"Syntheses and crystal structures of iron co-ordination polymers with 4,4'-bipyridine (4,4'-bpy) and 4,4'-azopyridine (azpy). Two-dimensional Networks supported by hydrogen bonding, $\{[Fe(azpy)(NCS)_2(MeOH)_2](azpy)\}_n$ and $\{[Fe(4,4'\text{-}bpy)(NCS)_2(H_2O)_2](4,4'\text{-}bpy)\}_n$"
Noro, S.; Kondo, M.; Ishii, T.; Kitagawa, S.; Matsuzaka, H.
J. Chem. Soc., Dalton Trans. **1999**, 1569-1574.

"Synthesis and Crystal Structure of New Sulfate-Bridged Coordination Polymer, $\{(4,4'\text{-}bpyH_2)[Fe_3(4,4'\text{-}bpy)_3(SO_4)_4(H_2O)_6]\cdot 10H_2O\}_n$ (4,4'-bpy = 4,4'-Bipyridine). Three-Dimensional Network with Microporous Channels"
Noro, S.; Kondo, M.; Kitagawa, S.; Ishii, T.; Matsuzaka, H.
Chem. Lett. **1999**, 727-728.

"Structural Transformation by Removal of Coordinated Solvents and Concomitant Spin-Crossover Phenomenon of Fe(II) Coordination Polymer $\{[Fe(NCS)_2(azpy)(MeOH)_2]\cdot azpy\}_n$ (azpy = 4,4'-Azopyridine)"
Noro, S.; Kitagawa, S.; Okubo, T.; Mitani, T.; Katada, M.; Wada, T.
to be submitted.

Chapter II
"New microporous coordination polymer affording guest-coordination sites at channel walls"
Noro, S.; Kitagawa, S.; Yamashita, M.; Wada, T.
Chem. Commun. **2002**, 222-223.

Chapter III
"Novel 2-Dimensional Coordination Polymer Constructed form a Multi-Functional Metalloligand"
Noro, S.; Kitagawa, S.; Yamashita, M.; Wada, T.
CrystEngComm. **2002**, *4*, 162-164. .

"Control of Frameworks by a Multi-Functional Metalloligand: New Synthetic Approach toward Crystal Engineering"
Noro, S.; Kitagawa, S.; Miyasaka, H.; Yamashita, M.; Okubo, T.; Mitani, T.; Wada, T.
J. Am. Chem. Soc., to be submitted.

Part 2

Chapter IV
"A New, Methane Adsorbents, Porous Coordination Polymer [{$CuSiF_6$(4,4'-bipyridine)$_2$}$_n$]"
Noro, S.; Kitagawa, S.; Kondo, M.; Seki, K.
Angew. Chem., Int. Ed. Engl. **2000**, *39*, 2082-2084 (published as Very Important Paper (VIP)).

Chapter V
"Framework Engineering by Anions and Porous Functionalities of Cu(II)/4,4'-bpy Coordination Polymers"
Noro, S.; Kitaura, R.; Kondo, M.; Kitagawa, S.; Ishii, T.; Matsuzaka, H.; Yamashita, M.
J. Am. Chem. Soc. **2002**, *124*, 2568-2583.

"Dynamic porous frameworks of coordination polymers controlled by anions"
Noro, S.; Kitagawa, S.
Studies in Surface Science and catalysis **2002**, *141*, 363-370.

Chapter VI
"Syntheses, Structures, and Methane Adsorption Properties of Stable Microporous Networks of Coordination Polymers with 4,4'-Azopyridine"
Kondo, M.; Shimamura, M.; Noro, S.; Minakoshi, S.; Asami, A.; Seki, K.; Kitagawa, S.
Chem. Mater. **2000**, *12*, 1288-1299.

"Effective Interpenetration and π-π Interaction for Construction of Azpy-Containing Coordination Networks: Syntheses, Crystal Structures, and Microporous Functionalities with Soft Dynamic Channels"
Noro, S.; Kitaura, R.; Kitagawa, S.; Wada, T.
Inorg. Chem., to be submitted.

Other Publications

"Rational Synthesis of Stable Channel-Like Cavities with Methane Gas Adsorption Properties: $[\{Cu_2(pzdc)_2(L)\}_n]$ (pzdc = pyrazine-2,3-dicarboxylate; L = a Pillar Ligand)"
Kondo, M.; Okubo, T.; Asami, A.; Noro, S.; Yoshitomi, T.; Kitagawa, S.; Ishii, T.; Matsuzaka, H.; Seki, K.
Angew. Chem., Int. Ed. Engl. **1999**, *38*, 140-143.

"Novel Extended Linear Structure of Decavanadate Anions Linked by Bis(4-Pyridinium) Disulfide (H_2dpds), $\{(H_2dpds)_2[V_{10}O_{26}(OH)_2].10H_2O\}_n$"
Kondo, M.; Fujimoto, K.; Asami, A.; Noro, S.; Kitagawa, S.; Ishii, T.; Matsuzaka, H.
Chem. Lett. **1999**, 291-292.

"New Coordination Network of $[Cd_2(bpob)_3(NO_3)_4]_n$ (bpob = 1,4-bis(4-pyridoxy)benzene) Constructed from Two Structural Isomers of the Ligand"
Kondo, M.; Asami, A.; Fujimoto, K.; Noro, S.; Kitagawa, S.; Ishii, T.; Matsuzaka, H.
J. Inorg. Mat. **1999**, 73-75.

"Synthesis and Structures of Zn Coordination Polymers with 4,4'-Bipyridine and 4,4'-Azopyridine. Effect of Counter Anion on the Network System"
Kondo, M.; Shimamura, M.; Noro, S.; Yoshitomi, T.; Minakoshi, S.; Kitagawa, S.
Chem. Lett. **1999**, 285-286.

"Synthesis and Crystal Structure of $[Cu(N\text{-salicylidene-3-aminopyridine})_2]_n$ Constructed from Unsymmetric Bridging Ligand with Two Dissimilar Metal-Binding Sites"
Noro, S.; Kondo, M.; Kitagawa, S.; Ishii, T.; Matsuzaka, H.; Yamashita, M.
Mol. Cryst. Liq. Cryst. **1999**, *342*, 231-236.

"Synthesis and Structures of Coordination Polymers with 4,4'-Dipyridyldisulfide"
Kondo, M.; Shimamura, M.; Noro, S.; Kimura, Y.; Uemura, K.; Kitagawa, S.
J. Solid State Chem. **2000**, *152*, 113-119.

"Novel Pillared-Layer Coordination Polymer Network with Hysteretic Sorption: $[Cu_2(pzdc)_2(dpyg)]_n$ (pzdc = pyrazine-2,3-dicarboxylate; dpyg = 1,2-di(4-pyridyl)glycol)"
Kitaura, R.; Fujimoto, K.; Noro, S.; Kondo, M.; Kitagawa, S.
Angew. Chem., Int. Ed. Engl. **2002**, *41*, 133-135.

List of Presentations

(1) Syntheses and Gas Adsorption Properties of Coordination Polymers Having 3-D Structure Constructed from Bipyridine Derivatives
Noro, S.; Okubo, T.; Kondo, M.; Seki, K.; Kitagawa, S.
74th Annual Meeting of Chemical Society of Japan, Kyoto, March 1998.

(2) Syntheses and Gas Adsorption Properties of Porous Coordination Polymers Containing 4,4'-Bipyridine Derivatives as Bridging Ligand
Noro, S.; Kondo, M.; Ishii, T.; Matsuzaka, H.; Kitagawa, S.; Seki, K.
48th Symposium on Coordination Chemistry of Japan, Kochi, September 1998.
(Poster presentation)

(3) Syntheses and Gas Adsorption Properties of Coordination Polymers Having Three-Dimensional Structure Constructed from Bipyridine Derivative
Noro, S.; Kondo, M.; Okubo, T.; Seki, K.; Kitagawa, S.
First International Conference of Inorganic Materials (ICIM), France, September 1998.
(Poster presentation)

(4) Syntheses and Gas Adsorption Properties of Coordination Polymers with Bridging 4,4'-Bipyridine Derivatives
Noro, S.; Kondo, M.; Kitagawa, S.; Matsuzaka, H.; Ishii, T.; Seki, K.
76th Annual Meeting of Chemical Society of Japan, Yokohama, March 1999.

(5) Selective Syntheses and Gas Adsorption Properties of 3-Dimensional Highly Porous Coordination Polymers $[Cu(AF_6)(4,4'\text{-bipyridine})_2]_n$ (A = Si, Ge)
Noro, S.; Kondo, M.; Seki, K.; Kitagawa, S.; Ishii, T.; Matsuzaka, H.; Yamashita, M.
49th Symposium on Coordination Chemistry of Japan, Sapporo, September 1999.

(6) Syntheses, Crystal Structures, and Methane Gas Adsorption Properties of Coordination Polymers Constructed from Pyrazine-2,3-dicarboxylate and Bipyridine Derivatives
Noro, S.; Okubo, T.; Yoshitomi, T.; Asami, A.; Seki, K.; Kondo, M.; Kitagawa, S.; Ishii, T.; Matsuzaka, H.; Yamashita, M.
International Symposium, Molecular Design and Functionalities of Assembled Metal Complexes, Kyoto, November 1999.
(Poster presentation)

(7) Synthesis and Crystal Structure of a Novel Porous Coordination Polymer Constructed from Cu(II) and 2,3-Pyridinedicarboxylate Ligand
Noro, S.; Kondo, M.; Kitagawa, S.; Ishii, T.; Matsuzaka, H.; Yamashita, M.
78th Annual Meeting of Chemical Society of Japan, Funabashi, March 2000.

(8) Novel Coordination Polymers Containing Pyridinedicarboxylate Bridges – Chemical Adsorption of Small Molecules
Noro, S.; Kondo, M.; Kitagawa, S.; Ishii, T.; Matsuzaka, H.; Yamashita, M.
50th Symposium on Coordination Chemistry of Japan, Kusatsu, September 2000.
(Poster presentation)

(9) Novel Coordination Polymers Containing Pyridinedicarboxylate Bridges -- Chemical Adsorption of Small Molecules
Noro, S.; Kondo, M.; Kitagawa, S.; Ishii, T.; Matsuzaka, H.; Yamashita, M.
International Symposium on New Horizons of Coordination Chemistry towards the 21th Century, Kusatsu, September 2000.
(Poster presentation)

(10) New Methane Adsorbents of Porous Coordination Polymers, $[CuAF_6(4,4'\text{-bipyridine})_2]_n$ (A = Si, Ge)
Noro, S.; Kondo, M.; Kitagawa, S.; Ishii, T.; Matsuzaka, H.; Yamashita, M.; Seki, K.
International Chemical Congress of Pacific Basin Societies (PACIFICHEM 2000), Honolulu, December 2000.
(Poster presentation)

(11) Synthesis and Crystal Structure of Porous Coordination Polymer Containing the Metallo Ligand $\{[Cu(2,4\text{-pydca})_2(H_2O)]\cdot 2Et_3NH\}$
Noro, S.; Kondo, M.; Kitagawa, S.; Miyasaka, H.; Ishii, T.; Matsuzaka, H.; Yamashita, M.
79th Annual Meeting of Chemical Society of Japan, Kobe, March 2001.

(12) Syntheses and Functionalities of Anion-Responding-Type Dynamic Cu–4,4'-Bipyridine Porous Coordination Polymers
Noro, S.; Kondo, M.; Kitagawa, S.; Wada, T.
50th Polymer Symposium of Japan, Shinjuku, September 2001.

(13) Construction of Anion-Responding-Type Dynamic Porous Coordination Polymers
Noro, S.; Kitaura, R.; Kondo, M.; Kitagawa, S.; Wada, T.

51th Symposium on Coordination Chemistry of Japan, Matsue, September 2001.

(14) Syntheses and Functionalities of Cu(II) Porous Coordination Polymers Induced from PF_6^- Anion
Noro, S.; Kitaura, R.; Kitagawa, S.; Wada, T.
81th Annual Meeting of Chemical Society of Japan, Shinjuku, March 2002.

(15) Molecular Design of Self-Assembled Chromium Complexes
Noro, S.; Chang, H.-C.; Kitagawa, S.; Wada, T.
16th Symposium on Optical and Electrical Properties of Organic Materials, Ohta, May 2002.

(16) Syntheses and Properties Responding to External Stimuli of Chromium(III)-Quinone Complexes
Noro, S.; Chang, H.-C.; Kitagawa, S.; Wada, T.
52th Symposium on Coordination Chemistry of Japan, Meguro, September 2002.